Self-Assembly of Merocyanines: Thermodynamic and Kinetic Insights into the Formation of Well-Defined Dye Aggregates

Dissertation zur Erlangung des
naturwissenschaftlichen Doktorgrades
der Julius-Maximilians-Universität Würzburg

vorgelegt von
Andreas Lohr
aus Illertissen

Würzburg 2008

Eingereicht am 4. August 2008
bei der Fakultät für Chemie und Pharmazie

1. Gutachter: Prof. Dr. Frank Würthner
2. Gutachter: Prof. Dr. Anke Krüger
der Dissertation

1. Prüfer: Prof. Dr. Frank Würthner
2. Prüfer: Prof. Dr. Anke Krüger
3. Prüfer: Prof. Dr. Christoph Lambert
des Öffentlichen Promotionskolloquiums

Tag des Öffentlichen Promotionskolloquiums: 24. September 2008

Doktorurkunde ausgehändigt am:

für Valerie

List of Abbreviations

AFM	atomic force microscopy
CD	circular dichroism
COSY	correlated spectroscopy
DCE	1,2-dichloroethane
DEPT	distorsionless enhancement by polarisation transfer
DMSO	dimethylsulfoxide
DMF	*N*,*N*-dimethylformamide
DPFA	*N*,*N*′-diphenylformamidine
ee	enantiomeric excess
ESI	electron spray ionization
HOPG	highly ordered pyrolytic graphite
HPLC	high performance liquid chromatography
HRMS	high resolution mass spectrometry
HSQC	heteronuclear single quantum coherence
HMBC	heteronuclear multiple bond correlation
LD	linear dichroism
MALDI-TOF	matrix-assisted laser desorption/ionization-time of flight
NMR	nuclear magnetic resonance
NOE	nuclear Overhauser effect
ROESY	rotating-frame Overhauser enhancement spectroscopy
rt	room temperature
MCH	methylcyclohexane
Mp	melting point
STM	scanning tunneling microscopy
TCE	trichloroethylene
THF	tetrahydrofuran
TLC	thin layer chromatography
TMS	tetramethylsilane
UV–vis	ultraviolet–visible

Table of Contents

Chapter 1

Introduction and Aim of this Thesis

Self-assembly is an efficient approach for the creation of defined molecular architectures which employs weak interactions such as metal-ion coordination, hydrogen bonding, and π–π interactions to effect noncovalent linkages between molecular building blocks.[1] In the last decades much research has been devoted into the exploration of various ways of how to apply this "bottom-up" approach for the development of nanoscale functional devices[2] as well as novel organic materials for optoelectronic and photonic applications.[3] For that, strong effort has been focused on the functionalization of organic dyes in order to program their self-assembly towards multi-chromophore architectures with appealing topology and intriguing properties.[4] However, in the meantime it has been recognized that the creation of more complex systems demands not only a detailed understanding of the thermodynamics involved in the self-assembly process, but that also deeper knowledge about the kinetic pathways for the morphogenesis of complex structures has to be gained.[5]

Merocyanine dyes are a class of chromophores that is promising for nonlinear optical and photorefractive applications owing to their outstanding dipolar and polarizability properties.[6] Besides several reports in which self-assembly of such dyes is directed via complex formation with hydrogen-bonding receptors,[7] in 2000 Würthner and Yao have shown that highly dipolar merocyanine dyes *themselves* can form self-assembled structures, *i.e.*, they form centrosymmetric dimer aggregates with very high binding constants in nonpolar solvents.[8] This dimerization arises primarily from dipole–dipole interaction between these chromophores owing to their exceptionally large ground-state dipole moment μ_g of about 17 D for merocyanine dyes **1** (Figure 1a).[9] Even though such dimer aggregates were discovered owing to unfavorable low nonlinear optical susceptibilities in polymeric materials based on electric-field-poled dipolar dyes,[6c] it was realized that this dimerization is a very promising supramolecular binding motif for the creation of more elaborate dye assemblies due to its high binding strength and directionality.

Later, in 2003 Würthner and coworkers reported a first application of dipolar aggregation in the self-assembly of ditopic bis(merocyanine) building blocks **2** into highly defined cylindrical dye assemblies through supramolecular polymerization and hierarchical self-organization (Figure 1b).[10] Various levels of organization could be addressed in this system by means of adjusting solvent polarity and monomer concentration.[11] Thus, pairing of the chromophoric units of these bis(merocyanine) dyes driven by dipolar aggregation leads to single-stranded supramolecular oligomers/polymers, which self-assemble into rod-shaped dye assemblies upon further increase of the monomer concentration or decrease of the solvent polarity. However, these studies were focused on the thermodynamics of this self-assembly process whilst little is known about the kinetic pathways on which these structures form. Owing to the achiral nature of the monomers applied so far only racemic mixtures of left- and right-handed helical nanorods were obtained, which precluded the characterization of their helical nature by CD spectroscopy.[11b]

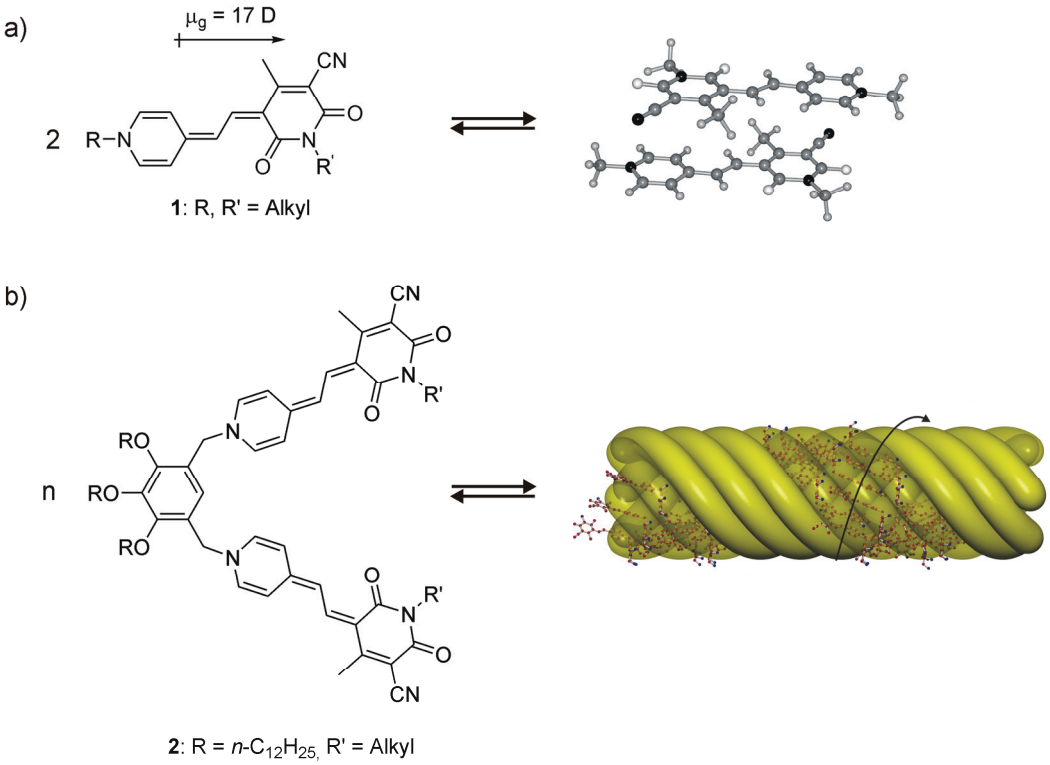

Figure 1. Schematic representation of the a) dimerization of a highly dipolar merocyanine dye **1** into centro-symmetric dimers and b) self-assembly of ditopic bis(merocyanine) dyes **2** into highly defined nanorods.

Since no dipolar interaction-driven self-assembly of merocyanine dyes into discrete architectures beyond simple dimers has been reported to date, the aim of the first part of this thesis is the application of this novel binding motif for the construction of more elaborate discrete merocyanine assemblies, *i.e.* extended π-stacks and cyclic arrays (Figure 2). To realize this objective, suitable merocyanine building blocks had to be synthesized, and their self-assembly studied by spectroscopic and microscopic methods (see Chapter 3 and 4).

The second part of this thesis aims on the elucidation of the kinetic pathways on which the self-assembly of bis(merocyanine) dye nanorods proceeds (see Chapter 5). Such studies are highly desirable since, as noted above, the kinetic pathways towards complex self-assembled systems are not yet understood. Bis(merocyanine) dye nanorods represent a promising system for studying such processes owing to the existence of several levels of organization. In the present studies, chiral bis(merocyanine) dyes will be applied which should induce the formation of helices of only one helical sense and, therefore, should give the possibility to gain valuable information about the self-assembly mechanisms from circular dichroism measurements. Moreover, co-aggregation studies with monomers of different enantiomeric excess and mixtures of achiral and chiral monomers will show whether chiral amplification, a set of phenomena that might allow to control the helicity of these nanorods by only small chiral bias in the monomers,[12] can be observed in these systems and, if so, what are the kinetic pathways for such processes.

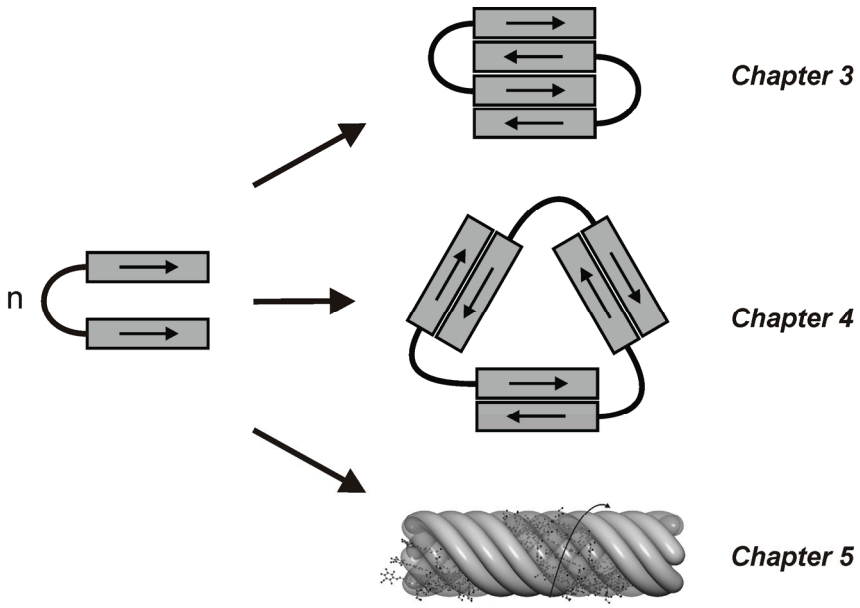

Figure 2. Schematic representation for the self-assembly of appropriately designed merocyanine building blocks into extended π-stacks, cyclic arrays, and homochiral helical nanorods as studied in this thesis.

References

(1) (a) Whitesides, G. M.; Mathias, J. P.; Seto, C. T. *Science* **1991**, *254*, 1312–1319. (b) Lehn, J. M. *Supramolecular Chemistry: Concepts and Perspectives*; VCH: Weinheim, 1995. (c) *Comprehensive Supramolecular Chemistry*; Atwood, J. L.; Davies, J. E. D.; MacNicol, D. D.; Vögtle, F.; Lehn, J.-M., Eds; Pergamon: Oxford, 1996. (d) Prins, L. J.; Reinhoudt, D. N.; Timmerman, P. *Angew. Chem., Int. Ed.* **2001**, *40*, 2382–2426. (e) Holliday, B. J.; Mirkin, C. A. *Angew. Chem., Int. Ed.* **2001**, *40*, 2022–2043. (f) Hof, F.; Craig, S. L.; Nuckolls, C.; Rebek, J., Jr. *Angew. Chem., Int. Ed.* **2002**, *41*, 1488–1508.

(2) (a) *Molecular Switches*; Feringa, B. L., Ed.; VCH: Weinheim, 2001. (b) Balzani, V.; Credi, A.; Venturi, M. *Molecular Devices and Machines*; VCH: Weinheim, 2003. (c) Schmittel, M.; Kalsani, V. *Top. Curr. Chem.* **2005**, *245*, 1–53.

(3) Gregory, P. *High Technology Application of Organic Colorants*; Plenum: New York, 1991.

(4) (a) *Supramolecular Dye Chemistry: Topics in Current Chemistry, Vol. 258*; Würthner, F., Ed.; Springer: Berlin, 2005. (b) Hoeben, F. J. M.; Jonkheijm, P.; Meijer, E. W.; Schenning, A. P. H. J. *Chem. Rev.* **2005**, *105*, 1491–1546.

(5) (a) Jonkheijm, P.; van der Schoot, P.; Schenning, A. P. H. J.; Meijer, E. W. *Science* **2006**, *313*, 80–83. (b) Percec, V.; Ungar, G.; Peterca, M. *Science* **2006**, *313*, 55–56.

(6) (a) Verbiest, T.; Houbrechts, S.; Kauranen, M.; Clays, K.; Persoons, A. *J. Mater. Chem.* **1997**, *7*, 2175–2189. (b) Wolff, J. J.; Wortmann, R. *Adv. Phys. Org. Chem.* **1999**, *32*, 121–217. (c) Würthner, F.; Wortmann, R.; Meerholz, K. *ChemPhysChem* **2002**, *3*, 17–31. (d) Pereverzev, Y. V.; Prezhdo, O. V.; Dalton, L. R. *ChemPhysChem* **2004**, *5*, 1821–1830.

(7) (a) Ahuja, R.; Caruso, P.-L.; Möbius, D.; Paulus, W.; Ringsdorf. H.; Wildburg, G. *Angew. Chem., Int. Ed. Engl.* **1993**, *32*, 1033–1036. (b) Prins, L. J.; Thalacker, C.; Würthner, F.; Timmerman, P.; Reinhoudt, D. N. *Proc. Natl. Acad. Sci. USA* **2001**, *98*, 10042–10045. (c) Würthner, F.; Yao, S.; Heise, B.; Tschierske, C. *Chem. Commun.* **2001**, 2260–2261. (d) Yagai, S.; Higashi, M.; Karatsu, T.; Kitamura, A. *Chem. Commun.* **2006**, 1500–1502. (e) Würthner, F.; Schmidt, J.; Stolte, M.; Wortmann, R. *Angew. Chem., Int. Ed.* **2006**, *45*, 3842–3846.

(8) Würthner, F.; Yao, S. *Angew. Chem., Int. Ed.* **2000**, *39*, 1978–1981.

(9) (a) Würthner, F.; Yao, S.; Debaerdemaker, T.; Wortmann, R. *J. Am. Chem. Soc.* **2002**, *124*, 9431–9447. (b) Rösch, U.; Yao, S.; Wortmann, R.; Würthner, F. *Angew. Chem., Int. Ed.* **2006**, *45*, 7026–7030.

(10) Würthner, F.; Yao, S.; Beginn, U. *Angew. Chem., Int. Ed.* **2003**, *42*, 3247–3250.

(11) (a) Yao, S.; Beginn, U.; Gress, T.; Lysetska, M.; Würthner, F. *J. Am. Chem. Soc.* **2004**, *126*, 8336–8348. (b) Lohr, A.; Gress, T.; Deppisch, M.; Knoll, M.; Würthner, F. *Synthesis* **2007**, 3073–3082.

(12) Palmans, A. R. A.; Meijer, E. W. *Angew. Chem., Int. Ed.* **2007**, *46*, 8948–8968.

Chapter 2

Literature Survey on Merocyanine Dye Self-Assembly

Abstract: The progress in the construction of extended supramolecular structures composed of dipolar merocyanine dyes is reviewed, starting with the observation of antiparallel dimer aggregates of simple merocyanine dyes in 2000 and the observation of of well-defined nanorods based on bis(merocyanine) dyes in 2003. The influence of solvent polarity as well as steric effects on the hierarchical self-assembly process of these dyes is discussed. In the second part of this chapter literature examples for hydrogen bond-directed self-assembly of merocyanine dyes are given.

2.1 Dipolar Aggregation of Merocyanine Dyes

The work of Würthner and coworkers showed that highly polar merocyanine dyes form centrosymmetric dimer aggregates and that this dimerization arises predominantly from dipolar interactions of the two dye dipoles (Figure 1).[1] The exceptionally strong ground-state dipole moment found for merocyanine dye **1** ($\mu_g \approx 17$ D) was attributed to a major contribution of zwitterionic resonance structures as revealed by significant bond length equilibration within the conjugated path by single crystal X-ray crystallography and intense cyanine-type absorption spectra. High dimerization constants of $K_D > 10^6\ M^{-1}$ for dyes **1** could be determined by concentration-dependent UV–vis absorption measurements in low-polar solvents, as for example in dioxane or CCl_4.[1] The UV–vis spectra of dye **1a** ($R^1 = R^2 = n\text{-}C_{12}H_{25}$) in diluted dioxane solution shown exemplarily in Figure 2, can be ascribed to the monomeric dyes with the most intensive charge-transfer (CT) band occurring at longest wavelength (568 nm) and subsidiary vibronic maxima or shoulders at shorter wavelengths.[1] With increasing concentration, the intensity of the CT band is reduced and concomitantly a hypsochromically shifted new band owing to the excitonic coupling of the chromophores appears, revealing the aggregation of the dyes.[2] Over a considerable range of concentration, a well-defined isosbestic point occurs which is a clear indication for the presence of an equilibrium between two species, *i.e.*, monomers (M) and dimers (D).

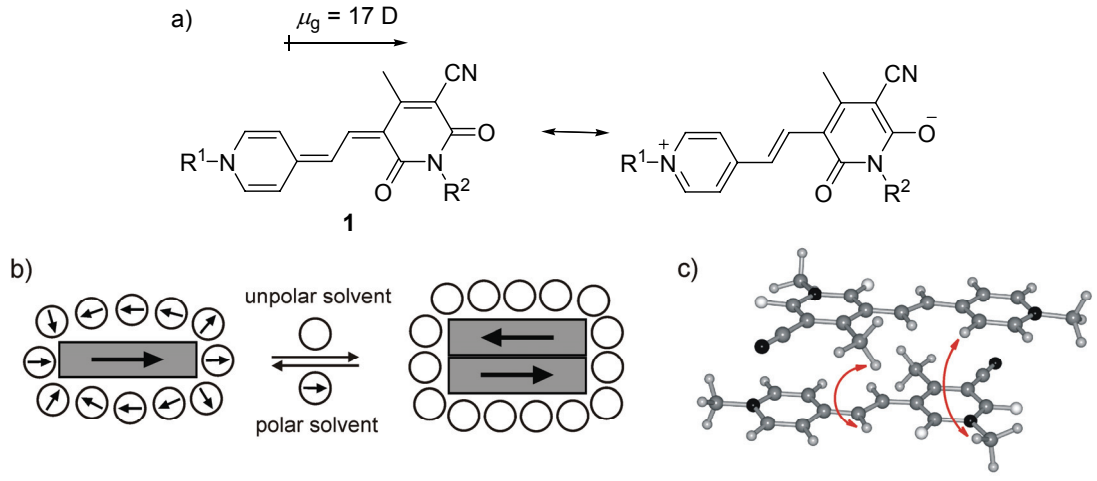

Figure 1. a) Resonance structures of highly dipolar merocyanine dyes **1** and b) formation of dimer aggregates in nonpolar solvents driven by dipole-dipole interactions and stabilization of the monomers by polar solvents. c) Structural model for the dimeric unit in solution based on NMR studies and AM1 geometry-optimized molecules. The curved arrows indicate spatial proximities as evidenced by ROESY NMR cross coupling peaks. All alkyl substituents were replaced by methyl for simplicity.[1]

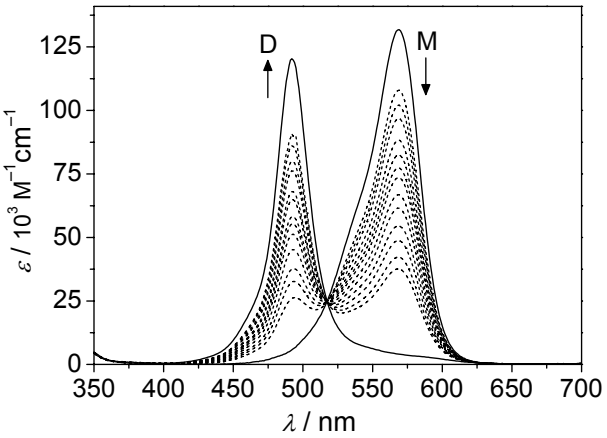

Figure 2. Concentration-dependent optical absorption spectra of dye **1a** ($R^1 = R^2 = n\text{-}C_{12}H_{25}$) in dioxane (- -). The arrows indicate the decrease of the intensity of the monomer band and the appearance of a dimer band with increasing concentration from 1.0×10^{-6} M to 3.0×10^{-5} M. The spectra of the monomer (–, M) and the dimer (–, D) were calculated from the data at two different concentrations and the binding constant.[1]

By analyzing these concentration-dependent UV–vis data with a simple dimerization model (eq. 1), where α_M denotes the fraction of dyes present as monomers and c_0 denotes the overall dye concentration, the dimerization constant K_D can be determined.[1]

$$\alpha_M = \frac{\sqrt{8K_D c_0 + 1} - 1}{4K_D c_0} \tag{1}$$

A simple electrostatic model with two contributions was found to account for the solvent dependent dimerization constants of dyes **1** (Figure 1b).[1] The first contribution is due to the electrostatic interaction of two interacting monomer dipole moments, which serve as driving force for dimerization. The magnitude of this interaction can be calculated from electrostatic theory within a dielectric with permittivity ε_r. The second contribution is due to the interaction of the monomer dipole moment with the solvent, which leads to stabilization of the monomers relative to the dimers. The dimers show a vanishing dipole moment and are, therefore, not stabilized by dipolar solvation. Both contributions are dependent on the permittivity of the solvent and lead to a shift of the equilibrium towards the dimers with decreasing solvent permittivity (Figure 3). Thus at a concentration of 10^{-5} M (as typically applied in UV–vis absorption spectroscopy) dye **1a** is dimerized to 55% in dioxane ($\varepsilon_r = 2.22$), 1% in chloroform ($\varepsilon_r = 4.81$), and 0.1% in tetrahydrofuran ($\varepsilon_r = 7.52$). At higher concentration of 10^{-2} M (as typically applied in NMR spectroscopy) the respective numbers are 98% (dioxane), 73% ($CHCl_3$), and 43% (THF). The centrosymmetric structure of these dimers was proved by ROESY NMR (Figure 1c) and also confirmed by X-ray analysis.[1] Even though these dimer

aggregates support an often proposed mechanism to explain unexpected low nonlinear optical susceptibilities in polymeric materials based on electric-field-poled dipolar dyes,[3] the dimerization was found to be a very promising supramolecular binding motif for the creation of functional structures due to its high binding strength and directionality.

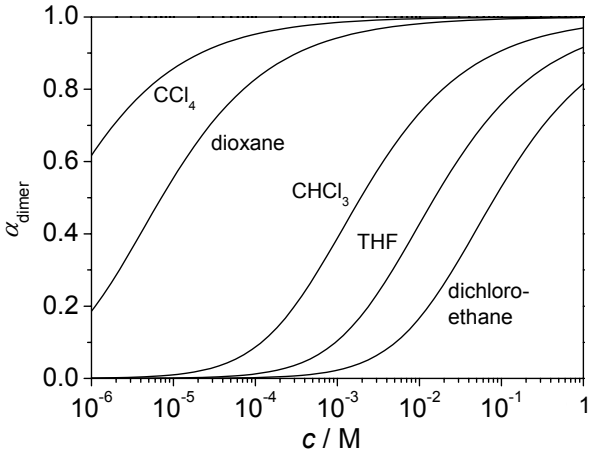

Figure 3. Fraction of dimerized dyes **1a** ($\alpha_{dimer} = 1-\alpha_M$) dependent on concentration calculated from the equilibrium constants for the dimerization at 20 °C in solvents of different polarity.[1]

2.2 Bis(merocyanine) Dye Nanorods

2.2.1 Hierarchical self-assembly

By utilizing this dipolar aggregation, the self-assembly of ditopic merocyanine building blocks **2** into highly defined cylindrical dye assemblies through supramolecular polymerization and hierarchical self-organization was achieved.[4] In dependence on the solvent polarity and the concentration, several levels of organization were observed (Figure 4). Pairing of the chromophoric units of the ditopic monomers (A) by dipolar aggregation leads to single-stranded supramolecular oligomers/polymers (B) (these species are formed by dimer aggregation, thus they are designated as D species). Further aggregation of these strands leads to rod-shaped dye assemblies (C). Based on structural data (AFM, TEM, and X-ray diffraction) and supported by optical spectroscopy, viscosity data, and molecular modeling, a structural model could be derived showing the dyes aggregated in helical fashion to give rod-shaped fibers where all alkyl groups of the tris(dodecyloxy)xylylene substituents point to the outside. Upon increasing concentration in non-polar solvents, the alkyl chains at the periphery entangle leading to gel formation and lyotropic mesophases (D).

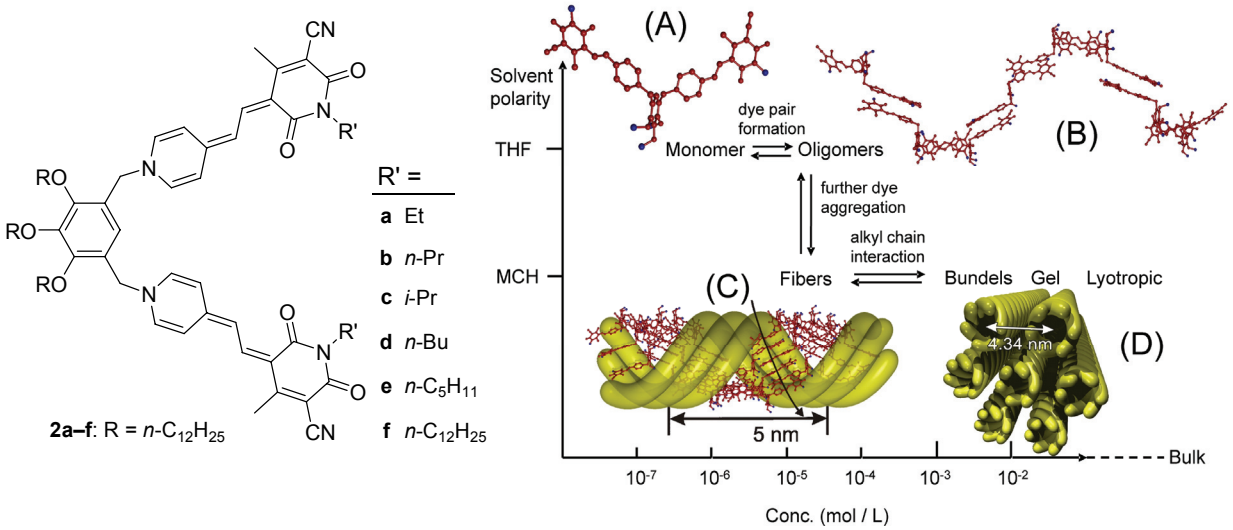

Figure 4. Structural models for the different levels of organization observed for bis(merocyanine) dye **2f** in dependence on the solvent polarity and the concentration. In MCH/THF mixtures all processes can be controlled in a reversible manner at ambient temperature. (A) Monomer structure according to MM+ force field calculations. For clarity, in the drawing all dodecyl substituents are replaced by methyl groups (marked in blue) and hydrogens are omitted. (B) Polymeric chain constituted by antiparallel pairing of merocyanine dyes, calculated by MM+ force field. (C) Tubular fiber consisting of H-aggregated dyes. The arrow around the fiber indicates the direction of H-aggregation. Note that the dodecyl chains attached to the xylylene spacer (blue) point outwards, and that for simplicity only one of the two possible helical aggregates is shown. (D) Hexagonal packing of the rods at a distance of 4.34 nm according to X-ray diffraction (also in this case only one helical conformation has been chosen tentatively). Figure taken from ref. 4b. Reproduced with permission from the *Journal of the American Chemical Society* **2004**, *126*, 8336–8348. Copyright 2004 American Chemical Society.

2.2.2 Solvent effect

The effect of the solvent polarity on the organization level is shown exemplarily for dye **2f** by UV–vis absorption spectra in solvents of different polarity at an identical concentration of 10^{-5} M (Figure 5).[4] Within the series of solvents of intermediate polarity, dichloromethane (CH_2Cl_2), THF, chloroform ($CHCl_3$) and trichloroethylene (TCE), a gradual transition from monomers to D species shows the oligomerization process by pairing of the chromophoric units as indicated by the decrease of the monomer band and the increase of the dimer band with decreasing solvent polarity. This behavior is explained in terms of the high polarity of CH_2Cl_2 ($\varepsilon_r = 8.93$) and THF ($\varepsilon_r = 7.52$) that enables a very good solvation of these strongly dipolar dyes (Figure 1). Accordingly, in these solvents the monomeric species is present predominantly. Upon decreasing the polarity of the solvent, here $CHCl_3$ ($\varepsilon_r = 4.81$) and TCE ($\varepsilon_r = 3.39$), the chromophores self-aggregate in an antiparallel fashion to form oligomeric single-stranded chains because these solvents cannot effect the solvation of the dipolar merocyanine chromophores. For the least polar solvents, tetrachloromethane (CCl_4) and

methylcyclohexane (MCH) the existence of the cylindrical dye assemblies is indicated by the band with a much more pronounced hypsochromic shift compared to the absorption of the monomeric dye and a very narrow bandwidth. This narrow and intense band is called as H-band and is due to excitonic coupling of the dyes to more than one closest neighbor dye. In the present case the monomers self-assemble into densely packed nanorods where all alkyl groups of the tris(dodecyloxy)xylylene group point to the outside and provide solubility in such solvents that completely lack a dipole moment like CCl_4 ($\varepsilon_r = 2.24$) and MCH ($\varepsilon_r = 2.02$). Notably, in such nonpolar solvents a monomeric dye with a dipole moment of 17 D would not dissolve at all.

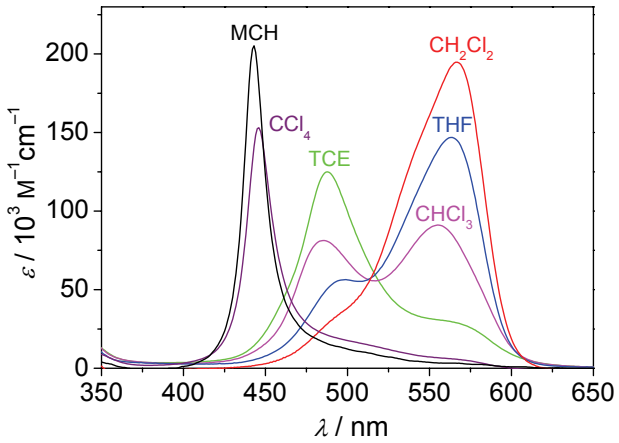

Figure 5. UV–vis absorption spectra of 10^{-5} M solutions of dye **2f** at 293 K in pure solvents of different polarity.[4]

2.2.3 Steric influence on structure and stability

By employing different alkyl substituents at the imide N atoms it was shown that even subtle structural changes at the periphery of the π-conjugated monomeric unit strongly influence the stability and structure of such aggregates.[5] The ability of monomers **2a**–**f** to self-assemble into nanorod aggregates in nonpolar THF/MCH = 1:9 mixtures was evidenced by the narrow and strongly blue-shifted UV–vis absorption bands at about 441 nm (Figure 6a). The nanorod aggregates formed from dodecyl-substituted monomers **2f** show a less blue-shifted aggregate band at 445 nm that was attributed to a more expanded packing induced by the long dodecyl chains at the imide N atoms. According to the structural model for the nanorod aggregates (Figure 4), half of the side chains at the imide N atoms point outward and the other half point inward the tubular fiber, revealing a significant effect of these long-chained alkyl substituents on the packing of the dyes. Furthermore, the influence of the side chains at the

imide N atoms on the stability of the nanorod aggregates was studied. UV–vis absorption spectroscopy in THF/MCH solvent mixtures with varying volume fractions of nonpolar MCH at a constant monomer concentration of 10^{-5} M allowed monitoring of the formation of nanorod aggregates with decreasing polarity of the solvent composition as shown for dye **2a** in Figure 6b. Upon raising the volume fraction of nonpolar MCH from 10 to 30%, the UV–vis absorption band at 441 nm (**H**) that corresponds to the nanorod species increases, while the absorption bands at 495 nm (**D**) and 562 nm (**M**) relating to oligomeric species and monomers, respectively, decrease.

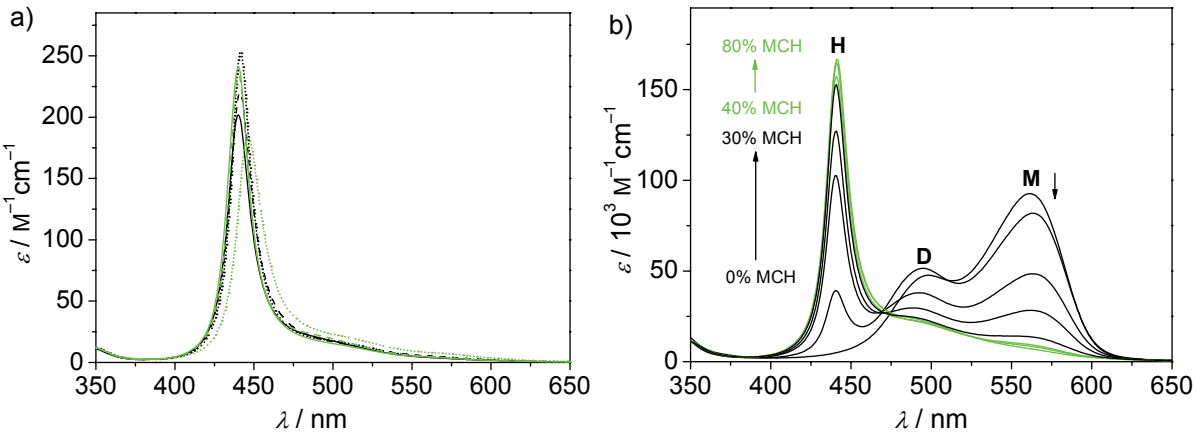

Figure 6. a) UV–vis absorption spectra of 10^{-5} M solutions of bis(merocyanine) dyes **4** in THF/MCH = 1:9 mixtures at 298 K after an equilibration period of 8 days: **2a** (black, —), **2b** (black, ---), **2c** (black, ···), **2d** (green, —), **2e** (green, ---), and **2f** (green, ···). b) UV–vis absorption spectra of 10^{-5} M solutions of dye **2a** in MCH/THF mixtures of different composition at 298 K.[5]

The transition from D- to H-aggregate species was found to take place in different solvent composition regimes depending on the substituents at the imide N atoms (Figure 7). The median (50%) value of the H-band absorbance, which corresponds to 50% of the monomers incorporated into nanorod aggregates, is in the range of only 13 vol% MCH for ethyl-substituted **2a**. Accordingly, nanorod formation occurs already in a pretty polar environment in case of **2a**. The *n*-propyl-, *n*-butyl-, and *n*-pentyl-substituted monomers **2b,d,e** require higher MCH contents of 20–25 vol% to reach the median value, whilst even higher MCH contents are required for isopropyl-substituted **2c** and dodecyl-substituted **2f** monomers with 30 and 40 vol% MCH, respectively. These results indicate that the thermodynamic stability of the nanorods is strongly influenced by the bulkiness of the respective substituents at the imide N atoms. Thus, the most stable nanorods are formed for monomers **2a** with small ethyl substituents, while increased chain length and branching of the substituents as in the case of **2c**

and **2f**, respectively, leads to decreased stability. This is reasonable in view of the compact packing of the dyes within the nanorod aggregates.

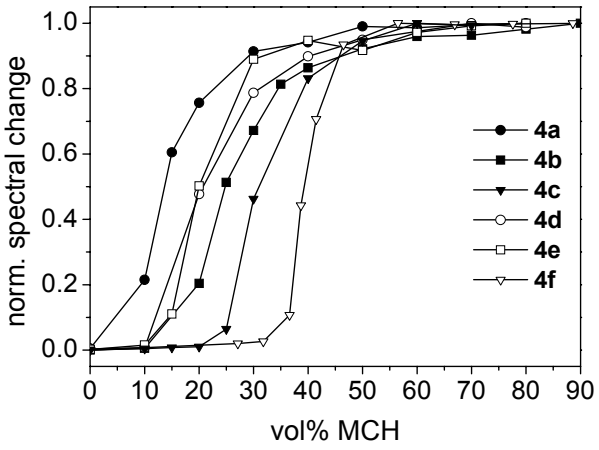

Figure 7. Change of normalized absorption at the maximum of the H-band depending on solvent composition showing the abrupt transition from D- to H-aggregates upon slight decrease of the solvent polarity.[5]

2.3 Hydrogen Bond-Directed Self-Assembly of Merocyanine Dyes

The following section will give an overview over hydrogen bond-directed self-assembly of merocyanine dyes in solution, at interfaces, and in the bulk. The merocyanine dyes applied in these studies mostly contain a barbituric acid group as the electron acceptor part of the dye that allows the formation of multiple hydrogen bonds between this group offering two ADA-arrays of hydrogen-bonding donor (D) and acceptor (A) sites, and additional building blocks bearing complementary DAD-type hydrogen-bonding arrays.

2.3.1 Self-Assembly in solution

Würthner and coworkers reported the complex formation between merocyanine dye **3** containing a barbituric acid acceptor group and a complementary Hamilton receptor-functionalized merocyanine dye **4** by 6-fold hydrogen bonding (Scheme 1).[6] From NMR titration experiments high association constants K_a of about $10^4\ M^{-1}$ in dioxane-d_8 and $>10^6\ M^{-1}$ in $CDCl_3$ were obtained. In this complex the merocyanine units are forced to adopt a head-to-tail arrangement, which leads to a summation of the ground state dipole moments of the respective merocyanine units and precludes dipolar aggregation of the merocyanine chromophores into antiparallel dimers with vanishing dipole moment as shown above. According to electrooptical absorption measurements it has been shown, that the increased

dipole moment of the head-to-tail complex **3·4** with respect to that of the individual components **3** and **4** leads to a higher degree of chromophore alignment in electric fields.

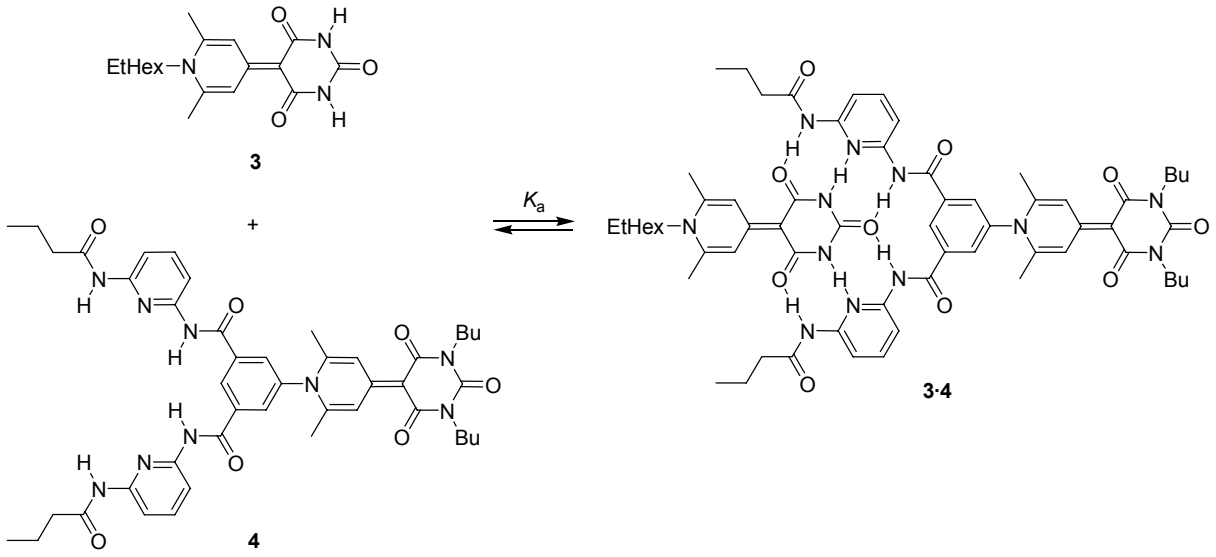

Scheme 1. Hydrogen bond-directed association of mercyanine dye **3** with the Hamilton receptor-functionalized merocyanine **4** (EtHex = 2-Ethylhexyl).[6]

The self-assembly of multichromophoric architectures consisting of three calixarene units **5**, each of them diametrically functionalized with triaminotriazine hydrogen receptor groups, and six merocyanine dyes **6** was reported by Prins *et al*. (Scheme 2).[7] These assemblies are hold together through cooperative formation of 36 hydrogen bonds and π–π interactions. Concentration-dependent UV/vis studies revealed a considerable high thermodynamic stability of these assemblies. For example, half of the assemblies formed from three equivalents **5a** and six equivalents **6** are present at an calixarene unit concentration of only 7.5×10^{-5} M in chloroform and 6×10^{-6} M in benzene, respectively. The merocyanine chromophores are arranged in two planes with each plane containing a cyclic array of three dyes. It was observed that the incorporated chromophores exhibit a hypsochromic shift in the UV–vis absorption maximum compared with that of the non-complexed chromophores. This complexation-induced spectral shift was attributed to excitonic coupling of the transition dipoles of the chromophores. Furthermore, the helicity of these assemblies could be controlled by the application of chiral calix[4]arene building blocks (*R*,*R*)-**5b** and (*S*,*S*)-**5c**, which induce a preferential *M*- or *P*-helical form of the complex, respectively. As a result of the excitonic coupling of the pairwise stacked chromophores in the assembly, strong bisignate CD effects were observed which show mirror-image relation for assemblies (*M*)-$\mathbf{5b}_3\cdot\mathbf{6}_6$ and (*P*)-$\mathbf{5c}_3\cdot\mathbf{6}_6$.

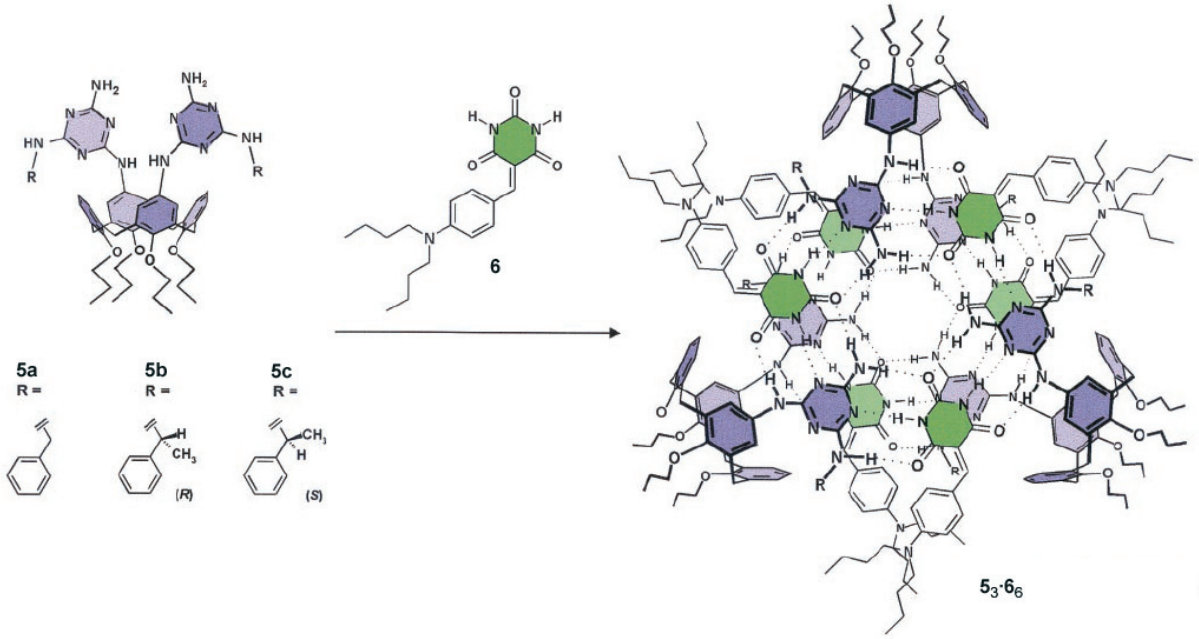

Scheme 2. Formation of a nine-component hydrogen-bonded assembly from calixarenes **5a**–**c** and barbiturate merocyanine **6**. Figure taken from ref. 12. Reproduced with permission from *Proceedings of the National Academy of Sciences of the United States of America* **2001**, *98*, 10042–10045. Copyright 2001 National Academy of Sciences, U.S.A.

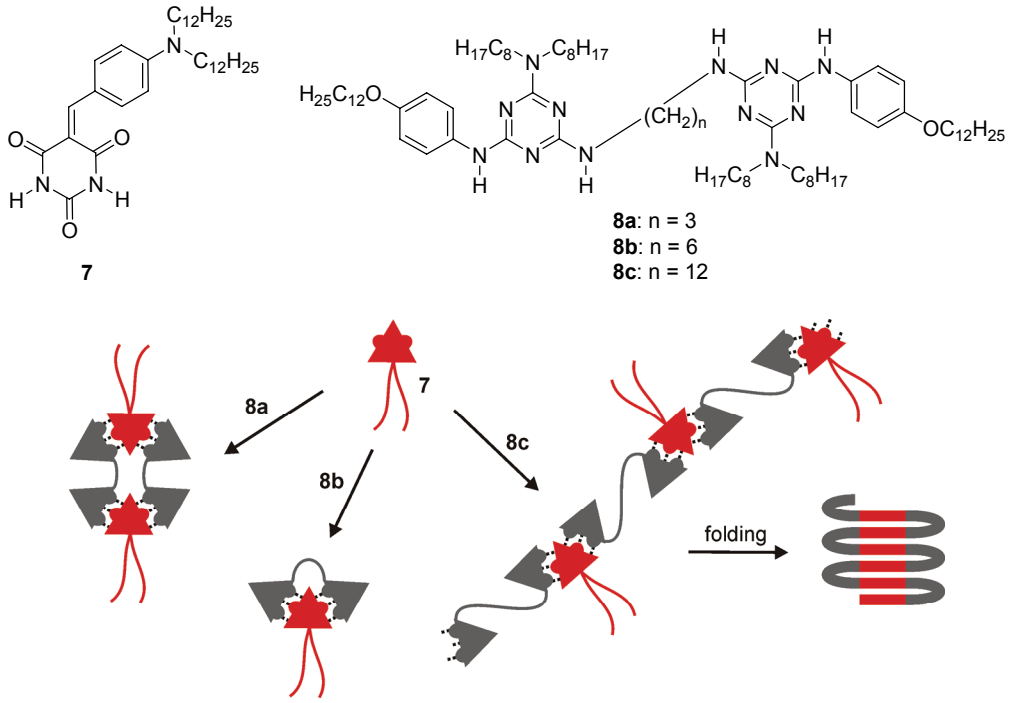

Figure 8. Structures of merocyanine **7** and bismelamine receptors **8a**–**c**, and schematical representation of their self-assembly into different complex geometries in dependence on the length of the alkyl-tether that connects the two melamine receptor units.[8]

Yagai and coworkers studied the complexation of a barbituric acid merocyanine dye **7** with a series of bismelamine hydrogen bond receptors **8a**–**c** in methylcyclohexane (Figure 8).[8] Depending on the length of the alkyl tether between the two melamine units different complex structures were obtained as schematical depicted in Figure 10. The various structures show different optical properties owing to the different arrangement and, thus, different excitonic coupling mode of the transition dipoles of the chromophores. Bismelamine **8b** containing a hexamethylene linker forms a simple 1+1 complex where both melamine units bind to the barbituric acid moiety of one merocyanine dye. In this case the UV–vis spectrum of the merocyanine chromophore is hardly affected by the complex formation. If bismelamine **8a** containing a shorter linker of only three methylene units was applied, a complex was formed which showed a strongly red-shifted absorption band and an increased fluorescence quantum yield with respect to the non-complexed dye. The authors suggested that these changes in the optical properties arise from J-type excitonic coupling of two chromophores in a cyclic oligomer where the spatial orientation of the chromophores is fixed in a head-to-head arrangement. On the other hand, if bismelamine **8c** equipped with a long dodecamethylene tether was combined with merocyanine **7**, supramolecular polymerization and folding of this polymer by stacking of the dye units was observed. The H-type coupling of the transition dipole moments of the chromophores in this stacked arrangement leads to a hypsochromically shifted absorption maximum of the polymer compared to that observed for the monomeric dyes. It was further reported that the polymer solution transforms into a gel-like viscoelastic material above a certain concentration in aliphatic solvents owing to the formation of an entangled fiber network.[9]

A further example for the formation of supramolecular polymers has been given by Würthner and coworkers.[10] In this study the self-assembly was achieved by a combination of hydrogen-bonding between melamine **9** and merocyanine dye **10** bearing a unsubstituted imide group, and dimer formation of this highly polar merocyanine chromophores by dipolar aggregation as revealed by UV–vis measurements. However, no significant increase of the viscosity of the solutions was observed and the authors conclude that these system forms rather weakly bound colloidal assemblies.[10]

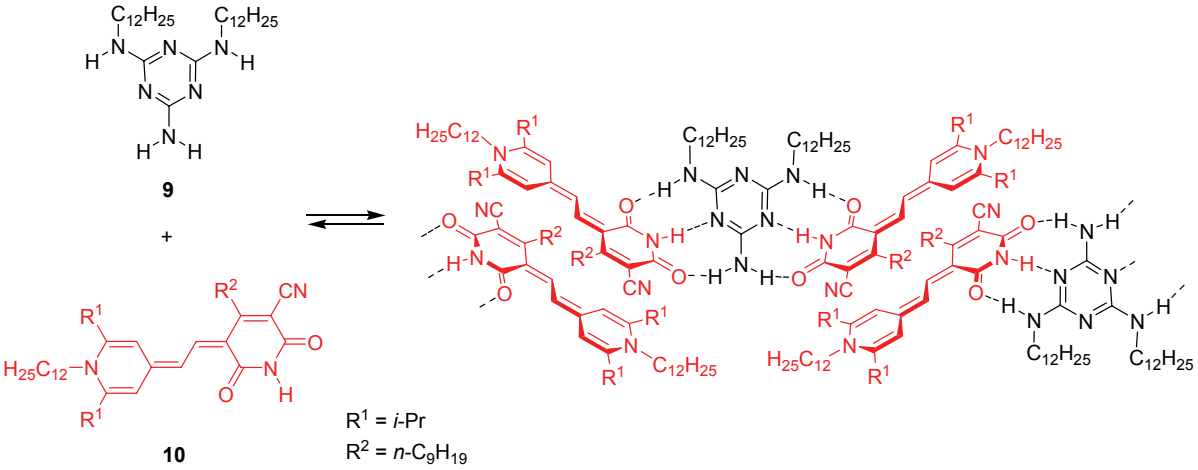

Scheme 3. Formation of a supramolecular polymer through dimerization of merocyanine dye **10** and triple hydrogen bonding to melamine **9**.[10]

2.3.3 Self-Assembly at interfaces

A two-dimensional self-assembled structure of a merocyanine dye at the liquid-solid interface was achieved by De Feyter *et al.* by heterocomplexation of barbituric acid merocyanine **11** with two triazine units **12** bearing long alkyl chains (Figure 9), and deposition of this complex from a 1-phenyloctane solution onto HOPG.[11] Scanning tunneling investigations showed that this complex forms a regular pattern at the surface and gave evidence for the termolecular nature of this heterocomplex from the observation of clusters consisting of three bright spots (Figure 9b). In addition, it was observed that all alkyl chains adopt an orientation on the surface which is nearly parallel to a main graphite symmetry axis.

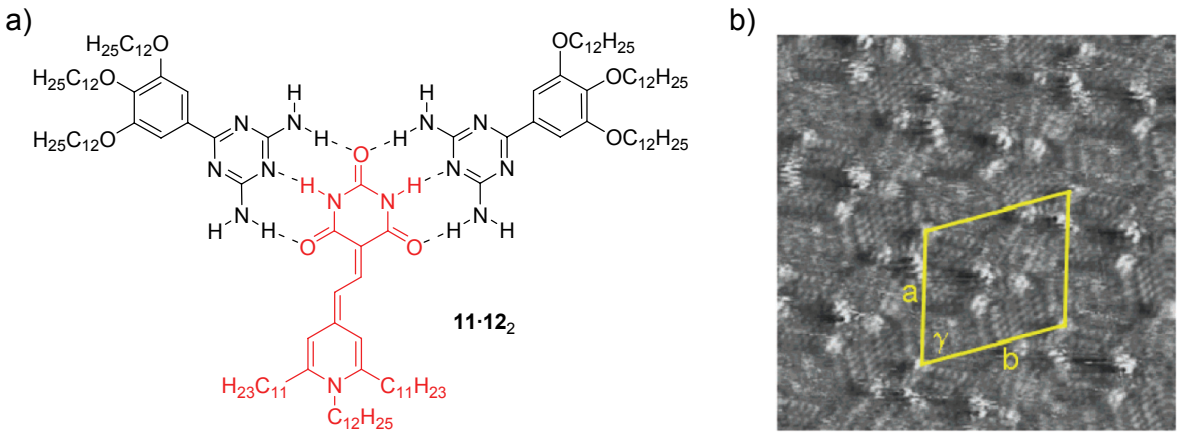

Figure 9. a) Structure of the heterocomplex formed from merocyanine dye **11** and triazine derivatives **12**. b) STM image of a monolayer of the heterocomplexes at the liquid–solid interface (image size: 11.5×11.5 nm^2). Figure 12b taken from ref. 12. Reproduced with permission from *Nano Letters* **2005**, *5*, 77–81. Copyright 2005 American Chemical Society.

In a paper in the early 90s, Ringsdorf and coworkers reported the formation of hydrogen-bonded molecular strands at the gas–water interface which consist of lipidic dioctadecyl-functionalized merocyanine dyes **13** and 2,4,6-triaminopyrimidine units (**14**).[12] As shown by measuring the surface pressure–surface area isotherms, Brewster angle microscopic studies, and UV–vis reflectivity measurements, the self-assembly proceeds *via* hydrogen bond-directed insertion of **14**, which was present in the aqueous subphase, into a monolayer of **13** that has been spread on the gas–water interface (Figure 10). However, a stable structure was obtained only at pH 3, while at higher pH a second process succeeded the formation of the molecular strands and led to hydrolysis of the dyes.

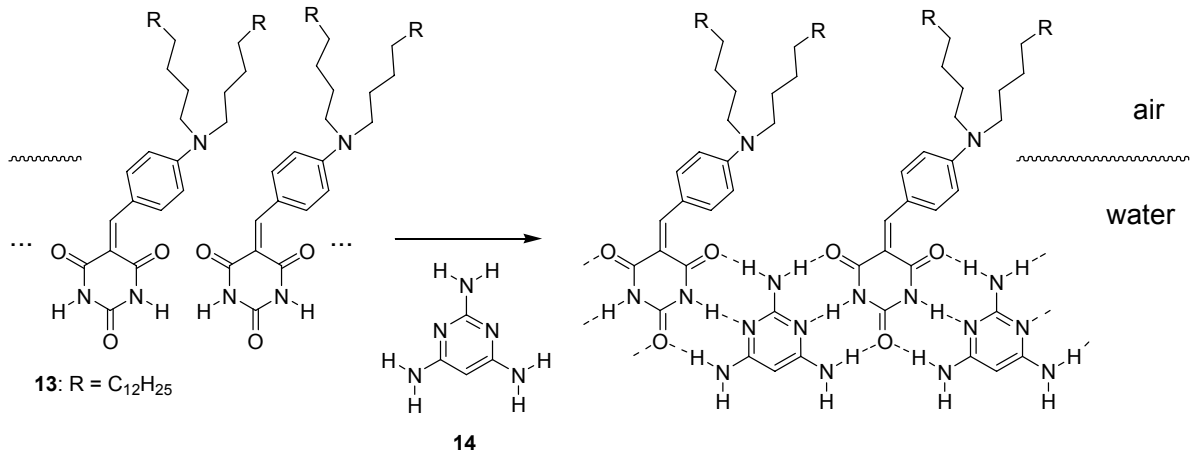

Figure 10. Schematic representation of the self-assembly of molecular strands from barbituric acid lipid **13** and triaminopyrimidine **14** at the gas-water interface by insertion of **14** from the subphase into a monolayer of **13**.[12]

2.3.4 Self-Assembly in the bulk

A similar supramolecular motif formed from barbiturate merocyanine dye **15** and melamine building block **16** was applied by Würthner *et al.* for the hydrogen bond-directed formation of liquid crystalline merocyanine dye assemblies (Figure 11).[13] In order to induce liquid crystalline properties to this assembly the melamine building block **16** was functionalized with two mesogenic tridodecyloxyphenyl units. According to optical polarising microscopic, differential scanning calorimetric and X-ray diffraction studies these assemblies form a columnar mesophase in the bulk where the hydrogen bonds and the aromatic cores are organized parallel to the column axes. The authors explained such a three-dimensional organization by a combination of triple hydrogen-bonding, dipolar π–π aggregation, and micro-segregation of the polar aromatic units and the nonpolar alkyl chains as shown schematically in Figure 11.

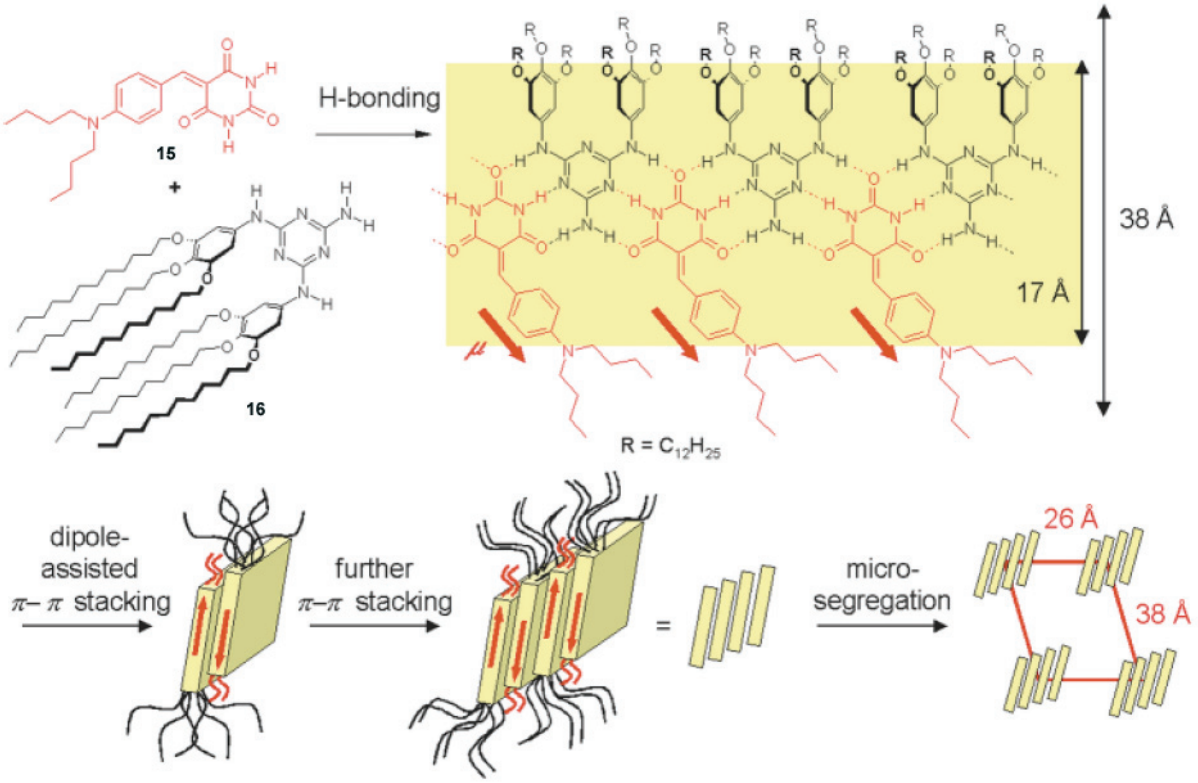

Figure 11. Formation of a columnar assembly from merocyanine **15** and melamine **16** involving hydrogen bond-directed growth of tapes and dipole-driven π–π stacking of these tapes to give ribbons, which finally assemble into a columnar structure by microsegregation and steric effects. The yellow shaded area represents the π-conjugated parts of the structures. Figure taken from ref. 13, *Chemical Communications* **2001**, 2260–2261 – Reproduced by permission of The Royal Society of Chemistry.

2.4 Conclusion

The high binding strength and directionality of dipolar aggregation of merocyanine dyes into antiparallel dimers enables the creation of defined nanorod structures, which were characterized by variety of methods. The studies on self-assembled merocyanine dye nanorods demonstrate that noncovalent synthesis of large assemblies requires well adjusted reaction conditions like those demanded in covalent organic synthesis. Solvent polarity and steric effects influence the level of organization, and the thermodynamic stability and structure. Therefore, a masterful optimization of the monomer structures with regard to the functional π-system and the lateral substituents, together with optimized conditions for preparation, is mandatory to obtain most stable assemblies. It has further been shown how multiple hydrogen bond formation between merocyanine dyes containing a barbituric acid acceptor group and properly designed complementary building blocks can lead to well-defined supramolecular architectures.

2.5 References

(1) (a) Würthner, F.; Yao, S. *Angew. Chem., Int. Ed.* **2000**, *39*, 1978–1981. (b) Würthner, F.; Yao, S.; Debaerdemaeker, T.; Wortmann, R. *J. Am. Chem. Soc.* **2002**, 124, 9431–9447.

(2) Kasha, M.; Rawls, H. R.; Ashraf El-Bayoumi M. *Pure Appl. Chem.* **1965**, *11*, 371–392.

(3) Würthner, F.; Wortmann, R.; Meerholz, K. *ChemPhysChem* **2002**, *3*, 17–31.

(4) Würthner, F.; Yao, S.; Beginn, U. *Angew. Chem., Int. Ed.* **2003**, *42*, 3247–3250. (b) Yao, S.; Beginn, U.; Gress, T.; Lysetska, M.; Würthner, F. *J. Am. Chem. Soc.* **2004**, *126*, 8336–8348.

(5) Lohr, A.; Gress, T.; Deppisch, M.; Knoll, M.; Würthner, F. *Synthesis* **2007**, 3073–3082.

(6) Würthner, F.; Schmidt, J.; Stolte, M.; Wortmann, R. *Angew. Chem., Int. Ed.* **2006**, *45*, 3842–3846. (b) Schmidt, J.; Schmidt, R.; Würthner, F. *J. Org. Chem.* **2008**, *in print*.

(7) Prins, L. J.; Thalacker, C.; Würthner, F.; Timmerman, P.; Reinhoudt, D. N. *Proc. Natl. Acad. Sci. USA* **2001**, *98*, 10042–10045.

(8) Yagai, S.; Higashi, M.; Karatsu, T.; Kitamura, A. *Chem. Commun.* **2006**, 1500–1502

(9) Yagai, S.; Higashi, M.; Karatsu, T.; Kitamura, A. *Chem. Mater.* **2005**, *17*, 4392–1398.

(10) Würthner, F.; Yao, S. *J. Org. Chem.* **2003**, *68*, 8943–8949.

(11) De Feyter, S.; Miura, A.; Yao, S.; Chen, Z.; Würthner, F.; Jonkheijm, P.; Schenning, A. P. H. J.; Meijer, E. W.; De Schryver, F. C. *Nano Lett.* **2005**, *5*, 77–81.

(12) (a) Ahuja, R.; Caruso, P.-L.; Möbius, D.; Paulus, W.; Ringsdorf. H.; Wildburg, G. *Angew. Chem., Int. Ed. Engl.* **1993**, *32*, 1033–1036. (b) Bohanon, T. M.; Denzinger, S.; Fink, R.; Paulus, W.; Ringsdorf, H.; Weck, M. *Angew. Chem., Int. Ed. Engl.* **1995**, *34*, 58–60. (c) Bohanon, T. M.; Caruso, P.-L.; Denzinger, S.; Fink, R.; Möbius, D.; Paulus, W.; Preece, J. A.; Ringsdorf, H.; Schollmeyer, D. *Langmuir* **1999**, *15*, 174–184.

(13) Würthner, F.; Yao, S.; Heise, B.; Tschierske, C. *Chem. Commun.* **2001**, 2260–2261.

Chapter 3

Self-Assembly of Bis(merocyanine) Tweezers into Discrete Bimolecular π-Stacks

Abstract: A novel class of tweezer molecules has been achieved through tethering of two dipolar merocyanine chromophores by a naphthalenedimethylene or dimethylenediphenylmethane spacer. The electrostatic interaction directed self-assembly of these bis(merocyanine) tweezers affords centrosymmetric bimolecular complexes with very high dimerization constants of up to $>10^9$ M^{-1}, even in the good solvating solvent chloroform. This pronounced self-association of bis(merocyanine) tweezers is attributed to the strong dipolar nature of the merocyanine chromophores and a unique aggregate geometry of four π-stacked chromophores with alternate arrangement of their dipole moments. The structural assignment of the tetrachromophoric π-stack has been accomplished by MALDI-TOF mass spectrometry and ROESY NMR spectroscopy. Furthermore, molecular modeling studies accounted for the relationship of dimerization constants and optical properties of the bimolecular complexes of the present bis(merocyanine) dyes with the structure of the spacer and position of attachment to the merocyanine chromophores.

3.1 Introduction

The construction of nanoscale supramolecular architectures by specially designed directed interactions offers tremendous potential in the area of nanotechnology. Thus, an impressive number of discrete, nanoscale assemblies have been constructed by modern methods of supramolecular chemistry employing a variety of weak interactions including metal-ion coordination, hydrogen bonding, and π–π interactions.[1,2] However, for the further development of such assemblies into molecular-level devices,[3] functional elements have to be incorporated which enable applications in supramolecular catalysis,[4] sensorics,[5] and molecular electronics.[6] The required functionality may be provided by chromophores with unique photophysical and electrochemical properties,[7] which enable optical or electrochemical addressing and readout in devices,[8,9] as well as serve as sensitizers[10] or light-harvesting antennae.[11]

There has been considerable interest in the self-assembly of merocyanine dyes,[12–15] a class of chromophores which is promising for nonlinear optical and photorefractive applications due to their outstanding dipolar and polarizability properties.[16,17] In the work of Würthner and coworkers, it has been shown that dipolar merocyanine dyes **1** form centrosymmetric dimer aggregates with high binding constants in nonpolar solvents such as dioxane or CCl_4 in the range of $K_D = 10^6\ M^{-1}$, and that this dimerization arises primarily from electrostatic interactions between these chromophores that can be traced back to the exceptionally large ground-state dipole moment μ_g of about 17 D for merocyanine dyes **1** (Figure 1a,b).[12a] This exceptionally large dipole moment is attributed to a major contribution of zwitterionic resonance structures as revealed by significant bond length equilibration within the conjugated path explored by single crystal X-ray analysis and intense cyanine-type absorption spectra.[12]

As the structure of these dimer aggregates is well-defined, the dipolar interactions of merocyanines are highly directional and, therefore, promising for the construction of more elaborate supramolecular architectures in which both, the binding interaction and functionality are provided by the chromophores. Indeed, highly defined supramolecular polymers could be recently obtained by dipolar aggregation of ditopic bis(merocyanine) monomers.[13] However, no programmed aggregation of merocyanine dyes into well-defined discrete aggregates beyond simple dimers has been reported to date.[18]

Therefore, we have taken inspiration from a class of compounds generally referred to as molecular tweezers or clips that contain two aromatic chromophores covalently linked by a single spacer unit. Such molecular hosts are able to complex aromatic guest molecules between

their two π-surfaces, which converge on the two divergent π-faces of the guest, thus forming a sandwich complex held together by two π-stacking interactions (Figure 1c).[19,20] In organic solvents, a favorable host–guest interaction between the molecular tweezers and the guest molecules occurs only if one partner is a π-donor and the other one is a π-acceptor, or *vice versa*. Such host–guest complexes are generally weak with association constants ranging from 0.1–1000 M^{-1} and are believed to be held together by electrostatic, polarization, dispersion, and charge-transfer forces. In contrast to the vast number of studies on such tweezer-based host-guest systems, there are only few reports on self-association of such host molecules (tweezers) in solution which is obviously a possible competition process for the complexation of aromatic guests (Figure 1d).[21–23] However, in most cases the self-association constants are such low that the guest complexation is not significantly effected. Stronger self-association occurrs mainly in aqueous media owing to the hydrophobic effect, or if additional noncovalent interactions such as hydrogen bonding are involved. The weak self-association of common tweezer systems in organic solvents is reasonable since favorable dispersion interactions from the van-der-Waals contact between the π-walls are often sterically prevented by the spacers and, more importantly, the electron donor–acceptor (EDA) forces responsible for strong complexation of electron-deficient guests are very weak between the mostly electron-rich π-walls of the tweezers (Figure 1d). Accordingly, more favorable EDA interactions can be

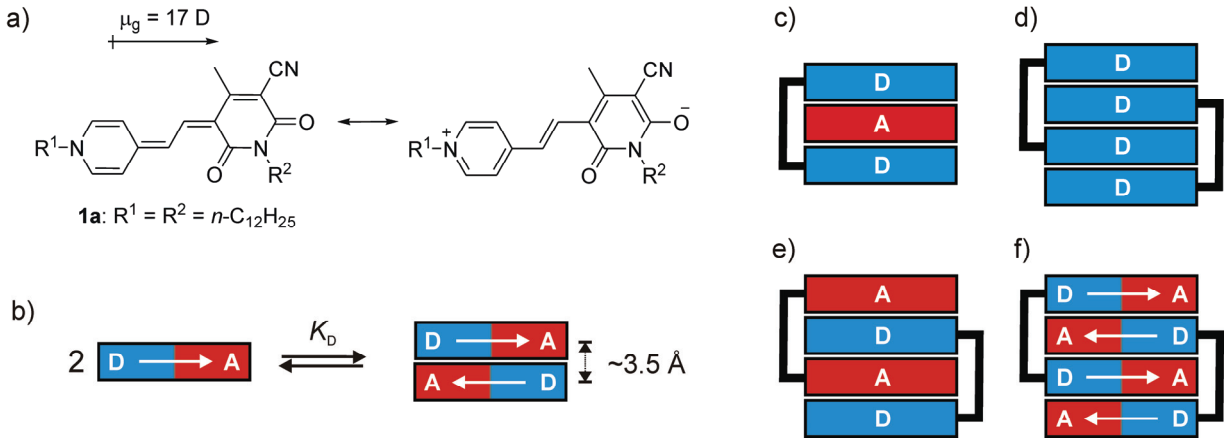

Figure 1. a) Resonance structures of highly dipolar merocyanine dyes **1** and schematic representations for b) the formation of merocyanine dimer aggregates by dipole-dipole interactions, c) a π-stack formed from a tweezer with electron-rich chromophores and an electron-deficient guest as host–guest complex (it can also be *vice versa*), d) a dimer of molecular tweezers with electron-rich chromophores, e) a heterodimer of an electron-rich and electron-deficient building block, and f) the concept for a bimolecular aggregate of dipolar bis(merocyanine) tweezers.

achieved in the case of heteroaggregates of electron-rich and electron-deficient building blocks (Figure 1e), where the alternately stacking of donor and acceptor groups allows for multiple EDA interactions.[24] Now, if such a concept is extended to tweezers of highly dipolar merocyanine dyes, we can expect the formation of bimolecular complexes of high thermodynamic stability (Figure 1f).

According to this concept, bis(merocyanine) dyes equipped with a spacer allowing an interplanar distance between chromophores of twice the distance observed for a simple merocyanine dimer of **1** (Figure 1b) should facilitate self-association into a sandwich-type bimolecular complex of four merocyanine chromophore units (Figure 1f). Under the premise that there are no sterical constraints for a π-stacked arrangement, such dimeric aggregates should be thermodynamically most favorable as they facilitate multiple and cooperative dipolar interactions. The closest interplanar distance of the dyes **1** in crystal structures was determined to be 3.2–3.5 Å, which approaches the smallest possible van-der-Waals distance between two π-systems.[12b] Thus, an appropriate tether for enabling a tight sandwich-like packing of the chromophores should provide an interplanar distance of the two chromophores in the range of 7 Å. Molecular building blocks that possess these desired structural specifications are well known from supramolecular hosts that are capable of complexing extended π-systems, and the special importance of the host geometry on the complexation properties has been discussed.[25,26] Based on literature examples and preliminary molecular modeling studies, we chose 2,7-naphthalenedimethylene and 4,4′-dimethylenediphenylmethane spacers to design bis(merocyanine) tweezers for our present study (Chart 1). The former spacer was found to be the best suited candidate to promote efficient packing, while the latter one provides a slightly larger distance between the two chromophore planes. Notably, the merocyanine chromophore of type **1** offers two positions for the attachment of the spacer, *i.e.*, via the pyridine donor group N atom or the imide N atom. On the basis of the above-mentioned considerations, we have synthesized the naphthalenedimethylene- and dimethylenediphenylmethane-tethered bis(merocyanine) dye tweezers **2**, **3** and **4**, **5** (Chart 1) and investigated in detail their self-association properties. Here we report that these properly designed tweezers indeed self-assemble into discrete bimolecular complexes, a novel class of strongly bound π-stacks which is so far unprecedented.

Chart 1. Chemical Structures of Bis(merocyanine) Dye Tweezers **2**–**5**.

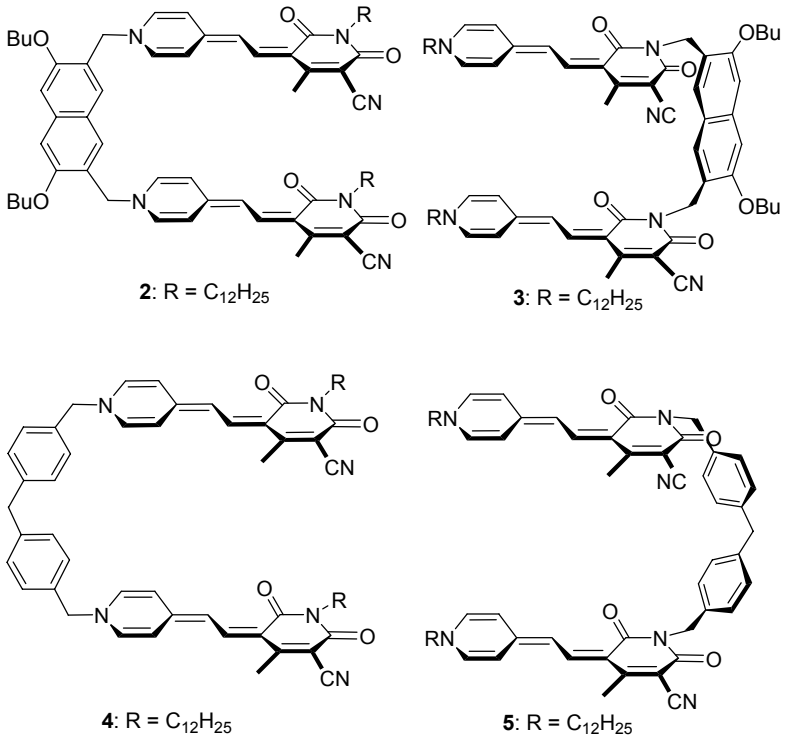

3.2 Results and Discussion

3.2.1 Synthesis of bis(merocyanine) tweezers

The bis(merocyanine) dyes **2**–**5** were synthesized according to Scheme 1. The detailed procedures and product characterization data are given in the Experimental Section. The spacer precursor naphthalene dicarbaldehyde **6** was prepared in 3 steps according to literature procedures starting with commercially available 2,7-naphthalenediol.[27] Alkylation of **6** with butyl bromide gave dialdehyde **7** in 43% yield. The synthesis of bis(pyridinium) salt **9** was achieved by reduction of dialdehyde **7** with $NaBH_4$ into diol **8**, followed by tosylation and substitution with 4-methylpyridine, and isolated as tetrafluoroborate in 79% yield. For the synthesis of bis(pyridone) **12**, dialdehyde **7** was converted into Cbz-protected diamine **10** by reductive amination with benzyl carbamate in 70% yield.[28] After deprotection by catalytic hydrogenation, the free amine intermediate was reacted with ethyl cyanoacetate to afford bis(cyanoacetamide) **11** in 66% yield. Condensation of **11** with ethyl acetoacetate gave bis(pyridone) **12** in 72% yield and the reaction of **12** with DMF and salt **13**[29] afforded the bis(merocyanine) dye **3** in 10% yield. Bis(merocyanine) dye **2** was obtained by the reaction of pyridone **16** with *N,N′*-diphenylformamidine (DPFA) and salt **9** in 28% yield.

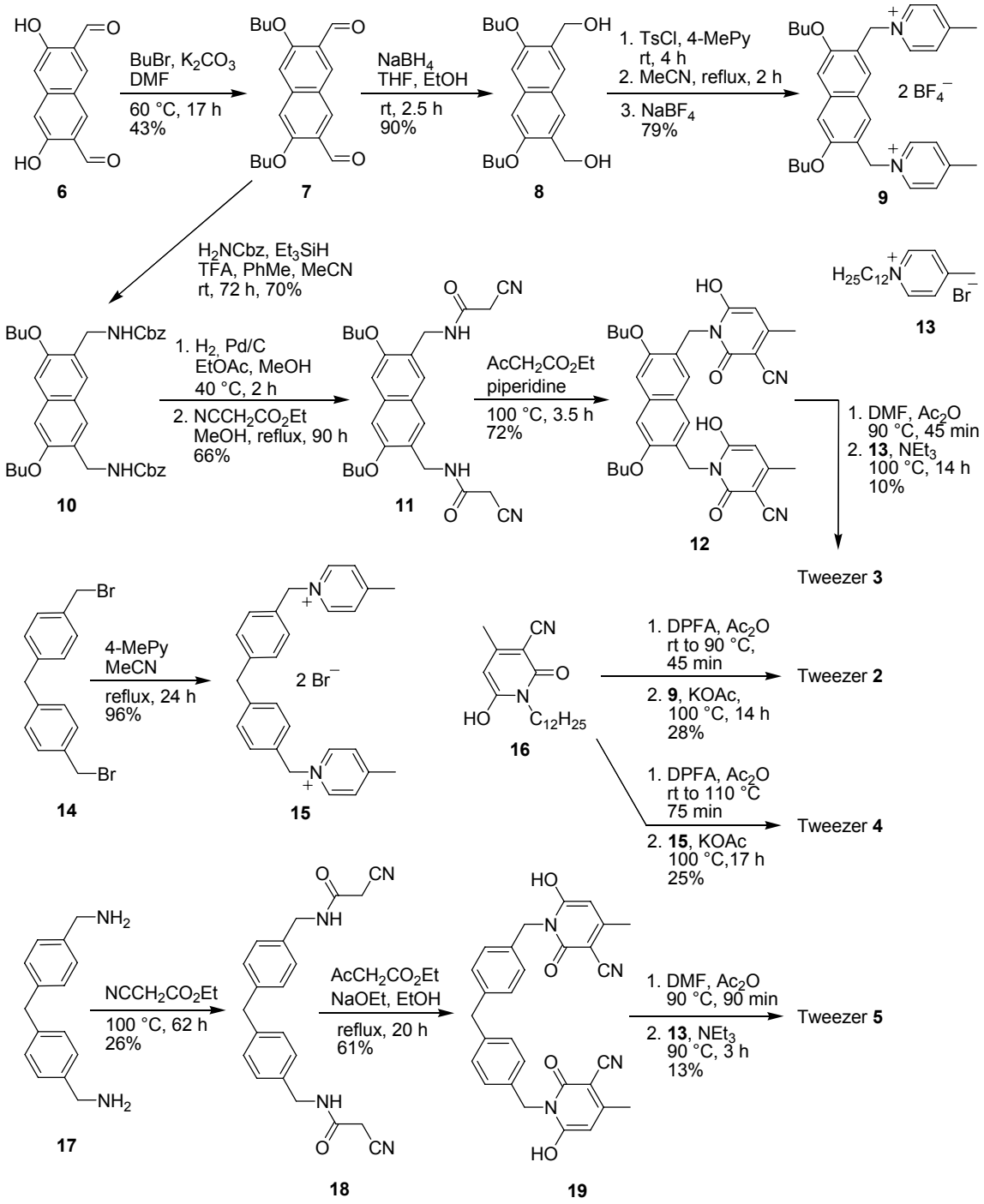

Scheme 1. Synthesis of bis(merocyanine) dyes **2**–**5**. For the structures of tweezers **2**–**5** see Chart 1.

Dibromide **14**, which was prepared from diphenylmethane according to literature procedure, was converted into dipyridinium salt **15** by nucleophilic substitution with 4-picoline in 96% yield.[30] Diamine **17** was obtained from dibromide **14** in two steps according to literature.[31] Amidation of **17** with ethyl cyanoacetate afforded diamide **18** in 26% yield, which was condensed with ethyl acetoacetate to produce bis(pyridone) **19** in 61% yield. Bis(merocyanine)

dyes **4** and **5** were obtained in 25% and 13% yield, respectively, by the reaction of either pyridone **16**[12b] with DPFA or **19** with DMF and subsequent reaction with salts **15** and **13**[29], respectively.

3.2.2 Mass spectrometric studies

First evidence for the self-assembly of the present bis(merocyanine) tweezers into bimolecular complexes was obtained by mass spectrometry.[32] Samples for MALDI-TOF mass spectroscopy were prepared by solvent evaporation from chloroform solutions of **2**–**5** containing 2-[(2*E*)-3-(4-*tert*-butylphenyl)-2-methylprop-2-enylidene]malononitrile (DCTB) as matrix. The spectra recorded in positive ion mode display peaks that correspond to the respective singly charged dimer cations ($[M_2]^+$), along with the signals for singly charged monomer cations (Figure 2 and Table 1). The measured isotope patterns of the aggregate signals match very well the calculated natural abundances, thus confirming the elemental composition and the dimeric nature of the aggregates in the gas phase. The observation of the respective dimer signals in the mass spectra corroborates the formation of discrete bimolecular complexes in solution and partial fragmentation in the gas phase.

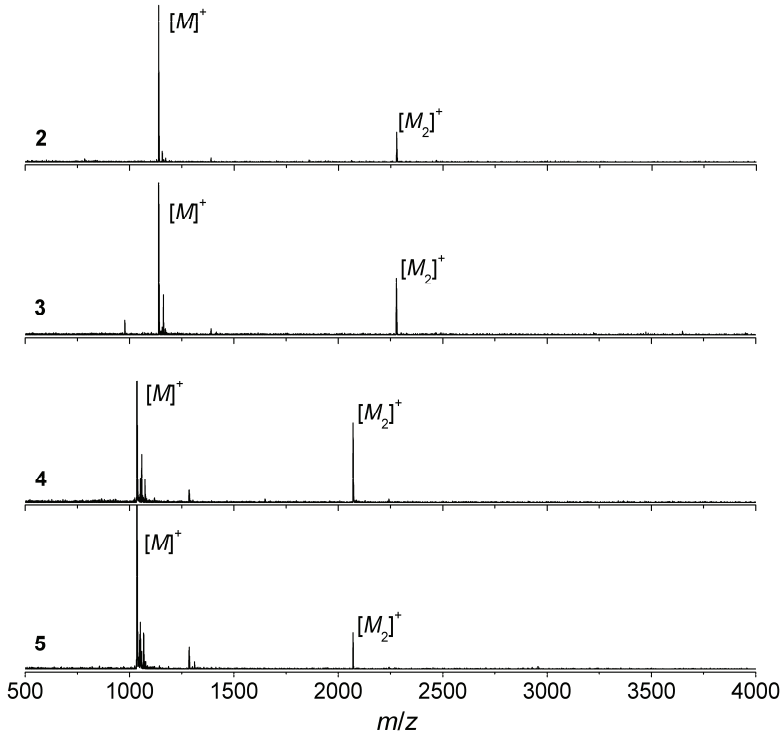

Figure 2. MALDI-TOF spectra of bis(merocyanine) dyes **2**–**5**. The peaks corresponding to singly charged monomer and dimer cations are marked with $[M]^+$ and $[M_2]^+$, respectively.

Table 1. Monoisotopic mass peaks observed in MALDI-TOF MS spectra of bis(merocyanine) dyes that correspond to bimolecular aggregates.

dye	calculated *m*/*z* (ion)	found *m*/*z*
2	2277.447 ($[M_2]^+$)	2277.431
3	2277.447 ($[M_2]^+$)	2277.430
4	2069.279 ($[M_2]^+$)	2069.301
5	2069.279 ($[M_2]^+$)	2069.274

3.2.3 Aggregation studies by UV–vis spectroscopy

UV–vis dilution experiments have been extensively utilized to study dye aggregation in solution. By this method, electronic interactions between the π-conjugated systems of dyes may be elucidated and the concentration range for aggregate formation can be easily assessed. For simple processes such as dimerization or polymerization, binding constants and Gibbs binding enthalpies may be obtained from such experiments.[33] In addition, structural information can be obtained from the splitting of the absorption band due to excitonic coupling of the transition dipole moments of the chromophores.[34] Thus, we have performed UV–vis dilution studies for bis(merocyanine) dyes **2**–**5** as well as for the reference dye **1a**. Since the dipolar interactions between merocyanine dyes are strongly dependent on solvent polarity, the dilution experiments were performed in chloroform, which is a solvent of intermediate polarity and was found to be best suited for studying the aggregation equilibria of the present series of bis(merocyanine) dyes in the concentration range suitable for UV–vis absorption spectroscopy.

Significant spectral changes were observed for dyes **2**–**5** and **1a** upon variation of the concentration in the range from 1×10^{-7} to 1.4×10^{-3} M using cells with path length of between 0.01 and 5 cm (Figure 3). For the reference dye **1a**, the UV–vis spectra in dilute solution can be ascribed to the monomers with an intensive charge-transfer band occurring at longest wavelength (denoted as M).[12] With increasing concentration, the intensity of the monomer band is reduced with the concomitant appearance of a hypsochromically shifted band (denoted as D) owing to excitonic coupling of the two chromophores in the formed dimer unit (Figure 3a). A second excitonic band observed at longer wavelength (~560 nm) is indicative for a slightly twisted arrangement of the two chromophores in the aggregate.[12c,35] The spectral changes observed for the bis(merocyanine) dyes are similar to those observed for **1a**, revealing an intense hypsochromically shifted absorption band and less intense absorption band at longer wavelength (a more detailed discussion of the bis(merocyanine) dye spectra is provided later).

Thus, they can be attributed to an equilibrium between two species, *i.e.* the monomers and the bimolecular complexes. Whilst both species are clearly identified in the concentration-dependent spectra of bis(merocyanine) dyes **2**, **4**, and **5**, only little dissociation of the

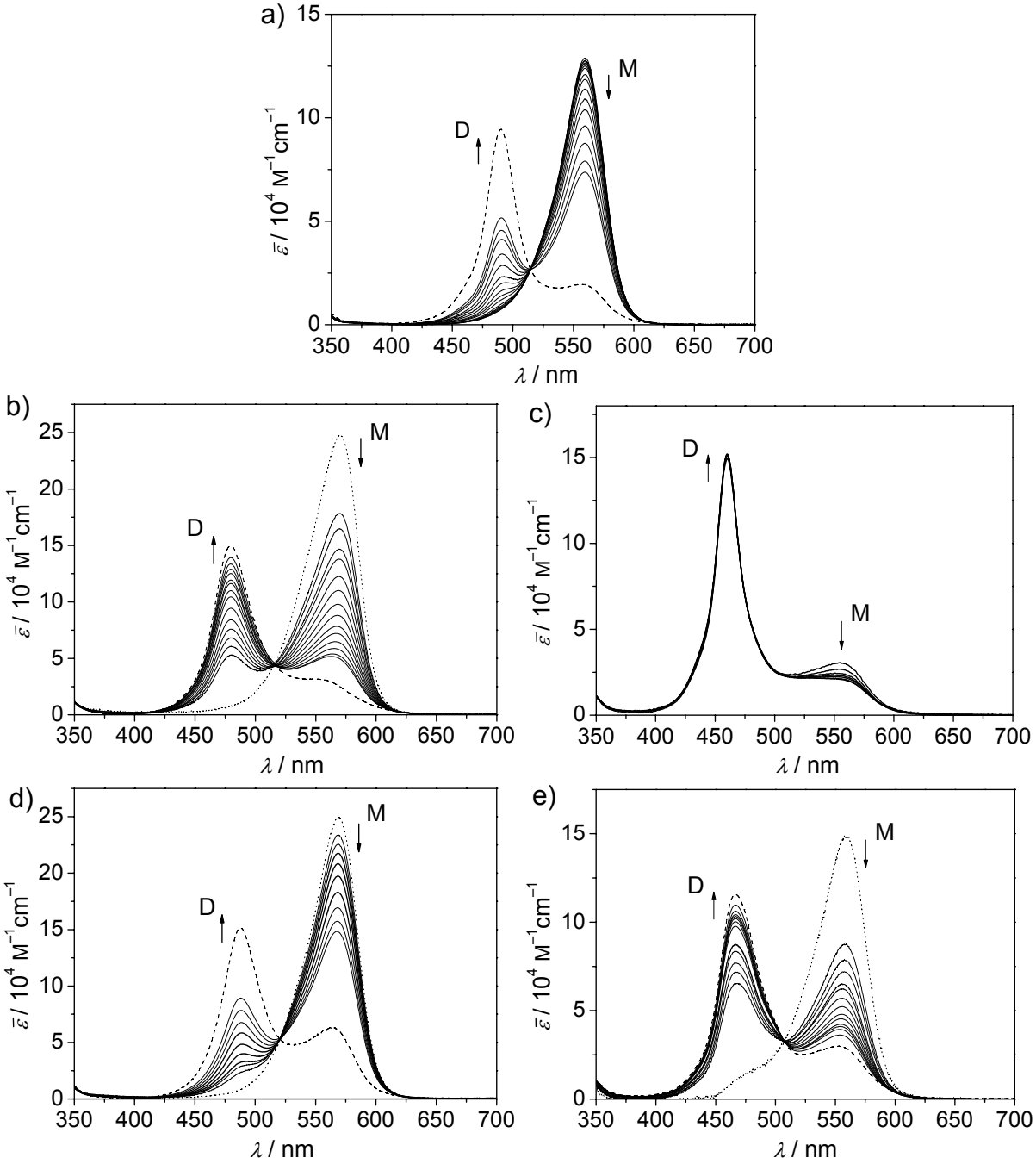

Figure 3. Concentration-dependent UV–vis spectra in $CHCl_3$ at 298 K. The arrows indicate the decrease in the intensity of the monomer band (denoted as M) and the appearance of a dimer band (denoted as D) with increasing concentration. The spectra of the monomer (···) and the dimer (---) were calculated from the data at two different concentrations and the binding constants. a) **1a** (c =1.4×10^{-3} to 4.5×10^{-6} M); b) **2** (c = 1×10^{-4} to 7×10^{-7} M); c) **3** (c = 1×10^{-4} to 1×10^{-7} M); d) **4** (c = 2×10^{-5} to 1×10^{-6} M); e) **5** (c =5×10^{-5} to 4.5×10^{-7} M).

aggregates of **3** into monomers was observed in $CHCl_3$ down to a concentration of 10^{-7} M, revealing a very strong aggregation for dye **3** (Figure 3c). However, in 1,2-dichloroethane (DCE), a solvent of higher dielectric permittivity but similar refractive index, the dissociation of the aggregates into monomers could be observed in the applicable concentration regime (see Figure A1).[36]

Over a considerable range of concentration, well-defined isosbestic points occur, which clearly indicate the presence of an equilibrium between two species, *i.e.*, monomer (M) and dimer (D) species. In this case a simple dimerization model according to the equation

$$K_D = \frac{c_D}{c_M^2} = \frac{1-\alpha_M}{2\alpha_M^2 c_0} \tag{1}$$

can be applied, where K_D denotes the dimerization constant, c_M and c_D are the concentrations of monomer and dimer, respectively, c_0 is the total dye concentration, and α_M (= c_M/c_0) is the fraction of the monomeric dye in solution.[12b] By solving eq 1, we obtain:

$$\alpha_M = \frac{\sqrt{8K_D c_0 + 1} - 1}{4K_D c_0} \tag{2}$$

The apparent molar absorptivity $\bar{\varepsilon}$ of the dye in solution may be expressed as

$$\bar{\varepsilon} = \alpha_M \varepsilon_M + (1-\alpha_M)\varepsilon_D \tag{3}$$

where ε_M and ε_D are the molar absorptivities of a free and dimer-bound monomeric unit, respectively.

Combining eqs 2 and 3, we obtain eq 4:

$$\bar{\varepsilon} = \frac{\sqrt{8K_D c_0 + 1} - 1}{4K_D c_0}(\varepsilon_M - \varepsilon_D) + \varepsilon_D \tag{4}$$

Nonlinear regression analysis of the apparent molar absorptivity of the dyes as a function of total monomer concentration c_0 at certain wavelengths based on eq 4 provides the dimerization constants and related Gibbs dimerization energies,

$$\Delta_D G^\circ = -RT \ln K_D \tag{5}$$

in $CHCl_3$ and DCE (for **3**) which are collected in Table 2. Figure 4 shows the fraction of monomer (α_M) calculated from the UV–vis data at certain wavelength in dependence of

concentration, as well as the resulting dimerization isotherms of the nonlinear regression analysis.

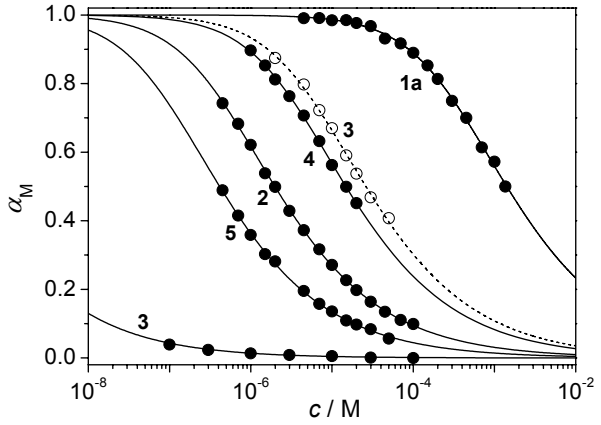

Figure 4. Fraction of monomer (α_M) calculated from UV–vis data at certain wavelength and results of the nonlinear regression analysis based on the dimerization model for dyes **3** (555 nm), **5** (555 nm), **2** (570 nm), **4** (485 nm), and **1a** (505 nm) in $CHCl_3$ (● and solid lines), and **3** (450 nm) in DCE (○ and dashed lines).

Table 2. Dimerization constants K_D and corresponding Standard Gibbs Free Dimerization Energies $\Delta_D G°$ from analysis based on the dimerization model,[a] and Absorption Maxima of reference dye **1a** and bis(merocyanine) dyes **2**–**5** from UV–vis dilution studies at 298 K.

dye	solvent	$-\Delta_D G°$ ($kJmol^{-1}$)	K_D (M^{-1})	EM[b] (M)	λ_M (nm)	λ_{D1} (nm)	λ_{D2} (nm)	$\Delta\tilde{\nu}_{D1-M}$ (cm^{-1})	$\Delta\tilde{\nu}_{D1-D2}$ (cm^{-1})
1a	$CHCl_3$	15.8	590		559	490	559	2520	2520
4	$CHCl_3$	27.3	6.2×10^4	1.1×10^{-2}	569	488	564	2917	2760
2	$CHCl_3$	32.3	4.5×10^5	8.1×10^{-2}	570	479	554	3333	2830
5	$CHCl_3$	36.1	2.1×10^6	0.38	558	466	553	3538	3376
3	$CHCl_3$	>50	$>10^9$	>180	555	460	554	3721	3688
1a	DCE	6.1	12		548	492	561	2077	2500
3	DCE	26.3	4.1×10^4	7.4×10^{-3}	539	464	520	2999	2321

[a]Average from nonlinear regression analysis at four to six different wavelengths of the monomer and aggregate absorption band. [b] Effective molarity calculated according to eq 6 assuming $K_D = 590\ M^{-1}$.

Dyes **4** and **2** that are tethered at the N atoms of the pyridine donor groups show dimerization constants of $K_D = 6.2\times10^4\ M^{-1}$ and $4.5\times10^5\ M^{-1}$, respectively, while dyes **5** and **3** that are tethered at the imide N atoms show considerably higher dimerization constants of $K_D = 2.1\times10^6\ M^{-1}$ and $>10^9\ M^{-1}$, respectively (Figure 4 and Table 2). The last value was approximated because only little dissociation was observed in the applicable concentration regime down to 10^{-7} M that precludes an exact determination. These values are about two to

six orders of magnitude higher than the value obtained for the reference dye **1a** and the corresponding Gibbs energies of dimerization $\Delta_D G°$ are about two- to fourfold higher than that of **1a**. This strong increase of the binding strength for bis(merocyanine) dyes **2**–**5** with respect to that of **1a** can be attributed to multiple interactions made possible by tethering the chromophores in the bis(merocyanines). These data further show that the position for the attachment of the spacers to the chromophores as well as the structure of the spacer have strong influence on the dimerization constants. Thus, tethering of the chromophores at the imide N atoms allows for stronger dimerization of the respective bis(merocyanine) dyes with respect to tethering at the N donor atom, and the 2,7-naphthalenedimethylene spacer provides higher binding constants than the 4,4′-dimethylenediphenylmethane spacer. These relations can be ascribed to varying spatial restrictions imposed upon the aggregate structure by the type of the spacer and position of tethering. Unfortunately, the determination of the enthalpic and entropic contribution, $\Delta H°$ and $\Delta S°$, to the Gibbs energy of dimerization $\Delta_D G°$ by means of a van't Hoff plot was not successful owing to the strong dependence of ε_r of chloroform on the temperature.[37]

It is important to note that the formation of linear oligomers by dimerization of the chromophores can be ruled out for all bis(merocyanine) dyes studied here, since the analysis of the UV–vis dilution data based on the isodesmic model[33] gave only poor fits. Also, the high aggregation constants obtained from the analysis based on the isodesmic model cannot be explained by the simple dimerization of two chromophores to form linear oligomers. Theoretically, however, above a certain overall monomer concentration known as the effective molarity *EM*, the formation of linear chains will be favored over cyclic aggregates.[38] The effective molarity for the formation of a macrocyclic aggregate consisting of *i* molecules can be calculated according to

$$EM = K_i / (\sigma K)^i \tag{6}$$

where K_i denotes the aggregation constant of the cyclic assembly, σ is a symmetry number (4 in the present cases), and K denotes the dimerization constant of the respective monotopic dye. The effective molarities for the present dimerization process in chloroform was calculated assuming K to equal $590\ M^{-1}$, which is the dimerization constant for reference dye **1a** (Table 2).[38] Since the obtained *EM* values are well above the concentration regime under

consideration in the performed dilution studies, the formation of linear chains can be excluded for the aggregation of the bis(merocyanine) dyes studied here.[39]

As noted before, the spectral changes caused by aggregation of dyes can provide information on their aggregate structure. Thus, the absorption spectra of the monomers and the bimolecular complexes of the present series of bis(merocyanine) dyes were derived from the spectra at two different concentrations and the dimerization constant according to eq 4 (dashed and dotted spectra in Figures 3 and A1), and the respective absorption maxima are collected in Table 2. The monomer spectra of the bis(merocyanine) dyes **2** and **4** are in good accordance with that observed for reference dye **1a**, showing absorption coefficients that are about twice as large as those obtained for mono-chromophoric **1a** (Figures 3a,b,d). However, it has to be noted that the monomer maxima of dyes **2** (λ_{max} = 570 nm) and **4** (569 nm) are red-shifted by about 10 nm with respect to that of **1a** (559 nm) that may be owing to a weak intramolecular J-type coupling between the chromophores.[13a,18] On the other hand, dye **5** shows nearly the same monomer maximum (λ_{max} = 558 nm) as reference **1a**, but its absorption coefficient is less than twice as large compared to that obtained for mono-chromophoric **1a** (Figures 3a,e). A closer look reveals that the absorption band of monomeric **5** is broader (FWHM = 1605 cm^{-1}) with respect to that of **1a** (FWHM = 1385 cm^{-1}) and has an additional shoulder at lower wavelength (~480 nm). The even more pronounced spectral broadening and the additional absorption band at lower wavelength of monomeric **3** (Figure A1) with respect to **1a** suggest a conformational distribution of monomeric **3** that involves a folded species besides of other conformations with more randomly oriented chromophores. Molecular modeling of monomeric **3** reveals that such a folded conformation with antiparallel stacked chromophores can be adopted, thus explaining the hypsochromic band as a result of H-type coupling.

The dimer spectra of bis(merocyanines) **2**–**5** show two absorption bands centered at considerably shorter and comparable wavelength with respect to the monomer absorption bands (Table 2). Such a split absorption spectrum was previously observed for merocyanine dimers of type **1a** and attributed to an excitation in the higher- and lower-lying exciton state of the dimer.[12] However, for the present dimers of bis(merocyanines) **2**–**5** such a simple treatment according to Kasha's dimer model is not feasible since four chromophores are kept in close proximity as suggested by the high dimerization constants. Thus, four transition dipole moments have to be considered for excitonic coupling. Nevertheless, some qualitative information can be elucidated from the spectral changes. The hypsochromic shift of the main

dimer maxima with respect to the monomer maxima in terms of the wavenumber difference $\Delta\tilde{\nu}_{D1-M}$ increases from 2520 cm^{-1} to 3721 cm^{-1} in the order of the series **1a**, **4**, **2**, **5**, and **3** (Table 2). It is noteworthy that the same order is given for the binding constants for bimolecular association. Thus, the tightest bound complex exhibits the strongest coupled chromophores which can be related to a smallest distance between the chromophores according to Kasha's theory.[34] Additionally, also the splitting between both dimer bands $\Delta\tilde{\nu}_{D1-D2}$ increases from 2520 cm^{-1} to 3688 cm^{-1} in this series. Thus, for the bis(merocyanine) dyes, stronger hypsochromically shifted main dimer bands as well as stronger splitting between the dimer maxima are observed in comparison with those for the reference dye **1a**. These data are in good accordance with a stacked arrangement of four chromophores where excitonic coupling to more than one neighbor dye may occur (Figure 1f). Along with the most pronounced hypsochromic shift in the present series of bis(merocyanine) dyes, the dimer band of **3** has a very narrow bandwidth (FWHM = 1200 cm^{-1}), implying a most tightly packed stacking of the chromophores. Notably, the hypsochromic shift of the absorption band of this tetrameric stack (in regard to the monomers) is not as pronounced as that observed for bis(merocyanine) nanorods, where a much larger number of chromophores are packed in close proximity.[13] Interestingly, the dimers of **3** show fluorescence that might be a result of the rigidified arrangement of the chromophores within the chromophore stack (see Figure A3). However, the quantum yield is still quite low (<10%) since fluorescence arises from the forbidden electronic transition of the lowest excited state to the ground state.

3.2.4 Structural elucidation of dimer aggregates by NMR spectroscopy

Structural characterization of the dimer aggregate of bis(merocyanine) **3** was performed as a representative example by NMR spectroscopy. For this purpose, ^{1}H NMR spectra of **3** were measured in $CDCl_3$ (c = 10 mM), where this dye dimerizes almost completely (see Figure 4), and in highly polar DMF-d_7 (c = 3 mM), in which the dimerization is negligible. The assignment of the proton NMR signals was achieved by (^{1}H,^{1}H)-COSY, (^{1}H,^{13}C)-HSQC and (^{1}H,^{13}C)-HMBC experiments. In Table 3, the assignment of significant proton signals of bis(merocyanine) dye **3** in DMF-d_7 and $CDCl_3$ is shown. For the complete assignment of ^{1}H and ^{13}C NMR spectra, see the Table A1 in the Appendix.

For monomeric bis(merocyanine) **3**, a simple ^{1}H NMR spectrum with a single set of signals was obtained in DMF-d_7 (Figure 5a). The respective positions at both halves of the dye **3** numbered with and without prime (see Table 3) are chemically equivalent in the monomeric compound, which is in accordance with rotational freedom around the single-bonds connecting the chromophores to the naphthalene spacer, thus leading to a C_{2v}-symmetric average geometry of the bis(merocyanine) dye on the NMR time scale. Furthermore, the presence of only one doublet for the protons at positions 1 and 2 (at 8.52 ppm) as well as for those at positions 3 and 4 (at 7.82 ppm) in DMF-d_7 strongly suggests a fast rotation around the C5–C6 bond. Such rotational motion is known for these merocyanine dyes and attributed to their zwitterionic properties, imparting strong single-bond character for the C5–C6 bond.[40]

A more complex spectrum is obtained for the bimolecular complex of **3** in $CDCl_3$ (Figure 5b), which shows a greater number and considerably broader signals in comparison with the monomer spectrum in DMF-d_7. The assignment of the signals in the dimer spectrum reveals that the chemical equivalency of the positions on both halves of the molecule is lost upon dimerization, since different chemical shifts are observed for the protons at the positions numbered with and without prime (Table 3). This splitting of the NMR signals is highlighted for selected protons in Figure 5 by the lines connecting the corresponding peaks. Notably, the methylene protons at position 15 and 15′, respectively, show two sets of geminally coupled

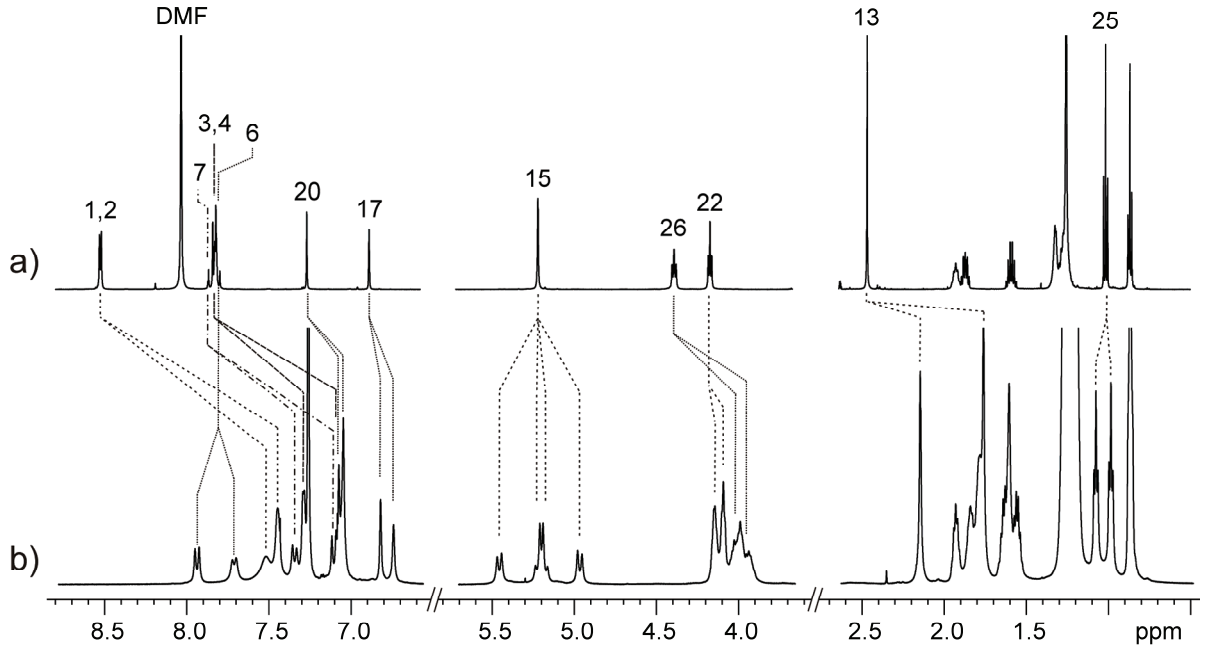

Figure 5. Parts of the 600 MHz ^{1}H NMR spectrum of **3** in a) DMF-d_7 (c = 3 mM) and b) $CDCl_3$ (c = 10 mM) at 293 K. The connecting dotted lines highlight the splitting of selected monomer signals upon dimerization.

Table 3. Assignment of the significant proton signals of bis(merocyanine) **3** in DMF-d_7 and $CDCl_3$.

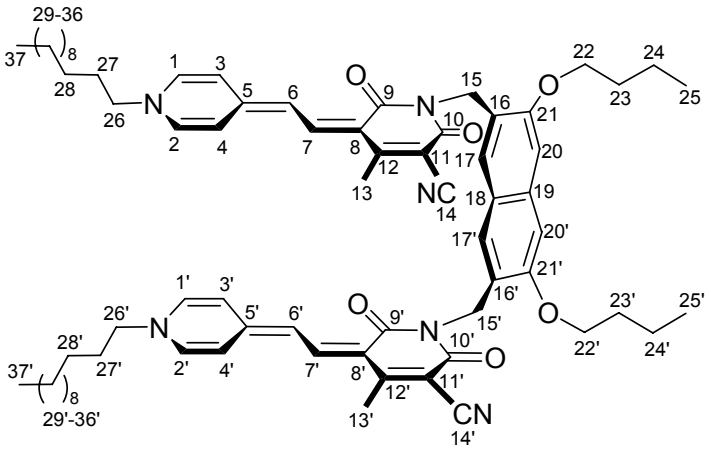

3

position	DMF-d_7 δ_H (J / Hz)	$CDCl_3$ δ_H (J / Hz)	$\Delta\delta_H$
1,2	8.52 (d, 7.0, 4H)	7.44 (br, 2H)	−1.08
1′,2′		7.52 (br, 2H)	−1.00
3,4	7.82 (d, 7.0[a], 4H)	7.05[a] (br, 2H)	−0.77
3′,4′		7.29 (d, 4.8, 2H)	−0.53
6	7.81 (d,14.8, 2H)	7.71 (d, 14.8, 1H)	−0.10
6′		7.94 (d, 14.8, 1H)	0.13
7	7.85 (d, 14.9, 2H)	7.34 (d, 14.7, 1H)	−0.51
7′		7.10 (d, 15.2[a], 1H)	−0.75
13	2.47 (s, 6H)	2.15 (s, 3H)	−0.32
13′		1.76 (s, 3H)	−0.71
15α	5.22 (s, 4H)	5.22 (d, 16.3, 1H)	0.00
15β		5.18 (d, 16.3, 1H)	−0.04
15′α		5.45 (d, 16.0, 1H)	0.23
15′β		4.97 (d, 16.0, 1H)	−0.25
17	6.89 (s, 2H)	6.82 (s, 1H)	−0.07
17′		6.73 (s, 1H)	−0.16
20	7.27 (s, 2H)	7.04 (s, 1H)	−0.23
20′		7.07 (s, 1H)	−0.20
22	4.17 (t, 6.5, 4H)	4.09 (br, 2H)	−0.08
22′		4.14 (br, 2H)	−0.03
25	1.02 (t, 7.4, 6H)	0.98 (t, 7.3, 3H)	−0.04
25′		1.08 (t, 7.3, 3H)	0.06
26,26′	4.39 (t, 7.4, 4H)	3.9–4.1 (br, 4H)	−0.4

[a] Estimated value due to partial overlap or broadening of signals

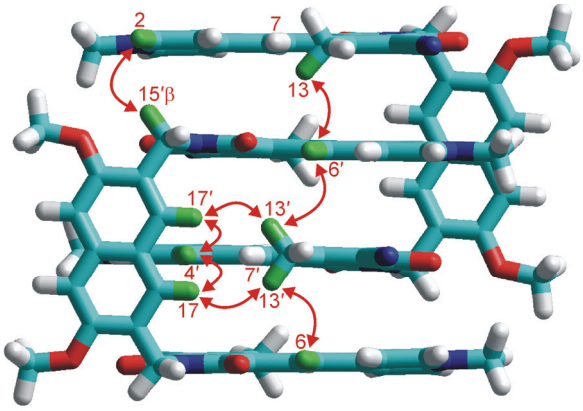

Figure 6. Structural model for the centrosymmetric dimer of **3** based on NMR studies and molecular modeling. The arrows indicate spatial proximities between the green highlighted protons as evidenced by ROESY cross-coupling peaks (see Figure 7). The alkyl chains are replaced by methyl groups for simplicity.

proton signals in the dimer spectrum which indicates restrained rotation around the methylene bridge between the spacer and chromophore units, and a different magnetic environment for each methylene proton in this rigidified dimer structure. For most of the protons, an upfield shift (negative $\Delta\delta_H$ values in Table 3) is observed upon dimerization, which can be attributed to shielding of the protons by the anisotropic contributions of the aromatic chromophores and spacers in the dimer structure. The signals for the pyridine-donor protons (at positions 1–4 and 1′–4′) become considerably broader, indicating a slower rotation of the pyridine-donor ring in the dimer, compared to that of the monomer. These results are in accordance with a centrosymmetric dimer structure as shown in Figure 6. Within this structure, the protons on the two halves of each monomer unit clearly have a different chemical environment, which leads to different chemical shifts (*i.e.*, splitting of monomer signals) of the protons at positions numbered with and without prime, while the respective protons on both of the monomer units with the same notation are chemically equivalent due to the overall centrosymmetric geometry.

In such a closely packed dimer, spatial proximities between the protons of the two individual molecules in close vicinity should lead to through-space couplings that can be studied by nuclear Overhauser enhancement (NOE) spectroscopy. Since the signal intensity of the NOE may become very low in the intermediate mass range, in the present case (the masses of the dimers are around 2280 g/mol) the rotating-frame Overhauser enhancement spectroscopy (ROESY) technique was applied. The through-space connections were then determined for dye **3** by ROESY NMR in $CDCl_3$ at a concentration of 10 mM (Figure 7). All the observed cross-peaks can be unambiguously assigned to *inter*molecular through-space couplings because none of them was found in DMF-d_7.

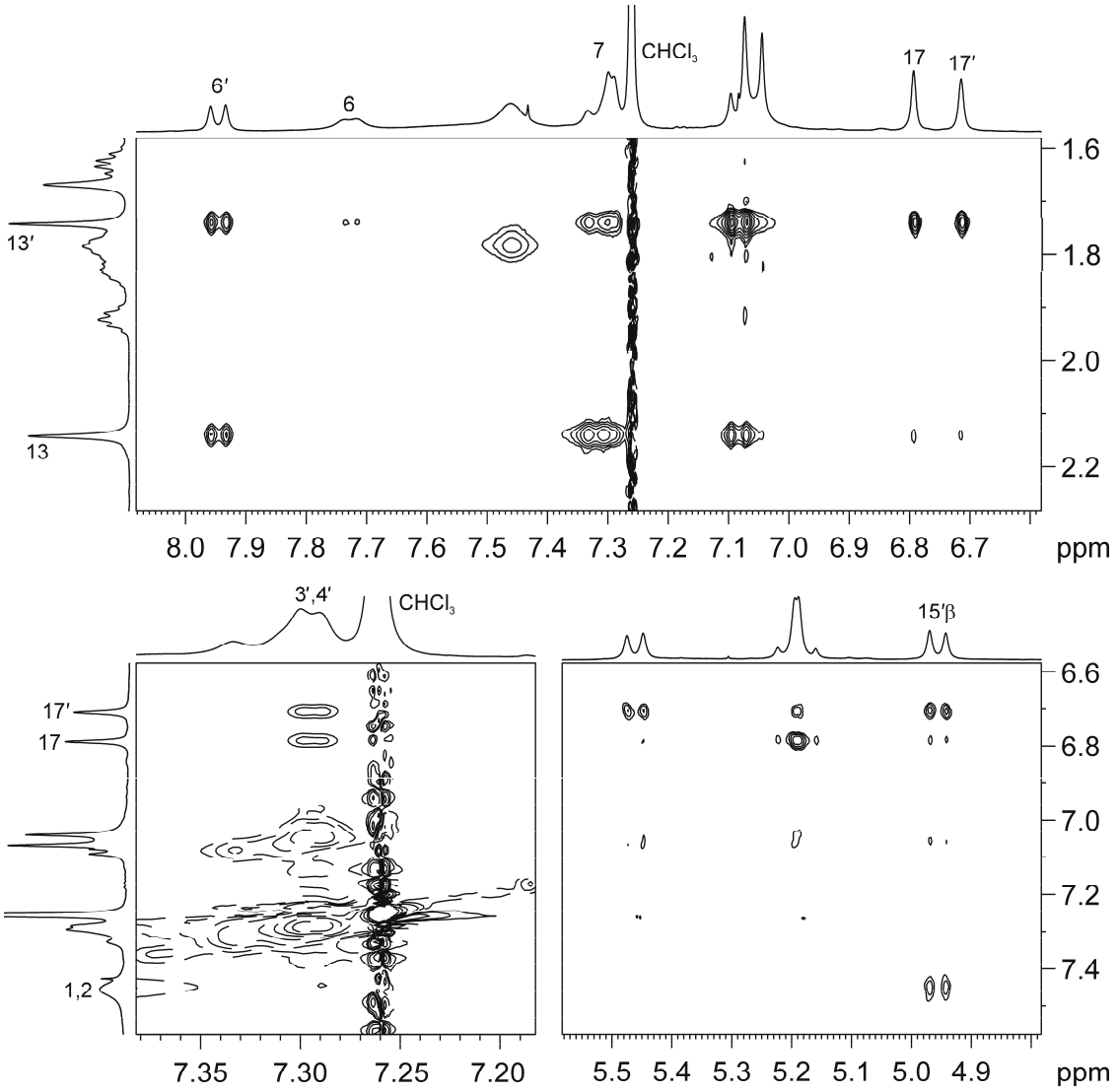

Figure 7. Selected areas of the 600 MHz ROESY NMR spectrum of dye **3** in $CDCl_3$ (c = 10 mM) at 274 K and 100 ms mixing time. Positive and negative signals are represented by solid and dashed contours, respectively.

For the pairs of protons which show cross-peaks in the ROESY spectrum (Figure 7), the intermolecular distances in a centrosymmetric dimer according to Figure 6 are in the range of 2.5–2.9 Å (based on MM+ optimized dimers, see below), which is well within the range of ROESY experiments. The intramolecular distances between these protons within the same molecule are far beyond the sensitivity of this technique. Thus, the results of the ROESY experiments in $CDCl_3$ provide clear evidence for the centrosymmetric dimer structure as illustrated in Figure 6. The through-space connectivity of protons 15′β and 2 found in the ROESY spectrum is in accordance with the proximity of these protons in the dimer model shown in Figure 6 and reveals that the positions denoted with prime are those at the inner halves of the monomer units in the dimer. This notation is also in agreement with the

significantly stronger shielding of protons 13′ and 7′ with respect to protons 13 and 7, respectively. Notably, in the ROESY spectra of **3** in $CDCl_3$ the signals of the protons denoted with and without prime are connected to each other by cross-peaks of the same sign as the diagonal peaks (both negative), which reveals a supramolecular exchange between the halves of the molecules with and without prime on the time scale of the mixing times of the ROESY experiments (100 and 300 ms).

3.2.5 Molecular modeling

We performed molecular modeling studies for the present series of bis(merocyanine) dyes aiming at a qualitative explanation for the dependence of the dimerization constants and absorption properties on the molecular structure of the bis(merocyanine) monomers, as revealed by the UV–vis studies (*vide supra*). However, the structural characterization of supramolecular assemblies by computational methods is still very limited because an accurate description of the involved intermolecular forces requires higher-level calculations that are limited to small systems. Simple force-field calculations are in general not applicable since they cannot account for the non-uniform charge distribution in the delocalized π-system responsible for the strong dipolar character of the merocyanine chromophore **1**. As shown recently, the dimerization of simple merocyanine chromophores **1** can be described with accuracy only by more demanding DFT-D methods, whilst even semi-empirical or standard DFT methods fail due to missing dispersion corrections.[41]

Keeping in mind the noted deficiency of this method, the packing of the chromophores in the dimer structures of bis(merocyanine) monomers **2**–**5** was assessed by geometry optimization applying a simple force-field calculations (HYPERCHEM™, MM+).[42] A molecular dynamics simulation was used to equilibrate each supramolecule, followed by energy minimization of the resulting structures to full convergence. As shown in Figure 8, the geometry-optimized dimer models of all bis(merocyanine) compounds in the present series adopt a centrosymmetric structure, which is experimentally confirmed for dye **3** by the 2D NMR experiments. The chromophores are arranged in a stacked fashion and interlock like two tweezers from opposite directions. In such a dimer structure, the electron-rich and electron-deficient parts of the chromophores are positioned on top of each other to maximize the electrostatic interactions. These multiple dipolar interactions account for the strong increase of the dimerization constant of the bis(merocyanine) dyes with respect to simple dimers of reference dye **1a**.

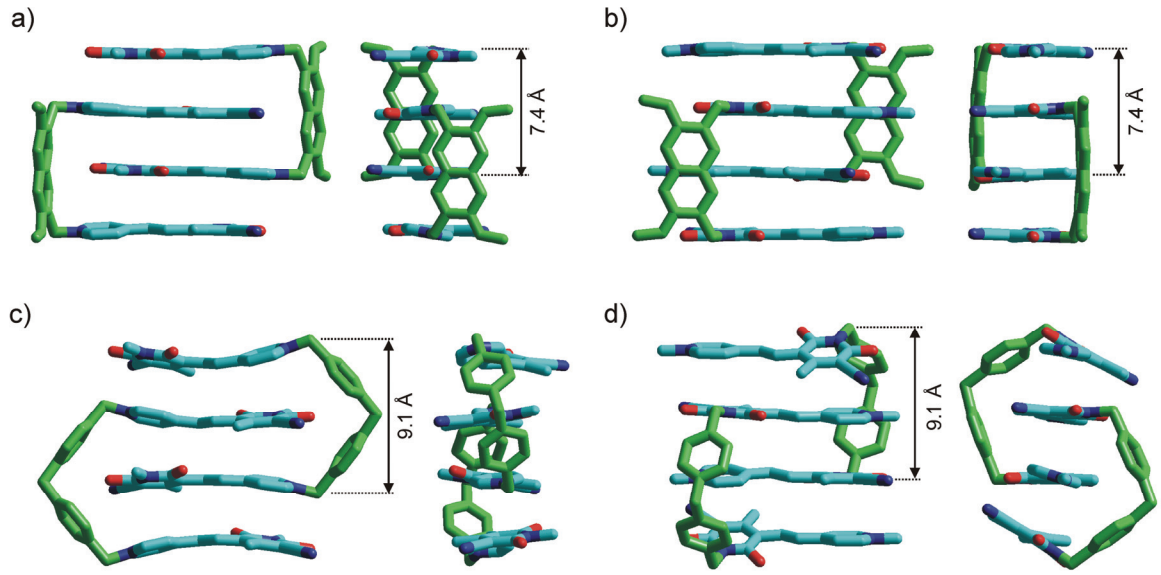

Figure 8. MM+ geometry-optimized models for dimer aggregates of bis(merocyanine) dyes: a) **2**, b) **3**, c) **4**, and d) **5**. The spacer units are shown in green and all alkyl chains were replaced by methyl substituents.

A more detailed inspection reveals that the 2,7-naphthalenedimethylene-tethered bis(merocyanines) **2** and **3** adopt a very tight packing of the two inner chromophores in the bimolecular complex with an ideal van-der-Waals distance to both neighboring chromophores in the range of 3.5–3.6 Å (Figure 8a,b). The intramolecular distance between the methylene C atoms of the spacers is 7.4 Å (arrows), which is nearly twice the distance between the chromophore planes, and suggests that the monomers do not have to assume a distorted geometry for the formation of these tightly packed dimer structure. On the other hand, the dimers of bis(merocyanine) dyes **4** and **5** provided with the 4,4′-dimethylenediphenylmethane spacer show a considerably larger distance between the methylene C atoms of 9.1 Å (Figure 8c,d). Thus, the molecular geometry of the monomeric units is strongly distorted in these cases to allow the approach of the chromophore planes to a close van-der-Waals contact. From these structural differences between the monomers, provided either with the 2,7-naphthalenedimethylene spacer or the 4,4′-dimethylenediphenylmethane spacer, it is apparent that the latter one is less suited to support a tight chromophore stack. In addition, higher entropic losses have to be overcome in the dimerization of 4,4′-dimethylenediphenylmethane-tethered dyes in comparison with the 2,7-naphthalenedimethylene-tethered ones, since a larger number of rotors have to be frozen out in the former case for the formation of the rigid dimers.[43] These considerations account for the higher dimerization constants of the naphthalene-tethered dyes **2** and **3** compared to those of the diphenylmethane-tethered dyes **4** and **5**, respectively.

Higher dimerization constants were also found for the bis(merocyanine) dyes tethered via the imide N atoms (**3** and **5**) with respect to those tethered via the donor N atom (**2** and **4**). A closer look at the dimer models of the bis(merocyanine) dyes **2** and **4** reveals that the terminal carbonyl groups of the chromophores are in close proximity to the aromatic spacers, which might evoke repulsive forces between the carbonyl oxygen with negative partial charge and the π-cloud of the spacers (Figure 8a,c). Such repulsive forces are avoided in the case of the bis(merocyanine) dyes **3** and **5** tethered at the imide N atoms where the dyes can be slipped against each other to the point of a most suitable electrostatic interaction (Figure 8b,d). Such a slipped arrangement might even allow aromatic edge-to-face interactions between the pyridine donor group with partial positive charge and the aromatic spacers.[44] Edge-to-face interactions can be quite strong (of the order of several kJ/mol) and may contribute substantially to the stronger dimerization constants observed in the case of the bis(merocyanine) dyes tethered via the imide N atoms with respect to those tethered *via* the pyridin donor group N atom.

The dimer structures obtained from molecular modeling can also account for the UV–vis absorption properties of the bis(merocyanine) dimers. The strong hypsochromic shifts $\Delta\tilde{\nu}_{\mathrm{D1-M}}$ of the main dimer absorption bands with respect to the monomer bands as well as the stronger splitting of the dimer bands $\Delta\tilde{\nu}_{\mathrm{D1-D2}}$ compared to that of the reference merocyanine **1a** result from the tightly packed bimolecular complexes of the bis(merocyanine) dyes, which allows excitonic coupling between four chromophores with almost parallel transition dipole moments.[35] Moreover, the increase of $\Delta\tilde{\nu}_{\mathrm{D1-M}}$ and $\Delta\tilde{\nu}_{\mathrm{D1-D2}}$ in the series of **4**, **2**, **5**, and **3**, which corresponds to the series of increasing dimerization constant (see Table 2), can be attributed to increasingly tight packing of the chromophores since exciton coupling theory predicts an inverse third power relationship between the coupling energy of the transition dipoles *J* and the distance of the dipole centers.[45]

3.3 Conclusion

Tweezers obtained by tethering of two identical, highly dipolar merocyanine chromophores to appropriate spacer units self-assemble into centrosymmetric dimers containing a π-stacked arrangement of four chromophores. Owing to the alternating orientation of the dipole moments of the four chromophores in these bimolecular complexes and ideal interplanar distances for π–π stacking of about 3.5 Å, very high dimerization constants up to $>10^{-9}$ M^{-1} became possible even in the good solvating solvent like chloroform. These self-association constants are indeed

several orders of magnitude higher than those reported for traditional tweezer systems.[21] Thus, a new design principle for ultra strong bimolecular association has been introduced based on the antiparallel stacking of highly dipolar chromophores (Figure 1f). This novel design principle may be applied to create further discrete architectures of dipolar systems.

3.4 Experimental Section

Materials and Methods. Solvents and reagents were obtained from commercial suppliers and purified according to standard procedures.[46] Naphthalene dicarbaldehyde **6**,[27] pyridinium salt **13**,[29] dibromide **14**,[30] hydroxypyridone **16**,[12b] and diamine **17**,[31] were prepared according to literature procedures. Column chromatography was performed on silica gel (Merck Silica 60, particle size 0.04−0.063 mm) and TLC was conducted on silica gel plates (60 F_{254}, Merck). Melting points were determined on a Linkam TP 94 heating stage and are uncorrected. NMR experiments were conducted on a Bruker Avance 400 and a Bruker DMX 600 spectrometer with TMS or residual solvent signal as internal standard. High-resolution ESI-TOF and EI mass spectrometry was carried out on a microTOF focus instrument (Bruker Daltronik GmbH) in positive mode and a Finnigan MAT 90 instrument, respectively. MALDI-TOF MS measurements were performed on a Bruker Autoflex II. Elemental analyses were furnished with a CHNS 932 analyzer (Leco Instruments GmbH).

UV–vis Absorption. UV–vis spectra were measured on a Perkin Elmer Lambda 950 spectrometer in conventional quartz cells of 0.001–5.0 cm path length to cover a suitable concentration range. The spectral bandwidth and the scan rate were 2 nm and 140 nm/min, respectively. The stock solutions of each compound were accurately prepared, and dilutions of these stocks were used for absorption measurements over a concentration range by taking into account the solubility and absorbance of the respective compound. The temperature was controlled with a PTP-1 peltier element (Perkin Elmer). The solvents for UV–vis absorption were of spectroscopic grade and used as received.

2D NMR Spectroscopy. Measurements were performed at 274 K and 293 K in standard 5 mm NMR tubes on a Bruker DMX 600 spectrometer equipped with a 5 mm $^{13}C/^{1}H$ cryoprobe. Prior to two-dimensional NMR measurements, the samples were degassed by bubbling with dry argon gas for at least 30 min. A set of standard ^{1}H, ^{13}C, DEPT, (^{1}H,^{1}H)-COSY, (^{1}H,^{13}C)-HSQC and (^{1}H,^{13}C)-HMBC spectra was recorded for compound **3** in $CDCl_3$ and in DMF-d_7

using the ^{1}H and ^{13}C solvent signals as internal standard (7.26 and 77.00 ppm for $CDCl_3$ and 2.75 and 29.76 ppm for the high-field methyl signal of DMF-d_7). Two-dimensional ROESY spectra of **3** in $CDCl_3$ were acquired with a standard pulse sequence over a sweep width of 7184 Hz using 8192 data points in the t_2 dimension and 512 increments in the t_1 dimension for different mixing times of τ_m = 300 ms (at 274 and 293 K) and 100 ms (at 274 K). A total of 32 scans were collected for each t_1 increment with an acquisition time of 0.57 s, followed by an additional relaxation delay of 2.5 s. The spectra were acquired at different temperatures and mixing times to differentiate between ROE connections and chemical exchange peaks. A 2D ROESY spectrum of **3** in DMF-d_7 was recorded at 293 K with 300 ms mixing time and similar experimental conditions.

3,6-Dibutoxynaphthalene-2,7-dicarbaldehyde (7). Dihydroxynaphthalene **6** (6.0 g, 27.8 mmol) and K_2CO_3 (19 g, 139 mmol) were suspended in DMF (100 mL) and the mixture was heated under argon atmosphere to 60 °C. *n*-Butylbromide (7.62 g, 55.6 mmol) was added within 5 min and the mixture was heated for additional 17 h. The hot mixture was poured into 200 mL ice water under vigorous stirring and the suspension was stirred for additional 10 min. The precipitate was filtered, washed with water and chromatographed with a short column (SiO_2, CH_2Cl_2). The crude product was recrystallized twice from acetone. The product was obtained as pale yellow needles. Yield: 3.88 g (11.8 mmol, 43%). Mp 131–133 °C. TLC (CH_2Cl_2) R_f = 0.21. ^{1}H NMR (400 MHz, $CDCl_3$, 25 °C): δ 10.53 (s, 2H, C*H*O), 8.37 (s, 2H, naph-H), 7.04 (s, 2H, naph-H), 4.18 (t, J = 6.4 Hz), 1.91 (m, 4H, OCH_2CH_2), 1.57 (m, 4H, CH_2CH_3), 1.03 (t, J = 7.5 Hz, 6H, CH_3). HRMS (ESI, pos. mode, MeCN/$CHCl_3$ = 1:1): calcd m/z for $C_{20}H_{24}O_4Na$ ($[M+Na]^+$) 351.15668, found 351.15691. Anal. Calcd for $C_{20}H_{24}O_4$ (328.40): C, 73.15; H, 7.37. Found: C, 72.95; H, 7.30.

3,6-(Dibutoxynaphthalene-2,7-diyl)dimethanol (8). Dialdehyde **7** (1.0 g, 3.05 mmol) was suspended in a mixture of THF (2 mL) and EtOH (13 mL). $NaBH_4$ (248 mg, 6.53 mmol) was added and the suspension was stirred at room temperature (rt) for 2.5 h. Hydrochloric acid (10%, 7 mL) was added carefully and the mixture was extracted four times with CH_2Cl_2, subsequently the combined organic phase was washed with brine and water. The organic phase was dried over Na_2SO_4 and the solvent was removed under vacuum. Column chromatography (SiO_2, CH_2Cl_2/MeOH = 9:1) and crystallization from methyl *tert*-butyl ether/*n*-hexane afforded a pale pink colored solid. Yield: 910 mg (2.74 mmol, 90%). Mp 93–94 °C. TLC

(CH_2Cl_2/MeOH = 9:1) R_f = 0.42. ^{1}H NMR (400 MHz, $CDCl_3$, 25 °C): δ 7.60 (s, 2H, naph-H), 7.02 (s, 2H, naph-H), 4.79 (s, 4H, C*H*$_2$OH), 4.12 (t, *J* = 6.4 Hz, 4H, OC*H*$_2$CH$_2$), 2.25 (br, 2H, OH), 1.86 (m, 4H, OCH$_2$C*H*$_2$), 1.55 (m, 4H, C*H*$_2$CH$_3$), 1.01 (t, *J* = 7.4 Hz, 6H, CH_3). HRMS (ESI, pos. mode, MeCN/$CHCl_3$ = 1:1): calcd *m*/*z* for $C_{20}H_{28}O_4Na$ ([*M*+Na]$^+$) 355.18798, found 355.18842. Anal. Calcd for $C_{20}H_{28}O_4$ (332.43): C, 72.26; H, 8.49. Found: C, 72.27; H, 8.48.

1,1′-[(3,6-Dibutoxynaphthalene-2,7-diyl)bis(methylene)]bis(4-methylpyridinium) ditetrafluoroborate (9). Diol **8** (500 mg, 1.50 mmol) was dissolved in 4-methylpyridine (3.5 mL, 35 mmol). Tosylchloride (572 mg, 3.00 mmol) was added and the solution was stirred at rt for 2 h. Additional tosylchloride (143 mg, 0.75 mmol) was added and the mixture was stirred for further 2 h. Acetonitrile (7 mL) was added and the solution was refluxed for 2 h. The solvent was removed under reduced pressure and the residue was dissolved in MeOH (2 mL). In a second flask, a saturated aqueous $NaBF_4$ solution (22.5 mL) was diluted with water (7.5 mL) and the methanolic solution was dropped to it under mild stirring. The solution was shortly heated to reflux and cooled slowly and kept over night at room temperature. The precipitate was filtrated and recrystallized from *i*-PrOH/EtOAc. An additional recrystallization from *i*-PrOH afforded pale brown needles. Yield: 780 mg (1.18 mmol, 79%). Mp 117–120 °C. ^{1}H NMR (400 MHz, MeOD-d_4, 25 °C): δ 8.81 (d, *J* = 6.7 Hz, 4H, py-H), 8.11 (s, 2H, naph-H), 7.91 (d, *J* = 6.3 Hz, 4H, py-H), 7.31 (s, 2H, naph-H), 5.84 (s, 4H, -CH_2N), 4.09 (t, *J* = 6.6 Hz, 4H, OCH_2), 2.67 (s, 6H, py-CH_3), 1.75 (m, 4H, OCH$_2$C*H*$_2$), 1.37 (m, 4H, C*H*$_2$CH$_3$), 0.97 (t, *J* = 7.4 Hz, 6H, CH_3). HRMS (ESI, pos. mode, MeOH): calcd *m*/*z* for $C_{32}H_{40}BN_2O_2F_4$ ([*M*–BF_4]$^+$) 570.31546, found 570.31469. Anal. Calcd for $C_{32}H_{40}B_2F_8N_2O_2{\cdot}2H_2O$ (694.31): C, 55.36; H, 6.39; N, 4.03. Found: C, 55.36; H, 6.24; N, 3.97.

Dibenzyl [(3,6-dibutoxynaphthalene-2,7-diyl)bis(methylene)]biscarbamate (10). Dialdehyde **7** (2.75 g, 8.37 mmol) and benzylcarbamate (2.79 g, 18.5 mmol) was dissolved in acetonitrile (90 mL) and toluene (90 mL). Under stirring, Et_3SiH (2.96 mL, 18.6 mmol) and then TFA (0.94 mL) were added and stirring was continued at rt for 48 h. Additional portions of Et_3SiH (2.96 mL, 18.6 mmol) and TFA (0.94 mL) were added and the solution was stirred for further 24 h. The reaction mixture was washed with saturated aqueous $NaHCO_3$ solution (2×90 mL) and brine (90 mL). After drying over Na_2SO_4 the solvent was removed under reduced pressure and the oily residue was subjected to columns chromatography (SiO_2, CH_2Cl_2/EtOAc = 95:5). Repeated recrystallization from EtOH afforded fine white needles.

Yield: 3.49 g (5.83 mmol, 70%). Mp 103–104 °C. TLC (CH_2Cl_2/EtOAc = 95:5) R_f = 0.34. ^{1}H NMR (400 MHz, $CDCl_3$, 25 °C): δ 7.59 (br, 2H, naph-H), 7.3 (m, 10H, ph-H), 6.98 (s, 2H, naph-H), 5.27 (br, 2H, NH), 5.11 (s, 4H, OCH_2Ph), 4.48 (d, J = 5.9 Hz, 4H, CH_2NH), 4.07 (t, J = 6.4 Hz, 4H, OCH_2CH$_2$), 1.84 (m, 4H, OCH$_2$CH_2), 1.53 (m, 4H, CH_2CH$_3$), 1.00 (t, J = 7.4 Hz, 6H, CH_3). HRMS (ESI, pos. mode, MeCN/$CHCl_3$ = 1:1): calcd m/z for $C_{36}H_{42}N_2O_6Na$ ([M+Na]$^+$) 621.29351, found 621.29399. Anal. Calcd for $C_{36}H_{42}N_2O_6$ (598.73): C, 72.22; H, 7.07; N, 4.68. Found: C, 72.14; H, 7.03; N, 4.71.

***N,N′*-[(3,6-Dibutoxynaphthalene-2,7-diyl)bis(methylene)]bis(2-cyanoacetamide) (11).** In an argon gas flooded flask, the Cbz-protected diamine **10** (3.0 g, 5.01 mmol) was dissolved in a mixture of EtOAc (120 mL) and MeOH (60 mL) and the solution was degassed by applying vacuum and flooding with argon. Afterwards Pd/C (10%, 100 mg) was added to the solution and H_2 gas was supplied by means of a balloon. Under vigorous stirring and slight heating to 40 °C for 2 h, the mixture was filtered over celite. The solvent was removed under reduced pressure, and the resulting colorless oil (1.64 g) was dissolved in MeOH (20 mL) and degassed as described above. Ethyl cyanoacetate (1.17 mL, 11.0 mmol) was added and the solution stirred at rt for 1 h. Additional MeOH (20 mL) was added and the mixture was refluxed for 90 h. After cooling to rt, the precipitate was filtered and washed with MeOH. After drying under vacuum a white powder was obtained. For elemental analysis, the product was recrystallized from MeCN/AcOH (1:1). Yield: 1.54 g (3.31 mmol, 66%). Mp 248–249 °C. TLC (CH_2Cl_2/MeOH = 95:5) R_f = 0.30. ^{1}H NMR (400 MHz, DMSO-d_6, 25 °C): δ 8.53 (t, ^3J = 5.6 Hz, 2H, NH), 7.56 (s, 2H, naph-H), 7.23 (s, 2H, naph-H), 4.36 (d, J = 5.6 Hz, 4H, CH_2NH), 4.08 (t, J = 6.4 Hz, 4H, OCH_2CH$_2$), 3.73 (s, 4H, CH_2CN), 1.79 (m, 4H, OCH$_2$CH_2), 1.50 (m, 4H, CH_2CH$_3$), 0.97 (t, J = 7.4 Hz, 6H, CH_3). HRMS (ESI, pos. mode, MeOH): calcd m/z for $C_{26}H_{32}N_4O_4Na$ ([M+Na]$^+$) 487.23158, found 487.23181. Anal. Calcd for $C_{26}H_{32}N_4O_4$ (464.56): C, 67.22; H, 6.94; N, 12.06. Found: C, 66.89; H, 6.88; N, 11.72.

1,1′-[(3,6-Dibutoxynaphthalene-2,7-diyl)bis(methylene)]bis(6-hydroxy-4-methyl-2-oxo-1,2-dihydropyridine-3-carbonitrile) (12). Cyanoacetamide **11** (2.0 g, 4.31 mmol) was suspended in piperidine (7 mL) and ethyl acetoacetate (3.25 mL, 25.7 mmol) was added to the suspension. The mixture was then heated to 100 °C for 3.5 h and subsequently the solvent was distilled under reduced pressure. After addition of conc. HCl (10 mL), the mixture was sonicated until a homogeneous suspension was formed. The mixture was diluted with water to

the threefold volume. The product was filtered off (G3 frit) and washed several times with water and Et_2O to give the product with sufficient purity (>85%) for further reaction. Owing to the very poor solubility of **12** in all considered solvents, except dimethylsulfoxide, only small amounts were purified by column chromatography for the characterization purpose (SiO_2, CH_2Cl_2/MeOH = 7:3). Yield: 1.85 g (3.10 mol, 72%). TLC (CH_2Cl_2/MeOH = 7:3) R_f = 0.45. ^{1}H NMR (400 MHz, DMSO-d_6, 25 °C): δ 7.24 (s, 2H, naph-H), 6.91 (s, 2H, naph-H), 5.58 (s, 2H, pyridone-H), 5.10 (s, 4H, CH_2N), 4.11 (t, J = 6.3 Hz, 4H, OCH_2CH$_2$), 2.24 (s, 6H, pyridone-CH$_3$), 1.79 (m, 4H, OCH$_2$CH_2), 1.51 (m, 4H, CH_2CH$_3$), 0.98 (t, J = 7.4 Hz, 6H, -CH$_3$). HRMS (ESI, pos. mode, MeCN): calcd m/z for $C_{34}H_{36}N_4O_6Na$ ([M+Na]$^+$) 619.25271, found 619.25274.

(5*Z*,5′*Z*)-5,5′-{(3,6-Dibutoxynaphthalene-2,7-diyl)bis[methylenepyridin-1-yl-4-ylidene-(1*Z*)ethane-2,1-diylidene]}bis(1-dodecyl-4-methyl-2,6-dioxo-1,2,5,6-tetrahydropyridine-3-carbonitrile) (2). A mixture of dodecyl pyridone **16** (275 mg, 0.836 mmol) and *N,N*′-diphenylformamidine (170 mg, 0.866 mmol) in Ac_2O (1.5 mL) was stirred at room temperature for 15 min. The mixture was then heated to 90 °C for additional 30 min to complete the reaction. The reaction mixture being cooled to room temperature, dipyridinium salt **9** (217 mg, 0.33 mmol) and KOAc (97 mg, 1 mmol) were added, and the mixture was heated at 100 °C for 14 h. The solution was concentrated in vacuo and the crude product was purified by column chromatography (SiO_2, CH_2Cl_2/MeOH = 95:5). Yield: 105 mg (92 µmol, 28%). Mp 297 °C. TLC (CH_2Cl_2/MeOH = 93:7) R_f = 0.27. ^{1}H NMR (400 MHz, CD_2Cl_2/MeOD-d_4 = 4:1 vol%, 25 °C) δ 8.02 (d, J = 7.0 Hz, 4H, py-H), 7.87 (s, 2H, naph-H), 7.70 (s, 4H, met-H), 7.47 (d, J = 7.1 Hz, 4H, py-H), 7.14 (s, 2H, naph-H), 5.43 (s, 4H, CH$_2$N), 4.09 (t, J = 6.6 Hz, 4H, CH$_2$O), 3.90 (t, J = 7.6 Hz, 4H, CH$_2$N), 2.41 (s, 6H, pyridone-CH$_3$), 1.79 (m, 4H, OCH$_2$CH_2), 1.55 (m, 4H, NCH$_2$CH_2), 1.44 (m, 4H, CH$_2$), 1.4–1.2 (m, 36H, CH$_2$), 0.98 (t, J = 7.4 Hz, 6H, CH$_3$), 0.85 (t, J = 6.8 Hz, 6H, CH$_3$). HRMS (ESI, pos. mode, MeOH): m/z calcd for $C_{72}H_{94}N_6O_6Na$ ([M+Na]$^+$) 1161.71271, found 1161.71164. UV–vis (CH_2Cl_2, 25 °C, 10^{-5} M): λ_{max} (ε) = 560 nm (226900 $M^{-1}cm^{-1}$).

(5*Z*,5′*Z*)-1,1′-[(3,6-Dibutoxynaphthalene-2,7-diyl)bis(methylene)]bis{5-[2-(1-dodecylpyridin-4(1*H*)-ylidene)ethylidene]-4-methyl-2,6-dioxo-1,2,5,6-tetrahydropyridine-3-carbonitrile} (3). A mixture of bis(pyridone) **12** (597 mg, 1 mmol) and dimethylformamide (220 mg, 3 mmol) in Ac_2O (0.8 mL) was heated to 90 °C for 45 min. After cooling down to rt,

1-dodecyl-4-methylpyridinium bromide (**13**) (685 mg, 2 mmol) and Et_3N (0.2 g, 2 mmol) were added and the mixture was heated at 100 °C for 14 h. The solution was concentrated in vacuo and the crude product was purified by column chromatography (SiO_2, CH_2Cl_2/MeOH = 96.5:3.5). Yield: 110 mg (97 μmol, 10%). Mp 270 °C (decomp.). TLC (CH_2Cl_2/MeOH = 93:7) R_f = 0.58. ^{1}H NMR (600 MHz, DMF-d_7, 20 °C): δ 8.52 (d, J = 7.0 Hz, 4H, py-H), 7.82 (m, 8H, met-H, py-H), 7.27 (s, 2H, naph-H), 6.89 (s, 2H, naph-H), 5.22 (s, 4H, naph-CH_2N), 4.39 (t, J = 7.4 Hz, 4H, CH_2N), 4.17 (t, J = 6.5 Hz, 4H, CH_2O), 2.47 (s, 6H, pyridone-CH_3), 1.93 (m, 4H, CH_2), 1.87 (m, 4H, CH_2), 1.59 (m, 4H, CH_2), 1.4–1.2 (m, 36H, CH_2), 1.02 (t, J = 7.4 Hz, 6H, CH_3), 0.88 (t, J = 7.0, 6H, CH_3). ^{13}C NMR (150 MHz, DMF-d_7, 20 °C): 163.30, 163.03, 156.89, 156.05, 155.44, 142.46, 138.94, 133.86, 125.81, 123.29, 122.80, 121.12, 119.89, 114.68, 105.44, 105.17, 86.15, 67.86, 59.08, 38.69, 32.10, 31.60, 31.21, 29.72, 29.22, 26.26, 22.81, 19.62, 18.39, 13.97, 13.85. HRMS (ESI, pos. mode, MeCN): m/z calcd for $C_{72}H_{94}N_6O_6Na$ ([M+Na]$^+$) 1161.71271, found 1161.71166. UV–vis (DMF, 25 °C, 5×10^{-5} M): λ_{max} (ε) = 510 nm (126000 $M^{-1}cm^{-1}$).

1,1′-[Methylene-bis(4,1-phenylenemethylene)]bis(4-methylpyridinium) dibromide (15). A mixture of dibromide **14** (800 mg, 2.26 mmol) and 4-picoline (0.92 mL, 9.2 mmol) in acetonitrile (25 mL) was heated to reflux for 24 h. Removal of the solvent and the excess 4-picoline under reduced pressure yielded dipyridinium salt **15** as a white powder. Yield: 1.17 g (2.16 mmol, 96%). Mp 220 °C (decomp.). ^{1}H NMR (400 MHz, D_2O, 25 °C): δ 8.63 (d, J = 6.7 Hz, 4H, py-H), 7.81 (d, J = 6.7 Hz, 4H, py-H), 7.32 (d, J = 8.1 Hz, 4H, ph-H), 7.26 (d, J = 8.1 Hz, 4H, ph-H), 5.66 (s, 4H, CH_2N), 3.93 (s, 2H, PhCH_2Ph), 2.63 (s, 6H, py-CH_3). ^{13}C NMR (100 MHz, D_2O, 25 °C): δ 163.9, 146.3, 146.2, 134.4, 133.1, 132.5, 132.1, 66.7, 43.8, 24.7. HRMS (ESI, pos. mode, MeOH): calcd m/z for $C_{27}H_{27}N_2$ ([M−H−2Br]$^+$) 379.21688, found 379.21688.

***N*,*N*′-[Methylene-bis(4,1-phenylenemethylene)]bis(2-cyanoacetamide) (18).** A mixture of diamine **17** (8.3 g, 36.7 mmol) and ethyl cyanoacetate (380 mL) was heated to 100 °C for 62 h. After cooling to rt, ethyl acetate (500 mL) was added and the mixture was kept overnight. The precipitated solid was filtered, washed with ethyl acetate, and dried under vacuum. Recrystallization from acetonitrile yielded bis(cyanoacetamide) **18** as a slight brown powder. Yield: 3.50 g (9.71 mmol, 26%). Mp 215–218 °C. ^{1}H NMR (400 MHz, DMSO-d_6, 25 °C): δ 8.64 (br, 2H, NH), 7.17 (s, 8H, ph-H), 4.23 (d, J = 5.7 Hz, 4H, CH_2NH), 3.89 (s, 2H,

$PhCH_2Ph$), 3.65 (s, 4H, CH_2CN). ^{13}C NMR (100 MHz, $CDCl_3$, 25 °C): δ 162.0, 140.1, 136.0, 128.5, 127.5, 116.1, 42.3, 40.3, 25.2. MS (EI, 70 eV): *m*/*z*: 360 ($[M]^+$), 276. Anal. Calcd for $C_{21}H_{20}N_4O_2$ (360.41): C, 69.98; H, 5.59; N, 15.55. Found: C, 70.01; H, 5.78; N, 15.39.

1,1′-[Methylene-bis(4,1-phenylenemethylene)]bis(6-hydroxy-4-methyl-2-oxo-1,2-dihydro-pyridine-3-carbonitrile) (19). Metallic sodium (2.5 g, 110 mmol) was added to ethanol (45 mL) and the mixture was heated to reflux until all sodium was reacted to sodium ethanolate. Cyano acetamide **18** (3.0 g, 8.32 mmol) and ethyl acetoacetate (24 mL, 190 mmol) were added and the mixture was heated to reflux for 20 h. After addition of water (90 mL) and further heating for 20 min, hydrochloric acid (10%, 190 mL) was added carefully to the hot solution. During cooling down of the solution a brown solid precipitated, which was filtered and washed with water. After drying under vacuum, the crude product was dissolved in DMSO (50 mL) and precipitated by adding ethyl acetate (200 mL). The solid was washed three times with ethyl acetate and after drying under vacuum bis(hydroxypyridone) **19** was obtained as a light-brown powder in sufficient purity for further reaction. Yield: 2.49 g (5.05 mmol, 61%). Mp >300 °C (decomp.). ^1H NMR (400 MHz, DMSO-d_6, 25 °C): δ 7.14 (s, 8H, ph-H), 5.60 (s, 2H, pyridone-H), 5.05 (s, 4H, CH_2N), 3.85 (s, 2H, $PhCH_2Ph$), 2.21 (s, 6H, pyridone-CH_3). ^{13}C NMR (100 MHz, $CDCl_3$, 25 °C): δ 161.0, 160.7, 158.8, 140.6, 134.8, 129.0, 128.0, 117.9, 92.7, 88.8, 43.7, 40.7, 21.0.

(5*Z*,5′*Z*)-5,5′-{Methylene-bis[4,1-phenylenemethylenepyridin-1-yl-4-ylidene(1*Z*)ethane-2,1-diylidene]}bis(1-dodecyl-4-methyl-2,6-dioxo-1,2,5,6-tetrahydropyridine-3-carbonitrile) (4). A mixture of hydroxypyridone **16** (353.5 mg, 1.11 mmol) and *N,N′*-diphenylformamidine (217.8 mg, 1.11 mmol) in acetic anhydride (1.85 ml) was stirred for 30 min at rt and then heated to 110 °C for further 45 min. After cooling to rt, bis(pyridinium) salt **15** (200 mg, 370 µmol) and KOAc (107 mg, 1.11 mmol) were added and the mixture was heated to 100 °C for 17 h. The solvent was removed under reduced pressure and the residue was subjected to column chromatography (SiO_2, CH_2Cl_2/MeOH = 95:5). The product was dissolved in a little amount of CH_2Cl_2/MeOH (9:1) mixture and precipitated by adding an excess amount of MeOH to obtain a dark powder. Yield: 95 mg (92 µmol, 25%). Mp 232–233 °C. TLC (CH_2Cl_2/MeOH = 9:1) R_f = 0.54. ^1H NMR (400 MHz, DMSO-d_6, 25 °C): δ 8.49 (d, *J* = 7.1 Hz, 4H, py-H), 7.80–7.68 (m, 8H, py-H, met-H), 7.36 (d, *J* = 8.2 Hz, 4H, ph-H), 7.28 (d, *J* = 8.2 Hz, 4H, ph-H), 5.45 (s, 4H, NCH_2Ph), 3.93 (s, 2H, $PhCH_2Ph$), 3.79 (t, *J* = 7.4 Hz, 4H,

NC*H*$_2$CH$_2$), 2.39 (s, 6H, pyridone-CH$_3$), 1.44 (m, 4H, NCH$_2$C*H*$_2$), 1.22 (m, 36H, CH$_2$), 0.83 (t, *J* = 6.8 Hz, 6H, CH$_3$). HRMS (ESI, pos. mode, MeCN/CHCl$_3$ = 1:1): calcd *m*/*z* for $C_{67}H_{83}N_6O_4$ ([*M*+H]$^+$) 1035.64703, found 1035.64030.

(5*Z*,5′*Z*)-1,1′-[Methylenebis(4,1-phenylenemethylene)]bis{5-[2-(1-dodecylpyridin-4(1*H*)-ylidene)ethylidene]-4-methyl-2,6-dioxo-1,2,5,6-tetrahydropyridine-3-carbonitrile} (5). A mixture of bis(hydroxypyridone) **19** (100 mg, 203 µmol), DMF (44 mg, 602 µmol) and acetic anhydride (0.1 mL) was heated to 90 °C for 90 min. After cooling to rt, 1-dodecyl-4-methylpyridinium bromide (**13**) (139 mg, 406 µmol) and triethyl amine (0.56 mL, 406 µmol) were added and the mixture was heated to 90 °C for additional 3 h. After removal of the solvent under reduced pressure, MeOH was added to the residue. The precipitated solid was filtered and washed with diethyl ether. The crude product was subjected to column chromatography (SiO_2, CH_2Cl_2/MeOH = 95:5). The product was dissolved in a little amount of CH_2Cl_2/MeOH (9:1) mixture and precipitated by adding an excess amount of MeOH. After filtration and drying, bis(merocyanine) dye **5** was obtained as a dark-red powder. Yield: 28 mg (27 µmol, 13%). Mp 291–292 °C. TLC (CH_2Cl_2/MeOH = 9:1) R_f = 0.31. ^{1}H NMR (400 MHz, DMSO-d_6, 25 °C): δ 8.46 (d, *J* = 7.2 Hz, 4H, py-H), 7.83 (d, *J* = 7.2 Hz, 4H, py-H), 7.74 (m, 4H, met-H), 7.15 (d, *J* = 8.3 Hz, 4H, ph-H), 7.08 (d, *J* = 8.2 Hz, 4H, ph-H), 4.98 (s, 4H, NCH$_2$Ph), 4.28 (t, *J* = 7.04 Hz, 4H, NC*H*$_2$CH$_2$), 3.82 (s, 2H, PhCH$_2$Ph), 2.42 (s, 6H, pyridone-CH$_3$), 1.82 (m, 4H, CH$_2$C*H*$_2$), 1.23 (m, 36H, CH$_2$), 0.85 (t, *J* = 7.0 Hz, 6H, CH$_3$). HRMS (ESI, pos. mode, CH_2Cl_2): calcd *m*/*z* for $C_{67}H_{83}N_6O_4$ ([*M*+H]$^+$) 1035.64703, found 1035.64607.

3.5 References and Notes

(1) Lehn, J.-M. *Supramolecular Chemistry: Concepts and Perspectives*; VCH: Weinheim, 1995.

(2) (a) Prins, L. J.; Reinhoudt, D. N.; Timmerman, P. *Angew. Chem., Int. Ed.* **2001**, *40*, 2382–2426. (b) Holliday, B. J.; Mirkin, C. A. *Angew. Chem., Int. Ed.* **2001**, *40*, 2022–2043. (c) Hof, F.; Craig, S. L.; Nuckolls, C.; Rebek, J., Jr. *Angew. Chem., Int. Ed.* **2002**, *41*, 1488–1508. (d) Schmittel, M.; Kalsani, V. *Top. Curr. Chem.* **2005**, *245*, 1–53.

(3) (a) Balzani, V.; Credi, A.; Venturi, M. *Molecular Devices and Machines*; VCH: Weinheim, 2003. (b) *Molecular Switches*; Feringa, B. L., Ed.; VCH: Weinheim, 2001.

(4) (a) Merlau, M. L.; del Pilar Mejia, M.; Nguyen, S. T.; Hupp, J. T. *Angew. Chem., Int. Ed.* **2001**, *40*, 4239–4242. (b) Slagt, V. F.; Van Leeuven, P. W. N. M.; Reek, J. N. H. *Angew. Chem., Int. Ed.* **2003**, *42*, 5619–5623. (c) Masar, M. S., III; Gianneschi, N. C.; Oliveri, C. G.; Stern, C. L.; Nguyen, S. T.; Mirkin, C. A. *J. Am. Chem. Soc.* **2007**, *129*, 10149–10158.

(5) (a) Wright, A. T.; Anslyn, E. V. *Chem. Soc. Rev.* **2006**, *35*, 14–28. (b) Thomas, S. W., III; Joly, G. D.; Swager, T. M. *Chem. Rev.* **2007**, *107*, 1339–1386.

(6) (a) Meijer, E. W.; Schenning, A. P. H. J. *Chem. Commun.* **2005**, 3245–3258. (b) Carroll, R. L.; Gorman, C. B. *Angew. Chem., Int. Ed.* **2002**, *41*, 4378–4400.

(7) Gregory, P. *High Technology Applications of Organic Colorants*; Plenum Press: New York, 1991.

(8) (a) Yagai, S.; Karatsu, T.; Kitamura, A. *Chem.–Eur. J.* **2005**, *11*, 4054–4063. (b) Sun, S.-S.; Anspach, J. A.; Lees, A. J. *Inorg. Chem.* **2002**, *41*, 1862–1869. (c) Collin, J. P.; Dietrich-Buchecker, C.; Gavina, P.; Jimenez-Molero, M. C.; Sauvage, J. P. *Acc. Chem. Res.* **2001**, *34*, 477–487. (d) Funeriu, D. P.; Lehn, J.-M.; Fromm, K. M.; Fenske, D. *Chem.–Eur. J.* **2000**, *6*, 2103–2111. (e) Balzani, V.; Credi, A.; Raymo, F. M.; Stoddart, J. F. *Angew. Chem., Int. Ed.* **2000**, *39*, 3349–3391.

(9) (a) Lee, S. J.; Luman, C. R.; Castellano, F. N.; Lin. W. *Chem. Commun.* **2003**, 2124–2125. (b) Ruben, M.; Lehn, J.-M.; Vaughan, G. *Chem. Commun.* **2003**, 1338–1339. (c) Tsuda, A.; Sakamoto, S.; Yamaguchi, K.; Aida, T. *J. Am. Chem. Soc.* **2003**, *125*, 15722–15723. (d) Mines, G. A.; Tzeng, B. C.; Stevenson, K. J.; Li, J.; Hupp, J. T. *Angew. Chem., Int. Ed.* **2002**, *41*, 154–157. (e) Castellano, R. K.; Craig, S. L.; Nuckolls, C.; Rebek, J., Jr. *J. Am. Chem. Soc.* **2000**, *122*, 7876–7882.

(10) (a) Bonchio, M.; Carofiglio, T.; Carraro, M.; Fornasier, R. Tonellato, U. *Org. Lett.* **2002**, *26*, 4635–4637. (b) Cibulka, R.; Vasold, R.; König, B. *Chem.–Eur. J.* **2004**, *10*, 6223–6231. (c) Bauer, A.; Westkämper, F.; Grimme, S.; Bach, T. *Nature* **2005**, *436*, 1139–1140.

(11) (a) Balzani, V.; Campagna, S.; Denti, G.; Juris, A.; Serroni, S.; Venturi, M. *Acc. Chem. Res.* **1998**, *31*, 26–34. (b) Kuramochi, Y.; Satake, A.; Kobuke, Y. *J. Am. Chem. Soc.* **2004**, *126*, 8668–8669. (c) De Schryver, F. C.; Vosch, T.; Cotlet, M.; van der Auweraer,

M.; Müllen, K. Hofkens, J. *Acc. Chem. Res.* **2005**, *38*, 514–522. (d) You, C.-C.; Hippius, C.; Grüne, M.; Würthner, F. *Chem.–Eur. J.* **2006**, *12*, 7510–7519.

(12) (a) Würthner, F.; Yao, S. *Angew. Chem., Int. Ed.* **2000**, *39*, 1978−1981. (b) Würthner, F.; Yao, S.; Debaerdemaker, T.; Wortmann, R. *J. Am. Chem. Soc.* **2002**, *124*, 9431−9447. (c) Rösch, U.; Yao, S.; Wortmann, R.; Würthner, F. *Angew. Chem., Int. Ed.* **2006**, *45*, 7026−7030. (d) Seibt, J.; Lohr, A.; Würthner, F.; Engel, V. *Phys. Chem. Chem. Phys.* **2007**, *9*, 6214−6218.

(13) (a) Yao, S.; Beginn, U.; Gress, T.; Lysetska, M.; Würthner, F. *J. Am. Chem. Soc.* **2004**, *126*, 8336−8348. (b) Lohr, A., Gress, T., Deppisch, M., Knoll, M., Würthner, F. *Synthesis* **2007**, 3073−3082. (c) Lohr, A.; Lysetska, M.; Würthner, F. *Angew. Chem., Int. Ed.* **2005**, *44*, 5071−5074.

(14) (a) Würthner, F.; Yao, S.; Heise, B.; Tschierske, C. *Chem. Commun.* **2001**, 2260−2261. (b) Würthner, F.; Yao, S. *J. Org. Chem.* **2003**, *68*, 8943−8949. (c) Würthner, F.; Schmidt, J.; Stolte, M.; Wortmann, R. *Angew. Chem., Int. Ed.* **2006**, *45*, 3842−3846.

(15) (a) Yagai, S.; Higashi, M.; Karatsu, T.; Kitamura, A. *Chem. Mater.* **2005**, *17*, 4392−1398. (b) Yagai, S.; Higashi, M.; Karatsu, T.; Kitamura, A. *Chem. Commun.* **2006**, 1500−1502.

(16) (a) Pereverzev, Y. V.; Prezhdo, O. V.; Dalton, L. R. *ChemPhysChem* **2004**, *5*, 1821–1830. (b) Wolff, J. J.; Wortmann, R. *Adv. Phys. Org. Chem.* **1999**, *32*, 121–217. (c) Verbiest, T.; Houbrechts, S.; Kauranen, M.; Clays, K.; Persoons, A. *J. Mater. Chem.* **1997**, *7*, 2175–2189.

(17) Würthner, F.; Wortmann, R.; Meerholz, K. *ChemPhysChem* **2002**, *3*, 17−31.

(18) For the optical properties and formation of intramolecular aggregates of tethered merocyanine or squaraine dyes, see: (a) Lu, L.; Lachicotte, R. J.; Penner, T. L.; Perlstein, J.; Whitten, D. G. *J. Am. Chem. Soc.* **1999**, *121*, 8146−8156. (b) Katoh, T.; Inagaki, Y.; Okazaki, R. *J. Am. Chem. Soc.* **1998**, *120*, 3623−3628. (c) Zeena, S.; Thomas, G. K. *J. Am. Chem. Soc.* **2000**, *123*, 7859−7865. (d) Ushakov, E. N.; Gromov, S. P.; Fedorova, O. A.; Pershina, Y. V.; Alfimov, M. V.; Barigelletti, F.; Flamigni, L.; Balzani, V. *J. Phys. Chem. A* **1999**, *103*, 11189−11193. (e) Arankumar, E.; Chithra, P.; Ajayaghosh, A. *J. Am. Chem. Soc.* **2004**, *126*, 6590−6598.

(19) For a general review on molecular tweezers, see: Harmata, M. *Acc. Chem. Res.* **2004**, *37*, 862−873.

(20) (a) Chen, C.-W.; Whitlock, H. W., Jr. *J. Am. Chem. Soc.* **1978**, *100*, 4921–4922. (b) Wilcox, C. S.; Greer, L. M.; Lynch, V. *J. Am. Chem. Soc.* **1987**, *109*, 1865–1867. (c) Zimmerman, S. C.; Mrksich, M.; Baloga, M. *J. Am. Chem. Soc.* **1989**, *111*, 8528–8530. (d) Harmata, M.; Barnes, C. L.; Karra, S. R.; Elahmad, S. *J. Am. Chem. Soc.* **1994**, *116*, 8392–8393. (e) Klärner, F.-G.; Panitzky, J.; Bläser, D.; Boese, R. *Tetrahedron* **2001**, *57*, 3673–3687.

(21) For self-association of molecular tweezers in organic solvents, see: (a) Reek, J. N. H.; Elemans, J. A. A. W.; de Gelder, R.; Beurskens, P. T.; Rowan, A. E.; Nolte, R. J. M. *Tetrahedron* **2003**, *59*, 175–185. (b) Wu, A.; Chakraborty, A.; Fettinger, J. C.; Flowers, R. A., II; Isaacs, L. *Angew. Chem., Int. Ed.* **2002**, *41*, 4028−4031. (c) Wu, A.; Mukhopadhyay, P.; Chakraborty, A.; Fettinger, J. C.; Isaacs, L. *J. Am. Chem. Soc.* **2004**, *126*, 10035–10043. (d) Reek, J. N. H.; Rowan, A. E.; Crossley, M. J.; Nolte, R. J. M. *J. Org. Chem.* **1999**, *64*, 6653−6663. (e) Haino, T.; Fujii, T.; Fukazawa, Y. *J. Org. Chem.* **2006**, *71*, 2572–2580.

(22) For self-association of molecular tweezers in water, see: (a) Elemans, J. A. A. W.; Rowan, A. E.; Nolte, R. J. M. *J. Am. Chem. Soc.* **2002**, *124*, 1532–1540. (b) Isaacs, L.; Witt, D.; Lagona, J. *Org. Lett.* **2001**, *3*, 3221–3224. (c) Reek, J. N. H.; Kros, A.; Nolte, R. J. M. *Chem. Commun.* **1996**, 245–247. (d) Klärner, F.-G.; Kahlert, B.; Nellesen, A.; Zienau, J.; Ochsenfeld, C.; Schrader, T. *J. Am. Chem. Soc.* **2006**, *128*, 4831−4841. (e) Isaacs, L.; Witt, D. *Angew. Chem., Int. Ed.* **2002**, *41*, 1905–1907. (f) Elemans, J. A. A. W.; de Gelder, R.; Rowan, A. E.; Nolte, R. J. M. *Chem. Commun.* **1998**, 1553–1554.

(23) For self-assembly of molecular clips into lamellar films, see: (a) Holder, S. J.; Elemans, J. A. A. W.; Donners, J. J. J. M.; Boerakker, M. J.; de Gelder, R.; Barberá, J.; Rowan, A. E.; Nolte, R. J. M. *J. Org. Chem.* **2001**, *66*, 391–399.

(24) For self-assembly of heteroaggregates see, for example: (a) Gabriel, G. J.; Iverson, B. L. *J. Am. Chem. Soc.* **2002**, *124*, 15174–15175. (b) Zhou, Q.-Z.; Jiang, X.-K.; Shao, X.-B.; Chen, G.-J.; Jia, M.-X.; Li, Z.-T. *Org. Lett.* **2003**, *5*, 1955–1958. (c) Colquhoun, H. M.; Zhu, Z.; Williams, D. J. *Org. Lett.* **2003**, *5*, 4353–4356. (d) Zhou, Q.-Z.; Jia, M.-X.; Shao, X.-B.; Wu, L.-Z.; Jiang, X.-K.; Li, Z.-T.; Chen, G.-J. *Tetrahedron* **2005**, *61*, 7117–7124. (e) Talukdar, P.; Bollot, G.; Mareda, J.; Sakai, N.; Matile, S. *Chem.–Eur. J.* **2005**, *11*, 6525–6532. (f) Ghosh, S.; Ramakrishnan, S. *Angew. Chem., Int. Ed.* **2005**, *44*, 5441–

5447. (g) Pease, A. R.; Jeppesen, J. O.; Stoddart, J. F.; Luo, Y.; Collier, C. P.; Heath, J. R. *Acc. Chem. Res.* **2001**, *34*, 433–444.

(25) (a) Bühner, M.; Geuder, W.; Gries, W.-G.; Hünig, S.; Koch, M.; Poll, T. *Angew. Chem., Int. Ed. Engl.* **1988**, *27*, 1553–1556. (b) Odell, B.; Reddington, M. V.; Slawin, A. M. Z.; Spencer, N.; Stoddart, J. F.; Williams, D. J. *Angew. Chem., Int. Ed. Engl.* **1988**, *27*, 1547–1550.

(26) (a) Whitlock, B. J.; Whitlock, H. W. *J. Am. Chem. Soc.* **1994**, *116*, 2301–2311. (b) Izatt, R. M.; Bradshaw, J. S.; Pawlak, K.; Bruening, R. L.; Tarbet, B. J. *Chem. Rev.* **1992**, *92*, 1261–1354.

(27) (a) Bamberger, E. *Ann. d. Chem.* **1890**, *257*, 1–55. (b) Katz, T. J.; Liu, L.; Willmore, N. D.; Fox, J. M.; Rheingold, A. L.; Shi, S.; Nuckolls, C.; Rickman, B. H. *J. Am. Chem. Soc.* **1997**, *119*, 10054–10063. (c) Zagotto, G.; Palumbo, M.; Uriarte, E.; Bonsignore, L.; Delogu, G.; Podda, G. *Il Farmaco* **1998**, *53*, 675–679.

(28) For reductive aminations using triethylsilane as reductant, see: Dubé, D.; Scholte, A. A. *Tetrahedron Lett.* **1999**, *40*, 2295–2298.

(29) (a) Coleman, B. D.; Fuoss, R. M. *J. Am. Chem. Soc.* **1955**, *77*, 5472–5476. (b) Morley, J. O.; Morley, R. M.; Docherty, R.; Charlton, M. H. *J. Am. Chem. Soc.* **1997**, *119*, 10192–10202.

(30) Blacker, J.; Jazwinski, J.; Lehn, J.-M. *Helv. Chim. Acta* **1987**, *70*, 1–12.

(31) Rosa, J. C.; Galanakis, D.; Piergentili, A.; Bhandari, K.; Ganellin, C. R.; Dunn, P. M.; Jenkinson, D. H. *J. Med. Chem.* **2000**, *43*, 420–431.

(32) For reviews on mass spectroscopy in supramolecular chemistry, see: (a) Schalley, C. A. *Int. J. Mass Spectrom.* **2000**, *194*, 11–39. (b) Baytekin, B.; Baytekin, H. T.; Schalley, C. A. *Org. Biomol. Chem.* **2006**, *4*, 2825–2841.

(33) (a) Connors, K. A. *Binding Constants*; Wiley: New York, 1987. (b) Martin, R. B. *Chem. Rev.* **1996**, *96*, 3043–3064.

(34) Kasha, M.; Rawls, H. R.; Ashraf El-Bayoumi M. *Pure Appl. Chem.* **1965**, *11*, 371–392.

(35) The transition dipole moment of the merocyanine chromophore is oriented along the long molecular axis.

(36) The electric permittivity ε_r of $CHCl_3$ and DCE are 4.81 and 10.42, while the refractive indices n_D^{20} are 1.444 and 1.446, respectively. Data from *CRC Handbook of Chemistry and Physics*; Lide, D. R., Ed.; CRC Press: Boca Raton, 1995.

(37) For the determination of $\Delta H°$ and $\Delta S°$, a linear relationship between ln K_D and T^{-1} is required. In the present cases such a linear relation is not observed, which was attributed to the strong dependence of ε_r of chloroform on temperature from ε_r = 5.02 at 283 K to ε_r = 4.29 at 323 K. For comparison, these values correspond to the ε_r values of BuOAc and Et_2O at 293 K, respectively. Thus, ΔH shows a temperature dependence in the present case where bimolecular association is driven by electrostatic attractions (see ref. 12). Interestingly, the strong dependence of ε_r on temperature is also expressed in the value of the absorption maximum λ_{max} of this strongly solvatochromic type of merocyanine dyes (see Figure A2).

(38) (a) Ercolani, G. *Chem. Commun.* **2001**, 1416–1417. (b) Ercolani, G. *J. Phys. Chem. B* **1998**, *102*, 5699–5703. (c) Chi, X.; Guerin, A. J.; Haycock, R. A.; Hunter, C. A.; Sarson, L. D. *J. Chem. Soc.*, *Chem. Commun.* **1995**, 2563–2565.

(39) Since also the condition $EM\sigma K \geq 185n$ is verified for the present cases, a nearly complete aggregation into the dimers can be obtained at a certain initial monomer concentration, see ref. 38 for details.

(40) Crystal structures of this type of merocyanine chromophores reveal a significant bond length equilibration within the conjugated path (ref. 12a,b). Thus, a bond length of 1.435 Å was obtained for the bond between C5 and C6, which is very close to that for a standard single-bond (1.46 Å).

(41) Grimme, S.; Antony, J.; Schwabe, T.; Mück-Lichtenfeld, C. *Org. Biomol. Chem.* **2007**, *5*, 741–758.

(42) *Hyperchem*™; Hypercube Inc.: 1115 NW 4th Street, Gainesville, FL 32601, USA.

(43) (a) Rebek, J., Jr.; Askew, B.; Killoran, M.; Nemeth, D.; Lin, F.-T. *J. Am. Chem. Soc.* **1987**, *109*, 2426–2431. (b) Zimmerman, S. C.; Mrksich, M.; Baloga, M. *J. Am. Chem. Soc.* **1989**, *111*, 8528–8530.

(44) (a) Cloninger, M. J.; Whitlock, H. W. *J. Org. Chem.* **1998**, *63*, 6153–6159. (b) Adams, H.; Harris, K. D. M.; Hembury, G. A.; Hunter, C. A.; Livingstone, D.; McCabe, J. F.

Chem. Commun. **1996**, 2531–2531. (c) Carver, F. J.; Hunter, C. A.; Jones, P. S.; Livingstone, D. J.; McCabe, J. F.; Seward, E. M.; Tiger, P.; Spey, S. E. *Chem.–Eur. J.* **2001**, *7*, 4854–4862.

(45) (a) Davydov, A. S. *Theory of Molecular Excitons*; Plenum Press: New York, 1971. (b) Fidder, H.; Knoester, J.; Wiersma, D. A. *J. Chem. Phys.* **1991**, *95*, 7880–7890.

(46) Perrin, D. D.; Armarego, W. L. F. *Purification of Laboratory Chemicals*; Pergamon Press: Oxford, 1980.

3.6 Appendix

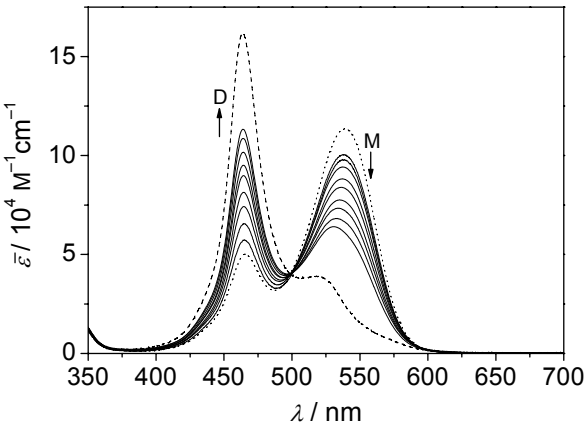

Figure A1. Concentration-dependent UV–vis spectra of **3** in 1,2-dichloroethane at 298 K ($c = 5\times10^{-5} - 1.5\times10^{-6}$ M). The arrows indicate the decrease in the intensity of the monomer band and the appearance of a dimer band with increasing concentration. The spectra of the monomer (···) and the dimer (---) were calculated from the data at two different concentrations and the dimerization constant.

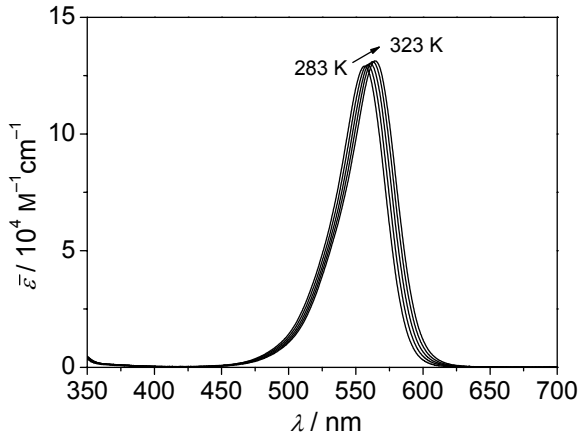

Figure A2. Temperature-dependent UV–vis spectra of dye **1a** in $CHCl_3$ at 4.5×10^{-6} M. The arrow indicates the spectral shift upon increasing temperature from 283 to 323 °C.

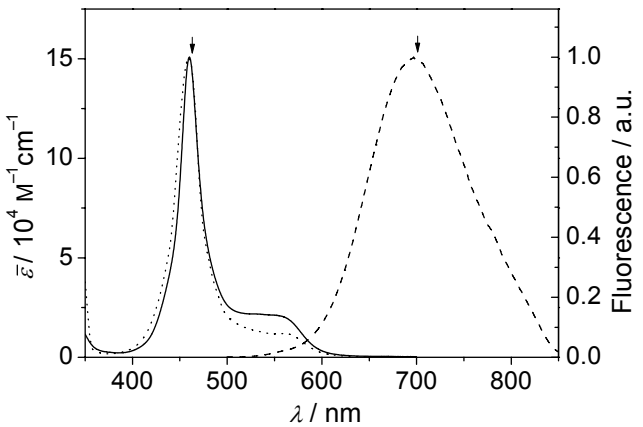

Figure A3. UV–vis absorption (—, left scale), fluorescence emission (---, right scale, λ_{ex} = 462 nm) and excitation (···, right scale, λ_{em} = 700 nm) spectra of dye **3** dimers in $CHCl_3$ at 1×10^{-6} M (298 K).

Table A1. ^{1}H and ^{13}C NMR spectral data of bis(merocyanine) **3** recorded in DMF-d_7 (c = 3 mM) and $CDCl_3$ (c = 10 mM) at 293 K.

position	DMF-d_7		$CDCl_3$	
	δ_H (J / Hz)	δ_C	δ_H (J / Hz)	δ_C
1,2	8.52 (d, 7.0, 4H)	142.46	7.44 (br, 2H)	139.67 (br)
1′,2′			7.52 (br, 2H)	141.20 (br)
3,4	7.82 (d, 7.0[a], 4H)	121.12	7.05[a] (br, 2H)	
3′,4′			7.29 (d, 4.8, 2H)	
5		156.89		156.34
5′				155.53
6	7.81 (d,14.8, 2H)	114.68	7.71 (d, 14.8, 1H)	113.10
6′			7.94 (d, 14.8, 1H)	114.77
7	7.85 (d, 14.9, 2H)	138.94	7.34 (d, 14.7, 1H)	139.26
7′			7.10 (d, 15.2[a], 1H)	136.43
8		156.05		156.16
8′				155.86
9		163.30		163.59
9′				163.05
10		163.03		162.57
10′				162.40
11		86.15		88.21
11′				86.76
12		105.44		105.35
12′				104.76
13	2.47 (s, 6H)	18.39	2.15 (s, 3H)	18.86
13′			1.76 (s, 3H)	18.11
14,14′		119.89		118.47, 118.84
15α	5.22 (s, 4H)	38.69	5.22 (d, 16.3, 1H)	39.36
15β			5.18 (d, 16.3, 1H)	
15′α			5.45 (d, 16.0, 1H)	38.82
15′β			4.97 (d, 16.0, 1H)	
16		125.81		125.23
16′				123.72
17	6.89 (s, 2H)	122.80	6.82 (s, 1H)	120.91
17′			6.73 (s, 1H)	120.71
18		123.29		122.99
19		133.86		133.88
20	7.27 (s, 2H)	105.17	7.04 (s, 1H)	104.82
20′			7.07 (s, 1H)	104.98
21		155.44		155.53
21′				155.02
22	4.17 (t, 6.5, 4H)	67.86	4.09 (br, 2H)	67.40
22′			4.14 (br, 2H)	67.40

23	1.87 (m, 4H)	31.60	1.84 (m, 2H)	31.36
23′			1.93 (m, 2H)	31.52
24	1.59 (m, 4H)	19.62	1.55 (m, 2H)	19.46
24′			1.63 (m, 2H)	19.57
25	1.02 (t, 7.4, 6H)	13.85	0.98 (t, 7.3, 3H)	13.96
25′			1.08 (t, 7.3, 3H)	14.12
26,26′	4.39 (t, 7.4, 4H)	59.08	3.9–4.1 (br, 4H)	60.16, 59.60
27,27′	1.93 (mbr, 4H)	31.21	1.79 (br, 4H)	30.48, 30.59
28–36, 28′–36′	1.35–1.22 (m, 36H)	22.81, 26.26, 29.22, 29.72, 32.10	1.60 (br, 4H), 1.14–1.12 (m, 32 H)	22.67, 26.20, 28.97, 29.33, 29.35, 29.44, 29.56, 29.64, 29.66, 31.88, 31.92
37,37′	0.87 (t, 7.0, 6H)	13.97	0.89–0.83 (br, 6H)	14.12

[a] Estimated value due to partial overlap or broadening of signals

Chapter 4

Self-Assembly of a Calix[4]arene-tethered Bis(merocyanine) into a Trimeric Cyclic Array

Abstract: In this chapter the supramolecular construction of a discrete cyclic architecture of merocyanine chromophores that contains three merocyanine dimer units is reported. This trimeric cyclic array was achieved by dipolar interaction directed self-assembly of an appropriately designed calixarene-bis(merocyanine) conjugate. UV–vis aggregation study of this calixarene-tethered bis(merocyanine) dye accompanied by a mathematical treatment for cyclic trimerization revealed the formation of a trimeric complex with high thermodynamic stability, which can be attributed to the formation of three intermolecular chromophore dimer units by dipolar aggregation. Further evidence for the formation of trimeric complex was obtained from MALDI-TOF MS and scanning tunneling microscopy (STM).

4.1 Introduction

The synthesis of molecules that utilize noncovalent interactions including metal-ion coordination, hydrogen bonding and π–π interactions to form defined linear, cyclic, or three-dimensional structures by self-assembly has been a field of considerable interest.[1,2] In the work of Würthner and coworkers, it has been shown that dipolar merocyanine dyes **1** form centrosymmetric dimer aggregates with high binding constants in nonpolar solvents like dioxane or CCl_4 in the range of $K_D = 10^6\ M^{-1}$ (Figure 1a,b).[3a] This dimerization arises predominantly from dipole–dipole interaction between these chromophores, which possess an exceptionally strong ground-state dipole moment μ_g of about 17 D owing to a major contribution of the zwitterionic resonance structure. The geometry of these dimer aggregates is highly defined, which shows that the dipolar interactions are directional and, therefore, highly promising for the construction of more elaborate supramolecular architectures. Accordingly, the formation of highly defined supramolecular polymers (see Chapters 2.2 and 5) as well as discrete bimolecular π-stacks (see Chapter 3) was achieved from ditopic bis(merocyanine) monomers that are tethered by appropriate spacers to guide self-assembly into desired architectures.[4,5] Thus, we envisaged that even cyclic arrays of merocyanine dimers should be accessible by self-assembly of properly tethered bis(merocyanine) dyes. From a functional point of view such noncovalent cyclic dye arrays composed of dimeric pairs of chromophores may be of interest because of their structural resemblance to natural light-harvesting systems.[6-8]

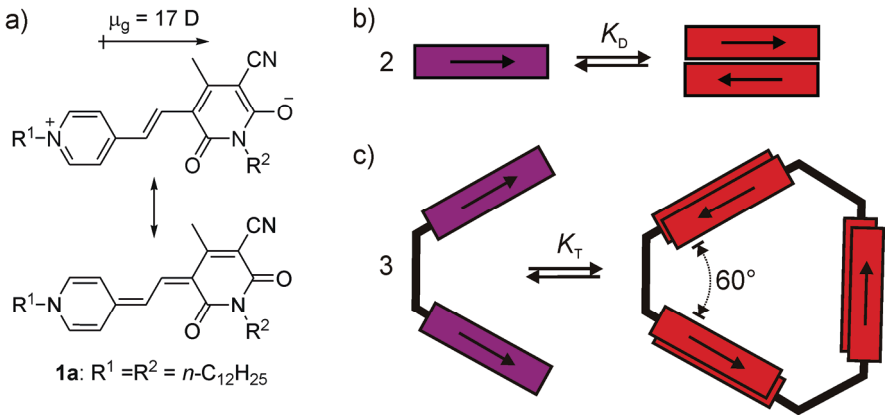

Figure 1. a) Resonance structures of highly dipolar merocyanine dyes **1**. b) Schematic representation of dimerization of merocyanine dyes into centrosymmetric aggregates by dipole–dipole interactions. c) Schematic representation of our concept for the construction of cyclic trimers containing three merocyanine dimer units that are formed by self-assembly of appropriately tethered bis(merocyanine) building blocks. The different colors represent the hypsochromic color shift upon formation of sandwich-type aggregates of merocyanine chromophores.

Our approach for the construction of such hitherto unknown cyclic self-assembled structures of merocyanine dyes is based on the intermolecular aggregation of merocyanine dyes into dimeric pairs that directs the self-assembly of suitably tethered bis(merocyanine) building blocks into a cyclic geometry (Figure 1c). To realize this concept, bis(merocyanine) building block **6** in which two merocyanine chromophores are attached at the wide upper-rim of a calix[4]arene in cone conformation was synthesized (see Scheme 1).[9,10] This calixarene-bis(merocyanine) conjugate should meet the required structural properties for self-assembly into a trimeric cyclic array since the calixarene scaffold provides structural predisposition of the chromophores which can easily adopt an angle of 60° as well as the structural rigidity to minimize the entropic costs for self-assembly.[11]

4.2 Results and Discussion

4.2.1 Synthesis

Calixarene-tethered bis(merocyanine) dye **6** was prepared according to Scheme 1. The starting material dinitrocalixarene **2** was synthesized according to a literature procedure.[12] Reduction of **2** to the diamino derivative and further reaction with pyrylium salt **3**[13] afforded dipyridinium salt **4** in 55% yield. Condensation of **4** with enamino pyridone **5**[3b] gave the desired calix[4]arene-bis(merocyanine) conjugate **6** in 7% yield. Notably, the methyl substituents at the *ortho* positions of the pyridine donor group of the merocyanine chromophore

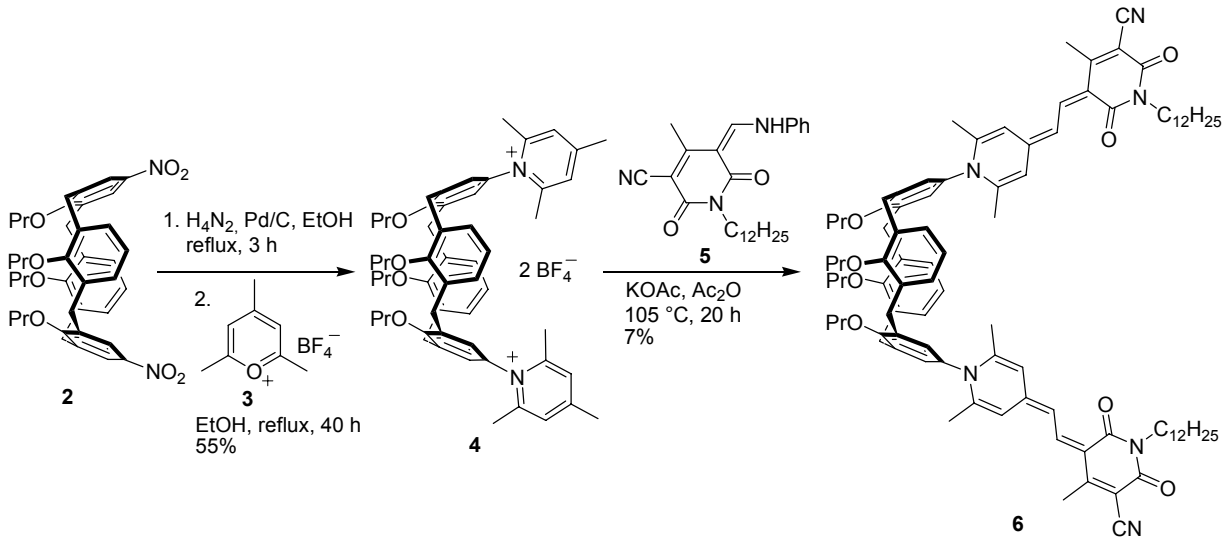

Scheme 1. Synthesis of calixarene-tethered bis(merocyanine) dye **6**.

demand a twisted arrangement of the chromophore plane with respect to the calixarene phenylene unit as revealed by the distinct chemical shifts of the towards inward and outward of calixarene scaffold directed methyl protons.

4.2.2 UV–vis aggregation studies

Concentration-dependent UV–vis experiments have been extensively utilized to study dye aggregation in solution. With this method, electronic interactions between the π-conjugated systems of the dyes may be elucidated and the concentration range for aggregate formation can be easily assessed. For simple processes such as dimerization or polymerization, binding constants and Gibbs binding enthalpies may be obtained from these data.[14] In addition, structural information is accessible from the absorption spectrum of the aggregate due to excitonic coupling of the transition dipole moments of the chromophores.[15] Thus, UV–vis dilution studies were conducted for calixarene-tethered bis(merocyanine) dye **6** as well as for the simple alkyl-substituted merocyanine dye **1a** (Figure 2). Since the dipolar interactions between merocyanine dyes are strongly dependent on solvent polarity, the dilution experiments were performed in chloroform, which is a solvent of intermediate polarity and was found to be best suited for studying the aggregation equilibria of the present dyes in the concentration range suitable for UV–vis absorption spectroscopy. Significant spectral changes were observed for dyes **6** and **1a** upon variation of concentration in the range from 10^{-6} to 10^{-3} M using cells with path length between 0.01 and 1 cm (Figure 2).

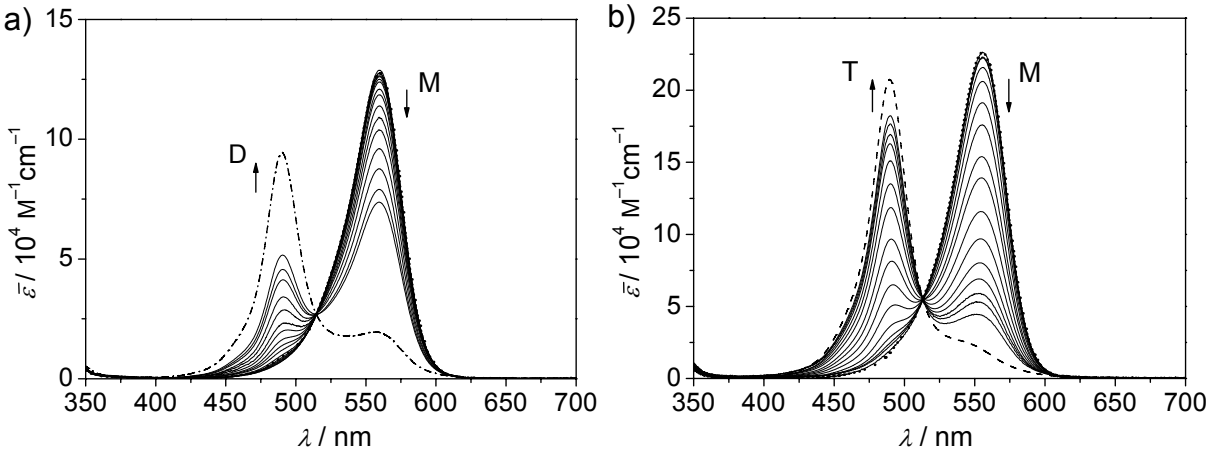

Figure 2. Concentration-dependent UV–vis spectra of a) **1a** ($c = 1.4\times10^{-3}$ to 4.5×10^{-6} M) and b) **6** ($c = 3\times10^{-4}$ to 1×10^{-6} M) in $CHCl_3$ at 298 K. The arrows indicate the decrease in the intensity of the monomer band and the appearance of the aggregate band with increasing concentration. The spectra of pure monomeric dyes (M, ····) and the respective pure dimer (D, -·-·) and trimer (T, ---) aggregates were derived from the data at two different concentrations and the aggregation constants.

For dye **1a**, the UV–vis spectra in dilute solution can be ascribed to the pure monomeric dyes with the most intensive charge-transfer band occurring at longer wavelength (denoted as M in Figure 2a).[3] With increasing concentration, the intensity of the monomer band at 559 nm (M) is reduced along with the concomitant appearance of a hypsochromically shifted D-band at 490 nm due to the excitonic coupling of the two chromophores in the dimer formed.[3] A second excitonic band at longer wavelength (~560 nm) is indicative for a slightly twisted arrangement of the two chromophores in the dimer.[3,16] In the case of calixarene-tethered bis(merocyanine) dye **6** very similar spectral changes are observed (Figure 2b). With increasing concentration, the monomer band at 556 nm (M) decreases and a hypsochromically shifted aggregate band at 490 nm (T) arises concomitantly. Over a considerable concentration range, a well-defined isosbestic point at 513 nm occurs which clearly indicates the presence of a two-state equilibrium between the monomers and well-defined aggregates. Both the monomer and the aggregate spectrum of **6** are in close agreement with the respective spectra observed for reference dye **1a**, showing absorption coefficients that are about twice as large as those obtained for mono-chromophoric **1a**. Thus, the spectral properties of monomeric and aggregated **6** are barely affected by the calixarene scaffold. The similar monomer absorption spectrum **1a** is quite reasonable since the twisted arrangement of the chromophore planes with respect to the phenylene units of the calixarene scaffold prevents further conjugation of the chromophore, while the repulsive interactions of the parallel oriented dipole moments prevents intramolecular aggregation in a pinched cone calixarene conformation with two closely stacked dyes.[9] More importantly, the close agreement of the aggregate spectrum of **6** to the dimer spectrum of **1a** indicates that the chromophores of **6** form independent intermolecular

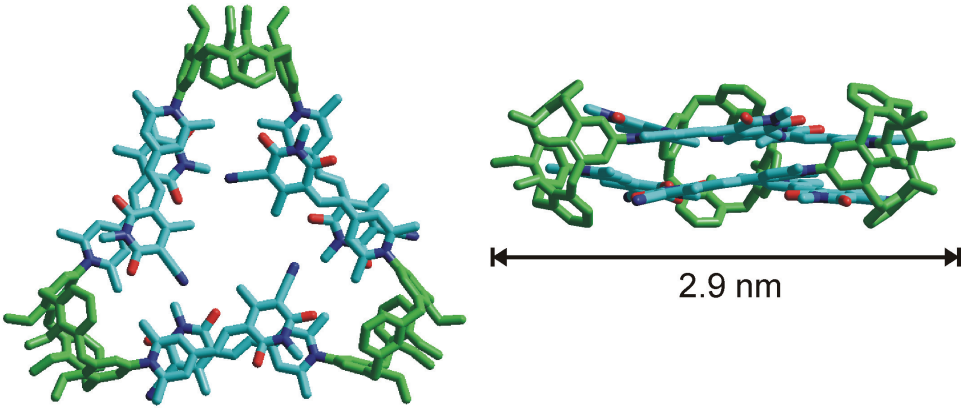

Figure 3. Top- and sideview of the MM+ geometry-optimized molecular model for cyclic trimers of **6**.[17] For simplicity, all alkyl substituents are replaced for methyl groups and hydrogen atoms are omitted.

chromophore pairs, which is in accordance with the cyclic trimer structure obtained from molecular modeling (Figure 3) and clearly excludes an extended stack arrangement as observed for self-assemblies of other bis(merocyanine) dyes which show a more hypsochromically shifted aggregate band. (see Chapters 2.3, 3, and 5).[4]

To elucidate the self-assembly of **6** into cyclic trimers and also to exclude the possibility of formation of linear oligomers, the concentration-dependent spectral changes were evaluated according to a mathematical model that describes a two-state equilibrium between monomers and cyclic trimers. As shown below, this model was derived in accordance to the dimerization model (see Chapter 3), but in the present case of trimerization a more elaborate method for solving a cubic equation is required.

For the two-state equilibrium between monomer (**M**) and trimer (**T**) species

$$3\,\mathbf{M} \rightleftharpoons[K_T] \mathbf{T} \tag{1}$$

the trimerization constant K_T can be given as

$$K_T = \frac{c_T}{c_M^3} \tag{2}$$

where c_M and c_T denote the respective concentration of monomers and trimers in solution. By introducing a fraction of monomers denoted as α_M, the concentrations of monomer and trimer c_M and c_T can be given as fraction of the total dye concentration c_0:

$$c_M = \alpha_M c_0 \tag{3}$$

$$c_T = \frac{(1-\alpha_M)}{3} c_0 \tag{4}$$

Combining eqs 2 to 4 yields the trimerization constant K_T as a function of monomer fraction α_M and the overall monomer concentration c_0:

$$K_T = \frac{1-\alpha_M}{3\alpha_M^3 c_0^2} \tag{5}$$

Equation 5 can be rewritten as:

$$\alpha_M^3 + \frac{1}{3K_T c_0^2}\alpha_M - \frac{1}{3K_T c_0^2} = 0 \tag{6}$$

This cubic equation can be analytically solved using Cardano's method[18] to yield the fraction of monomers α_M as a function of the overall monomer concentration c_0 and the trimerization constant K_T as given in eq 7:

$$\alpha_M = \sqrt[3]{\frac{1}{6K_T c_0^2} + \sqrt{\left(\frac{1}{9K_T c_0^2}\right)^3 + \left(\frac{1}{6K_T c_0^2}\right)^2}} + \sqrt[3]{\frac{1}{6K_T c_0^2} - \sqrt{\left(\frac{1}{9K_T c_0^2}\right)^3 + \left(\frac{1}{6K_T c_0^2}\right)^2}} \quad (7)$$

The apparent molar absorptivity $\bar{\varepsilon}$ of the dye in solution may be expressed in the form

$$\bar{\varepsilon} = \alpha_M \varepsilon_M + (1 - \alpha_M)\varepsilon_T \quad (8)$$

where ε_M and ε_T are the molar absorptivities of a free and the trimer-bound monomer unit, respectively.

Nonlinear regression analysis of the apparent molar absorptivities of **6** at certain wavelengths as a function of dye concentration according to this cyclic trimerization model (eqs 7 and 8) gave an excellent fit and yielded a trimerization constant K_T of 1.9×10^9 M^{-2} (Figure 4). This value corresponds to a Gibbs energy of trimerization $\Delta_T G° = -RT\ ln\ (K / M^{-2})$ of -52.9 kJ mol^{-1}. In comparison, for simple alkyl-substituted dye **1a** a dimerization constant K_D of 590 M^{-1} and a corresponding Gibbs energy of dimerization $\Delta_D G°$ of -15.8 kJ mol^{-1} was found according to the analysis based on the dimerization model (see Chapter 3).[14] Thus, the Gibbs energy of trimerization for **6** is slightly higher than three times the Gibbs energy of dimerization for **1a** which is in accordance with the formation of three chromophore pairs in the cyclic trimer complex of **6**. Unfortunately, the determination of the enthalpic and entropic contribution, $\Delta H°$ and $\Delta S°$, to these Gibbs energies by means of a van't Hoff plot was not successful due to the strong dependence of ε_r of chloroform on the temperature.[19] Nevertheless, the considerably increased thermodynamic stability of the present trimolecular aggregates from calixarene bis(merocyanine) dye **6** with respect to the dimers of reference **1a** is evident from the concentration where half of the monomers are incorporated into the respective aggregates, *i.e.*, where α_M equals 0.5 (Figure 4). For **6**, this α_M value is already reached at a total monomer concentration of 2.6×10^{-5} M, which is nearly two orders of magnitude lower than the respective concentration for **1a** (1.4×10^{-3} M). Thus, the increased enthalpic contribution due to the formation of three chromophore pairs in the trimeric cyclic complex of **6** with respect to one chromophore pair in the dimer of **1a** strongly overweighs the higher entropic loss for the

former caused by the self-assembly of three units with respect to only two in the case of the latter dye.

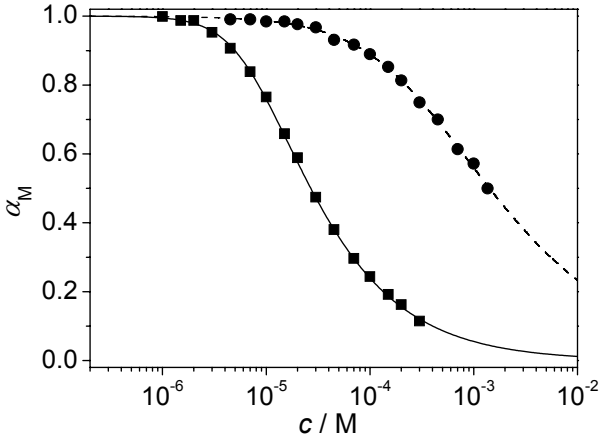

Figure 4. Fraction of monomer (α_M), calculated from UV–vis data at certain wavelengths, as a function of dye concentration and nonlinear regression analysis of the data points for **6** (■, at 535 nm) and **1a** (●, at 505 nm) in $CHCl_3$ based on the trimerization (solid curve) and dimerization (dashed curve) model.

It is important to note that the formation of linear oligomers of bis(merocyanine) **6** by the intermolecular dimerization of the chromophores can be ruled out, since the analysis of the UV–vis dilution data based on the isodesmic model[14] gave only poor fits. Also, the enhanced aggregation constant obtained from such analysis can hardly be explained by non-cooperative formation of dimeric chromophore pairs to form linear oligomers of **6**. Theoretically, however, above a certain overall monomer concentration known as the effective molarity *EM*, the formation of linear chains will be favored over cyclic aggregates.[20] The effective molarity for the formation of a macrocyclic assembly consisting of *i* molecules is given as:

$$EM = K_i / (\sigma K)^i \tag{9}$$

where K_i denotes the oligomerization constant (here trimerization constant K_T) of the cyclic assembly, σ is a symmetry number (equals 4 in the present case), and K denotes the dimerization constant of the respective monotopic dye.[20] For the present trimerization process in chloroform an effective molarity *EM* of 0.145 M can be obtained if we assume that K equals to 590 M^{-1}, which is the dimerization constant for reference dye **1a**. Since this *EM* value is far higher than the concentration range under consideration in the present studies, the formation of linear chains can be excluded for the aggregation of bis(merocyanine) dye **6** under the present conditions.

From the structural point of view, the aggregate model presented in Figure 3 is related to so-called double rosette aggregates developed by Reinhoudt and coworkers since in both systems three calix[4]arene units constitute the corners of triangular cyclic aggregate structure.[21] In the case of these double rosettes the calixarene scaffolds are diametrically functionalized with two melamine units at the upper-rim and these calixarene-melamine conjugates form thermodynamically very stable cyclic aggregates by co-aggregation with a large variety of different barbiturates and cyanurates. These aggregates are held together by the cooperative formation of 36 hydrogen bonds and π-stacking interactions. It was also reported that, when a hydrogen-bonding barbiturate-acceptor merocyanine dye was co-aggregated a circular array of six merocyanine chromophores was formed.[21b] UV–vis dilution studies in chloroform revealed that half of these aggregates were formed at a calixarene unit concentration of 7.5×10^{-5} M, a value which is similar to the one found for the present aggregates of calixarene bis(merocyanine) **6**. However, in the latter case the aggregate is hold together only by the formation of three merocyanine dimer units by dipolar interaction between the merocyanine chromophores whilst hydrogen-bonds are totally absent. This comparison underlines the strength of the "dipolar aggregation" binding motif.[3a]

4.2.3 Mass spectrometric study

Further evidence for the self-assembly of the present bis(merocyanine) dye into a trimolecular complex was provided by mass spectrometry.[22] A sample for MALDI-TOF mass spectrometry was prepared by solvent evaporation from a chloroform solution of **6** containing 2-[(2*E*)-3-(4-*tert*-butylphenyl)-2-methylprop-2-enylidene]malononitrile (DCTB) as matrix. The mass spectrum recorded in positive ion mode showed a peak corresponding to the singly charged trimer cation (*m*/*z* found 4463.97, calcd. for $[M_3]^+$ 4464.09)[23] along signals

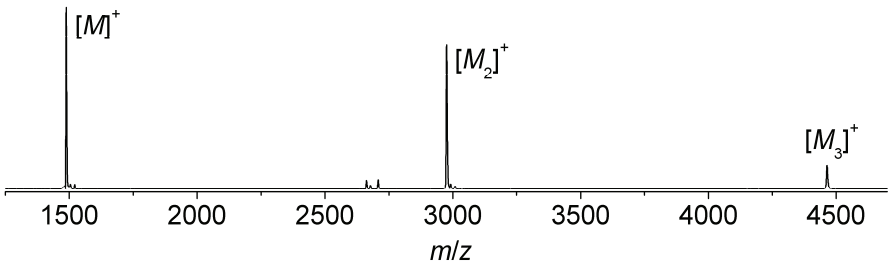

Figure 5. MALDI-TOF spectra of bis(merocyanine) dye **6** (matrix: DCTB, solvent: $CHCl_3$). $[M]^+$, $[M_2]^+$, and $[M_3]^+$ denote the mass peaks corresponding to the singly charged monomer, dimer, and trimer cation, respectively.

corresponding to the singly charged dimer and monomer cation (Figure 5) which supports the formation of discrete trimer aggregates in solution and partial fragmentation into dimers and monomers in the gas phase.

4.2.4 STM study[i]

Scanning tunneling microscopy (STM) measurements at the liquid-solid interface were performed aiming at a direct visualization of the self-assembled cyclic trimer structure of dye **6**. For this, a drop of a solution of **6** in 1,2,4-trichlorobenzene (TCB) was applied on a Au(111) substrate and the STM tip was immersed in the solution. TCB was used as solvent because it provides both, a low vapor pressure required for STM measurements at the liquid-solid interface and nearly complete aggregation even at low concentration due to the lower polarity of TCB with respect to $CHCl_3$.[24] Figure 6 shows the STM images at a tunneling current of 0.15 nA. In the large-scale image globular objects can be observed, which are randomly adsorbed over the whole surface (Figure 6a). The higher resolution image reveals that these objects are discrete and have a diameter of 3.4 ± 0.9 nm as obtained from cross-section analysis (Figure 6b,c).

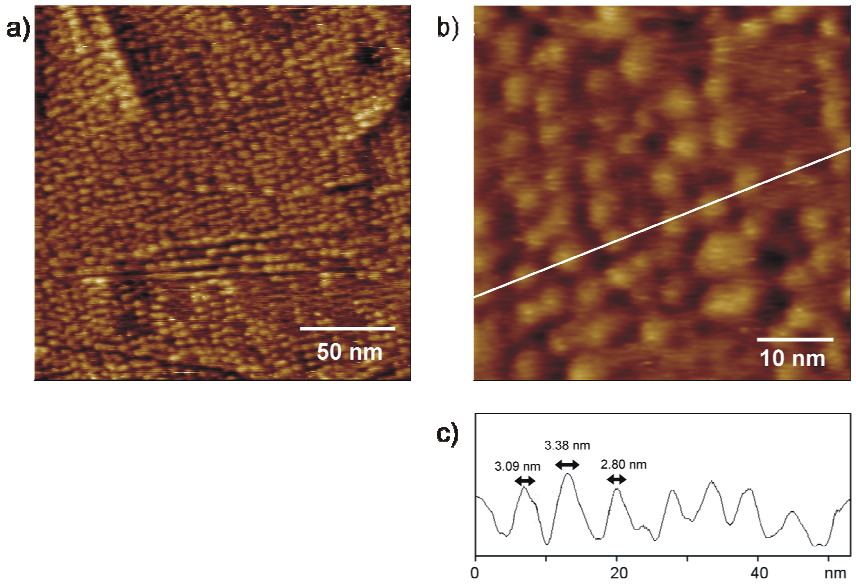

Figure 6. a,b) STM images of cyclic trimers of calixarene bis(merocyanine) **6** at the Au(111)/trichlorobenzene interface (E_{bias} = −0.6 V, I = 0.15 nA). c) Cross-section analysis along the line in Figure 6b.

[i] STM studies were performed by Dr. Shinobu Uemura

According to the MM+ geometry-optimized model of the trimolecular complex of **6** shown in Figure 3 the lateral dimension of the cyclic trimers from calixarene to calixarene corner is 2.9 nm. Taking into account the dimensions of the alkyl substituents at the calixarene units and at the imide N atoms of the chromophores, this value corresponds well to the diameter of the objects observed by STM. High-resolution images like those reported for monolayers of adsorbed organic dyes were attempted.[25] However, upon increasing the tunneling current to 0.20 nA and above, the spherical objects disappeared due to scratching of the aggregates by the tip. This effect indicates a considerable height of the aggregates as well as a weak aggregate–substrate interaction. From the dimensions of the obtained objects and the scratching behavior at higher tunneling current a cyclic trimer structure like the one shown in Figure 3 is very reasonable.

4.3 Conclusion

In summary, the present chapter described the construction of a trimolecular bis(merocyanine) complex containing three chromophore dimer units in a cyclic topology. For this, a bis(merocyanine) dye tethered with a preorganizing calix[4]arene scaffold was synthesized and self-assembly was studied by concentration-dependent UV–vis absorption measurements and evaluated by a mathematical model for cyclic trimerization, as well as MS and STM measurements. The present study demonstrates the potential of dipolar aggregation as a novel directional and specific supramolecular binding motif for the creation of more elaborate supramolecular architectures beyond simple dimer aggregates.

4.4 Experimental Section

Solvents and reagents were obtained from commercial suppliers and purified according to standard procedures.[26] Dinitrocalixarene **2**,[12] pyrylium salt **3**,[13] and pyridone **5**[3b] were prepared according to literature procedures. Column chromatography was performed on silica gel (Merck Silica 60, particle size 0.04−0.063 mm) and TLC was conducted on silica gel plates (60 F_{254}, Merck). Semi-preparative HPLC was performed on a JASCO system (PU 2080 PLUS) with a UV–vis detector (UV 2077 PLUS) using a semi-preparative NUCLEOSIL 100-5 NO_2 column (Macherey&Nagel). Melting points were determined on a Linkam TP 94 heating stage and are uncorrected. NMR experiments were conducted on a Bruker Avance 400 with TMS or residual undeuterated solvent as internal standard. High-resolution ESI-TOF mass spectrometry was carried out on a microTOF focus instrument (Bruker Daltronik GmbH) and

MALDI-TOF measurements were carried out on a Bruker Autoflex II. Elemental analysis was performed on a CHNS 932 analyzer (Leco Instruments GmbH).

UV–vis Absorption. UV–vis spectra were measured on a Perkin Elmer Lambda 950 spectrometer in conventional quartz cells of 0.01–1 cm path length to cover a suitable concentration range. The spectral bandwidth and the scan rate were 2 nm and 140 nm/min, respectively. The stock solutions of each compound were accurately prepared, and dilutions of these stocks were used for absorption measurements over a concentration range. The temperature was controlled with a PTP-1 peltier element (Perkin Elmer). The solvents for UV–vis absorption were of spectroscopic grade and used as received.

STM Measurements. Measurements at the liquid-solid interface were performed using a Nanoscope IV Multimode with low-current module (Veeco Instruments Inc., Santa Barbara, USA) at room temperature. STM tips were mechanically cut from a Pt/Ir (90/10, 0.25 mm) wire and tested on cleaved HOPG surfaces. Au(111) surface (MaTeck) was used as a substrate. Before each measurement, Au(111) surface was annealed in a flame. A droplet of **6** in 1,2,4-trichlorobenzene (Aldrich) was put onto a Au(111) surface, the tip was then immersed into the solution, and the sample was imaged in the constant current mode at the negative sample bias.

1,1′-[25,26,27,28-Tetrapropoxypentacyclo[19.3.1.1^{3,7}.1^{9,13}.1^{15,19}]octacosa-1(25),3(28),4,6,9(27),10,12,15(26),16,18,21,23-dodecaene-5,17-diyl]bis(2,4,6-trimethylpyridinium) ditetrafluoroborate (4). A mixture of dinitrocalixarene **2** (1.0 g, 1.46 mmol) and Pd/C (10%, 100 mg) in EtOH (26 mL) was heated to reflux and a solution of hydrazine monohydrate (1.42 mL) in EtOH (4 mL) was added within 20 min. The solution was refluxed for further 3 h. After cooling to rt the solution was filtered and the filter cake was washed with CH_2Cl_2. The filtrate was washed with H_2O, brine and again H_2O, and dried over $MgSO_4$. The solvent was removed under reduced pressure. The residue was dissolved in EtOH (25 mL) and pyrylium salt **3** (573 mg, 2.73 mmol) was added. The solution was refluxed for 40 h and cooled down slowly to rt. A precipitate was formed slowly, which was filtered off and washed with cold EtOH. Recrystallization from EtOH afforded a white powder. Yield: 0.81 g (0.80 mmol, 55%). Mp 247–250 °C (decomp.). ^{1}H NMR (400 MHz, MeOH-d_4, 25 °C): δ 7.85 (s, 2H, py-H), 7.82 (s, 2H, py-H), 7.33 (s, 4H, ph-H), 6.3 (m, 6H, ph-H), 4.61 (AX, 4H, ^2J = 13.2 Hz, ph-CH_2-ph), 4.28 (t, ^3J= 8.14 Hz, 4H, OCH_2), 3.71 (t, ^3J = 6.7 Hz, 4H, OCH_2), 3.34 (AX, 4H, ^2J = 13.5 Hz,

ph-C*H*$_2$-ph), 2.68 (s, 6H, py-CH$_3$), 2.59 (s, 6H, py-CH$_3$), 2.45 (s, 6H, py-CH$_3$), 2.12 (m, 4H; CH$_2$C*H*$_2$CH$_3$), 1.94 (m, 4H, CH$_2$C*H*$_2$CH$_3$), 1.16 (t, ^3J = 7.3 Hz, 6H, CH$_2$C*H*$_3$), 1.00 (t, ^3J = 7.4 Hz, 6H, CH$_2$C*H*$_3$). HRMS (ESI, pos. mode, MeOH): calc. *m*/*z* for $C_{56}H_{68}BF_4N_2O_4$ ([*M*−BF$_4$]$^+$) 918.52391, found 918.52402. Anal. Calcd for $C_{56}H_{68}B_2F_8N_2O_4 \cdot 2H_2O$ (1042.79): C, 64.50; H, 6.96; N, 2.69. Found: C, 64.62; H, 6.82; N, 2.76.

(5*Z*,5′*Z*)-5,5′-{[25,26,27,28-Tetrapropoxypentacyclo[19.3.1.1^{3,7}.1^{9,13}.1^{15,19}]octacosa-1(25),3(28),4,6,9(27),10,12,15(26),16,18,21,23-dodecaene-5,17-diyl]bis[(2,6-dimethylpyridin-1-yl-4-ylidene)(1*Z*)ethane-2,1-diylidene]}bis(1-dodecyl-4-methyl-2,6-dioxo-1,2,5,6-tetrahydro-pyridine-3-carbonitrile) (6). Dipyridinium salt **4** (483 mg, 0.48 mmol), pyridone **5** (404 mg, 0.96 mmol) und KOAc (94 mg, 0.96 mmol) were suspended in Ac$_2$O (3 mL) and heated to 105 °C for 20 h. The solvent was removed under reduced pressure and the residue was subjected to column chromatography (SiO$_2$, CH$_2$Cl$_2$/MeOH = 96.5:3.5) and subsequently purified by preparative HPLC (NUCLEOSIL 100-5 NO$_2$, CH$_2$Cl$_2$/MeOH = 97:3). The product was precipitated from CH$_2$Cl$_2$ by adding MeOH and a red powder was obtained. Yield: 50 mg (34 mmol, 7%). Mp >320 °C. TLC (CH$_2$Cl$_2$/MeOH = 10:1) R_f = 0.56. ^{1}H NMR (400 MHz, CD$_2$Cl$_2$/MeOD-d_4 = 4:1, 25 °C): δ 7.80 (d, ^3J = 15.2 Hz, 2H, met-H), 7.72 (d, ^3J = 15.0 Hz, 2H, met-H), 7.50 (s, 2H, py-H), 7.44 (s, 2H, py-H), 7.14 (s, 4H, ph-H), 6.33 (t, 2H, ph-H), 6.15 (d, ^3J = 7.7 Hz, 4H, ph-H), 4.57 (AX, 4H, ^2J = 13.4 Hz, ph-C*H*$_2$-ph), 4.22 (t, ^3J= 8.2 Hz, 4H, OCH$_2$), 3.96 (t, ^3J= 7.6 Hz, 4H, NCH$_2$), 3.69 (t, ^3J = 6.6 Hz, 4H, OCH$_2$), 3.29 (AX, 4H, ^2J = 17.5 Hz, ph-C*H*$_2$-ph), 2.50 (s, 6H, py-CH$_3$), 2.47 (s, 6H, pyridone-CH$_3$), 2.31 (s, 6H, py-CH$_3$), 2.04 (m, 4H, CH$_2$C*H*$_2$CH$_3$), 1.91 (m, 4H, CH$_2$C*H*$_2$CH$_3$), 1.59 (m, 4H, CH$_2$), 1.4–1.1 (m, 36H, CH$_2$), 1.12 (t, ^3J = 7.5 Hz, 6H, CH$_2$CH$_2$C*H*$_3$), 0.97 (t, ^3J = 7.5 Hz, 6H, CH$_2$CH$_2$C*H*$_3$), 0.86 (t, ^3J = 6.8 Hz, 6H, CH$_3$). HRMS (ESI, pos. mode, MeCN/CHCl$_3$ = 1:1): calc. *m*/*z* for $C_{96}H_{123}N_6O_8$ ([*M*+H]$^+$) 1487.94024, found 1487.93778. UV–vis (CH$_2$Cl$_2$, 25 °C, 10^{-5} M): λ_{max} (ε) = 546 nm (217600 M^{-1}cm^{-1}).

4.5 References and Notes

(1) (a) Whitesides, G. M.; Mathias, J. P.; Seto, C. T. *Science* **1991**, *254*, 1312–1319. (b) *Comprehensive Supramolecular Chemistry*; Atwood, J. L.; Davies, J. E. D.; MacNicol, D. D.; Vögtle, F.; Lehn, J.-M., Eds; Pergamon: Oxford, 1996. (c) Lehn, J.-M. *Science* **2002**, *295*, 2400–2403.

(2) For general reviews see: (a) Holliday, B. J.; Mirkin, C. A. *Angew. Chem., Int. Ed.* **2001**, *40*, 2022–2043. (b) Prins, L. J.; Reinhoudt, D. N.; Timmerman, P. *Angew. Chem., Int. Ed.* **2001**, *40*, 2382–2426. (c) Hof, F.; Craig, S. L.; Nuckolls, C.; Rebek, J., Jr. *Angew. Chem., Int. Ed.* **2002**, *41*, 1488–1508. (d) Schmittel, M.; Kalsani, V. *Top. Curr. Chem.* **2005**, *245*, 1–53. (e) Hoeben, F. J. M.; Jonkheijm, P.; Meijer, E. W.; Schenning, A. P. H. J. *Chem. Rev*. **2005**, *105*, 1491–1546.

(3) (a) Würthner, F.; Yao, S. *Angew. Chem., Int. Ed.* **2000**, *39*, 1978–1981. (b) Würthner, F.; Yao, S.; Debaerdemaker, T.; Wortmann, R. *J. Am. Chem. Soc.* **2002**, *124*, 9431–9447. (c) Rösch, U.; Yao, S.; Wortmann, R.; Würthner, F. *Angew. Chem., Int. Ed.* **2006**, *45*, 7026–7030. (d) Seibt, J.; Lohr, A.; Würthner, F.; Engel, V. *Phys. Chem. Chem. Phys.* **2007**, *9*, 6214–6218.

(4) (a) Yao, S.; Beginn, U.; Gress, T.; Lysetska, M.; Würthner, F. *J. Am. Chem. Soc.* **2004**, *126*, 8336–8348. (b) Lohr, A.; Lysetska, M.; Würthner, F. *Angew. Chem., Int. Ed.* **2005**, *44*, 5071–5074. (c) Lohr, A.; Gress, T.; Deppisch, M.; Knoll, M.; Würthner, F. *Synthesis* **2007**, 3073–3082.

(5) For the optical properties and formation of intramolecular aggregates of tethered merocyanine or squaraine dyes, see: (a) Katoh, T.; Inagaki, Y.; Okazaki, R. *J. Am. Chem. Soc.* **1998**, *120*, 3623–3628. (b) Lu, L.; Lachicotte, R. J.; Penner, T. L.; Perlstein, J.; Whitten, D. G. *J. Am. Chem. Soc.* **1999**, *121*, 8146–8156. (c) Ushakov, E. N.; Gromov, S. P.; Fedorova, O. A.; Pershina, Y. V.; Alfimov, M. V.; Barigelletti, F.; Flamigni, L.; Balzani, V. *J. Phys. Chem. A* **1999**, *103*, 11189–11193. (d) Zeena, S.; Thomas, G. K. *J. Am. Chem. Soc.* **2000**, *123*, 7859–7865. (e) Arankumar, E.; Chithra, P.; Ajayaghosh, A. *J. Am. Chem. Soc.* **2004**, *126*, 6590–6598.

(6) (a) McDermott, G.; Prince, S. M.; Freer, A. A.; Hawthornthwaite-Lowless, A. M.; Papiz, M. Z.; Cogdell, R. J.; Isaacs, N. W. *Nature* **1995**, *374*, 517–521. (b) Koepke, J.; Hu, X.; Muenke, C.; Schulten, K.; Michel, H. *Structure* **1996**, *4*, 581–597.

(7) For general reviews on cyclic dye arrays, see: (a) Nakamura, Y.; Aratani, N.; Osuka, A. *Chem. Soc. Rev.* **2007**, *36*, 831−845. (b) Satake, A.; Kobuke, Y. *Tetrahedron* **2005**, *61*, 13–41. (c) You, C.-C.; Dobrawa, R.; Saha-Möller, C. R.; Würthner, F. *Top. Curr. Chem.* **2005**, *258*, 39–82.

(8) For noncovalent cyclic porphyrin arrays, see for example: (a) Anderson, S.; Anderson, H. L.; Bashall, A.; McPartlin, M.; Sanders, J. K. *Angew. Chem., Int. Ed. Engl.* **1995**, *34*, 1096−1099. (b) Knapp, S.; Vasudevan, J.; Emge, T. J.; Arison, B. H.; Potenza, J. A.; Schugar, H. J. *Angew. Chem., Int. Ed.* **1998**, *37*, 2368−2370. (c) Biemans, H. A. M.; Rowan, A. E.; Verhoeven, A.; Vanoppen, P.; Latterini, L.; Foekema, J.; Schenning, A. P. H. J.; Meijer, E. W.; de Schryver, F. C.; Nolte, R. J. M. *J. Am. Chem. Soc.* **1998**, *120*, 11054−11060. (d) Li, J.; Ambroise, A.; Yang, S. I.; Diers, J. R.; Seth, J.; Wack, C. R.; Bocian, D. F.; Holten, D.; Lindsey, J. S. *J. Am. Chem. Soc*. **1999**, *121*, 8927−8940. (e) Mongin, O.; Hoyler, N.; Gossauer, A. *Eur. J. Org. Chem*. **2000**, 1193−1197. (f) Haycock, R. A.; Hunter, C. A.; James, D. A.; Michelsen, U.; Sutton, L. R. *Org. Lett*. **2000**, *2*, 2435–2438. (g) Ikeda, C.; Nagahara, N.; Yoshioka, N.; Inoue, H. *New. J. Chem.* **2000**, *24*, 897–902. (h Shi, X.; Barkigia, K. M.; Fajer, J.; Drain, C. M. *J. Org. Chem.* **2001**, *66*, 6513–6522. (i) Hajjaj, F.; Yoon, Z. S.; Yoon, M.-C.; Park, J.; Satake, A.; Kim, D.; Kobuke, Y. *J. Am. Chem. Soc.* **2006**, *128*, 4612−4623.

(9) For general reviews on calixarenes, see: (a) *Calixarenes 2001*; Asfari, Z.; Böhmer, V.; Harrowfield, J., Eds.; Kluwer Academic Publishers: Dordrecht, 2001. (b) Gutsche, C. D. *Calixarenes ReVisited*; The Royal Society of Chemistry: Letchworth, 1998. (c) Böhmer, V.; *Angew. Chem., Int. Ed. Engl.* **1995**, *34*, 713−745. (d) *Calixarenes in Action*; Mandolini, L.; Ungaro, R., Eds.; Imperial College Press: London, 2000.

(10) For dye-functionalized calixarenes, see for example: (a) Kenis, P. J. A.; Kerver, E. G.; Snellink-Ruël, B. H. M.; van Hummel, G. J.; Harkema, S.; Flipse, M. C.; Woudenberg, R. H.; Engbersen, J. F. J.; Reinhoudt, D. N. *Eur. J. Org. Chem.* **1998**, 1089−1098. (b) Kim, E. J.; Choe, J.-I.; Chang, S.-K. *Tetrahedron Lett.* **2003**, *44*, 5299−5302. (c) Yu, H.-h.; Xu, B.; Swager, T. M. *J. Am. Chem. Soc.* **2003**, *125*, 1142–1143. (e) Hippius, C.; Schlosser, F.; Vysotsky, M. O.; Böhmer, V.; Würthner; F. *J. Am. Chem. Soc.* **2006**, *128*, 3870–3871. (f) Hippius, C.; van Stokkum, I. H. M.; Zangrando, E.; Williams, R. M.; Würthner, F. *J. Phys. Chem. C* **2007**, *111*, 13988–13996.

(11) (a) Rebek, J., Jr.; Askew, B.; Killoran, M.; Nemeth, D.; Lin, F.-T. *J. Am. Chem. Soc.* **1987**, *109*, 2426–2431. (b) Zimmerman, S. C.; Mrksich, M.; Baloga, M. *J. Am. Chem. Soc.* **1989**, *111*, 8528–8530.

(12) Timmerman, P.; Boerrigter, H.; Verboom, W.; Reinhoudt, D. N. *Recl. Trav. Chim. Pays-Bas* **1995**, *114*, 103–111.

(13) Tsai, Y.-C.; Stephens, F. H.; Meyer, K.; Mendiratta, A.; Gheorghiu, M. D.; Cummins, C. C. *Organometallics* **2003**, *22*, 2902–2913.

(14) (a) Connors, K. A. *Binding Constants*; Wiley: New York, 1987. (b) Martin, R. B. *Chem. Rev.* **1996**, *96*, 3043–3064.

(15) (a) Kasha, M.; Rawls, H. R.; Ashraf El-Bayoumi M. *Pure Appl. Chem.* **1965**, *11*, 371–392. (b) Davydov, A. S. *Theory of Molecular Excitons*; Plenum Press: New York, 1971. (c) Fidder, H.; Knoester, J.; Wiersma, D. A. *J. Chem. Phys.* **1991**, *95*, 7880–7890.

(16) The transition dipole moment of the merocyanine chromophore is oriented along the long molecular axis.

(17) *Hyperchem*™; Hypercube Inc.: 1115 NW 4th Street, Gainesville, FL 32601, USA.

(18) Papula, L. *Mathematische Formelsammlung für Ingenieure und Naturwissenschaftler*; Vieweg Verlag: Wiesbaden, 2006, p. 19.

(19) For the determination of $\Delta H°$ and $\Delta S°$, a linear relationship between ln K_D and T^{-1} is required. In the present cases such a linear relation is not observed, which can be attributed to the strong dependence of ε_r of chloroform on temperature from $\varepsilon_r = 5.02$ at 283 K to $\varepsilon_r = 4.29$ at 323 K. For comparison, these values correspond to the ε_r values of BuOAc and Et_2O at 293 K, respectively. Thus, ΔH shows an inherent temperature-dependence in the present case where bimolecular association is driven by electrostatic attractions (see ref. 3). Interestingly, the strong dependence of ε_r on temperature is also expressed in the value of the absorption maximum λ_{max} of this strongly solvatochromic type of merocyanine dyes (see Chapter 3.6, Figure A2).

(20) (a) Chi, X.; Guerin, A. J.; Haycock, R. A.; Hunter, C. A.; Sarson, L. D. *J. Chem. Soc., Chem. Commun.* **1995**, 2563–2565. (b) Ercolani, G. *J. Phys. Chem. B* **1998**, *102*, 5699–5703. (c) Ercolani, G. *Chem. Commun.* **2001**, 1416–1417. (d) Ercolani, G. *J. Am. Chem. Soc.* **2003**, *125*, 16097–16103.

(21) (a) Timmerman, P.; Vreekamp, R. H.; Hulst, R.; Verboom, W.; Reinhoudt, D. N.; Risannen, K. ; Udachin, K. A.; Ripmeester, J. *Chem.–Eur. J.* **1997**, *3*, 1823–1832. (b) Prins, L. J.; Thalacker, C.; Würthner, F.; Timmerman, P.; Reinhoudt, D. N. *Proc. Natl. Acad. Sci. USA* **2001**, *98*, 10042–10045.

(22) For a review on mass spectroscopy in supramolecular chemistry, see: Baytekin, B.; Baytekin, H. T.; Schalley, C. A. *Org. Biomol. Chem.* **2006**, *4*, 2825–2841.

(23) The given *m*/*z* values corresponds to the average isotopic mass since the isotopic pattern of the singly charged trimeric complex of **6** could not be resolved in the MALDI-TOF measurements.

(24) Since the dielectric constant of 1,2,4-trichlorobenzene (ε_r = 2.24) is lower than that of chloroform (ε_r = 4.81), we expect a higher aggregation constant in TCB.

(25) (a) De Feyter, S.; De Schryver, F. C. *Chem. Soc. Rev.* **2003**, *32*, 139–150. (b) De Feyter, S.; De Schryver, F. C. *J. Phys. Chem. B* **2005**, *109*, 4290–4302.

(26) Perrin, D. D.; Armarego, W. L. F. *Purification of Laboratory Chemicals*; Pergamon Press: Oxford, 1980.

Chapter 5

Morphogenesis of Helical Merocyanine Dye Nanorods

Abstract: This chapter reports on the self-assembly of xylylene-tethered bis(merocyanine) dyes bearing two chiral alkyl substituents at the imide N atoms. A complex self-assembly sequence into well-defined helical nanorod structures has been revealed spectroscopically by time-dependent CD spectroscopy and microscopically by atomic force microscopy. This self-assembly sequence proceeds over several kinetically formed supramolecular intermediates which are distinguished by their morphology and (chir)optical properties. Moreover, the kinetics for the formation of homochiral nanorods was studied and it was shown that chiral amplification mechanisms can operate at different stages of self-assembly to afford energetically favored structures. The rates of these processes decrease strongly with decreasing chiral bias in the monomers as realized by decreasing enantiomeric excess of the chiral monomers or decreasing fraction of chiral co-monomers in mixtures of chiral and achiral monomers. For the fully equilibrated nanorods, however, strong chiral amplification directed by the "majority-rules" or "sergeants-and-soldiers" effect is observed.

5.1 Introduction

Nature creates the most complex nanostructures not only through the formation of covalent bonds along efficient biosynthetic pathways, but also by self-organization controlled by noncovalent interactions.[1] The construction of artificial structures with comparable complexity and function is one of the ultimate goals in chemistry. Although a broad repertoire of synthetic methods is nowadays available to succeed in the synthesis of the most challenging organic compounds,[2] it has been recognized that self-assembly can open new opportunities in both the fields of biology and materials science because it enables the rapid formation of nano-sized complex architectures with stable conformations, despite their noncovalent, reversible nature.[3] Nevertheless, for such "bottom-up" construction of more complex structures, a detailed understanding of the mechanisms involved in self-assembly processes is required.[4] Thus, in contrast to biological self-assembly such as protein folding, which is considered to be a kinetically controlled process,[5] most self-assembled artificial systems are formed under thermodynamic control,[6] and only recently the importance of kinetic control in self-assembly processes towards large polydisperse aggregates as well as discrete supramolecular structures has been recognized.[7–10]

Since chirality is a ubiquitous feature of natural structures, much research has been devoted to artificial systems with molecular and supramolecular chirality which led to appealing architectures and intriguing properties.[11,12] An elegant way to control the chirality of self-assembled systems by small chiral bias is provided by a set of phenomena generally regarded as amplification of chirality,[13] which have been found in helical macromolecules[14,15] and supramolecular noncovalent polymers and aggregates.[16–18] The chiral amplification in some of these systems has been explained by the "majority-rules" effect,[17] which implies that a slight enantiomeric excess of chiral monomers dictates the overall helical sense of an assembly, and the sergeant-and-soldiers principle,[16] which means the control of the cooperative movements of a large number of achiral units (the soldiers) by a few chiral units (the sergeants). However, due to the lack of comprehensive knowledge in self-assembly mechanisms not much is known about the pathways for such amplification of chirality. In most cases only the thermodynamics have been explored in supramolecular systems in the past and reports on the mechanisms of chiral amplification in such systems are rather scarce.[19,20] In these studies, the time-dependence of the sergeants-and-soldiers effect was either due to a slow exchange of achiral and chiral building blocks among the respective pre-assembled racemic and homochiral aggregates,[19] or

based on the induction of homochirality into racemic helical assemblies formed from achiral building blocks by addition of chiral guest molecules that bound to the assembly.[20] Since chiral amplification phenomena create large enantiomeric excess from small initial chiral bias, they have been suggested to be of importance for the evolution of natural homochirality.[21,22] Thus, studies on the mechanisms leading to amplification in chiral systems may provide answers to the more fundamental question of how natural homochirality has originally been evolved.

Our group is particularly interested in the self-assembly of merocyanine dyes,[23,24] a class of chromophores that is of interest for nonlinear optical and photorefractive applications owing to their outstanding dipolar and polarizability properties.[25] In the work of Würthner and coworkers it was shown that aggregation of merocyanine dyes into centrosymmetric dimers arises predominantly from dipolar interactions with dimerization constants of $K_D > 10^6$ M^{-1} in low-polar solvents.[23a] By utilizing this dipolar aggregation the same group achieved the self-assembly of the achiral bis(merocyanine) dye **5** into highly defined nanorods through supramolecular polymerization and hierarchical self-organization.[24] Force-field calculations suggested that these nanorods are formed from six helically intertwined supramolecular single-stranded polymers. The chromophores are organized in a card-pack fashion and helically wound around the long axis of the rods.[24] Since achiral monomers were used left- and right-handed helices were formed in equal amounts, that is, a racemic mixture was obtained.[24c]

To achieve homochiral nanorods, we decided to investigate the self-assembly of a chiral bis(merocyanine) derivative (*R*,*R*)-**6** bearing two (*R*)-2-octyl side chains at the imide positions. This should lead to the preferential formation of nanorod aggregates of only one helical handedness. Indeed, pronounced supramolecular and macroscopic chirality effects were observed upon self-assembly of dye (*R*,*R*)-**6**, indicating a highly stereoselective self-assembly process. More interestingly, novel phenomena in the self-assembly of these dyes were revealed by studying the self-assembly kinetics of this system by a combination of (chir)optical spectroscopy and atomic force microscopy measurements. Accordingly, herein we report the kinetically controlled self-assembly of merocyanine (*R*,*R*)-**6** into helical nanorods that exhibit a change of the supramolecular structure upon subsequent transformation in the thermodynamically stable nanorods.[26] As the helical sense of these nanorods is determined by the absolute configuration of the 2-octyl side chains at the imide positions, we were also interested into the stereochemical behavior of aggregates that were co-assembled from (*R*,*R*)- and (*S*,*S*)-enantiomers of **6** as well as from mixtures of achiral **5** and enantiopure (*R*,*R*)-**6** under

the conditions identical to those applied for the single enantiomers. These co-aggregates allowed investigations of the kinetics of chiral amplification by means of the majority-rules and sergeant-and-soldiers principle due to the unique self-assembly kinetics found for the bis(merocyanine) dye nanorods.

5.2 Results and Discussion

5.2.1 Synthesis of chiral bis(merocyanine) dye monomers

Chiral pyridones (*R*)-**3** and (*S*)-**3** were obtained in 50–53% yield by a sequence of condensation reactions starting with the respective chiral 2-octylamine (*R*)-**2** or (*S*)-**2**. The subsequent reaction of pyridones **3** with *N,N′*-diphenylformamidine and bis(pyridinium) salt **4** gave chiral bis(merocyanine) dyes (*R*,*R*)-**6** and (*S*,*S*)-**6** in 24–25% yield. Achiral bis(merocyanine) dye **5** was synthesized according to literature procedure.[24b]

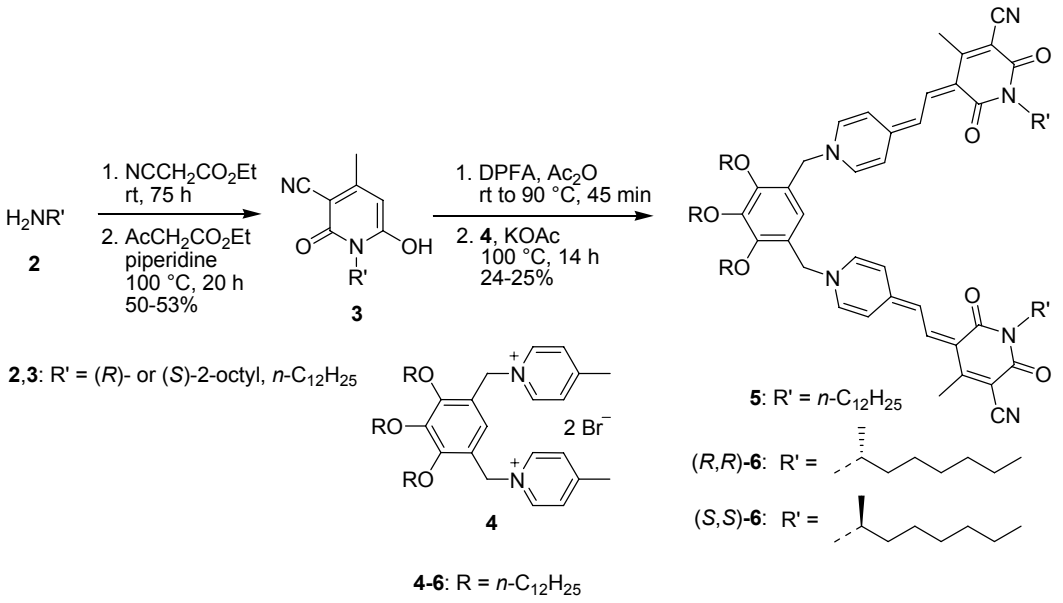

Scheme 1. Synthesis of bis(merocyanine) dyes.

5.2.2 Kinetic and thermodynamic self-assembly into H1 and H2 nanorods

The time course of the self-assembly of chiral bis(merocyanine) dye (*R*,*R*)-**6** was studied by UV–vis and CD spectroscopy, methods that are particularly suited to gain insight into the formation and packing properties of dye aggregates. As shown previously by solvent-dependent studies for a series of bis(merocyanine) dyes in THF/MCH mixtures of different composition, the polarity of the solvent affects the thermodynamic equilibrium between the different self-assembled species found for these dyes.[24] In pure THF these dyes are present

predominantly in the monomeric form owing to the high polarity of THF ($\varepsilon_r = 7.52$). With increasing fraction of nonpolar MCH ($\varepsilon_r = 2.02$) the chromophores of the bis(merocyanine) dyes form intermolecular dimers which leads to the formation of a single-stranded supramolecular polymer owing to the increased Coulomb forces between the dipolar chromophores.[24] Upon further increase of the MCH content above a certain value an abrupt transition to the H-aggregated nanorods takes place. Thus, the starting point for the self-assembly was defined by the addition of methylcyclohexane (MCH) to stock solutions of monomeric (*R*,*R*)-**6** in tetrahydrofuran (THF) to provide solutions with a total monomer concentration of 1×10^{-5} M in THF/MCH mixtures ranging from 40:60 to 20:80 vol% (see Experimental Section for details). Notably, in each of these solvent compositions full aggregation of the monomers into nanorods is observed after full equilibration. The time-dependent UV–vis spectra of (*R*,*R*)-**6** in THF/MCH = 30:70 vol% recorded at different time after initiation of aggregation (Figure 1, top panel) show the decrease of an absorption band at 484 nm with increasing time up to 14 min and a concomitant increase of a hypsochromically shifted sharp H-band at 443 nm. The occurrence of a well-defined isosbestic point at 462 nm indicates the conversion between two structurally defined species. As previously shown, the absorption band at 484 nm can be assigned to a pair of π-stacked merocyanine dyes in single-stranded polymers, which obviously have been instantly formed from the monomers after addition of MCH, while the sharp H-band at 443 nm can be assigned to nanorod aggregates that contain extended π-stacks of excitonically coupled chromophores.[24] Thus, the time-dependent spectral changes shown in Figure 1a can be assigned to the self-assembly of the single-stranded supramolecular polymers into H-aggregated nanorods, which in the following we will refer to as **D** and **H1**, respectively.

As the concentration of **H1** rises with time, strong induced Cotton effects appear in the CD spectra (Figure 1a, bottom panel), indicating chiral excitonic coupling of the chromophores in the self-assembled helical nanorods.[27,28] The CD spectra feature a very strong negative bisignate exciton couplet located at the most intensive absorption band of **H1**. The long wavelength shoulder at around 470 nm (negative) and the band at 506 nm (positive) may be attributed to a second bisignate CD signal with a positive sign which originates from partly forbidden low-energy transitions of the **H1**-aggregated dyes. Similar (−/+/−)-shaped CD spectra were observed for natural chlorin dye and artificial cyanine dye J-aggregates and

theoretical calculations have revealed that such a spectral shape is a common feature of helical cylindrical dye aggregates.[12a,29]

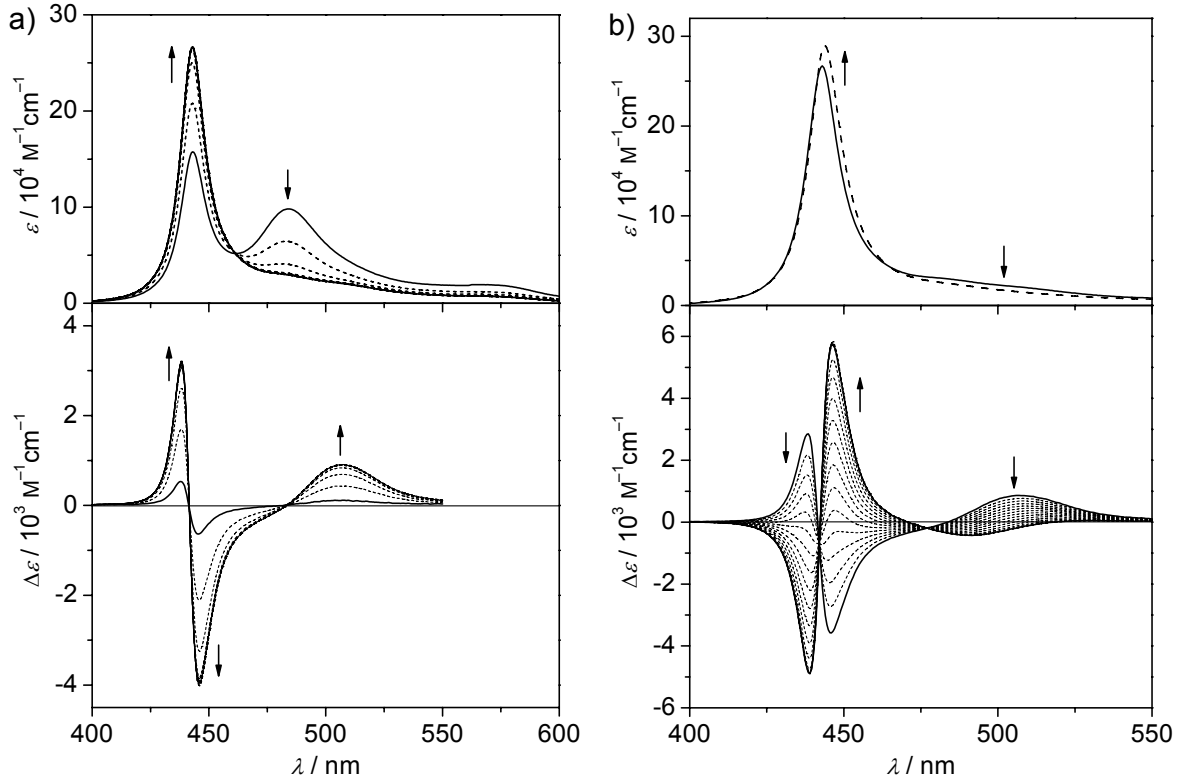

Figure 1. Time-dependent UV–vis (top) and CD spectra (bottom) showing the transition from a) D-aggregated species **D** into the kinetically formed H-aggregated species **H1** and b) the initially formed H-aggregated species **H1** into the thermodynamically more stable H-aggregated species **H2** for dye (*R*,*R*)-**6** in a mixture of THF/MCH= 30:70 vol% at 23 °C ($c = 1\times10^{-5}$ M). Arrows indicate changes with increasing time from a) 0 to 14 min and b) 34 min to 20 h.

As the time course of self-assembly progressed (spectra were recorded from 34 min to 20 h) a total inversion of the CD spectrum was observed, while the UV–vis spectra remained almost unchanged (Figure 1b). Since the formation of the initial **H1** aggregate is fast and the subsequent inversion is very slow, both processes can be studied independently with good approximation. Two well-defined isodichroic points at 441 nm and 476 nm reveal a transition between **H1** and another H-aggregated species with opposite exciton chirality, which in the following we denote as **H2**. The observed spectral changes can be explained in terms of kinetically and thermodynamically controlled self-assembly into two H-aggregated species **H1** and **H2** with opposite exciton chirality.[7a,b] First, the species **H1** is formed in a rapid process by kinetic self-assembly. Subsequently, **H1** is transformed in a much slower process into the thermodynamically more stable self-assembly product **H2**. The anisotropy factors *g* at 437 nm

for **H1** and **H2** were determined as 1.7×10^{-2} and -2.8×10^{-2}, respectively. These values are two to three orders of magnitude higher than the *g* values obtained for chiral dimers of related dyes suggesting a highly delocalized exciton state as well as a high stereoselective self-assembly process for both nanorod species.[30] A further comparison of the spectral data for **H1** and **H2** nanorods as summarized in Table 1 reveals that the wavelengths of the first and second CD maximum/minimum of **H2** are slightly bathochromically shifted by 1 nm with respect to that of the **H1** nanorods. This spectral shift is in accordance with the slight shift observed for the main absorption band in the UV–vis spectra of **H2** with respect to **H1** nanorods. The third maximum/minimum as well as the second zero-crossing is more strongly blue-shifted from 506 nm and 483 nm for **H1** to 490 nm and 470 nm for the **H2** nanorods, respectively. Thus, the two different nanorod species can be distinguished not only by their opposite exciton chirality but also by the maxima/minima as well as by the zero-crossing wavelengths of their CD spectra.

Table 1. UV–vis and CD spectroscopic data of species **D**, **H1**, and **H2**, and structural data determined by AFM in tapping mode.

Species	UV–vis	CD					AFM [a]		
	λ_{max} (nm)	λ_1 (nm)	λ_2 (nm)	λ_3 (nm)	λ_{zero} (nm)	g_{437} (10^{-2})	Helicity	Pitch (nm)	Height (nm)
D	484								
H1	443	437	445	506	483	1.7	*P*	10.4±0.6	3.34±0.40
H2	444	438	446	490	470	−2.8	*P*	4.9±0.60	3.16±0.25

[a] Helicity and helical pitch of observed morphology.

Similar spectral changes to those described above were observed for the corresponding self-assembly experiments with (*R*,*R*)-**6** monomers conducted in solvent compositions with THF/MCH = 40:60 and 20:80 vol%, that is, in solvent compositions with respectively higher and lower solvent permittivity compared to that in the previous experiment (THF/MCH = 30:70 vol%), as well as in the previous solvent composition but at elevated temperature. A comparison of the time-dependent CD data at 437 nm obtained from all self-assembly experiments is given in Figure 2. In all cases the fast increase of the CD amplitude owing to the self-assembly of the **D** species into **H1** nanorods is observed during the first 14 min, while the subsequent conversion of **H1** into **H2** nanorods is much slower. Remarkably, a linear relationship of the CD amplitude on the time is found for the latter process and the rate

in which this process proceeds strongly depends on the solvent composition (filled symbols). Thus, in THF/MCH = 30:70 vol% this process is complete after about 14 hours, while at higher fraction of MCH (THF/MCH = 20:80 vol%), which corresponds to lower solvent permittivity, this process becomes such slow that the kinetic product (species **H1**) can be trapped for days. On the contrary, at lower fraction of MCH (THF/MCH = 40:60 vol%), which corresponds to higher solvent permittivity with respect to THF/MCH = 30:70 vol%, the **H1**→**H2** conversion is strongly accelerated. These solvent-dependent studies reveal that the THF/MCH ratio and, thus, the polarity of the solvent affects not only the thermodynamic bias and driving force towards a particular self-assembled species,[24b] but also the kinetic rates of the self-assembly process.

The comparison of the data in THF/MCH = 30:70 vol% at 47 °C with those in the same solvent but at 23 °C provide further evidence, that the present process leading to the thermodynamically stable **H2** nanorods is strongly accelerated at elevated temperature. This temperature dependence is in good accordance with the theoretical understanding of classical organic reactions where product formation under kinetic control is favored at low temperature while product formation under thermodynamic control is favored at higher temperature.[31]

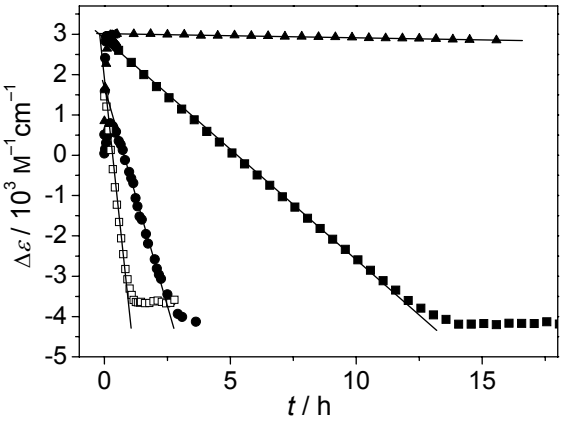

Figure 2. Molar circular dichroism $\Delta\varepsilon$ at 437 nm during self-assembly of (*R*,*R*)-**6** (10^{-5} M) in solvents of different composition and temperature: THF/MCH = 20:80 (▲), 30:70 (■), 40:60 vol% (●) at 23 °C, and 30:70 vol% at 47 °C (□).[32]

The observed linear relationship of the CD value for the **H1**→**H2** conversion on the time suggests that a pseudo-zero-order rate law applies for this process. Such kinetics are consistent with a fast pre-equilibrium between the starting material (*i.e.* **H1**) and an intermediate species (*i.e.* small oligomers) resulting in a "saturated" intermediate concentration and preceding the

rate-limiting product formation step.[33] This kinetic model is quite reasonable to apply for the present process since the observed solvent dependence of the conversion rate is in accordance with monomeric or D-aggregated intermediate species (a kind of randomly oriented supramolecular polymer) that are in equilibrium with both the **H1** nanorods (*i.e.* the starting material) and the **H2** nanorods (*i.e.* the product). Clearly, with decreasing solvent polarity a smaller amount of these intermediates will be present in solution leading to a decreased rate of the rate-limiting **H2** formation and, thus, a decreased rate for the overall **H1**→**H2** process. It can therefore be strongly suggested that the conversion from **H1** to **H2** requires disassembly of the **H1** nanorod aggregates and is not a reordering process that proceeds within the nanorods.

To gain more insight into the structural changes upon the **D**→**H1**→**H2** self-assembly process, we carried out atomic force microscopy (AFM) investigations.[i] Figure 3 illustrates tapping mode AFM images of samples prepared by spin-coating of solutions of bis(merocyanine) (*R*,*R*)-**6** ($c = 1\times10^{-5}$ M, THF/MCH = 30:70 vol%) onto highly ordered pyrolytic graphite (HOPG) at different time intervals after initiation of the self-assembly process (*i.e.* addition of MCH into the stock solution in THF). The 30:70 ratio of THF/MCH was used for this study since the CD spectroscopic investigations established this solvent composition as the best-suited solvent system to study both the self-assembly of the kinetically formed product and the subsequent transformation into the thermodynamically stable nanorods at room temperature on convenient time scales. After 1 min (Figure 3a) the height image shows wide disordered "grainy" regions that can be assigned to little ordered supramolecular polymers (**D** species) and some short **H1** rods in the initial stage of their formation. After 14 min, when the bisignate CD signal has reached its maximum negative amplitude, the disordered regions have mostly disappeared and much longer **H1** rods are formed. Figure 3b and Figure 3c show the height and the corresponding phase image of the **H1** rods after 14 min in higher resolution. A pronounced right-handed helical (*P*) structure with a pitch of 10.4±0.6 nm can be observed in the phase image (Figure 3c). The **H1** rods have a height of 3.34±0.40 nm. After 11 h the coexistence of the **H2** species is evident (Figure 3d). The **H2** rods have also right-handed helicity, but now with a helical pitch of only 4.9±0.6 nm, and a decreased height of 3.16±0.25 nm (see Table 1). Subsequently, after 22 h merely the **H2** rods

[i] AFM measurements were performed by Dr. Marina Knoll.

can be observed (Figure 3e and Figure A1). On the basis of the rod diameter (height values of AFM), a more compact structure is assigned to the thermodynamically more stable **H2** nanorods. In contrast to the phase images, the corresponding height images do not show the helical morphology, which suggests that regions of different "hardness" render the helical contrast in the phase images. We attribute this contrast to the density of alkyl chains at the periphery of the nanorods. Artifacts caused by sample preparation or measurements can surely be excluded as rods assembled out of the enantiomeric (*S*,*S*)-**6** monomers show opposite left-handed helicity (not shown).

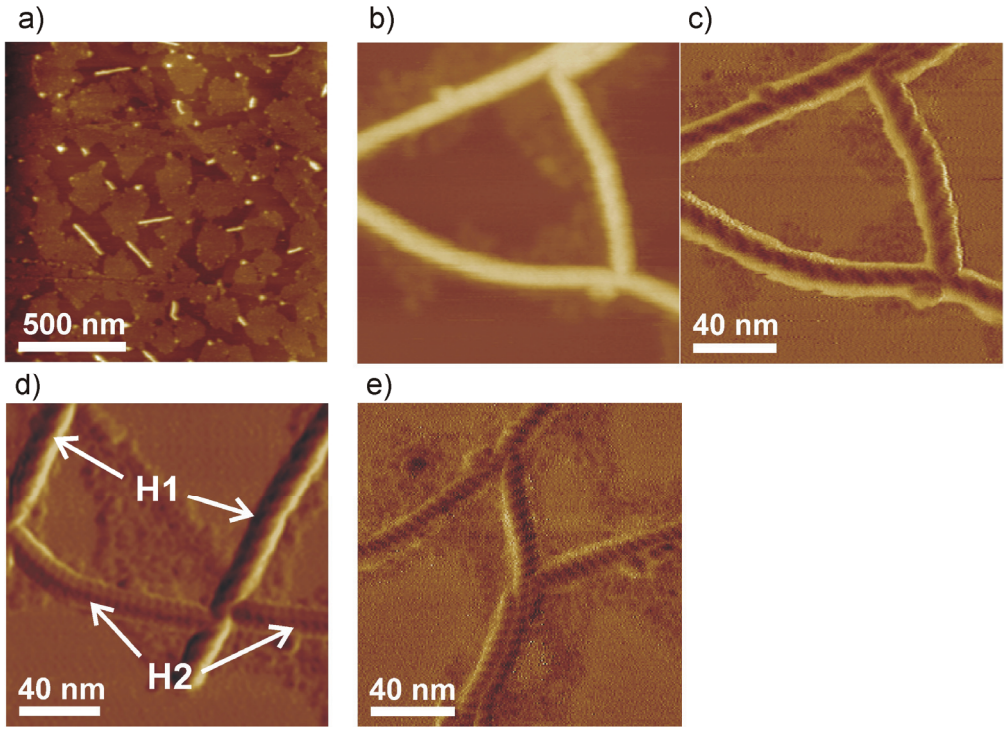

Figure 3. AFM height (a,b) and phase (c–e) images of samples prepared by spin-coating of solutions of bis(merocyanine) dye (*R*,*R*)-**6** ($c = 1\times10^{-5}$ M, THF/MCH = 30:70 vol%, 20 °C) onto HOPG at different times after initiation of self-assembly: a) 1 min; b,c) 14 min; d) 11 h; e) 22 h. In a and b the z scale is 10 nm and in c–e the z scale is 30°.

The observed self-assembly sequence of bis(merocyanine) dye (*R*,*R*)-**6** is schematically summarized in Figure 4a. After initiation of aggregation the instantly formed supramolecular D-species self-assembles into **H1** nanorods, which show a negative exciton couplet at the main absorption band and a right-handed morphology with about 10 nm helical pitch. This data is quite unexpected since the CD data indicates a left-handed helical arrangement of the chromophores in the aggregate that does not comply with the right-handed morphology observed by AFM. Subsequently, the kinetically formed **H1** species is slowly converted into

the thermodynamically equilibrated **H2** nanorods showing also right-handed morphology with 5 nm helical pitch and a positive exciton couplet at the main absorption band which now does comply with the right-handed helical arrangement of the chromophores in the nanorods. In accordance with the term stereomutation which generally applies for a change of configuration at a stereogenic unit brought about by physical or chemical means,[34] we have proposed to call the present phenomenon a supramolecular stereomutation.[26a] Although CD spectroscopic studies on achiral bis(merocyanine) dyes are not applicable since a silent CD spectrum is obtained owing to the presence of helices of both handedness in the same amount, AFM studies on a series of achiral bis(merocyanine) dyes suggest that the presence of a stereomutation process is not restricted to (*R*,*R*)-**6** but also applies for the formation of helical nanorods from bis(merocyanine) dyes with achiral alkyl substituents at the imide N atom.[24c]

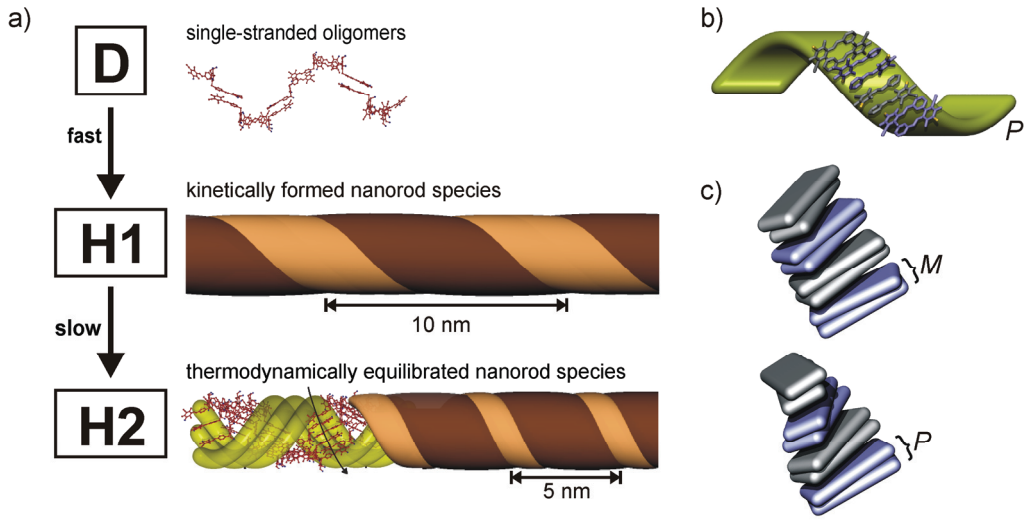

Figure 4. a) Self-assembly sequence of bis(merocyanine) dyes (*R*,*R*)-**6** into kinetically trapped **H1** nanorod aggregates and thermodynamically equilibrated **H2** nanorods. The brown windings in schematic representations of **H1** and **H2** indicate the right-handed helical morphology observed in AFM phase images with differing helical pitches for **H1** and **H2**. b) Model for right-handed (*P*) helically wound arrangement of the stacked chromophores in the rod aggregates. For the sake of clarity only a section of eight chromophores is shown. For more information on our dye packing model see ref 24b. c) Schematic illustration of the left- to right-handed (*M*→*P*) rearrangement between closest neighboring dyes during the **H1**→**H2** transition. The overall helical twist remains right-handed (*P*) for both **H1** and **H2**, but is more pronounced for **H2** than for **H1**.

We propose a structural model for the spatial arrangement of the chromophores in the **H1** and **H2** rods that may account for the apparent discrepancy between the excitonically coupled CD signals and the morphology of **H1** nanorods as well as for the smaller helical pitch of **H2** compared to **H1** nanorods. Since both species are very similar nanorods that contain the chromophores in helically wound stacks (CD, AFM) only a small difference between the two

aggregates structures can be assumed. Such a small structural difference is given in an opposite helical twist between the closest neighboring chromophores in the helically wound stacks (Figure 4b,c). Notably, the antiparallel stacking arrangement of these dipolar dyes with a next closest (d ~ 3.5 Å) and a second more distant neighboring dye unit (d > 4 Å) has been established by several crystal structures of dipolar merocyanine dyes.[23a] Thus, a left-handed helical arrangement of the closest neighboring chromophores in **H1** and a right-handed one in **H2** nanorods may account for the CD spectra of opposite exciton chirality that will be determined by the helical configuration of these next neighboring chromophores (Figure 4c). According to this model the overall twist of the dye stack is right-handed for both nanorod species but more pronounced for **H2** with respect to **H1** what accounts for the same right-handed (*P*) macroscopic helical twist in both dye aggregates but a smaller pitch for the first than for the latter.

5.2.3 "Majority-rules" effect in H1 and H2 nanorods

As shown in the previous section the helical sense of these nanorods is governed by the absolute configuration of the chiral 2-octyl side chains. Thus, we raised the question, whether amplification of chirality, in particular owing to the "majority-rules" effect, can be observed in these supramolecular assemblies and, if so, what are the mechanistic pathways for such amplification. To approach these questions, we have studied the formation of aggregates that are coassembled from enantiomeric (*R*,*R*)-**6** and (*S*,*S*)-**6** monomers of various enantiomeric excess (*ee*). The co-assembly experiments were performed by mixing stock solutions of (*R*,*R*)-**6** and (*S*,*S*)-**6** in THF (3.33×10^{-5} M) in different volumetric ratios. Subsequently, nonpolar methylcyclohexane (MCH) was added to give solutions with a total monomer concentration of 10^{-5} M in a mixture of THF/MCH = 30:70 vol% (for details see Experimental Section). As shown before, the formation of the initial **H1** aggregate is very fast compared to the subsequent transformation of **H1** into **H2** aggregates, and both **H1** and **H2** species could be studied independently with good approximation. Thus, also in the present case of the co-aggregated nanorods, the **H1** spectra were measured after completion of **H1** aggregate formation, which is indicated by attaining the maximum CD amplitude after initiation of aggregation (Figure 5a). The **H2** spectra were revealed after 8 days at room temperature, when the stereomutation from **H1** into **H2** nanorods was found to be complete (Figure 5b). The wavelengths of the maxima/minima of the bisignate Cotton effects of the major UV–vis absorption band as well as the zero-crossing points at 483 and 470 nm observed from the CD spectra are in very good

accordance with those previously observed for **H1** and **H2** nanorods formed from pure (*R*,*R*)-**6** monomers at room temperature, thus revealing the completed formation of the respective **H1** and **H2** nanorods which are co-aggregated from (*R*,*R*)- and (*S*,*S*)-**6**. As expected, the CD spectra corresponding to solutions of antipodal *ee* show mirror image relation, while the solution with racemic monomers (0% *ee*) is CD silent corresponding to the presence of same amounts of left- and right-handed helical nanorods.

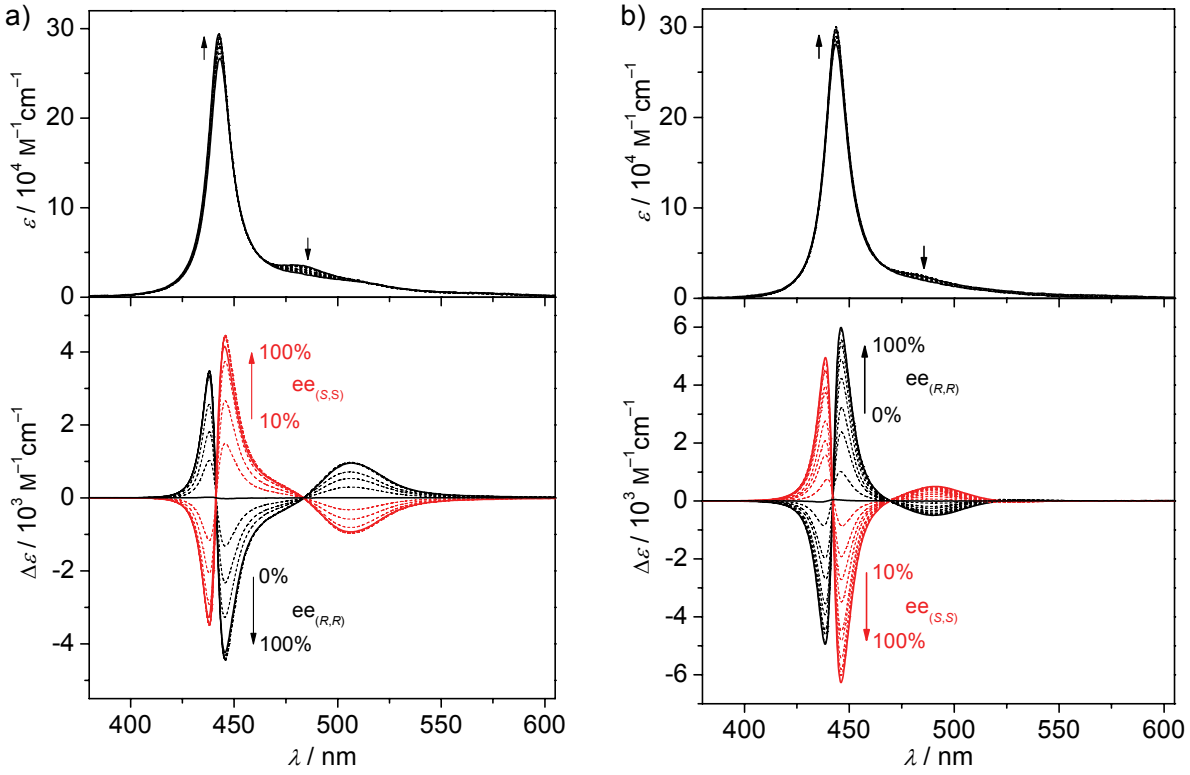

Figure 5. a) UV–vis (top panel) and CD spectra (bottom panel) of a) initially formed **H1** aggregates and b) **H2** aggregates in dependence on the enantiomeric excess (*ee*) of the monomer mixtures (10^{-5} M, THF/MCH = 30:70 vol%, 23 °C). The arrows indicate spectral changes with increasing enantiomeric excess in steps of 10% of the (*R*,*R*)- (black) and (*S*,*S*)-enantiomer (red), respectively. For **H2** the spectra were taken after 8 days at room temperature.

The anisotropy factors g ($\Delta\varepsilon/\varepsilon$) for **H1** and **H2** aggregates formed from enantiomeric mixtures of **6** with various *ee* values were determined from CD and UV–vis spectra at 437 nm (Figure 6).[35] For the kinetically formed **H1** nanorods a nonlinear dependence of the anisotropy factors g_{437} on the enantiomeric excess (*ee*) can be observed which reveals that the "majority-rules" effect is operative in this kind of nanorod species. Thus, an enantiomeric excess of only 15% is required to achieve 50% helical sense excess. Note, that the helical sense excess is defined as the fraction of right-handed helical material minus that of left-handed material and

that the g_{437}-values of ±1.7 and ±2.8 obtained for **H1** and **H2** nanorods formed from enantiopure monomers, respectively, relate to the presence of nanorods of only one helical handedness.[17b,36] In contrast to the kinetically formed **H1** nanorods, only a weakly nonlinear dependence of *g* on the *ee* value of the monomers is found for the **H2** nanorods after 8 days at room temperature. These results indicate that only a weak chiral amplification is operative for **H2** nanorods formed under these conditions and that the "majority-rules" effect must obviously have been disappeared during the conversion of **H1** into **H2** nanorods.[37] However, if the same solutions were kept for 8 days at 47 °C instead of room temperature, also for the **H2** nanorods chiral amplification can be found according to the nonlinear dependence of *g* on the *ee* value observed under these conditions. Under these conditions, an enantiomeric excess of 10% *ee* is required to achieve 50% helical sense excess. In the following this state where chiral amplification is present in **H2** nanorods will be denoted as **H2′**.

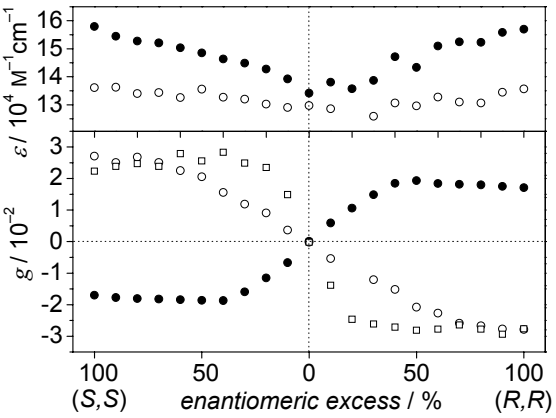

Figure 6. Absorption coefficients ε and anisotropy factors *g* at 437 nm of the initially formed **H1** nanorods at room temperature (●) as well as of the **H2** nanorods after 8 days at room temperature (○) and 47 °C (□, in arbitrary units of *g*) as a function of the enantiomeric excess of the monomer mixtures of (*R*,*R*)-**6** and (*S*,*S*)-**6**.[38]

To summarize, at room temperature the transformation of **H1** nanorods into **H2** nanorods leads to **H2** nanorods with almost absent chiral amplification and only at elevated temperature chiral amplification directed by the "majority-rules" effect can be observed. These observations can be rationalized by a considerably high kinetic barrier for the required reorganization of initially formed **H2** nanorods with non-favored helicity into such with favored one leading to **H2** nanorods with helical sense excess values that are higher than proportional to the *ee* of their monomers (denoted as the **H2′** state). Notably, the disappearance of chiral amplification during the **H1**→**H2** conversion gives further indication for the proposed stereomutation mechanisms where the **H1** nanorods have to be disassembled and thus, the chiral information of **H1**

nanorods is lost. Interestingly, also the UV–vis spectra show subtle changes depending on *ee* of the monomer mixture (Figure 5, top panels), more precisely, an increase of the sharp H-band at 443 nm and a decrease of a lower energy band at around 480 nm with increasing *ee* values. This behavior may be explained either in terms of lowering of the stability of the nanorods and therefore disassembly of the nanorods into random oligomers (denoted as species **D**), or − more likely − is attributed to a change of the excitonic interaction of the chromophores due to their increasingly distorted packing in the aggregates upon increasing amounts of mismatching monomers within the dominant helical sense.

AFM images of a sample prepared from a solution with racemic **6** (0% *ee*) show both **H1** and **H2** nanorods with left- and right-handed helicity, respectively, but no helix reversals within the respective nanorods (Figure 7). The latter observation can be rationalized according to the model of van Gestel, which predicts that the strength of the "majority-rules" effect depends on the free-energy penalty of a mismatch between the preferred helical handedness of a monomer and the actual helical sense of the assembly compared with the energetic penalty for a helical sense reversal.[18] Hence, the quite strong chirality amplification found in the present system indicates that the energetic penalty for a helical sense reversal must be very high compared to a mismatch which is reasonable in view of our aggregate model containing six helically intertwined single-stranded supramolecular polymers.[24b] Thus, as a result of the predicted unfavorable helical sense reversals long domains of the same helical handedness are formed as observed by AFM in the present case.

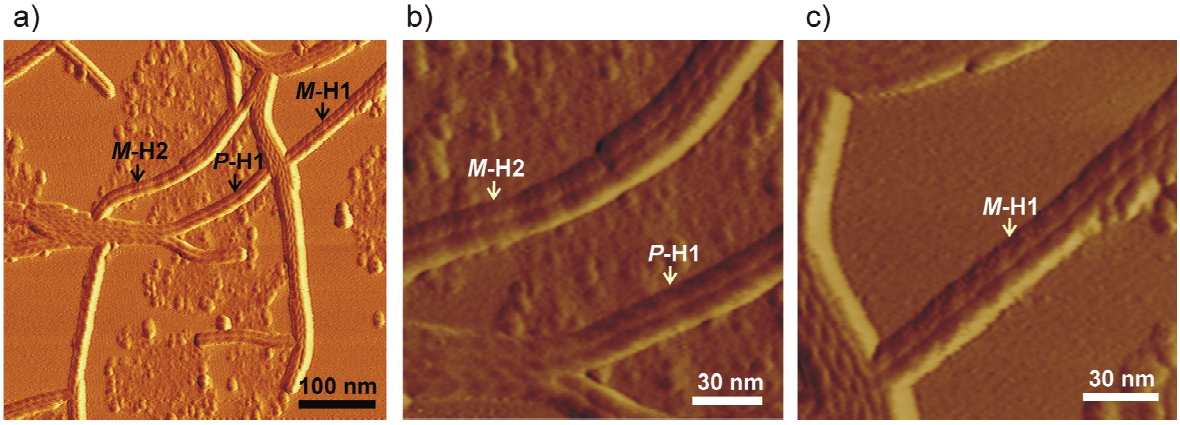

Figure 7. Tapping-mode AFM phase images of a sample prepared by spin-coating of a solution of a racemic mixture of bis(merocyanine) dyes (*R*,*R*)-**2** and (*S*,*S*)-**2** (total concentration 10^{-5} M, THF/MCH = 30:70 vol%) onto HOPG 3 h after initiation of self-assembly. The z scale of the height image is 10 nm. **H1** nanorods with left- and right-handed helicity are visible and the relevant sections are magnified in panels b,c.

5.2.4 Self-assembly kinetics of H1 nanorods with amplified chirality

Although the thermodynamic aspects of the "majority-rules" effect had previously been investigated for other supramolecular systems,[17] the kinetic course of this effect has not been explored so far. The **D**→**H1** aggregation process in the self-assembly sequence of **6** is ideally suited for such kinetic studies because, as shown above, the "majority-rules" effect is operative in **H1** nanorods, and their formation proceeds on a time scale that is convenient for UV–vis and CD spectroscopic studies at ambient temperature. Thus, the **D**→**H1** aggregation process of monomers with various *ee* values was monitored by time-dependent measurements of CD and UV–vis absorption at 437 nm after initiation of aggregation by addition of methylcyclohexane to a THF solution of **6**. The CD data were plotted as $\Delta\varepsilon/ee$, which denotes the molar circular dichroism divided by the respective enantiomeric excess of the monomers, against time (Figure 8a). From this plot the "majority-rules" effect can be easily recognized because the $\Delta\varepsilon/ee$ values should not exceed, but rather converge to the maximum $\Delta\varepsilon/ee$ value ($\Delta\varepsilon_{max} = 3.18\times10^3$ $M^{-1}cm^{-1}$) of the aggregate consisting of enantiopure monomers (100% *ee*) if the helical sense excess of the respective aggregate is proportional to the *ee* values of its monomers. In this case no amplification of chirality is present. On the other hand, if the "majority-rules" effect is operative, the $\Delta\varepsilon/ee$ values would exceed the maximum $\Delta\varepsilon/ee$ value of the homochiral aggregate (100% *ee*), which would indicate a higher helical sense excess than proportional to the *ee* values of the monomers.

The time-dependent UV–vis and CD profiles of samples containing monomers of various *ee* values do not differ significantly up to 110 seconds after initiation of aggregation, but strongly diverge after long times (Figure 8a). This behavior can be interpreted in terms of a nucleation-and-growth process.[4a,b] The first step constitutes the self-assembly of **H1**-type aggregate precursors (further denoted as **H1***) from the instantly formed randomly grown supramolecular oligomer chain species **D**.[39] The rates for this process are with good approximation independent of the *ee* values. This is shown by the time-dependent UV–vis absorption profiles revealing a fast and uniform increase of the aggregate band for all samples. Indeed, AFM images taken in this initial stage of self-assembly show only very small nanorod aggregates in the initial stage of their formation, which can be attributed to the **H1*** nanorod nuclei and wide disordered regions that can be assigned to the less structured supramolecular polymer species **D** (Figure 3a)**.** In this first step the "majority-rules" effect is apparently not involved because the $\Delta\varepsilon/ee$ versus *t* curves for samples of different *ee* do not diverge from the one that

corresponds to 100% *ee*. The helical sense excess of these initial aggregates is therefore proportional to the *ee* value of the monomers.

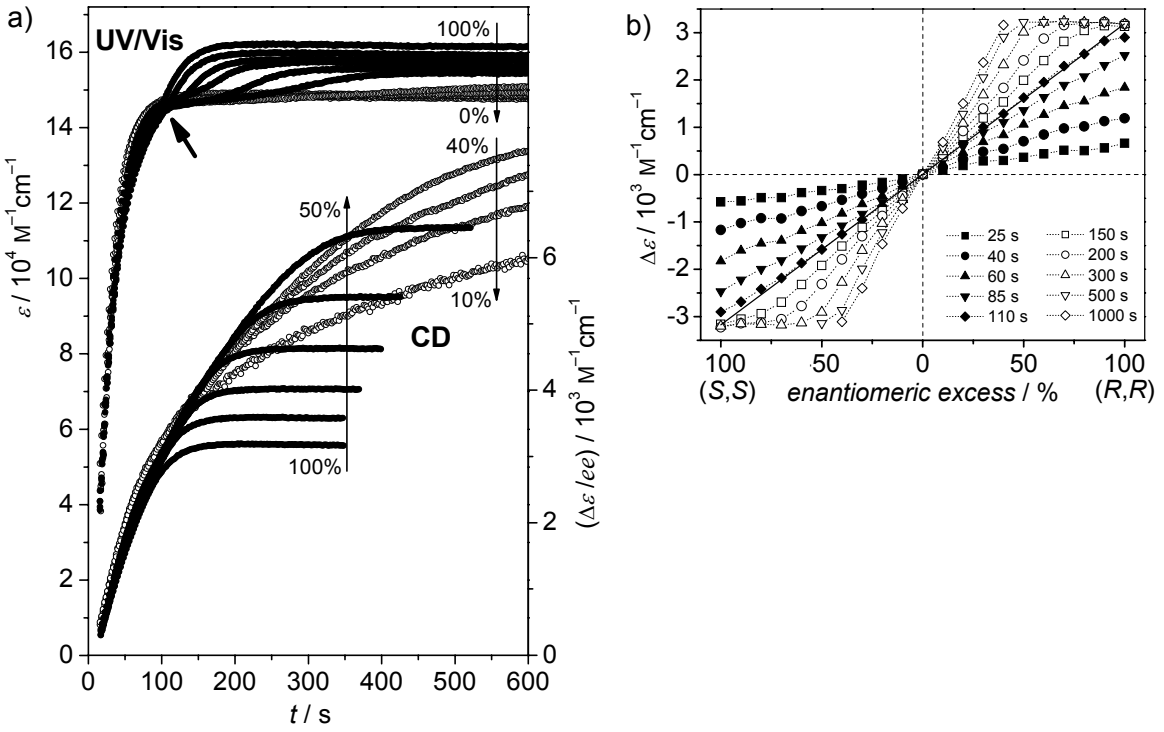

Figure 8. Kinetic study of the **D**→**H1***→**H1** sequence. a) UV–vis absorption (left scale) and circular dichroism (right scale) at 437 nm after initiation of aggregation by adding nonpolar MCH (10^{-5} M, THF/MCH = 30:70 vol%, 23 °C). Notice that the CD values are divided by the respective enantiomeric excess of the monomers for an easy recognition of the "majority-rules" effect. The arrows indicate the order of curves for solutions with decreasing *ee* values of the (*R*,*R*)-**6** enantiomer in steps of 10%: (●) 100–50% *ee*, (○) 40–10% *ee*. b) Molar circular dichroism $\Delta\varepsilon$ at 437 nm as a function of enantiomeric excess at different time after initiation of aggregation: Filled symbols: 25–110 s; open symbols: 150–1000 s. The solid straight line indicates the expected values for the **H1** aggregates in the absence of "majority-rules" effect.

In the subsequent second step, the initial **H1*** precursors grow into elongated **H1** nanorods. In this second step the "majority-rules" effect is operative as indicated by the $\Delta\varepsilon/ee$ values exceeding significantly the one corresponding to 100% *ee*. The action of the "majority-rules" effect in the second step (**H1***→**H1**) is also expressed in the UV–vis absorption profiles by a sigmoid step subsequent to the rapid increase of the H band absorption in the first step (Figure 8a, bold arrow). The height of this sigmoid step increases and the time span decreases with higher *ee* values. This two-step self-assembly pathway is further evident from the plots of the $\Delta\varepsilon$ values versus enantiomeric excess at different time after initiation of the aggregation (Figure 8b). In the initial time period of up to 110 s (filled symbols) the CD values show a linear dependence on the *ee* value, and the slope of the curve increases with increasing time,

thus indicating the formation of the **H1*** precursors. In the further time course (open symbols) the nonlinear behavior of the CD spectrum evolves, which indicates that nanorod growth is now governed by the "majority-rules" effect.

5.2.5 Analysis of the self-assembly kinetics of D species into H1 nanorods

The kinetics of the coupled two-step self-assembly sequence **D**→**H1***→**H1** were evaluated by nonlinear curve fitting of the time-dependent CD data with a kinetic model derived as shown below. Neglecting the initial **M**→**D** aggregation, as it proceeds very fast compared to the subsequent steps, and the respective reverse conversions, the following self-assembly sequence (Scheme 2) was considered for the derivation of the fit function for the time-dependent CD data.

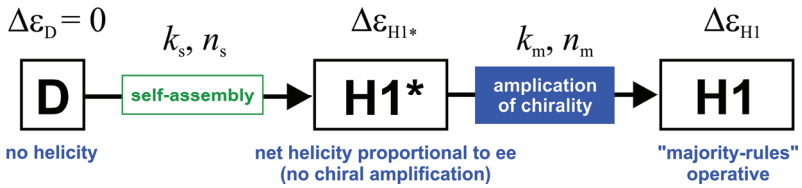

Scheme 2. Two-step self-assembly sequence of chiral bis(merocyanine) dyes **6** from supramolecular oligomers **D** into **H1** aggregates with operative "majority-rules" effect, with the respective optical and kinetic parameters used in the derivation of the fit function for the time-dependent CD data.

The time-dependent CD $\Delta\varepsilon(t)$ is composed of the CD signal of chromophores incorporated in **H1*** species $\Delta\varepsilon_{H1*}$ multiplied by their mole fraction x_{H1*}, plus the CD signal of chromophores incorporated in **H1** species $\Delta\varepsilon_{H1}$ multiplied by their mole fraction x_{H1} (eq 1). Chromophores in the **D** species are CD silent and, therefore, have not being considered for contribution to the CD.

$$\Delta\varepsilon(t) = \Delta\varepsilon_{H1*}x_{H1*}(t) + \Delta\varepsilon_{H1}x_{H1}(t) \qquad (1)$$

Since the time-dependent CD data of this consecutive two-step conversion could not be fitted with simple, standard forms such as coupled first-order or second-order, we have applied a modified first-order rate law (eq 2) with a time-dependent rate constant $\kappa(t)$ for each of the two steps. This rate equation is a simplified form of a "non-conventional autocatalytic mechanism" earlier proposed by Pasternack and was successfully applied to supramolecular polymerization processes.[40] The time-dependent rate constant $\kappa(t)$ is described by two kinetic

parameters, which are the rate coefficient k and the so-called "aggregate growth rate" parameter n. Note that if $n = 0$, the rate law complies with the conventional first-order kinetics.

$$\frac{dx}{dt} = -\kappa(t)x = -(kt)^n kx \tag{2}$$

By applying this rate law for the **D** → **H1*** conversion, the time-dependent mole fraction of monomers incorporated into species **D** $x_D(t)$ can be given as

$$\frac{dx_D(t)}{dt} = -(k_s t)^{n_s} k_s x_D(t) \tag{3}$$

where k_s and n_s denote the kinetic parameters for the **D** → **H1*** self-assembly process. Solving differential equation eq 3 yields:

$$x_D(t) = e^{-(k_s t)^{n_s+1}/(n_s+1)} \tag{4}$$

If one considers that **H1*** is formed from **D** and also further transformed into **H1**, and eq. 2 also applies to the **H1*** → **H1** conversion, the time-dependent mole fraction of monomers incorporated in **H1*** $x_{H1*}(t)$ reads as

$$\frac{dx_{H1*}(t)}{dt} = (k_s t)^{n_s} k_s x_D(t) - (k_m t)^{n_m} k_m x_{H1*}(t) \tag{5}$$

where k_m and n_m denote the kinetic parameters for the **H1*** → **H1** conversion. By combining eqs 4 and 5, we obtain

$$\frac{dx_{H1*}(t)}{dt} = (k_s t)^{n_s} k_s e^{-(k_s t)^{n_s+1}/(n_s+1)} - (k_m t)^{n_m} k_m x_{H1*}(t) \tag{6}$$

Solving this inhomogeneous differential equation 6 yields:

$$x_{H1*}(t) = e^{\left(-\frac{(k_m t)^{n_m+1}}{n_m+1}\right)} \cdot \int_0^t (k_s u)^{n_s} k_s e^{\left(-\frac{(k_s u)^{n_s+1}}{n_s+1} + \frac{(k_m u)^{n_m+1}}{n_m+1}\right)} du \tag{7}$$

The still missing time-dependent mole fraction of monomers incorporated in **H1** species $x_{H1}(t)$ can now be obtained by considering the mass balance law:

$$x_D(t) + x_{H1*}(t) + x_{H1}(t) = 1 \tag{8}$$

Combining eqs. 4, 7, and 8 gives eq. 9.

$$x_{\mathrm{H1}}(t) = 1 - e^{-(k_s t)^{n_s+1}/(n_s+1)} - e^{\left(-\frac{(k_m t)^{n_m+1}}{n_m+1}\right)} \cdot \int_0^t (k_s u)^{n_s} k_s e^{\left(-\frac{(k_s u)^{n_s+1}}{n_s+1} + \frac{(k_m u)^{n_m+1}}{n_m+1}\right)} du \tag{9}$$

The fit function for the time-dependent CD data $\Delta\varepsilon(t)$ can now be obtained by putting the respective time-dependent mole fractions $x_{\mathrm{H1}*}$ and x_{H1} (eqs 7 and 9, respectively) in eq 1 to give

$$\begin{aligned}\Delta\varepsilon(t) = \Delta\varepsilon_{\mathrm{H1}*}&\left(e^{\left(-\frac{(k_m t)^{n_m+1}}{n_m+1}\right)} \cdot \int_0^t (k_s u)^{n_s} k_s e^{\left(-\frac{(k_s u)^{n_s+1}}{n_s+1} + \frac{(k_m u)^{n_m+1}}{n_m+1}\right)} du \right) \\ + \Delta\varepsilon_{\mathrm{H1}}&\left(1 - e^{-(k_s t)^{n_s+1}/(n_s+1)} - e^{\left(-\frac{(k_m t)^{n_m+1}}{n_m+1}\right)} \cdot \int_0^t (k_s u)^{n_s} k_s e^{\left(-\frac{(k_s u)^{n_s+1}}{n_s+1} + \frac{(k_m u)^{n_m+1}}{n_m+1}\right)} du \right)\end{aligned} \tag{10}$$

Nonlinear least square curve fitting of the data by equation 10 was performed applying the Levenberg-Marquardt algorithm as implemented in the computer program given in the Appendix. Although $\Delta\varepsilon_{\mathrm{H1}}$ is well-defined from the asymptotic value of the CD profiles at extended time when merely **H1** nanorod aggregates are present, there are still five freely variable parameters remaining: k_s, n_s, k_m, n_m, and $\Delta\varepsilon_{\mathrm{H1}*}$. As nonlinear curve fitting with that high number of parameters yields ambiguous results, the full set of parameters could be only determined for the enantiomerically pure (*R*,*R*)- and (*S*,*S*)-**6** aggregate data with accuracy, and the so determined parameters k_s and n_s were kept constant for the curve fitting of the remaining samples ($k_s = 2.13\times10^{-2}$ s^{-1} and $n_s = 0.593$ for the series with excess of (*R*,*R*)-**6**; $k_s = 2.03\times10^{-2}$ s^{-1} and $n_s = 0.622$ for the series with excess of (*S*,*S*)-**6**). This procedure seems to be a reasonable approximation. The small deviations of k_s and n_s, respectively, between the samples of pure (*R*,*R*)-**5** and (*S*,*S*)-**5** are attributed to a small difference in the total monomer concentration of the two separately prepared series of samples with antipodal enantiomeric excess. If taking into account the empirical nature of this model and the above-mentioned approximations, the model yields excellent fits to the data with some systematical deviations in the early stages (Figure 9).

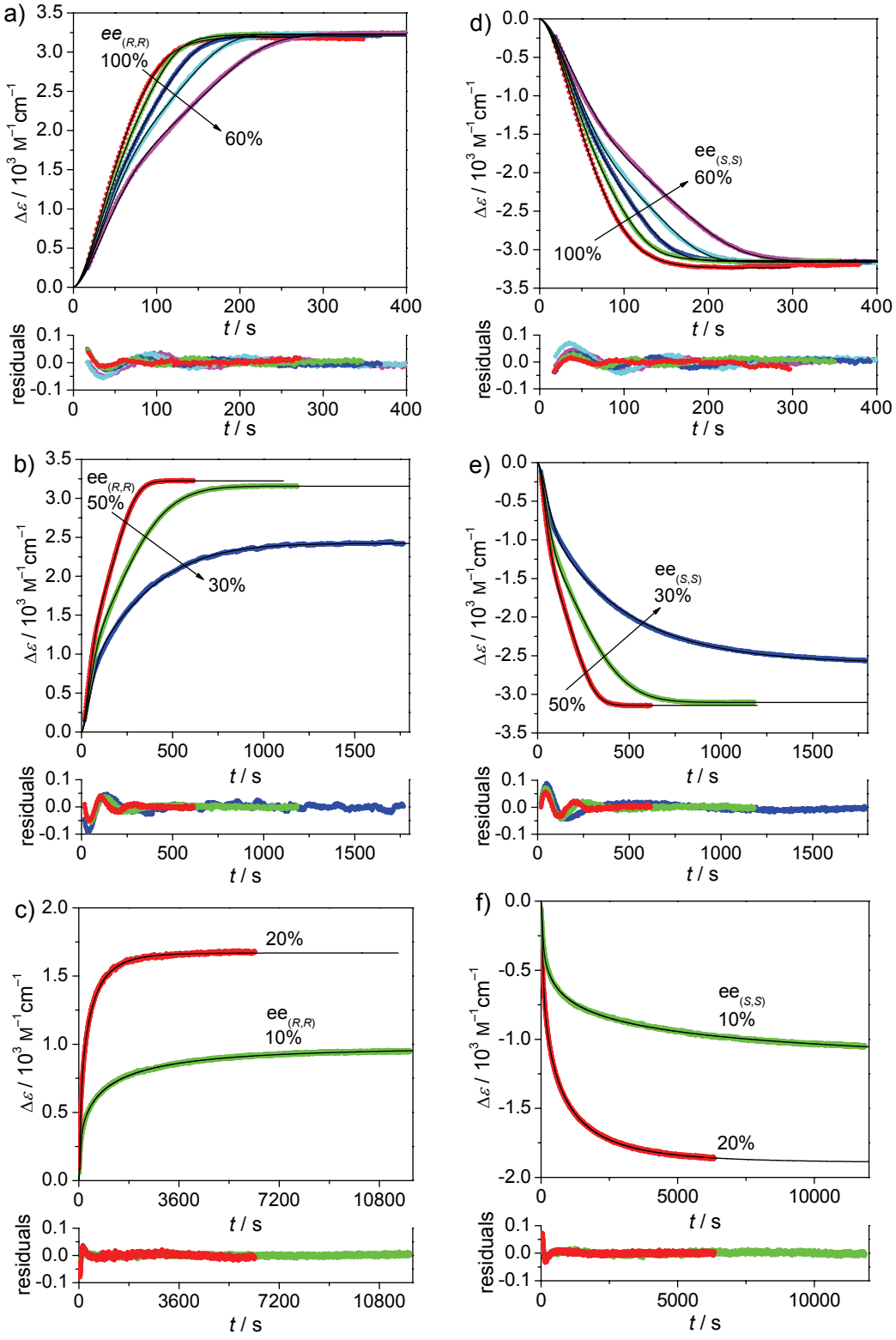

Figure 9. Kinetic profiles of the self-assembly of (*R*,*R*)-**6**/(*S*,*S*)-**6** mixtures with various ee values after initiation of aggregation by adding nonpolar MCH monitored by CD spectroscopy at 437 nm (○) and fitted curves according to equation 10 (—); the residuals panels show the deviation of the fitted curves from the measured data. The units of the residuals are 10^3 $M^{-1}cm^{-1}$. Panels (a–c): series with enantiomeric excess of (*R*,*R*)-**6** and panels (d–f) series with enantiomeric excess of (*S*,*S*)-**6**.

The optical and kinetic parameters k_m, n_m, $\Delta\varepsilon_{H1*}$, and $\Delta\varepsilon_{H1}$ obtained from this procedure are presented in Figure 10 which corroborate the qualitative interpretation of the kinetic data in Figure 8. The linear relationship of $\Delta\varepsilon_{H1*}$ with *ee* values well reflects the proposed proportional net helicity of **H1*** nanorod precursor aggregate, while the characteristic nonlinear relationship of $\Delta\varepsilon_{H1}$ to the enantiomeric excess shows the "majority-rules" effect operational in the formation of elongated **H1** nanorod aggregates. As noted above, the kinetic parameters for the **D**→**H1*** conversions, k_s and n_s, were kept constant for all *ee* values which implies that their rate is in approximation independent on the *ee* value. In contrast, both kinetic parameters for the "majority-rules" conversion **H1***→**H1**, k_m and n_m, respectively, increase strongly with higher *ee*.

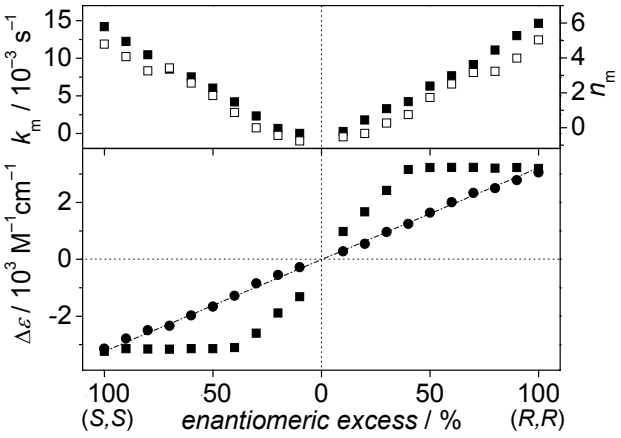

Figure 10. Optical data and kinetic parameters for the **D**→**H1***→**H1** self-assembly sequence dependent on the enantiomeric excess of the monomers obtained from nonlinear curve fitting of the time-dependent CD data. Molar circular dichroism of **H1*** ($\Delta\varepsilon_{H1*}$, ●) and **H1** ($\Delta\varepsilon_{H1}$, ■) aggregates at 437 nm (bottom panel) and kinetic parameters k_m (■) and n_m (□) for the "majority-rules" directed nanorod growth process (top panel).

With this procedure we could simulate both the kinetic profiles of the **D**→**H1*** nucleation and that of the "majority-rules" effect directed **H1***→**H1** growth decoupled from the respective subsequent or preceding step, *i.e.*, entangled from the coupled two-step sequence (Figure 11). For this purpose, we plotted the respective mole fraction $x_{H1*}(t)$ for the **D**→**H1*** conversion and $x_{H1}(t)$ for the **H1***→**H1** conversions versus time by applying the integrated form of the basic rate law (eq 11) with the corresponding kinetic parameters k_s and n_s (for **D**→**H1***), and k_m and n_m (for **H1***→**H1**). The parameters for the same enantiomeric excess of (*R*,*R*)-**2** and (*S*,*S*)-**2** monomers are averaged.

$$x(t) = e^{-(kt)^{n+1}/(n+1)} \tag{11}$$

Thus, for the **D→H1*** step, a kinetic profile with an induction period and a sigmoid shape is obtained (Figure 12, thick line). Such kinetic profiles have been previously observed in supramolecular polymerization and were attributed to an autocatalytic growth mechanism after the spontaneous formation of a "critical" nucleus.[41] More importantly, our analysis reveals that the second step, that is, the "majority-rules" directed chiral amplification as given in the **H1*→H1** process, is also governed by an autocatalytic mechanism that is strongly dependent on the enantiomeric excess. The kinetic profiles for greater than 20% *ee* show sigmoid profiles with induction periods that become more pronounced with higher *ee* values, while the sigmoid character is lost for *ee* values less than 20% *ee* (Figure 11). These kinetics may point at an autocatalytic generation of "secondary" nuclei with preferred helicity that grow into larger domains.[42] In other words, only those **H1*** nuclei that have the proper "majority-rules" governed chiral supramolecular organization act as proper templates for elongation into extended nanorods whilst the "wrong" nuclei convert back into D-species over time as discussed before in the context of the supramolecular stereomutation phenomena. Clearly, such **H1*→H1** reorganization can proceed faster with higher *ee* of the monomers as a higher excess of aggregates with the preferred helicity is initially formed as a consequence of the linear relationship of the net helicity of **H1*** precursor aggregates on the *ee* value. As a result, the rate of the **H1*→H1** transformation increases strongly with higher *ee* values, while full conversion requires up to several hours for 10% *ee* (Figure 11).

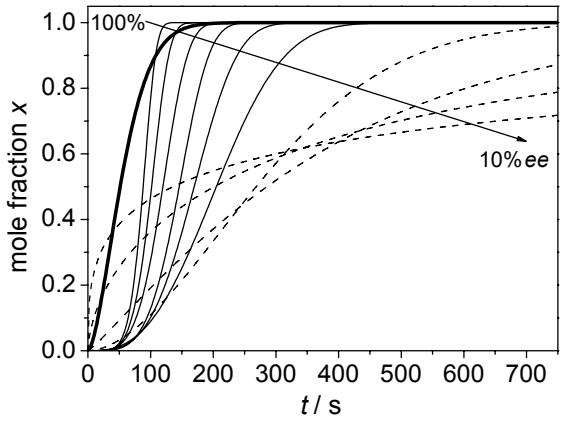

Figure 11. Simulations of the kinetic profiles for the decoupled **D→H1*** and **H1*→H1** step. The mole fractions x_{H1*} (thick line) corresponding to the fraction of monomers incorporated in **H1*** species for the **D→H1*** step and mole fractions x_{H1} (thin lines) corresponding to the fraction of monomers incorporated in **H1** species for the **H1*→H1** step. In the latter, the curves for samples with decreasing ee are indicated by the arrow.

5.2.6 Chiral amplification in H2 nanorods by the "sergeant-and-soldiers" principle

Although chiral amplification owing to the majority-rules effect is also operative in **H2** nanorods upon co-assembly of (*R*,*R*)- and (*S*,*S*)-**6** monomers at elevated temperature (see 5.2.3), the kinetics leading to the **H2′** state was not easily accessible at room temperature where it would take several months. On the other hand, experiments at higher temperature suffer from partial dissociation of the nanorods of lower *ee*. Thus, in order to gain deeper insight into the kinetics leading to the chiral amplification in **H2** nanorods, we applied mixtures of **5** and (*R*,*R*)-**6** monomers for the co-aggregation experiments and studied the kinetics of chiral amplification in **H2** nanorods directed by the sergeants-and-soldiers principle. For the present co-aggregates dissociation was not as pronounced at elevated temperature as in the "majority-rules" experiments. The co-assembly experiments were performed by mixing stock solutions of **5** and (*R*,*R*)-**6** in THF (3.33×10^{-5} M) in different volumetric ratios. Subsequently, nonpolar methylcyclohexane (MCH) was added to give solutions with a total monomer concentration of 10^{-5} M in a mixture of THF/MCH = 30:70 vol% (for details see Experimental Section). In the present case we heated the solutions to 47 °C after initiation of aggregation by MCH addition (instead of keeping them at room temperature) to accomplish quick formation of the **H2** nanorods as shown before for pure (*R*,*R*)-**6** (see Figure 2). Figure 12 shows CD spectra of aggregates containing 5% chiral "sergeant" molecules that are recorded at different time intervals (20 min−39 h) after initiation of aggregation and heating to 47 °C. With increasing time a uniform increase of the CD intensity can be observed for all wavelengths.[43] The wavelengths of the maxima/minima as well as the zero-crossing points observed from the CD spectra recorded during this time remain constant and are in good accordance with those previously observed for **H2** nanorods formed from pure (*R*,*R*)-**6** monomers at room temperature. However, a close comparison of the CD spectra of the here studied **H2** co-aggregates from mixtures of **5** and (*R*,*R*)-**6** (Figure 12b) with that of **H2** nanorods formed from pure (*R*,*R*)-**6** reveals a slight hypsochromic shift of the former ones (about 1 nm) which can be attributed to a slightly different packing in the former ones compared to **H2** nanorods from pure (*R*,*R*)-**6**. Importantly, this slight spectral shift indicates the co-aggregated nature of the **H2** nanorods. These spectral features clearly reveal that the formation of the co-aggregated **H2** nanorods is completed at elevated temperature already after 20 min.

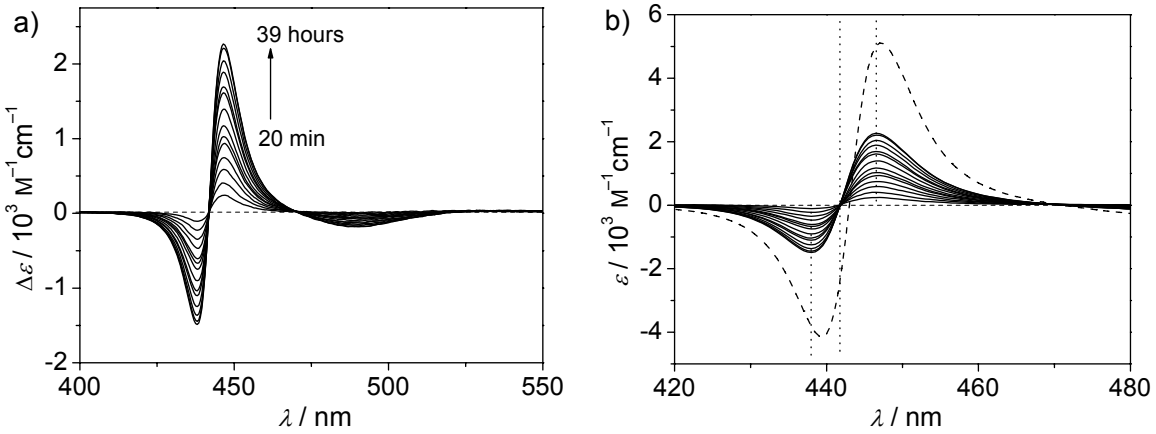

Figure 12. a) Time-dependent CD spectra of nanorods formed from dyes **5** and (*R,R*)-**6** (95:5 mol%) ($c_{tot} = 10^{-5}$ M, THF/MCH = 30:70 vol%, 47 °C). The arrow indicates spectral changes with increasing time. b) Magnified section of the spectra shown in Fig.12a (solid lines). For comparison the CD spectrum of **H2** aggregates formed from pure (*R,R*)-**6** monomers (dashed line) was added. The dotted lines serve as an orientation for the spectral shifts.

For the self-assembly experiments with other fraction of chiral sergeant monomers similar spectral changes were observed and Figure 13 shows the anisotropy factors *g* at 437 nm obtained at different time in dependence of fraction of chiral sergeant. The nonlinear behavior of the *g*-values on the fraction of chiral sergeant monomers provides evidence that chiral amplification directed by the sergeant-and-soldiers principle is operative in the present **H2** nanorods and, more importantly, that the uniform increase of the CD intensity (recorded for up to 39 h) for all wavelengths can be attributed to the reconstruction of coexisting **H2** nanorod aggregates with energetically disfavored left-handed (*M*) helicity into such with the preferred right-handed (*P*) helicity, thus, leading to increasing helical sense excess with time (Figure 13). A pronounced impact of the amount of (*R,R*)-**6** sergeants on the time required for this chiral amplification process can be observed. Thus, already after 6 h (Figure 13, filled squares), the anisotropy factors of nanorods containing 40% or more chiral sergeants are almost the same as those observed for nanorods assembled from pure chiral monomers (*R,R*)-**6**. In these cases the helical sense excess, which can be directly derived from the *g* values, reaches more than 93% during the first 6 h (Figure 13, right scale).[44] However, the kinetics of this chiral amplification slows down considerably for decreasing fraction of co-monomer (*R,R*)-**6**, as revealed by the increasing *g* factors of nanorods containing 5 to 20% chiral sergeants in the time period from 6 to 18 h. In the case of 20% chiral sergeants, a helical sense excess of 73% is obtained after 6 h, while 87% is reached after 18 h. Finally, the helical sense excess reached by nanorods containing 10 and 5% chiral sergeants is only 62 and 36%, respectively, after 18 h.

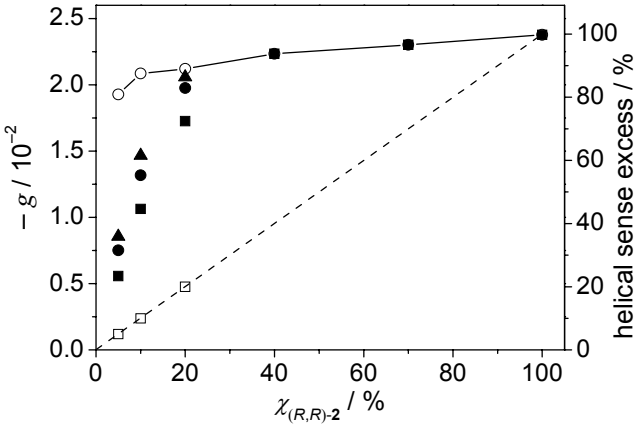

Figure 13. Dependence of the anisotropy factor g at 437 nm on the mole fraction $\chi_{(R,R)\text{-}\mathbf{2}}$ of chiral (*R*,*R*)-**6** after 6 h (■), 12 h (●), and 18 h (▲) of equilibration at 47 °C. Additionally, the g values for the start (□) and final state (○) obtained from nonlinear curve fitting of the time-dependent CD data are shown. The dashed line represents the expected g values in the absence of any chiral amplification.

For a detailed analysis of the kinetics of this chiral amplification process the anisotropy factors g at the minima of the Cotton effect at 437−438 nm were plotted versus time in Figure 14. The time-dependent g values could be properly described by a stretched exponential relaxation function,

$$g(t) = g_{\mathrm{H2'}} + (g_{\mathrm{H2}} - g_{\mathrm{H2'}}) \cdot e^{-\left(\frac{t-t_0}{\tau}\right)^{\beta}} \qquad (t \geq t_0) \tag{12}$$

where t_0 denotes the time for completion of **H2** aggregate formation after initiation of self-assembly, τ the relaxation time, β the stretching parameter, g_{H2} the anisotropy factor of **H2** nanorods before chiral amplification, and $g_{\mathrm{H2'}}$ that of **H2′** nanorods with operative chiral amplification. Notably, for reducing the number of free variable parameters of the nonlinear curve fitting, the g_{H2} values were set as the g value for nanorods consisting of pure (*R*,*R*)-**6** ($g = -2.38\times10^{-2}$) multiplied by the respective fraction of chiral monomers $\chi_{(R,R)\text{-}\mathbf{2}}$ which implies that the **H2** nanorods do not show chiral amplification right after their formation. As shown in Figure 14 the curve fitting of the time-dependent anisotropy factors g at 437 nm yielded excellent fits to the data with correlation coefficients higher than 0.99, and the parameters obtained from this procedure are collected in Table 2.

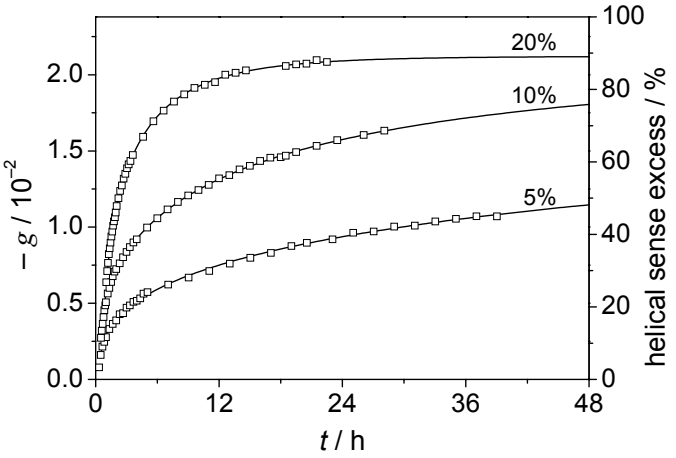

Figure 14. Time-dependent anisotropy factors *g* at 437 nm of nanorods formed from dyes **5** and (*R,R*)-**6** with various mole fractions of chiral (*R,R*)-**6** (5−20%) as indicated ($c_{tot} = 10^{-5}$ M, THF/MCH = 30:70 vol%, 47 °C). The solid lines represent the stretched exponential curve fits according to eq 12 with correlation coefficients $r^2 > 0.99$.

Table 2. Results from curve fitting of the time-dependent *g* values.

$\chi_{(R,R)\text{-}\mathbf{6}}$	g_{H2} (10^{-2}) [a]	$g_{H2'}$ (10^{-2})	τ (h)	β
5%	−0.119	−1.93	68.9	0.47
10%	−0.238	−2.09	13.9	0.55
20%	−0.476	−2.12	3.1	0.68

[a] The value for g_{H2} was not varied for the nonlinear curve fitting.

Table 2 shows an increase of the relaxation time from 3 to 69 hours upon decrease of the fraction of chiral sergeants from 20 to 5%. This indicates that the chiral amplification by means of a reconstruction of nanorods with unfavorable helicity into that with the favored one drastically slows down for decreasing fraction of chiral sergeants. The g_{H2} and $g_{H2'}$ values from the curve fitting for the nanorods of different ratios of **5**/(*R*,*R*)-**6** are included in Figure 13 by the open symbols and reveal that after complete formation of **H2** nanorods no chiral amplification is present while a final helical sense excess of more that 80% can be realized after long time for all investigated mixtures. Accordingly, at a fraction of 5 mol% of (*R*,*R*)-**6** a number of 17 soldier molecules are properly directed by the sergeant molecules. These observations found for the present "sergeant-and-soldiers" principle directed chiral amplification in **H2** nanorods are in excellent accordance with those for the "majority-rules" effect directed chiral amplification in **H2** nanorods (see 5.2.3), where the initially formed **H2** nanorods do not show chiral amplification, while after longer equilibration time at elevated temperature pronounced chiral amplification became evident.

It is important to note that this chiral amplification process is markedly distinguished from previous reports on the time-dependence of the sergeants-and-soldiers effect by a slow exchange of achiral and chiral building blocks among the respective pre-assembled racemic and homochiral aggregates.[19] However, we also have have conducted such type of experiments by adding a small amount of homochiral **H2** nanorods (pre-assembled from (*R*,*R*)-**2**) to the racemic mixture of **H2** nanorods (pre-assembled from achiral **1**). Also in this case amplification of helical bias could be observed indicating the exchange of chiral and achiral monomers among the pre-assembled nanorod aggregates.[45]

5.3 Summary of the Self-Assembly Processes

Previous studies on bis(merocyanine) dye nanorods by Würthner and coworkers were focused on the thermodynamics of the hierarchical self-assembly in dependence of concentration and solvent polarity.[24] Especially the latter was found to offer a unique parameter to control dye self-organization based on thermodynamic data derived from studies on merocyanine dimerization[23] that established the predominantly electrostatic nature of the noncovalent interaction between dipolar merocyanine dyes. Thus, with decreasing solvent polarity, the strength of the noncovalent dipole–dipole interaction increases, allowing for structural growth from the molecular to the macroscopic scale. In contrast, the present work investigated the self-assembly kinetics for the formation of bis(merocyanine) dye nanorods and revealed a complex self-assembly sequence for this superstructure formation. Figure 15 gives an overview of the observed self-assembly sequence which will be summarized in the following starting from the monomers and ending up with the thermodynamically stable **H2** nanorods with amplified chirality. The observation of several kinetically trapped intermediates in this self-assembly sequence can be rationalized by increasing kinetic barriers upon formation of the subsequent thermodynamically more stable species.

After addition of nonpolar MCH the bis(merocyanine) dye monomers **M** instantly aggregate into the single-stranded polymer species **D** with rates that were too fast to be studied with the applied spectroscopic methods. Since the formation of these supramolecular polymers requires only the antiparallel aggregation of two chromophores of the bis(merocyanine) dyes, it is reasonable that this process is the most rapid in the self-assembly sequence. In the subsequent step, this **D** species self-assembles into a first kinetic product with extended helically aggregated π-stacks, *i.e.* the **H1** nanorods, via a nucleation-and-growth mechanism. By studying the effect of the enantiomeric excess on the nanorod formation, we could reveal that

in the first step the **H1*** nuclei are formed with rates that are independent on the enantiomeric excess of the monomers and, in addition, the helicity of these nuclei is not governed by the "majority-rules" effect. Thus, the fast formation of these nanorod precursors is quite unspecific. However, in the subsequent growth of these nanorod precursors into elongated **H1** nanorods a strong impact of the *ee* of the monomers is observed. Here, the "majority-rules" effect is involved leading to helical sense excess of the nanorods that is higher than proportional to the *ee* of the monomers. Interestingly, the time-dependence of this growth is also strongly determined by the *ee* and, thus, the growth of the nanorods takes far longer from monomers of lower *ee* compared to that from enantiopure monomers. The different rates observed for this elongation and concomitant chiral amplification could be attributed to an autocatalytic formation of nuclei with the "majority-rules" governed helicity.

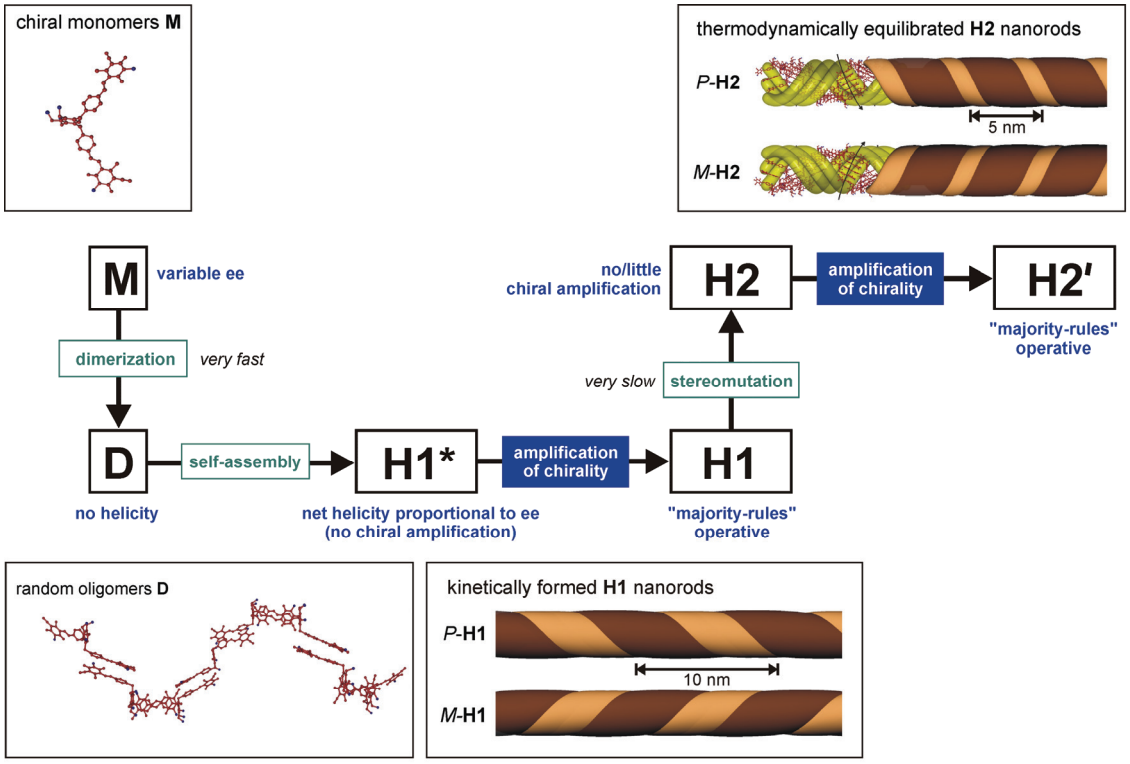

Figure 15. Self-assembly sequence of bis(merocyanine) monomer mixtures of (*R*,*R*)-**6** and (*S*,*S*)-**6** with variable *ee* into helical nanorods after initiation of aggregation. Instantaneous dimerization of chromophores leads to oligomeric species **D** without structural and helical preference, which self-assemble into nanorod precursors **H1***, showing a helical sense excess that is proportional to the *ee* values of the monomer mixtures. Directed by the "majority-rules" effect, the **H1*** precursors grow into elongated **H1** nanorods with supramolecular homochirality. In a much slower supramolecular stereomutation process the **H1** nanorods are converted into **H2** nanorods, followed by chiral amplification in the case of *ee* < 100%

In a subsequent much slower process these kinetically formed **H1** nanorods are converted into more compact **H2** nanorods that show nearly mirror image CD spectra as well as a smaller pitch of the helical morphology. In the case of enantiopure monomers these homochiral **H2** nanorods represent the thermodynamically stable self-assembly product. Solvent-dependent kinetic studies for this stereomutation of **H1** into **H2** nanorods with enantiopure monomers suggest that the **H1** nanorods have to be disassembled for this process to occur. Although the detailed kinetics of this supramolecular stereomutation was not investigated for mixtures of the enantiomeric monomers, the studies after 8 days at room temperature showed that the stereomutation was completed for the nanorods consisting of monomers of different *ee* at that time and, more importantly, the chiral amplification by means of the "majority-rules" effect was lost during the stereomutation process. This loss of the "majority-rules" effect governed chiral information in the **H1** nanorods might be a result of the above proposed disassembly of the **H1** nanorods for the conversion into **H2** nanorods. Thus, for the **H2** nanorods containing monomers with less than 100% *ee* a subsequent reconstruction of the nanorods with disfavored helicity occurs leading to chiral amplification in these **H2** nanorod aggregates. In the case of the sergeant-and-soldiers studies the same observation was made and detailed kinetic studies showed that this chiral amplification process slows down for a smaller fraction of chiral sergeants, but high excess of helical sense can still be reached with a small fraction of chiral sergeants after extended period of time.

The grave difference between the chiral amplification found in **H1** and **H2** nanorods is that the first one occurs in the early stage of nanorod formation, *i.e.*, the self-assembly of the monomers into a kinetic nanorod product (denoted as **H1**), while the latter is due to a time-dependent development of helical bias as a self-ordering phenomenon of pre-assembled **H2** nanorods with initial statistical *M*/*P* ratio. The latter chiral amplification process can be interpreted in terms of a reconstruction of initially formed **H2** nanorods with the "wrong" helicity into such with a helical sense that is favored by the enantiomer in majority or by the sergeant molecules.

5.4 Conclusion

To conclude, this chapter elucidated the helical nature of bis(merocyanine) dye nanorods and, more importantly, disclosed a complex self-assembly sequence of chiral bis(merocyanine) dyes into well-defined helical nanorod structures. As revealed spectroscopically by time-dependent CD spectroscopy and microscopically by atomic force microscopy this self-

assembly process proceeds over several kinetically formed supramolecular intermediates which are distinguished by their morphology, circular dichroism spectra, and helical sense excess. Moreover, these studies provided novel insights into the kinetics of chiral amplification in a supramolecular system and showed that chiral amplification mechanisms can operate at different stages of self-assembly to afford energetically favored structures. The enantiomeric excess in the monomers as well as the fraction of chiral monomers has a strong impact on the nanorod morphogenesis and chiral amplification kinetics. The rates of these processes decreases strongly with decreasing chiral bias in the monomers as realized by decreasing enantiomeric excess of the chiral monomers or decreasing fraction of chiral co-monomers in mixtures of chiral and achiral monomers. Nevertheless, after extended periods of time for the fully equilibrated nanorod structures strong chiral amplification directed by the "majority-rules" or "sergeants-and-soldiers" effect can be observed. These studies highlight the complexity of a self-assembly pathway in an artificial system and point out the importance of kinetic control in self-assembly.

5.5 Experimental Section

Materials and Methods. Solvents and reagents were obtained from commercial suppliers, unless otherwise stated, and used without further purification. Chiral amines (*R*)-**2** and (*S*)-**2** were purchased from Lancaster with an enantiomeric excess of higher than 99%. Dibromide **4** and bis(merocyanine) dye **5** were synthesized according to literature procedure.[9] Column chromatography was performed on silica gel (Merck Silica 60, particle size 0.04−0.063 mm) and thin layer chromatography (TLC) was conducted on silica gel plates (60 F_{254} Merck, Darmstadt). High performance liquid chromatography (HPLC) was carried out on Nucleosil 100-5 NO2 column (Macherey&Nagel, Düren/Germany) using purity-grade "pa" solvents. Melting points were determined on a Linkam TP 94 heating stage and are uncorrected. The solvents for UV–vis absorption, circular dichroism (CD), and atomic force microscopy (AFM) studies were of spectroscopic grade and used as received. ^{1}H NMR spectra were recorded on a Bruker Avance 400 spectrometer at 25 °C with TMS or residual undeuterated solvent as internal standard. High resolution ESI-TOF mass spectrometry was carried out on a microTOF focus instrument (Bruker Daltronik GmbH) in positive mode with MeOH or MeCN as solvent. UV–vis absorption was measured on a Perkin Elmer Lambda 950 UV–vis spectrophotometer with a spectral bandwidth of 2 nm and a scan rate of 140 nm/min using a conventional quartz cell (light path 5 mm). Temperature was regulated by a PTP-1 Peltier element (Perkin Elmer).

CD was measured on a Jasco J-950 spectropolarimeter with a spectral bandwidth of 1 nm, a response time of 1 s and a scan rate of 50 nm/min using the same quartz cell. AFM measurements were performed under ambient conditions using a MultiMode Nanoscope IV system operating in tapping mode in air. Silicon cantilevers (Olympus Corp.) with a resonance frequency of 300 kHz were used. Solutions of a racemic mixture of dye **6** in THF/MCH = 30:70) were spin-coated onto a HOPG (highly ordered pyrolytic graphite) surface under 3000 rpm.

Self-Assembly Experiments. Solutions for the self-assembly experiments in THF/MCH = 30:70 vol% containing a total monomer concentration of 10^{-5} M were prepared from stock solutions of **5**, (*R*,*R*)-**6**, and (*S*,*S*)-**6** in tetrahydrofuran (3.33×10^{-5} M) by mixing in different volumetric ratios to obtain monomer solutions with either enantiomeric excess ranging from 0% *ee* to 100% *ee* of both (*R*,*R*)-**6** or (*S*,*S*)-**6**, or containing a mixture of **5** and (*R*,*R*)-**6** with fractions of the chiral monomer ranging from 5 to 100%. The aggregation of the monomers into nanorods was initiated by addition of nonpolar methylcyclohexane (817 μL) to the respective THF monomer solution (350 μL). Accordingly, for the self-assembly experiments of (*R*,*R*)-**6** in THF/MCH = 40:60, MCH (675 μL) was added to a 2.5×10^{-5} M THF stock solution (450 μL), and for the self-assembly in 20:80 vol%, MCH (1000 μL) was added to a 5.0×10^{-5} M THF stock solution (250 μL).

General Procedure for the Synthesis of Chiral Hydroxypyridones 3: Ethyl cyanoacetate (880 mg, 7.74 mmol) was added dropwise to the (*R*)- or (*S*)-2-octylamine (**2**) (1.00 g, 7.74 mmol) within 15 min and stirred at room temperature for 72 h. Afterwards, ethyl acetoacetate (1.01 g, 7.74 mmol) and piperidine (0.77 mL) were added, and the mixture was stirred at 100 °C for 20 h. The solvent was evaporated and the pH value was adjusted to 1 with 32% aqueous HCl. The precipitated product was separated by filtration, washed with water (2×5 mL) and dried under vacuum. Recrystallization of the crude product with ethyl acetate afforded the analytically pure pyridones in 50–53% yield.

6-Hydroxy-4-methyl-1-[(1*R*)-1-methylheptyl]-2-oxo-1,2-dihydropyridine-3-carbonitrile ((*R*)-3): Yield: 1.08 g (4.12 mmol, 53%). Mp 183–185 °C. ^{1}H NMR (400 MHz, DMSO-d_6, 25 °C): δ 5.56 (s, 1H, 5-H), 5.26 (s, 1H, NCH), 2.19 (s, 3H, 4-CH_3), 1.95 (m, 1H, NCHCH_2), 1.65 (m, 1H, NCHCH_2), 1.36 (s, 3H, NCHCH_3), 1.25–1.00 (m, 8H, CH_2), 0.83 (t, J = 6.8 Hz, 3H,

CH_3). HRMS (ESI, pos. mode, MeOH): calcd *m*/*z* for $C_{15}H_{22}N_2O_2Na$ ([*M*+Na]$^+$) 285.1574, found 285.1574. Anal. Calcd for $C_{15}H_{22}N_2O_2$ (262.35): C, 68.67; H, 8.45; N, 10.68. Found: C, 68.50; H, 8.23; N, 10.39.

6-Hydroxy-4-methyl-1-[(1*S*)-1-methylheptyl]-2-oxo-1,2-dihydropyridine-3-carbonitrile ((*S*)-3): Yield: 1.02 g (3.39 mmol, 50%). Mp: 183–185 °C. ^{1}H NMR (400 MHz, DMSO-d_6, 25 °C) δ 5.56 (s, 1H, 5-H), 5.26 (s, 1H, NCH), 2.19 (s, 3H, 4-CH_3), 1.95 (m, 1H, NCHCH_2), 1.65 (m, 1H, NCHCH_2), 1.36 (s, 3H, NCHCH_3), 1.25–1.00 (m, 8H, CH_2), 0.83 (t, *J* = 6.8 Hz, 3H, CH_3). HRMS (ESI, pos. mode, MeOH): calcd *m*/*z* for $C_{15}H_{22}N_2O_2Na$ ([*M*+Na]$^+$) 285.15735, found 285.15734. Anal. Calcd. for $C_{15}H_{22}N_2O_2$ (262.35): C, 68.67; H, 8.45; N, 10.68. Found: C, 68.65; H, 8.31; N, 10.54.

General Procedure for the Synthesis of Chiral Bis(merocyanines) 6: The respective chiral pyridone **3** (1.0 mmol) and *N*,*N*′-diphenylformamidine (1.0 mmol) in Ac_2O (1.75 mL) were stirred at room temperature for 15 min. The mixture was then heated to 90 °C for additional 30 min to complete the reaction. After being cooled to room temperature, pyridinium salt **4** (0.33 mmol) and KOAc (1.0 mmol) were added, and the mixture was heated at 100 °C for 14 h. The solution was concentrated in vacuo, and the crude product was purified by column chromatography on silica using CH_2Cl_2/MeOH = 95:5 as eluent. After precipitation from CH_2Cl_2/MeOH and drying in vacuo, the dyes were obtained in analytically pure form. Prior to self-assembly experiments further purification was made by preparative HPLC using CH_2Cl_2/MeOH = 9:1 as eluent, followed by precipitation and drying as mentioned above.

(5*Z*,5′*Z*)-5,5′-{[4,5,6-Tris(dodecyloxy)-1,3-phenylene]bis[methylenepyridin-1-yl-4-ylidene(1*Z*)ethane-2,1-diylidene]}bis{4-methyl-1-[(1*R*)-1-methylheptyl]-2,6-dioxo-1,2,5,6-tetrahydropyridine-3-carbonitrile} ((*R*,*R*)-6): Yield: 330 mg (0.24 mmol, 24%). Mp: 261–263 °C. TLC (CH_2Cl_2/MeOH = 93:7) R_f = 0.37. ^{1}H NMR (400 MHz, CD_2Cl_2/MeOD-d_4 = 4:1): δ 8.09 (d, *J* = 7.0 Hz, 4H, py-H), 7.66 (d, *J* = 15.0 Hz, 2H, met-H), 7.61 (d, *J* = 14.9 Hz, 2H, met-H), 7.44 (d, *J* = 7.2 Hz, 4H, py-H), 7.37 (s, 1H, ph-H), 5.35 (s, 4H, NCH_2), 5.12 (m, 2H, NCH), 4.11 (t, *J* = 6.9 Hz, 4H, OCH_2), 3.91 (t, *J* = 6.7 Hz, 2H, OCH_2), 2.33 (s, 6H, CH_3), 2.06 (m, 2H, CH_2), 1.73 (m, 8H, CH_2), 1.41 (d, *J* = 6.8 Hz, 6H, CH_3), 1.40–1.08 (m, 70H, CH_2), 0.85 (m, 15H, CH_3). HRMS (ESI, pos. mode, MeOH): calcd *m/z* for $C_{88}H_{132}N_6O_7Na$ ([*M*+Na]$^+$): 1408.0050, found: 1408.0056. Anal. Calcd for $C_{88}H_{132}N_6O_7$ (1386.03): C, 76.26;

H, 9.60; N, 6.06. Found: C, 76.07; H, 9.92; N, 5.85. UV–vis (CH_2Cl_2, 25 °C, 10^{-6} M): λ_{max} (ε) = 572 nm (207000 $M^{-1}cm^{-1}$)

(5*Z*,5′*Z*)-5,5′-{[4,5,6-Tris(dodecyloxy)-1,3-phenylene]bis[methylenepyridin-1-yl-4-ylidene(1*Z*)ethane-2,1-diylidene]}bis{4-methyl-1-[(1*S*)-1-methylheptyl]-2,6-dioxo-1,2,5,6-tetrahydropyridine-3-carbonitrile} ((*S*,*S*)-6): Yield: 346 mg (0.25 mmol, 25%). Mp: 261–263 °C. TLC (CH_2Cl_2/MeOH = 93:7) R_f = 0.37. ^{1}H NMR (400 MHz, CD_2Cl_2/MeOD-d_4 = 4:1): δ 8.09 (d, J = 7.0 Hz, 4H, py-H), 7.66 (d, J = 15.0 Hz, 2H, met-H), 7.61 (d, J = 14.9 Hz, 2H, met-H), 7.44 (d, J = 7.2 Hz, 4H, py-H), 7.37 (s, 1H, ph-H), 5.35 (s, 4H, NCH_2), 5.12 (m, 2H, NCH), 4.11 (t, J = 6.9 Hz, 4H, OCH_2), 3.91 (t, J = 6.7 Hz, 2H, OCH_2), 2.33 (s, 6H, CH_3), 2.06 (m, 4H, CH_2), 1.73 (m, 6H, CH_2), 1.41 (d, J = 6.8 Hz, 6H, CH_3), 1.40–1.08 (m, 70H, CH_2), 0.85 (m, 15H, CH_3). HRMS (ESI, pos. mode, MeCN): calcd *m/z* for $C_{88}H_{132}N_6O_7Na$ ([M+Na]$^+$) 1408.0050, found 1408.0058. Anal. Calcd. for $C_{88}H_{132}N_6O_7$ (1386.03): C, 76.26; H, 9.60; N, 6.06. Found: C, 76.18; H, 9.73; N, 5.94. UV–vis (CH_2Cl_2, 25 °C, 10^{-6} M): λ_{max} (ε) = 572 nm (207000 $M^{-1}cm^{-1}$).

5.6 References and Notes

(1) Stryer, L. *Biochemie*, Spektrum: New York, 1999.

(2) Nicolaou, K.C.; Sorensen, E. J. *Classics in Total Synthesis*, Wiley-VCH: Weinheim, 1996

(3) (a) Whitesides, G. M.; Mathias, J. P.; Seto, C. T. *Science* **1991**, *254*, 1312–1319. (b) Prins, L. J.; Reinhoudt, D. N.; Timmerman, P. *Angew. Chem., Int. Ed.* **2001**, *40*, 2382–2426. (c) Brunsveld, L.; Folmer, B. J. B.; Meijer, E. W.; Sijbesma, R. P. *Chem. Rev.* **2001**, *101*, 4071–4097. (d) Rowan, A. E.; Nolte, R. J. M. *Angew. Chem., Int. Ed.* **1998**, *37*, 63–68.

(4) (a) Jonkheijm, P.; van der Schoot, P.; Schenning, A. P. H. J.; Meijer, E. W. *Science* **2006**, *313*, 80–83. (b) Percec, V.; Ungar, G.; Peterca, M. *Science* **2006**, *313*, 55–56. (c) Service, R. F. *Science* **2005**, *309*, 95.

(5) Dobson, C. M.; Sali, A.; Karplus, M. *Angew. Chem., Int. Ed.* **1998**, *37*, 868–893.

(6) (a) Lehn, J. M. *Supramolecular Chemistry: Concepts and Perspectives*, VCH, Weinheim, **1995**. (b) *Comprehensive Supramolecular Chemistry*; Atwood, J. L.; Davies, J. E. D.; MacNicol, D. D.; Vögtle, F.; Lehn, J.-M., Eds; Pergamon: Oxford, 1996.

(7) For polymeric assemblies, see: (a) Simonyi, M.; Bikadi, Z.; Zsila, F.; Deli, J. *Chirality* **2003**, *15*, 680–698. (b) Jonkheijm, P.; Miura, A.; Zdanowska, M.; Hoeben, F. J. M., De Feyter, S., Schenning, A. P. H. J.; De Schryver, F. C.; Meijer, E. W. *Angew. Chem., Int. Ed.* **2004**, *43*, 74–78. (c) Jyothish, K.; Hariharan, M.; Ramaiah, D. *Chem.–Eur. J.* **2007**, *13*, 5944–5951.

(8) For metallosupramolecular architectures, see: (a) Hasenknopf, B.; Lehn, J. M.; Boumediene, N. ; Leize, E.; Van Dorsselaer, A. *Angew. Chem., Int. Ed.* **1998**, *37*, 3265–3268. (b) Holliday, B. J. ; Jeon, Y.-M.; Mirkin, C. A.; Stern, C. L.; Incarvito, C. D.; Zakharov, L. N.; Sommer, R. D.; Rheingold, A. L. *Organometallics* **2002**, *21*, 5713–5725. (c) Hori, A.; Yamashita, K.; Fujita, M. *Angew. Chem., Int. Ed.* **2004**, *43*, 5016–5019.

(9) For hydrogen-bonded supramolecular architectures, see: (a) Mathias, J. P.; Simanek, E. E.; Seto, C. T.; Whitesides, G. M. *Angew. Chem., Int. Ed. Engl.* **1993**, *32*, 1766–1769. (b) Mathias, J. P.; Seto, C. T.; Simanek, E. E.; Whitesides, G. M. *J. Am. Chem. Soc.* **1994**, *116*, 1725–1736. (c) Prins, L. J.; De Jong, F.; Timmerman, P.; Reinhoudt, D. N. *Nature* **2000**, *408*, 181–184. (d) Prins, L. J.; Neuteboom, E. E.; Paraschiv, V.; Crego-Calama, M.; Timmerman, P.; Reinhoudt, D. N. *J. Org. Chem.* **2002**, *67*, 4808–4820. (e) Paraschiv, V.; Crego-Calama, M.; Ishi-i, T.; Padberg, C. J.; Timmerman, P.; Reinhoudt, D. N. *J. Am. Chem. Soc.* **2002**, *124*, 7638–7639. (f) Badjić, J. D.; Cantrill, S. J.; Stoddart, J. F. *J. Am. Chem. Soc.* **2004**, *126*, 2288–2289. (g) de Greef, T. F. A., Ligthart, G. B. W. L.; Lutz, M.; Spek, A. L.; Meijer, E. W.; Sijbesma, R. P. *J. Am. Chem. Soc.* **2008**, *130*, 5479–5486.

(10) For other systems, see: (a) Dyck, A. S. M.; Kisiel, U.; Bohne, C. *J. Phys. Chem. B* **2003**, *107*, 11652–11659. (b) Oshikiri, T.; Takashima, Y.; Yamaguchi, H.; Harada, A. *J. Am. Chem. Soc.* **2005**, *127*, 12186–12187. (c) Mukhopadhyay, P.; Zavalij, P. Y.; Isaacs, L. *J. Am. Chem. Soc.* **2006**, *128*, 14093–14102. (d) Nordel, P.; Westerlund, F.; Wilhelmsson, L. M.; Nordén, B.; Lincoln, P. *Angew. Chem., Int. Ed.* **2007**, *46*, 2203–2206.

(11) For general reviews on helical structures, see: (a) Rowan, A. E.; Nolte, R. J. M. *Angew. Chem., Int. Ed.* **1998**, *37*, 63–68. (b) Brunsveld, L.; Folmer, B. J. B.; Meijer, E. W.; Sijbesma, R. P. *Chem. Rev.* **2001**, *101*, 4071–4097. (c) Hill, D. J.; Mio, M. J.; Prince, R. B.; Hughes, T. S.; Moore, J. S. *Chem. Rev.* **2001**, *101*, 3893–4011. (d) Schmuck, C. *Angew. Chem., Int. Ed.* **2003**, *42*, 2448–2452. (e) Yashima, E.; Maeda, K.; Nishimura, T.

Chem.–Eur. J. **2004**, *10*, 43–51. (f) *Supramolecular Dye Chemistry: Topics in Current Chemistry, Vol. 258*; Würthner, F., Ed.; Springer: Berlin, 2005. (g) *Supramolecular Chirality: Topics in Current Chemistry, Vol. 265*; Crego-Calama, M.; Reinhoudt, D. N., Eds.; Springer: Berlin, 2006.

(12) (a) Pawlik, A.; Kirstein, S.; De Rossi, U.; Daehne, S. *J. Phys. Chem. B* **1997**, *101*, 5646–5651. (b) Oda, R.; Huc, I.; Schmutz, M.; Candau, S. J.; MacKintosh, F. C. *Nature* **1999**, *399*, 566–569. (c) Yashima, E.; Maeda, K.; Okamoto, Y. *Nature* **1999**, *399*, 449–451. (d) Engelkamp, H.; Middelbeek, S.; Nolte, R. J. M. *Science* **1999**, *284*, 785–788. (e) Prins, L. J.; De Jong, F.; Timmerman, P.; Reinhoudt, D. N. *Nature* **2000**, *408*, 181–184. (f) Ribo, J. M.; Crusats, J.; Sagues, F.; Claret, J.; Rubires, R. *Science* **2001**, *292*, 2063–2066. (g) S. Balaban, T.; Bhise, A. D.; Fischer, M.; Linke-Schaetzel, M.; Roussel, C.; Vanthuyne, N. *Angew. Chem., Int. Ed.* **2003**, *42*, 2140–2144. (h) de Jong, J. J. D.; Lucas, L. N.; Kellogg, R. M.; van Esch, J. H.; Feringa, B. L. *Science* **2004**, *304*, 278–281. (i) George, S. J.; Ajayaghosh, A.; Jonkheijm, P.; Schenning, A. P. H. J.; Meijer, E. W. *Angew. Chem., Int. Ed.* **2004**, *43*, 3422–3425. (j) Keith, C.; Reddy, R. A.; Baumeister, U.; Tschierske, C. *J. Am. Chem. Soc.* **2004**, *126*, 14312–14313. (k) Percec, V.; Dulcey, A. E.; Balagurusamy, V. S. K.; Miura, Y.; Smidrkal, J.; Peterca, M.; Nummelin, S.; Edlund, U.; Hudson, S. D.; Heiney, P. A.; Duan, H.; Magonov, S. N.; Vinogradov, S. A. *Nature* **2004**, *430*, 764–768. (l) Hill, J. P.; Jin, W.; Kosaka, A.; Fukushima, T.; Ichihara, H.; Shimomura, v; Ito, K.; Hashizume, T.; Ishii, N.; Aida, T. *Science* **2004**, *304*, 1481–1483.

(13) Palmans, A. R. A.; Meijer, E. W. *Angew. Chem., Int. Ed.* **2007**, *46*, 8948–8968.

(14) For chiral amplification in macromolecules, see: (a) Schlitzer, D. S.; Novak, B. M. *J. Am. Chem. Soc.* **1998**, *120*, 2196–2197. (b) Green, M. M.; Garetz, B. A.; Munoz, B.; Chang, H. *J. Am. Chem. Soc.* **1995**, *117*, 4181–4182. (c) Cornelissen, J. J. L. M.; Fischer, M.; Sommerdijk, N. A. J. M.; Nolte, R. J. M. *Science* **1998**, *280*, 1427–1430. (d) Green, M. M.; Park, J.-W.; Sato, T.; Teramoto, A.; Lifson, S.; Selinger, R. L. B.; Selinger, J. V. *Angew. Chem., Int. Ed.* **1999**, *38*, 3138–3154. (e) Jha, S. K.; Cheon, K.-S.; Green, M. M.; Selinger, J. V. *J. Am. Chem. Soc.* **1999**, *121*, 1665–1673. (f) Langeveld-Voss, B. M. W.; Waterval, R. J. M.; Jannsen, R. A. J.; Meijer, E. W. *Macromolecules* **1999**, *32*, 227–230. (g) Yashima, E.; Maeda, K.; Nishimura, T. *Chem.–Eur. J.* **2004**, *10*, 42–51.

(15) For foldamers with chiral induction, see for example: (a) Prince, R. B.; Brunsveld, L.; Meijer, E. W.; Moore, J. S. *Angew. Chem., Int. Ed.* **2000**, *39*, 228–230. (b) Dolain, C.;

Jiang, H.; Léger, J.-M.; Guionneau, P.; Huc, I. *J. Am. Chem. Soc.* **2005**, *127*, 12943–12951.

(16) For „sergeants-and-soldiers“ effect in supramolecular systems, see: (a) Palmans, A. R. A.; Vekemans, J. A. J. M.; Havinga, E. E.; Meijer, E. W. *Angew. Chem., Int. Ed. Engl.* **1997**, *36*, 2648–2651. (b) Prins, L. J.; Huskens, J.; de Jong, F.; Timmerman, P.; Reinhoudt, D. N. *Nature* **1999**, *398*, 498–502. (c) Prins, L. J.; Timmerman, P.; Reinhoudt, D. N. *J. Am. Chem. Soc.* **2001**, *123*, 10153–10163. (d) Hirschberg, J. H. K. K.; Koevoets, R. A.; Sijbesma, R. P.; Meijer, E. W. *Chem.–Eur. J.* **2003**, *9*, 4222–4231. (e) Ishi-i, T.; Kuwahara, R.; Takata, A.; Jeong, Y.; Sakurai, K.; Mataka, S. *Chem.–Eur. J.* **2006**, *12*, 736–776. (f) Wilson, A. J.; van Gestel, J.; Sijbesma, R. P.; Meijer, E. W. *Chem. Commun.* **2006**, 4404–4406. (g) Ajayaghosh, A.; Varghese, R.; George, S. J.; Vijayakumar, C. *Angew. Chem., Int. Ed.* **2006**, *45*, 1141–1144. (h) Wilson, A. J.; van Gestel, J.; Sijbesma, R. P.; Meijer, E. W. *Chem. Commun.* **2006**, 4404–4406. (i) Ajayaghosh, A.; Varghese, R.; Mahesh, S.; Praveen, V. K. *Angew. Chem., Int. Ed.* **2006**, *45*, 7729–7732.

(17) For “majority-rules” effect in supramolecular systems, see: (a) Green, M. M.; Garetz, B. A.; Munoz, B.; Chang, H.; Hoke, S.; Cooks, R. G. *J. Am. Chem. Soc.* **1995**, *117*, 4181–1482. (b) Van Gestel, J.; Palmans, A. R. A.; Titulaer, B.; Vekemans, J. A. J. M.; Meijer, E. W. *J. Am. Chem. Soc*. **2005**, *127*, 5490–5494. (c) Jin, W.; Fukushima, T.; Niki, M.; Kosaka, A.; Ishii, N.; Aida, T. *Proc. Natl. Acad. Sci. USA* **2005**, *102*, 10801–10806. (d) Wilson, A. J.; Masuda, M.; Sijbesma, R. P.; Meijer, E. W. *Angew. Chem., Int. Ed.* **2005**, *44*, 2275–2279.

(18) For a theoretical treatment of chiral amplification in supramolecular polymers, see: (a) van Gestel, J.; van der Schoot, P.; Michels, M. A. J. *Macromolecules* **2003**, *36*, 6668–6673. (b) Van Gestel, J. *Macromolecules* **2004**, *37*, 3894–3898.

(19) (a) Prins, L. J.; Timmerman, P.; Reinhoudt, D. N. *J. Am. Chem. Soc.* **2001**, *123*, 10153–10163. (b) Mateos-Timoneda, M. A.; Crego-Calama, M.; Reinhoudt, D. N. *Chem.–Eur. J.* **2006**, *12*, 2630–2638. (c) Smulders, M. M. J.; Schenning, A. P. H. J.; Meijer, E. W. *J. Am. Chem. Soc.* **2008**, *130*, 606–611.

(20) (a) Ishi-I, T.; Crego-Calama, M.; Timmerman, P.; Reinhoudt, D. N.; Shinkai, S. *J. Am. Chem. Soc.* **2002**, *124*, 14631–14641. (b) Morino, K.; Watase, N.; Maeda, K.; Yashima, E. *Chem.–Eur. J.* **2004**, *10*, 4703–4107. (c) George, S. J.; Tomović, Ž.; Smulders, M. M.

J.; de Greef, T. F. A.; Leclère, P. E. L. G.; Meijer, E. W.; Schenning, A. P. H. J. *Angew. Chem., Int. Ed.* **2007**, *46*, 8206–8211.

(21) (a) Bada, J. L. *Nature* **1995**, *374*, 594–595. (b) *Chirality in Natural and Applied Science* (Eds.: W. J. Lough, I. W. Wainer), Blackwell Scientific, Oxford, **2002**.

(22) (a) Feringa, B. L.; van Delden, R. A. *Angew. Chem., Int. Ed.* **1999**, *38*, 3418–3438. (b) Nanita, S. C.; Cooks, R. G. *Angew. Chem., Int. Ed.* **2006**, *45*, 554–569. (c) Soai, K.; Shibata, T.; Morioka, H.; Choji, K. *Nature* **1995**, *378*, 767–768. (d) Klussmann, M.; Iwamura, H.; Mathew, S. P.; Wells, D. H., Jr.; Pandya, U.; Armstrong, A.; Blackmond, D. G. *Nature* **2006**, *441*, 621–623.

(23) (a) Würthner, F.; Yao, S.; Debaerdemaeker, T.; Wortmann, R. *J. Am. Chem. Soc.* **2002**, *124*, 9431–9447. (b) Würthner, F.; Yao, S.; Heise, B.; Tschierske, C. *Chem. Commun.* **2001**, 2260–2261. (c) Würthner, F.; Yao, S. *J. Org. Chem.* **2003**, *68*, 8943–8949.

(24) (a) Würthner, F.; Yao, S.; Beginn, U. *Angew. Chem., Int. Ed.* **2003**, *42*, 3247–3250. (b) Yao, S.; Beginn, U.; Gress, T.; Lysetska, M.; Würthner, F. *J. Am. Chem. Soc.* **2004**, *126*, 8336–8348. (c) Lohr, A., Gress, T., Deppisch, M., Knoll, M., Würthner, F. *Synthesis* **2007**, 3073 – 3082.

(25) (a) Verbiest, T.; Houbrechts, S.; Kauranen, M.; Clays, K.; Persoons, A. *J. Mater. Chem.* **1997**, *7*, 2175–2189. (b) Wolff, J. J.; Wortmann, R. *Adv. Phys. Org. Chem.* **1999**, *32*, 121–217. (c) Würthner, F.; Wortmann, R.; Meerholz, K. *ChemPhysChem* **2002**, *3*, 17–31. (d) Pereverzev, Y. V.; Prezhdo, O. V.; Dalton, L. R. *ChemPhysChem* **2004**, *5*, 1821–1830.

(26) Parts of the present chapter have been communicated: (a) Lohr, A.; Lysetska, M.; Würthner, F. *Angew. Chem., Int. Ed.* **2005**, *44*, 5071–5074. (b) Lohr, A.; Würthner, F. *Angew. Chem., Int. Ed.* **2008**, *47*, 1232–1236. (c) Lohr, A.; Würthner, F. *Chem. Commun.* **2008**, 2227–2229.

(27) (a) Berova, N.; Nakanishi K. *in Circular Dichroism. Principles and Applications*, 2nd ed. (Eds.: Berova, N.; Nakanishi, K.; Woody, R. W.), Wiley, New York, **2000**, pp. 337–382. (b) Bußß, V.; Reichardt, C. *J. Chem. Soc. Chem. Commun.* **1992**, 1636–1638.

(28) Two recent reports on supramolecular dye aggregates show linear dichroism (LD) effects as a result of convective flow and resultant alignment of the fibers in the cuvette. Such LD effects may contribute to the apparent CD spectra of dye aggregates: (a) Wolffs, M.;

George, S. J.; Tomović, Ž.; Meskers, S. C. J.; Schenning, A. P. H. J.; Meijer, E. W. *Angew. Chem., Int. Ed.* **2007**, *46*, 8203–8205. (b) Tsuda, A.; Alam, M. A.; Harada, T.; Yamaguchi, T.; Ishii, N.; Aida, T. *Angew. Chem., Int. Ed.* **2007**, *46*, 8198–8202. Note that for the present merocyanine nanorods, no significant LD signal was observed, thus a contribution of LD to the CD spectra of these nanorods can be excluded.

(29) (a) Prokhorenko, V. I.; Steensgaard, D. B.; Holzwarth, A. R. *Biophys. J.* **2003**, *85*, 3173–3186. (b) Didraga, C.; Klugkist, J. A.; Knoester, J. *J. Phys. Chem. B* **2002**, *106*, 11474–11486.

(30) (a) Buß, V.; Reichardt, C. *J. Chem. Soc., Chem. Commun.* **1992**, 1636–1638; (b) Buss, V. *Angew. Chem., Int. Ed. Engl.* **1991**, *30*, 869–870; (c) Gargiulo, D.; Derguini, F.; Berova, N.; Nakanishi, K.; Harada, N. *J. Am. Chem. Soc.* **1991**, *113*, 7046–7047.

(31) Sykes, P. *Reaktionsmechanismen der Organischen Chemie*, VCH: Weinheim, 1988.

(32) The final CD value is lower for the experiment at 47 °C with respect to that at 23 °C owing to a slight spectral shift at elevated temperature.

(33) (a) Connors, K. A. *Chemical Kinetics: The Study of Reaction Rates in Solution*, VCH: New York, 1990, p. 24. (b) Rae, M.; Berberan-Santos, M. N. *Chem. Phys.* **2002**, *280*, 283–293.

(34) Moss, G. P. *Pure Appl. Chem.* **1996**, *68*, 2193–2222.

(35) Analysis of the CD data at the other maxima/minima revealed the same nonlinear behavior.

(36) The high anisotropy factors *g* and the single-handed helical morphology observed for nanorods of homochiral (*R*,*R*)-**6** (Figure 3 and Figure A1) suggest that the observed maximum helical sense excess does correspond to the presence of aggregates of one helical handedness.

(37) Interestingly, the disappearance of "sergeants-and-soldiers" directed chiral amplification was reported. In this case the monomers of initially formed co-aggregates separate into aggregates containing only sergeants and such containing only soldiers: van Gorp, J. J.; Vekemans, J. A. J. M.; Meijer, E. W. *J. Am. Chem. Soc.* **2002**, *124*, 14759–14769.

(38) Owing to a slight spectral shift observed at elevated temperature the *g* values at 47 °C were normalized with respect to those obtained after 8 days at room temperature. The measurements at 47 °C were performed by U. Mayerhöffer.

(39) Notably, according to our structural model (see ref. 24) six D-aggregated oligomeric chains form a well-ordered helically winded cluster of tightly packed merocyanine dyes during this process.

(40) Pasternack, R. F.; Gibbs, E. J.; Collings, P. J.; dePaula, J. C.; Turzo, L. C.; Terracina, A. *J. Am. Chem. Soc.* **1998**, *120*, 5873–5878. (b) Pasternack, R. F.; Fleming, C.; Herring, S.; Collings, P. J.; dePaula, J.; DeCastro, G.; Gibbs, E. J. *J. Biophys. J.* **2000**, *79*, 550–560. (c) Monti, D.; Venanzi, M.; Mancini, G.; Di Natale, C.; Paolesse, R. *Chem. Commun.* **2005**, 2471–2473.

(41) (a) Balaban, T. S.; Leitich, J.; Holzwarth, A. R.; Schaffner, K. *J. Phys. Chem. B* **2000**, *104*, 1362–1372. (b) Slavnova, T. D.; Chibisov, A. K.; Görner, H. *J. Phys. Chem. A* **2005***, 109*, 4758–4765.

(42) Kondepudi, D. K.; Kaufman, R. J.; Singh, N. *Science* **1990**, *250*, 975–976.

(43) Notably, the CD spectra recorded in the first 20 min show the inversion of the CD spectrum during the stereomutation from **H1** into **H2** nanorods as reported before (see 5.2.2).

(44) The *g* value of aggregates formed from pure (*R*,*R*)-**2** monomers corresponds to a helical sense excess of 100 %, see ref. 36.

(45) Notably, under these conditions the chiral amplification process was faster but still took several hours at elevated temperature. See: Mayerhöffer, U. Diploma thesis, Universität Würzburg, 2008.

5.7 Appendix

Additional AFM image

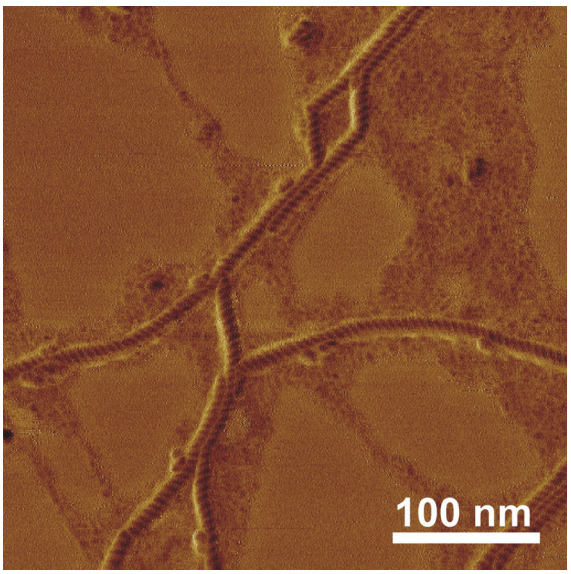

Figure A1. AFM phase image of a sample prepared by spin-coating of bis(merocyanine) dye (*R*,*R*)-**6** (c = 1×10^{-5} M, THF/MCH = 30:70 vol%, 20 °C) onto HOPG at 22 h after initiation of self-assembly.

Program for the nonlinear curve fitting of the time-dependent CD data[ii]

The following C++ code was applied for the nonlinear curve fitting procedure of the time-dependent CD according to eq. 10. It applies the Levenberg-Marquard algorithm for the curve fitting and uses the Romberg algorithm for the numerical integration of the integrand in eq. 10.

```
#include <iostream>
#include <fstream>
#include <cstdio>
#include <cmath>
#include <vector>
#include <cassert>
#include <algorithm>
#include <limits.h>

#define MAX_DIM 6
#define LOG(x)

#define FAST_INT
```

[ii] This program was written by Stefan Geschwentner, Ulm (Germany).

```
double EPS = 1;
double infinity = 1e+30;

bool read_data(char *filename, std::vector<double> & x, std::vector<double> & y,
double max_x)
{
   std::ifstream f(filename);
   if(!f)
   {
      std::cerr << "IO-error: can't open file " << filename << std::endl;
      return false;
   }
   double t1, t2;
   while((f >> t1 >> t2) && (fabs(t1) <= max_x))
   {
      x.push_back(t1);
      y.push_back(t2);
   }
   f.close();
   return true;
}

inline bool isinf(double x)
{
   return x > DBL_MAX;
}

inline bool isvalid(double x)
{
   return !isnan(x) && !isinf(x);
}

//---------------------------------------------------------------------------
// numerical integration with romberg
template <typename Func>
double integrate(Func f, double a, double b, double eps = 1e-15)
{
   if(a == b) return 0;
   LOG(std::cout << "--- begin romberg f = " << f.name() << " from " << a << " to "
<< b << std::endl;)
   std::vector<double> T;
   double h = b-a, erg = -1;
   int n = 1;
   double fa = f(a), fb = f(b);
   double S = 0.5*h*(fabs(fa)+fabs(fb));
   T.push_back(0.5*h*(fa+fb));
   LOG(std::cout << "f[" << a << "]=" << fa << std::endl;
   std::cout << "f[" << b << "]=" << fb << std::endl;)

   bool stop = false;

   for(int k = 1; !stop;++k)
   {
        double sum = 0, s = 0;
        h *= 0.5;
        n *= 2;
        double q = 1;

        for(int i = 1;  i <= n-1; i += 2)
        {
           double val = f(a+i*h);
           if(!isvalid(val)) return val;
           sum += val;
           s += fabs(val);
           LOG(if(k == 1) std::cout << "f[" << a+i*h << "]=" << val << std::endl;)
        }
        S = 0.5*S+s*h;
        T.push_back(0.5*T[k-1]+sum*h);
        LOG(std::cout << "k=" << k << " S=" << S << " T[k]=" << T[k] << std::endl;)
        for(int i = k-1; (i >= 0) && !stop; --i)
        {
           q *= 4;
           T[i] = T[i+1]+(T[i+1]-T[i])/(q-1);
```

```
            if(!isvalid(T[i])) return T[i];
            if(fabs(T[i]-T[i+1]) <= eps*S)
            {
               stop = true;
               erg = T[i];
            }
         }
   }

   LOG(std::cout << "--- end romberg f = " << f.name() << " from " << a << " to " <<
b << " erg=" << erg << std::endl;)
   return erg;
}

//------------------------------------------------------------------------
// helper functions

template <typename Function>
struct BindFunction : Function
{
  double *y;
  BindFunction(Function f, int n, double y[]) : Function(f), y(y) { }

  double operator()(double t)
  {
      return this->Function::operator()(t, y);
  }
};

template <typename Function>
BindFunction<Function> Bind(Function f, int n, double y[])
{
   return BindFunction<Function>(f, n, y);
}


template <typename Function>
struct Bind2Function : Function
{
  int n_param;
  double p[MAX_DIM];
  Bind2Function(Function f, int n_param, double bind_param[]) : Function(f),
n_param(n_param)
  {
     assert(n_param+2 <= MAX_DIM);
     p[0] = bind_param[0];
     p[1] = bind_param[1];
  }

  double operator()(double t, double param[], bool verbose = false)
  {
      if(verbose)
         std::cout << "Bind2  param=[" << p[0] << ", " << p[1] << "]" << std::endl;
      for(int i = 0; i < n_param; ++i)
         p[i+2] = param[i];
      return this->Function::operator()(t, p);
  }

  double diff(int n, double t, double param[], bool verbose = false)
  {
     assert(n < n_param);
     if(verbose)
         std::cout << "Bind2  param=[" << p[0] << ", " << p[1] << "]" << std::endl;
     for(int i = 0; i < n_param; ++i)
        p[i+2] = param[i];
     return Function::diff(n+2, t, p);
  }
};

template <typename Function>
Bind2Function<Function> Bind2(Function f, int n, double y[])
{
   return Bind2Function<Function>(f, n, y);
```

```
}

//------------------------------------------------------------------------
// non-linear least square curve fitting with Levenberg-Marquardt

template <typename Function>
double LSE(Function f, int n_param, int n_data,
                        std::vector<double> & x, std::vector<double> & y,
                        double param[], double bound = DBL_MAX)
{
   double lse = 0;
   for(int i = 0; i < n_data; ++i)
   {
      double res = y[i]-f(x[i],param);
      lse += res*res;
      if((lse >= bound) && !isvalid(lse)) return lse;
   }
   return lse;
}

template <typename Function>
void GetBeta(double beta[], Function f, int n_param, int n_data,
             std::vector<double> & x, std::vector<double> & y,
             double param[])
{
   for(int i = 0; i < n_param; ++i)
   {
      beta[i] = 0;
      for(int j = 0; j < n_data; ++j)
      {
         beta[i] += (y[j]-f(x[j], param))*f.diff(i, x[j], param);
      }
   }
}

template <typename Function, typename Matrix>
void GetAlpha(Matrix & alpha, double lambda, Function f, int n_param, int n_data,
             std::vector<double> & x, std::vector<double> & y,
             double param[])
{
   for(int i = 0; i < n_param; ++i)
   {
      for(int k = i; k < n_param; ++k)
      {
         alpha[i][k] = 0;
         for(int j = 0; j < n_data; ++j)
         {
            alpha[i][k] += f.diff(i, x[j], param)*f.diff(k, x[j], param);
         }
         alpha[k][i] = alpha[i][k];
      }
      alpha[i][i] *= (1+lambda);
   }
}

template <typename Function, typename Matrix>
bool GetAlphaBeta(Matrix & alpha, double beta[], double lambda, Function f, int
n_param, int n_data,
             std::vector<double> & x, std::vector<double> & y,
             double param[])
{
   for(int i = 0; i < n_param; ++i)
   {
      beta[i] = 0;
      for(int k = 0; k < n_param; ++k)
         alpha[i][k] = 0;
   }

   double d[MAX_DIM];
   for(int j = 0; j < n_data; ++j)
   {
      for(int i = 0; i < n_param; ++i)
      {
```

```
         d[i] = f.diff(i, x[j], param);
         beta[i] += (y[j]-f(x[j], param))*d[i];
         if(!isvalid(beta[i])) return false;
      }

      for(int i = 0; i < n_param; ++i)
      {
         for(int k = 0; k < n_param; ++k)
         {
            alpha[i][k] += d[i]*d[k];
            if(!isvalid(alpha[i][k])) return false;
         }
      }
   }

   for(int i = 0; i < n_param; ++i)
   {
      if(alpha[i][i])
         alpha[i][i] *= (1+lambda);
      else
         alpha[i][i] = 1+lambda;
      if(!isvalid(alpha[i][i])) return false;
   }

   return true;
}

template <typename Matrix>
bool SolveLGS(Matrix  alpha, double beta[], int n)
{
   for(int i = 0; i < n; ++i)
   {
      for(int j = i+1; j < n ; ++j)
      {
         double u = alpha[j][i]/alpha[i][i];
         if(!isvalid(u)) return false;
         for(int k = i+1; k < n; ++k)
         {
            alpha[j][k] -= u*alpha[i][k];
            if(!isvalid(alpha[j][k])) return false;
         }
         beta[j] -= u*beta[i];
         if(!isvalid(beta[j])) return false;
      }
   }

   for(int i = n-1; i >= 0; --i)
   {
      for(int j = i+1; j < n; ++j)
         beta[i] -= alpha[i][j]*beta[j];
      beta[i] /= alpha[i][i];
      if(!isvalid(beta[i])) return false;
   }
   return true;
}

template <typename Function>
double Levenberg_Marquardt(Function f, int n_param, int n_data,
                           std::vector<double> & x, std::vector<double> & y,
                           double param[], double min_param[], char* param_name[], bool
verbose = false)
{
   assert(n_param <= MAX_DIM);
   double lambda = 0.001;
   double new_lse = -1;
   LOG(std::cout << "get lse" << std::endl;)
   double lse = LSE(f, n_param, n_data, x, y, param), bound = lse;
   if(!isvalid(lse))
   {
      if(verbose)
         std::cout << "error: lse at initialpoint is undef." << std::endl;
      return lse;
   }
```

```
   int iter = 0;

   if(verbose)
   {
      std::cout << iter << ": " << "?" << "lamda=" << lambda << " lse=" << lse << "
param=[";
      for(int i = 0; i < n_param;++i)
      {
         if(i) std::cout << ",";
         std::cout << param_name[i] << "=" << param[i];
      }
      std::cout << "]" << std::endl << std::flush;
   }

   int cont = 0;
   double new_param[MAX_DIM];
   double beta[MAX_DIM];
   double alpha[MAX_DIM][MAX_DIM];

   do
   {
      ++iter;
      LOG(std::cout << "get beta" << std::endl;)
      if(GetAlphaBeta(alpha, beta, lambda, f, n_param, n_data, x, y, param))
      {
      if(verbose)
      {
         std::cout << "beta=[";
         for(int i = 0; i < n_param; ++i)
         {
            if(i) std::cout << ", ";
            std::cout << beta[i];
         }
         std::cout << "]" << std::endl << std::flush;
      }
      LOG(std::cout << "get alpha" << std::endl;)
      if(verbose)
      {
         std::cout << "alpha=[";
         for(int i = 0; i < n_param; ++i)
         {
            for(int j = 0; j < n_param; ++j)
            {
               if(j) std::cout << ", ";
               if(i&&!j) std::cout << std::endl << "     , ";
               std::cout << alpha[i][j];
            }
         }
         std::cout << "]" << std::endl << std::flush;
      }
      LOG(std::cout << "solve lgs" << std::endl;)
      if(SolveLGS(alpha, beta, n_param))
      {
      if(verbose)
      {
         std::cout << "delta=[";
         for(int i = 0; i < n_param; ++i)
         {
            if(i) std::cout << ", ";
            std::cout << beta[i];
         }
         std::cout << "]" << std::endl << std::flush;
      }

      for(int i = 0; i < n_param; ++i)
      {
         new_param[i] = param[i] + beta[i];
         if(new_param[i] < min_param[i])
         {
            if(verbose) std::cout << "Param " << param_name[i] << " is out of Range"
<< std::endl << std::flush;
         }
```

```
      }

      if(verbose)
      {
         std::cout << "new_param=[";
         for(int i = 0; i < n_param;++i)
         {
            if(i) std::cout << ",";
            std::cout << param_name[i] << "=" << new_param[i];
         }
         std::cout << "]" << std::endl << std::flush;
      }
      LOG(std::cout << "get lse" << std::endl;)
      new_lse = LSE(f, n_param, n_data, x, y, new_param, bound);
      if(verbose)
         std::cout << "new_lse=" << new_lse << std::endl << std::flush;
      }
      }
      bool ok;
      if(!isvalid(new_lse) || (new_lse >= lse))
      {
         lambda *= 10;
         if(!isvalid(lambda)) cont = 3;
         ok = false;
      }
      else
      {
         if((fabs(lse-new_lse) < 0.01) || (fabs(lse-new_lse) < 1e-3*lse)) ++cont;
         lambda *= 0.1;
         lse = new_lse;
         for(int i = 0; i < n_param; ++i)
            param[i] = new_param[i];
         ok = true;
      }

      if(verbose)
      {
         std::cout << iter << ": " << (ok ? '+' : '-' ) << "lambda=" << lambda << "
lse=" << lse << " param=[";
         for(int i = 0; i < n_param;++i)
         {
            if(i) std::cout << ",";
            std::cout << param_name[i] << "=" << param[i];
         }
         std::cout << "]" << std::endl << std::flush;
      }
   }
   while(cont < 2);

   // covariance
   GetAlphaBeta(alpha, beta, 0, f, n_param, n_data, x, y, param);

   double cov[MAX_DIM][MAX_DIM];
   double tmp[MAX_DIM][MAX_DIM];

   for(int i = 0; i < n_param; ++i)
   {
      for(int j = 0; j < n_param; ++j)
      {
         cov[i][j] = 0;
         for(int k = 0; k < n_param; ++k)
            tmp[j][k] = alpha[j][k];
      }
      cov[i][i] = 1;
      SolveLGS(tmp, cov[i], n_param);
   }

   if(verbose)
   {
      if(cont == 2)
        std::cout << "Stop iterations" << std::endl;
      else
        std::cout << "Abort iterations" << std::endl;
```

```
      std::cout << "covariance=" << std::endl;
      for(int i = 0; i < n_param; ++i)
      {
         for(int j = 0; j < n_param; ++j)
            std::cout << cov[i][j] << "\t";
         std::cout << std::endl;
      }
      std::cout << std::flush;
   }

   return lse;
}

//-------------------------------------------------------------------------
// function

struct xH1_star_integrand
{
   const char * name() { return "xH1_star_integrand";}

   double operator()(double t, double param[])
   {
      double ks = param[0], ns = param[1], km = param[2], nm = param[3];
      return pow(ks*t,ns)*ks*exp(pow(km*t,nm+1)/(nm+1)-pow(ks*t,ns+1)/(ns+1));
   }
};

struct xH1_star_integrand_diff_ks
{
   const char * name() { return "xH1_star_integrand_diff_ks";}

   double operator()(double t, double param[])
   {
      double ks = param[0], ns = param[1], km = param[2], nm = param[3];
      double e = pow(ks*t,ns), e1 = e*ks*t;
      return e*(ns+1-e1)*exp(pow(km*t,nm+1)/(nm+1)-e1/(ns+1));
   }
};

struct xH1_star_integrand_diff_ns
{
   const char * name() { return "xH1_star_integrand_diff_ns";}

   double operator()(double t, double param[])
   {
      double ks = param[0], ns = param[1], km = param[2], nm = param[3];
      double e1, e2, e3;
      return (e1 = log(ks*t)), (e2 = pow(ks*t,ns)),  (e3 = e2*ks*t/(ns+1)),
             ks*e2*((t ? e1 - e1*e3 : 0.0) + e3/(ns+1))*exp(pow(km*t,nm+1)/(nm+1)-e3);
   }
};

struct xH1_star_integrand_diff_km
{
   const char * name() { return "xH1_star_integrand_diff_km";}

   double operator()(double t, double param[])
   {
      double ks = param[0], ns = param[1], km = param[2], nm = param[3];
      double e1 = pow(ks*t,ns)*ks, e2 = pow(km*t,nm+1);
      return e1*e2/km*exp(e2/(nm+1)-(e1*t)/(ns+1));
   }
};

struct xH1_star_integrand_diff_nm
{
   const char * name() { return "xH1_star_integrand_diff_nm";}

   double operator()(double t, double param[])
   {
      double ks = param[0], ns = param[1], km = param[2], nm = param[3];
      double e1 = pow(ks*t,ns)*ks, e2 = pow(km*t,nm+1)/(nm+1);
```

```
      return e1*e2*((t ? log(km*t) : 0.0)-1.0/(nm+1))
                        *exp(e2-(e1*t)/(ns+1));
   }
};

struct xH1_star
{
#ifdef FAST_INT
   double int_last_t, int_val;

   xH1_star() : int_last_t(0), int_val(0) {}
#endif

   double operator()(double t, double param[])
   {
      double /*ks = param[0], ns = param[1],*/ km = param[2], nm = param[3];
#ifdef FAST_INT
      int_val = (t >= int_last_t
            ? int_val + integrate(Bind(xH1_star_integrand(), 4, param),int_last_t,t)
            : integrate(Bind(xH1_star_integrand(), 4, param),0,t));
      int_last_t = t;
      return int_val*exp(-pow(km*t,nm+1)/(nm+1));
#else
      return integrate(Bind(xH1_star_integrand(), 4, param),0,t)*exp(-
pow(km*t,nm+1)/(nm+1));
#endif
   }

   double diff(int n, double t, double param[])
   {
#ifdef FAST_INT
      static double last_t[4] = {0,0,0,0}, val[4] = {0,0,0,0};
#endif
      double /*ks = param[0], ns = param[1],*/ km = param[2], nm = param[3];
      switch(n)
      {
      case 0: // ks
#ifdef FAST_INT
         val[n] = (t >= last_t[n]
                  ? val[n] + integrate(Bind(xH1_star_integrand_diff_ks(), 4,
param),last_t[n],t)
                  : integrate(Bind(xH1_star_integrand_diff_ks(), 4, param),0,t));
         last_t[n] = t;
         return val[n]*exp(-pow(km*t,nm+1)/(nm+1));
#else
         return integrate(Bind(xH1_star_integrand_diff_ks(), 4, param),0,t)*exp(-
pow(km*t,nm+1)/(nm+1));
#endif
         break;
      case 1: // ns
#ifdef FAST_INT
         val[n] = (t >= last_t[n]
                  ? val[n] + integrate(Bind(xH1_star_integrand_diff_ns(), 4,
param),last_t[n],t)
                  : integrate(Bind(xH1_star_integrand_diff_ns(), 4, param),0,t));
         last_t[n] = t;
         return val[n]*exp(-pow(km*t,nm+1)/(nm+1));
#else
         return integrate(Bind(xH1_star_integrand_diff_ns(), 4, param),0,t)*exp(-
pow(km*t,nm+1)/(nm+1));
#endif
         break;
      case 2: // km
#ifdef FAST_INT
         int_val = (t >= int_last_t
                  ? int_val + integrate(Bind(xH1_star_integrand(), 4,
param),int_last_t,t)
                  : integrate(Bind(xH1_star_integrand(), 4, param),0,t));
         int_last_t = t;
         val[n] = (t >= last_t[n]
                  ? val[n] + integrate(Bind(xH1_star_integrand_diff_km(), 4,
param),last_t[n],t)
                  : integrate(Bind(xH1_star_integrand_diff_km(), 4, param),0,t));
```

```
         last_t[n] = t;
         return (val[n]-int_val*pow(km*t,nm+1)/km)*exp(-pow(km*t,nm+1)/(nm+1));
#else
         return integrate(Bind(xH1_star_integrand_diff_km(), 4, param),0,t)*exp(-
pow(km*t,nm+1)/(nm+1))
                -integrate(Bind(xH1_star_integrand(), 4,
param),0,t)*pow(km*t,nm)*t*exp(-pow(km*t,nm+1)/(nm+1));
#endif
         break;
      case 3: // nm
#ifdef FAST_INT
         int_val = (t >= int_last_t
                  ? int_val + integrate(Bind(xH1_star_integrand(), 4,
param),int_last_t,t)
                  : integrate(Bind(xH1_star_integrand(), 4, param),0,t));
         int_last_t = t;
         val[n] = (t >= last_t[n]
                  ? val[n] + integrate(Bind(xH1_star_integrand_diff_nm(), 4,
param),last_t[n],t)
                  : integrate(Bind(xH1_star_integrand_diff_nm(), 4, param),0,t));
         last_t[n] = t;
         return (val[n]-int_val*pow(km*t,nm+1)/(nm+1)*((t ? log(km*t) : 0.0)-
1./(nm+1)))*exp(-pow(km*t,nm+1)/(nm+1));
#else
         return integrate(Bind(xH1_star_integrand_diff_nm(), 4, param),0,t)*exp(-
pow(km*t,nm+1)/(nm+1))
                -integrate(Bind(xH1_star_integrand(), 4, param),0,t)
                 *((t ? log(km*t)*pow(km*t,nm+1)/(nm+1) : 0.0)-
pow(km*t,nm+1)/pow(nm+1,2))*exp(-pow(km*t,nm+1)/(nm+1));
#endif
         break;
      }
      return 0;
   }

};

struct xD
{
   double operator()(double t, double param[])
   {
      double ks = param[0], ns = param[1]/*, km = param[2], nm = param[3]*/;
      return exp(-pow(ks*t,ns+1)/(ns+1));
   }

   double diff(int n, double t, double param[])
   {
      double ks = param[0], ns = param[1]/*, km = param[2], nm = param[3]*/;
      switch(n)
      {
      case 0: // ks
         return -t*pow(ks*t,ns)*exp(-pow(ks*t,ns+1)/(ns+1));
         break;
      case 1: // ns
         return ((t ? -pow(ks*t,ns+1)/(ns+1)*log(ks*t) :
0.0)+pow(ks*t,ns+1)/pow(ns+1,2))*exp(-pow(ks*t,ns+1)/(ns+1));
         break;
      case 2: // km
         return 0;
         break;
      case 3: // nm
         return 0;
         break;
      }
      return 0;
   }
};

struct xH1
{
   xD xd;
   xH1_star xh1s;
```

```
   double operator()(double t, double param[])
   {
      return 1-xd(t, param)-xh1s(t, param);
   }

   double diff(int n, double t, double param[])
   {
      return -xd.diff(n, t, param)-xh1s.diff(n, t, param);
   }
};

struct xH1_star_manne
{
   double operator()(double t, double param[])
   {
      double ks = param[0], ns = param[1], km = param[2], nm = param[3];
      return (1-exp(-pow(ks*t,ns+1)/(ns+1)))/(1+pow(km*t,nm+1)/(nm+1));
   }

   double diff(int n, double t, double param[])
   {
      double ks = param[0], ns = param[1], km = param[2], nm = param[3];
      switch(n)
      {
      case 0: // ks
         return pow(ks*t, ns)*t*exp(-
pow(ks*t,ns+1)/(ns+1))/(1+pow(km*t,nm+1)/(nm+1));
         break;
      case 1: // ns
         return pow(ks*t,ns+1)/(ns+1)*((t ? log(ks*t) : 0.0)-1./(ns+1))*exp(-
pow(ks*t,ns+1)/(ns+1))/(1+pow(km*t,nm+1)/(nm+1));
         break;
      case 2: // km
         return -(1-exp(-
pow(ks*t,ns+1)/(ns+1)))/pow(1+pow(km*t,nm+1)/(nm+1),2)*(pow(km*t,nm+1)/km);
         break;
      case 3: // nm
         return -(1-exp(-pow(ks*t,ns+1)/(ns+1)))/pow(1+pow(km*t,nm+1)/(nm+1),2)
                *pow(km*t,nm+1)/(nm+1)*((t ? log(km*t) : 0.0)-1./(nm+1));
         break;
      }
      return 0;
   }

};

struct Delta_Epsilon
{
   xD xd;
   xH1_star xh1s;

   Delta_Epsilon() : xd(), xh1s() {}

   double operator()(double t, double param[])
   {
      return (param[4]-param[5]) * xh1s(t, param) + param[5] * (1-xd(t, param));
   }

   double diff(int n, double t, double param[])
   {
      switch(n)
      {
      case 4:
         return xh1s(t, param);
         break;
      case 5:
         return 1-xh1s(t, param)-xd(t, param);
         break;
      default:
         return (param[4]-param[5]) * xh1s.diff(n, t, param) - param[5] * xd.diff(n,
t, param);
         break;
      }
```

```
   }
};

template <typename Function>
void plot(std::ostream & out, Function f, int n_param, int n_data,
                          std::vector<double> & x, double param[])
{
   int offset = ((int)x[0])%2;
   if(offset == 1)
      out << 0 << ' ' << f(0.0, param) << std::endl;

   for(int i = offset; i < x[0]; i += 2)
      out << i << ' ' << f((double)i, param) << std::endl;

   for(int i = 0; i < n_data; ++i)
      out << x[i] << ' ' << f(x[i], param) << std::endl;

   for(double t = x[n_data-1]+2; t <= 2*x[n_data-1]; t += 2)
       out << t << ' ' << f(t, param) << std::endl;
}

void sample(const std::vector<double> & x, const std::vector<double> & y,
            std::vector<double> & x_new, std::vector<double> & y_new,
            int step, int offset = 0)
{
   for(int i = offset; i < (int)x.size(); i += step)
   {
      x_new.push_back(x[i]);
      y_new.push_back(y[i]);
   }
}

template <typename Function>
void resplot(std::ostream & out, Function f,
             int n_param, double param[],
             int n_data, std::vector<double> & x, std::vector<double> & y,
             int param1, int param2, double a1, double b1, double a2, double b2, int
n1 = 10, int n2 = 10)
{
   double h1 = (b1-a1)/n1;
   double h2 = (b2-a2)/n2;
   for(int i = 0; i < n1; ++i)
   {
      param[param1] = a1+h1*i;
      for(int j = 0; j < n2; ++j)
      {
         param[param2] = a2+h2*j;
         double lse = LSE(f, n_param, n_data, x, y, param, infinity);
         if(!isvalid(lse) || (lse > infinity)) lse = infinity;
         out << param[param1] << ' ' << param[param2] << ' ' << lse << std::endl;
      }
      out << std::endl;
   }
}

// --------------------------------
// main

int main(int argc, char *argv[])
{
   assert(argc == 3);
   int set = atoi(argv[1]);
   assert((set >= 0) && (set <= 1));
   int num = atoi(argv[2]);
   assert((num >= 2) && (num <= 11));
   char filename[100];
   sprintf(filename, "A32%dk%02d.TXT", set, num);
   double ee = fabs((num-1)/10.);

   double max_t[2][10] = {
                            {11086, 5738, 1702, 1098, 555, 371, 343, 267, 265, 208},
                            {11800, 6326, 2420, 1034, 599, 409, 353, 318, 226, 225}
                          };
```

```
   std::vector<double> x, y;
   if(!read_data(filename, x, y, max_t[set][num-2])) return -1;
   assert(x.size() == y.size());
   int n = (int)x.size();

   std::cout.precision(15);
   std::cout << "file=" << filename << std::endl;
   std::cout << "n=" << n << std::endl;
   double lse = 0;

   EPS = 2;
   double tmp;
   do
   {
      EPS *= 0.5;
      tmp = 1+EPS;
   }
   while(tmp > 1);
   EPS *= 2;
   std::cout << "EPS=" << EPS << std::endl;
   std::cout << "DBL_MAX=" << DBL_MAX << std::endl;


   if(num == 11)
   {
      int n_param = 6;
      double min_param[6] = {0, 0, 0, -1, -1e+30, -1e+30};
      char* param_name[6] = {"ks", "ns", "km", "nm", "delta_epsilon_xH1*",
"delta_epsilon_xH1"};
      double param[6];
      if(set == 0)
      {
         param[0] = 0.0212976564492344;
         param[1] = 0.592919410713291;
         param[2] = 0.0146407397230146;
         param[3] = 5.03382750873002;
         param[4] = 3057.47469365754;
         param[5] = 3191.509234599;
      }
      else
      {
         param[0] = 0.021;
         param[1] = 0.64;
         param[2] = 0.012;
         param[3] = 2.8;
         param[4] = y[n-1];
         param[5] = y[n-1];
      }

      Delta_Epsilon f;

#ifdef RESPLOT
      std::cout << "begin resplot" << std::endl;
      resplot(std::cerr, f, n_param, param, n, x, y,
              1, 4,
              0.54, 0.74,
              0, 6000,
              40, 40);

      std::cout << "end resplot" << std::endl;
      return 0;
#else
      lse = Levenberg_Marquardt(f, n_param, n, x, y, param, min_param, param_name,
true);
      std::cout << "lse=" << lse << std::endl;
      plot(std::cerr, f, n_param, n, x, param);
#endif
   }
   else
   {
      int n_param = 4;
      double param[4];
```

```
double min_param[4] = {0, -1, -1e+30, -1e+30};
char* param_name[4] = {"km", "nm", "delta_epsilon_xH1*", "delta_epsilon_xH1"};
double fixed_param[2];
if(set == 0)
{
   fixed_param[0] = 0.0212976564492344;
   fixed_param[1] = 0.592919410713291;
}
else
{
   fixed_param[0] = 0.020346410283696;
   fixed_param[1] = 0.62238354456176;
}
param[0] = 0.01;
param[1] = 0.01;
param[2] = ee*y[n-1];
param[3] = y[n-1];
switch(num)
{
case 2:
   if(set == 0)
   {
      param[0] = 0.00178349934833236;
      param[1] = -0.310101732933848;
      param[2] = 589.711462461509;
      param[3] = 1668.75060847215;
   }
   else
   {
      param[0] = 0.000664483153946286;
      param[1] = -0.44471638206304;
      param[2] = -550.545406193058;
      param[3] = -1892.37520931528;
   }
   break;
case 3:
   if(set == 0)
   {
      param[0] = 0.00324061639910703;
      param[1] = 0.322461019277507;
      param[2] = 1029.51127544456;
      param[3] = 2420.85155453692;
   }
   else
   {
      param[0] = 0.00233198864072955;
      param[1] = -0.010767489702333;
      param[2] = -845.56698680611;
      param[3] = -2598.45195629275;
   }
   break;
case 4:
   if(set == 0)
   {
      param[0] = 0.00415625741542247;
      param[1] = 0.833807729190313;
      param[2] = 1335.17500029092;
      param[3] = 3154.06138024185;
   }
   else
   {
      param[0] = 0.00420072445092931;
      param[1] = 0.870118108512702;
      param[2] = -1281.02325755439;
      param[3] = -3105.12895977142;
   }
   break;
case 5:
   if(set == 0)
   {
      param[0] = 0.00613291913513896;
      param[1] = 1.92947439722276;
      param[2] = 1759.44772458897;
```

```
            param[3] = 3221.59403514338;
        }
        else
        {
            param[0] = 0.00603909305044723;
            param[1] = 1.83895346648579;
            param[2] = -1662.75889438507;
            param[3] = -3142.06872609191;
        }
        break;
    case 6:
        if(set == 0)
        {
            param[0] = 0.00739040705561941;
            param[1] = 2.85846251072827;
            param[2] = 2154.80621253203;
            param[3] = 3228.70763463266;
        }
        else
        {
            param[0] = 0.00752055543151679;
            param[1] = 2.56047045300042;
            param[2] = -1973.67845302681;
            param[3] = -3146.8030284917;
        }
        break;
    case 7:
        if(set == 0)
        {
            param[0] = 0.00879158626030883;
            param[1] = 3.72019369041851;
            param[2] = 2511.42581430764;
            param[3] = 3230.71791661231;
        }
        else
        {
            param[0] = 0.00855421826024841;
            param[1] = 3.41631689706377;
            param[2] = -2338.03564941604;
            param[3] = -3162.78390700877;
        }
        break;
    case 8:
        if(set == 0)
        {
            param[0] = 0.0107103383257628;
            param[1] = 4.21993145540814;
            param[2] = 2711.66533192663;
            param[3] = 3209.32025025913;
        }
        else
        {
            param[0] = 0.0104709298445197;
            param[1] = 3.25739627661057;
            param[2] = -2493.02200124087;
            param[3] = -3154.67594510311;
        }
        break;
    case 9:
        if(set == 0)
        {
            param[0] = 0.0133515025333525;
            param[1] = 4.70060694480576;
            param[2] = 3016.83367948387;
            param[3] = 3238.14240477;
        }
        else
        {
            param[0] = 0.0122412366901099;
            param[1] = 4.07215429667012;
            param[2] = -2788.87325192761;
            param[3] = -3143.14943127697;
        }
```

```
         break;
      case 10:
         if(set == 0)
         {
            param[0] = 0.0146407399045361;
            param[1] = 5.03382723838358;
            param[2] = 3057.47468883476;
            param[3] = 3191.5092345739;
         }
         else
         {
            param[0] = 0.0141909588260316;
            param[1] = 4.78984290776663;
            param[2] = -3142.40527142199;
            param[3] = -3235.69880522798;
         }
         break;
      default:
         break;
      }

      Bind2Function<Delta_Epsilon> f(Bind2(Delta_Epsilon(), n_param, fixed_param));
      lse = Levenberg_Marquardt(f, n_param, n, x, y, param, min_param, param_name,
true);
      std::cout << "lse=" << lse << std::endl;
      plot(std::cerr, f, n_param, n, x, param);
   }

   return 0;
}
```

Chapter 6

Summary

The control of the spatial arrangment of functional dye molecules in the solid state, at interfaces and in solution is of fundamental importance for the development of nanoscale functional units for optoelectronics and photonics. In the last decades new routes have been explored which allow the efficient construction of such defined structures by self-assembly. Nevertheless, despite considerable progress most known dye assemblies are constructed as simple one-dimensional stacks through aggregation of their π-systems along one axis.

Recently, the dimer formation of highly dipolar merocyanine dyes, a class of chromophores which is of interest for nonlinear optical and photorefractive applications, was proposed as a novel and promising supramolecular binding motif for the construction of well-defined functional dye assemblies owing to its high binding strength and directionality (Figure 1a,b). The objective of this thesis was the supramolecular construction of such well-defined merocyanine assemblies based on dipolar aggregation of tailored merocyanine building blocks. For that, appropriate molecules were synthesized and their self-assembly properties were studied by NMR, UV–vis and CD spectroscopy, as well as scanning probe microscopy. The content of this thesis is summarized below:

In the introductory ***Chapter 2*** a short review on merocyanine dye aggregation is given starting with the dimer formation of simple merocyanine dyes and extending to the self-assembly of bis(merocyanine) dyes into well-defined nanorods. Special attention is given to the influence of solvent polarity as well as steric effects on the self-assembly of these dyes. Furthermore, literature examples for hydrogen bond-directed self-assembly of merocyanine dyes are given.

In the following chapters, studies on the construction of well-defined bi- and trimolecular aggregates by dipolar aggregation, as well as self-assembly studies towards homochiral supramolecular nanorods are described. The underlying concept was based on tethering two merocyanine chromophores by appropriate spacers that guide self-assembly of the respective bis(merocyanine) dyes into the desired geometry. Figure 1c shows a schematic representation of the studied systems.

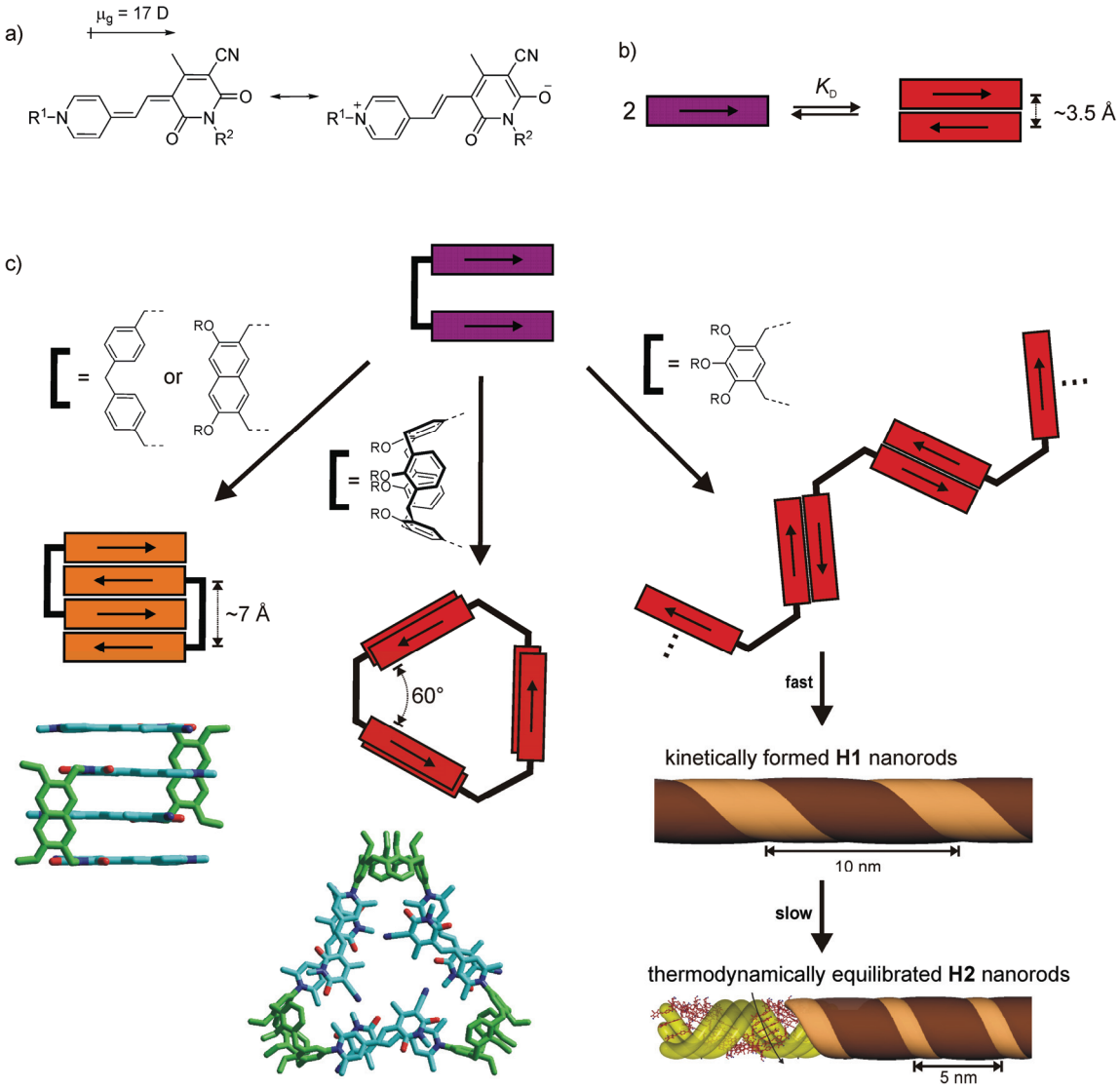

Figure 1. a) Resonance structures of the highly dipolar merocyanine chromophore applied in this thesis. b) Schematic representation of dimerization of merocyanine dyes into centrosymmetric aggregates by dipole–dipole interactions. c) Schematic representation of the supramolecular construction of well-defined merocyanine dye assemblies by self-assembly of appropriately designed bis(merocyanine) building blocks. Depending on the type of the tether that connects the two chromophores of the respective bis(merocyanine) dyes, bimolecular complexes containing a π-stack of four chromophores (left) and a cyclic trimer complex containing three intermolecular merocyanine dimer units (middle) were achieved. Studies on the self-assembly kinetics of xylylene-tethered bis(merocyanine) dyes revealed a complex self-assembly sequence into kinetically and thermodynamically formed helical nanorod aggregates (right).

In ***Chapter 3*** a novel class of dipolar tweezer molecules is presented which self-assemble into centrosymmetric bimolecular complexes featuring a π-stacked arrangement of four chromophores (Figure 1c, left). These tweezers have been achieved through tethering of two dipolar merocyanine chromophores by a naphthalenedimethylene or dimethylenediphenyl-methane spacer that provide an interplanar distance of the chromophores in the range of 7 Å.

Owing to the ideal interplanar chromophore distances for π–π stacking and the unique aggregate geometry with alternating orientation of the dipole moments of the four chromophores in these bimolecular complexes very high dimerization constants of up to $>10^{-9}$ M^{-1} became possible even in chloroform. These self-association constants are several orders of magnitude higher than those of traditional tweezer systems containing two electron-rich chromophores. The structural assignment of the tetrachromophoric π-stack has been accomplished by MALDI-TOF mass spectrometry and ROESY NMR spectroscopy. Molecular modeling studies accounted for the relationship of dimerization constants and optical properties of the bimolecular complexes of these bis(merocyanine) dyes on the type of spacer and position of attachment to the merocyanine chromophores.

In ***Chapter 4*** the self-assembly of a discrete cyclic architecture of merocyanine chromophores that contains three merocyanine dimer units is reported (Figure 1c, middle). This trimeric cyclic array was achieved by dipolar interaction directed self-assembly of a calixarene-bis(merocyanine) conjugate, which provides the structural predisposition for self-assembly into a trimeric cyclic array as well as the structural rigidity to minimize the entropic costs for self-assembly. Concentration-dependent UV–vis aggregation studies of this calixarene-tethered bis(merocyanine) dye revealed a high thermodynamic stability of the formed trimeric complex which can be attributed to the formation of three antiparallel chromophore pairs by dipolar aggregation. Further evidence for the formation of trimeric complex was obtained from MALDI-TOF MS and scanning tunneling microscopy (STM).

While *Chapters 3* and *4* focused on the creation of discrete aggregates, in ***Chapter 5*** a detailed study of the self-assembly of chiral xylylene-tethered bis(merocyanine) dyes into well-defined helical nanorod aggregates is presented (Figure 1c, right). Special attention was given to the kinetics of this self-assembly process. Thus, a complex self-assembly sequence into well-defined helical nanorod structures has been revealed spectroscopically by time-dependent CD spectroscopy and microscopically by atomic force microscopy. This self-assembly sequence proceeds over several kinetically formed supramolecular intermediates which are distinguished by their morphology and (chir)optical properties. Moreover, co-aggregation studies applying chiral monomers with different enantiomeric excess as well a mixtures of enantiopure and achiral monomers gave novel insights into the kinetics of chiral amplification in a supramolecular system directed by the "majority-rules" and "sergeants-and-soldiers" effect. It was shown that chiral amplification mechanisms can operate at different stages of

self-assembly to afford energetically favored structures. The enantiomeric excess in the monomers as well as the fraction of chiral monomers in mixtures of chiral and achiral monomers has a strong impact on the self-assembly and chiral amplification kinetics. These studies show for the first time that the rates of these processes decreases strongly with decreasing enantiomeric excess of the chiral monomers or decreasing fraction of chiral monomers in co-aggregates of chiral and achiral monomers. Thus, rapid self-assembly processes into helical nanostructures require enantiopure educts. However, within a slow evolution homochiral aggregates can be obtained from molecular mixtures with low enantiomeric excess.

In conclusion, the present thesis demonstrates the potential of dipolar aggregation as novel directional and specific supramolecular binding motif for the creation of more elaborate supramolecular architectures beyond simple dimers. Furthermore, the self-assembly studies into bis(merocyanine) nanorods gave new insights into the kinetics of morphogenesis in supramolecular aggregates.

Zusammenfassung

Die Kontrolle der räumlichen Anordnung von funktionellen Farbstoffmolekülen im Festkörper, an Grenzflächen und in Lösung ist von entscheidender Bedeutung für die Entwicklung nanoskaliger Funktionseinheiten für die Optoelektronik und die Photonik. In den letzten Jahrzehnten wurden Wege erforscht, auf denen sich der Aufbau solcher definierter Strukturen effizient mittels Selbstorganisation realisieren lässt. Trotz dieser Fortschritte sind die meisten bekannten Farbstoffaggregate jedoch nach wie vor einfache eindimensionale Stapel, welche durch Aggregation der π-Systeme entlang einer Achse entstehen.

Aufgrund ihrer hohen Bindungsstärke und Direktionalität wurde die Dimerisierung von hochpolaren Merocyaninfarbstoffen, einer Chromophorart welche für nicht-linear-optische und photorefraktive Anwendungen von Interesse ist, unlängst als neuartiges und vielversprechendes Bindungsmotif für die Realisierung von definierten funktionalen Farbstoffaggregaten vorgeschlagen (Abbildung 1a,b). Das Ziel dieser Dissertation war der supramolekulare Aufbau definierter Merocyaninaggregate durch dipolare Aggregation maßgeschneiderter Merocyanin-Bausteine. Hierzu wurden geeignete Moleküle synthetisiert und ihre Selbstorganisations-eigenschaften mittels NMR-, UV–vis- und CD-Spektroskopie sowie Rastersondenmikroskopie charakterisiert. Der Inhalt dieser Dissertation ist im Folgenden zusammengefasst:

Das einleitende ***Kapitel 2*** gibt einen kurzen Literaturüberblick über die Aggregation von Merocyaninfarbstoffen ausgehend von der Dimerbildung einfacher Merocyaninfarbstoffe bis hin zur Selbstorganisation von Bis(merocyanin)-Farbstoffen zu definierten Nanostäbchen. Besonderes Augenmerk wurde dabei auf die Einflüsse gelegt, welche die Lösungsmittel-polarität sowie sterische Effekte auf die Selbstorganisation dieser Farbstoffe ausüben. Desweiteren werden Literaturbeispiele vorgestellt, in denen die Selbstorganisation von Merocyanin-Farbstoffen durch Wasserstoffbrückenbindungen vermittelt wird.

Die folgenden Kapitel beschäftigen sich mit Studien zum Aufbau definierter bi- und trimolekularer Aggregate durch dipolare Aggregation von Bis(merocyanin)-Farbstoffen, sowie mit Selbstorganisationsstudien zu homochiralen supramolekularen Nanostäbchen. Das zugrunde liegende Konzept basiert auf der Verknüpfung zweier Merocyanin-Chromophore

durch einen geeigneten Verbindungsbaustein, welcher die Selbstorganisation dieser Bis(merocyanin)-Einheiten in die gewünschte Aggregatgeometrie bewirkt. Abbildung 1c zeigt eine schematische Darstellung der untersuchten Systeme.

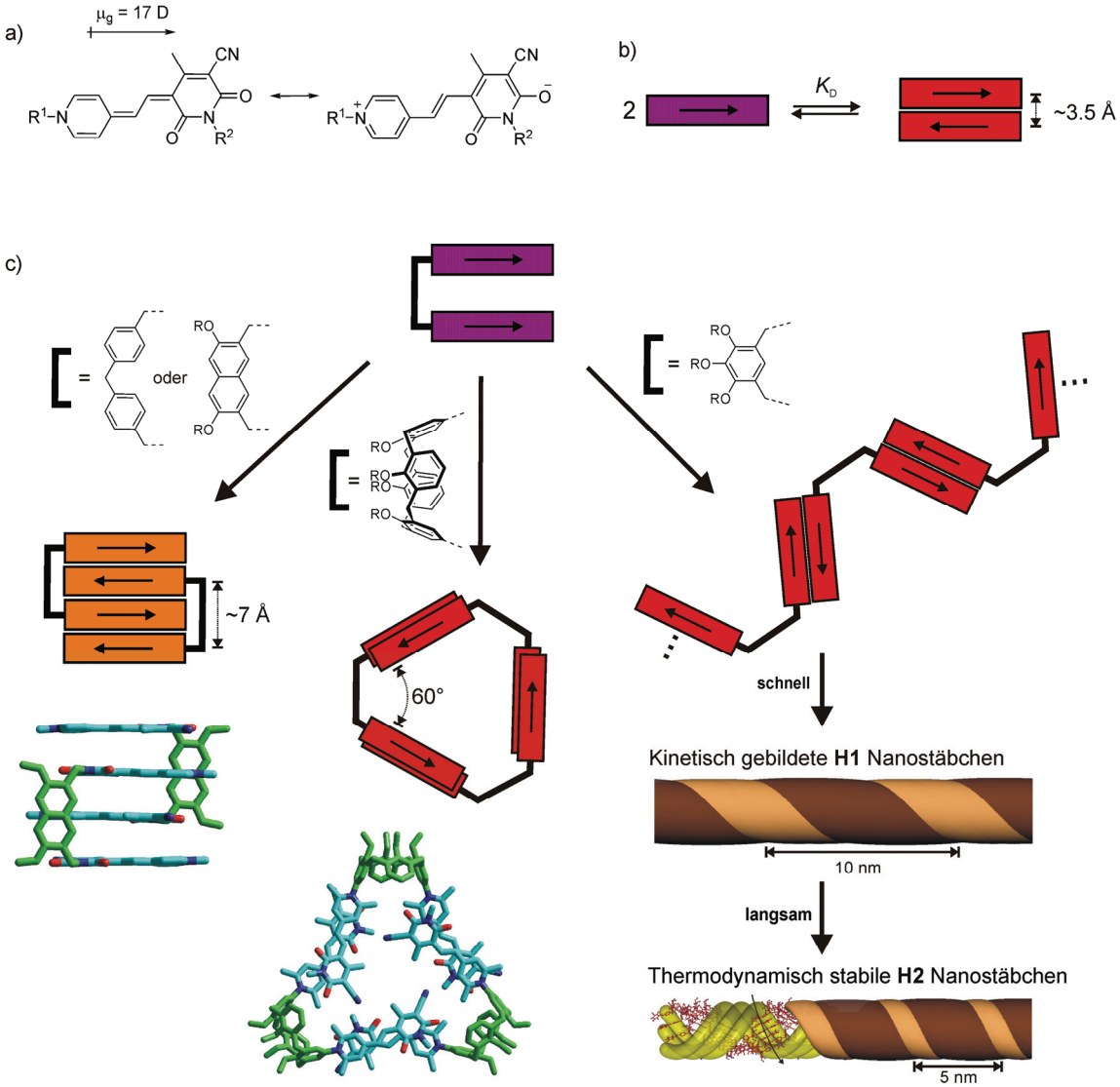

Abbildung 1. a) Resonanzstrukturen des in dieser Arbeit verwendeten hochpolaren Merocyanin-Chromophors. b) Schematische Darstellung der Merocyanin-Dimerisierung zu punktsymmetrischen Aggregaten durch Dipol–Dipol-Wechselwirkungen. c) Schematische Darstellung des supramolekularen Aufbaus von definierten Merocyanin-Farbstoffaggregaten durch Selbstorganisation von entsprechend konzipierten Bis(merocyanin)-Bausteinen. In Abhängigkeit vom Verknüpfungselement zwischen den Chromophoren des jeweiligen Bis(merocyanin)-Farbstoffes wurden bimolekulare Komplexe mit einem π-Stapel von vier Chromophoren, sowie ein zyklischer Trimerkomplex mit drei intermolekular gebildeten Dimereinheiten erhalten. Studien zur Selbstorganisationskinetik von Xylylen-verküpften Bis(merocyanin)-Farbstoffen zeigten eine komplexe Selbstorganisationssequenz zu kinetisch und thermodynamisch gebildeten helikalen Nanostäbchen (rechts).

In ***Kapitel 3*** ist eine neuartige Klasse dipolarer Pinzettenmoleküle beschrieben, deren Aggregation zu punktsymmetrischen bimolekularen Komplexen führt, welche einen aus vier Chromophoren bestehenden π-Stapel aufweisen (Abbildung 1c, links). Diese Pinzettenmoleküle wurden durch kovalente Verknüpfung zweier Merocyanin-Chromophore mit einem Naphthalindimethylen- oder Dimethylendiphenylmethan-Baustein erhalten, welcher einen interplanaren Abstand der beiden Chromophore im Bereich von 7 Å zur Verfügung stellt. Aufgrund eines idealen interplanaren Chromophorabstands für die π-Stapelung und einer einzigartigen Aggregatgeometrie, bei der die Dipolmomente der vier Chromophore abwechselnd orientiert sind, wurden in diesen bimolekularen Komplexen selbst in Chloroform sehr hohe Dimerisierungskonstanten von bis zu $>10^{-9}$ M^{-1} erreicht. Diese Selbst-assoziationskonstanten sind mehrere Größenordungen höher als die von herkömmlichen Pinzettenmolekülen welche zwei elektronenreiche Chromophore enthalten. Die Struktur der in dieser Arbeit beschriebenen tetrachromophoren π-Stapel wurde durch MALDI-TOF Massenspektroskopie sowie durch ROESY NMR Spektroskopie charakterisiert. Mittels Kraftfeldrechnungen konnte die Abhängigkeit der Dimerisierungskonstanten und der optischen Eigenschaften dieser bimolekularen Komplexe von der Art der Verknüpfungseinheit und der Verknüpfungsposition an den Merocyaninchromophoren erklärt werden.

Kapitel 4 behandelt die Selbstorganisation eines diskreten, drei Chromophor-Dimere enthaltenden, zyklischen Merocyanin-Aggregates (Abbildung 1c, mitte). Dies wurde durch die dipolare Aggregation eines Calix[4]aren-Bis(merocyanin) Konjugates erreicht, welches die strukturelle Prädisposition zur Selbstorganisation in ein zyklisches Trimer und zusätzlich die nötige Rigidität zur Minimierung des Entropieverlustes bei der Selbstorganisation aufweist. Durch konzentrationsabhängige UV–vis-Aggregationsstudien konnte eine hohe thermo-dynamische Stabilität des Trimerkomplexes nachgewiesen werden, welche auf die Bildung dreier antiparalleler Chromophorpaare durch dipolare Aggregation zurückzuführen ist. Weitere Belege für die Bildung des Trimerkomplexes wurden durch MALDI-TOF Massenspektrometrie und Rastertunnelmikroskopie erhalten.

Im Gegensatz zu Kapitel 3 und 4, die sich mit der Herstellung diskreter Aggregate beschäftigen, behandelt ***Kapitel 5*** die Untersuchung der Selbstorganisation von chiralen Xylylen-verknüpften Bis(merocyanin)-Bausteinen zu definierten helikalen Nanostäbchen (Abbildung 1c, rechts). Besonderes Augenmerk wurde dabei auf die Kinetik dieser Selbstorganisation gelegt. Durch CD-spektroskopische und rasterkraftmikroskopische

Untersuchungen konnte gezeigt werden, dass der Ausbildung dieser helikalen Stäbchenstrukturen eine komplexe Abfolge von Selbstorganisationsprozessen zugrunde liegt. Der Prozess der Selbstorganisation verläuft über mehrere kinetisch gebildete supramolekulare Intermediate, die sich in ihrer Morphologie und ihren (chir)optischen Eigenschaften unterscheiden. Darüber hinaus führten Co-Aggregations-Studien mit chiralen Monomeren für unterschiedliche Enantiomerenverhältnisse, sowie mit enantiomerenreinen und achiralen Monomeren zu einzigartigen Einblicken in die Kinetik der Chiralitätsverstärkung in supramolekularen Systemen durch den „majority-rules“ bzw. „sergeants-and-soldiers“ Effekt. Es zeigte sich, dass solche chirale Verstärkungsmechanismen in unterschiedlichen Phasen der Selbstorganisation wirksam sein können und zur Bildung energetisch begünstigter Strukturen führen. Der Enantiomerenüberschuß der Monomere bzw. der Anteil chiraler Monomere im Gemisch hat dabei einen großen Einfluss auf die Kinetik dieser Selbstorganisationsprozesse. Die Geschwindigkeit dieser Prozesse nimmt nach den hier erstmals beschriebenen Untersuchungen mit abnehmendem Enantiomerenüberschuß bzw. mit abnehmendem Anteil von chiralen Monomeren in Coaggregaten von chiralen und achiralen Monomeren dramatisch ab. Rasche Selbstorganisationsprozesse zu helikalen Nanostrukturen erfordern somit enantiomerenreine Ausgangsmaterialien. Im Rahmen einer langsamen Evolution können homochirale Aggregate jedoch auch aus Gemischen von Molekülen entstehen, welche nur einen geringen Enantiomerenüberschuss aufweisen.

Zusammenfassend konnte in der vorliegenden Arbeit das Potential der dipolaren Aggregation von Merocyaninfarbstoffen als neuartiges, gerichtetes und spezifisches Bindungsmotif zum Aufbau wesentlich komplexerer supramolekularer Architekturen als einfachen Dimeren gezeigt werden. Desweiteren lieferten Studien zur Selbstorganisation von Bis(merocyanin)-Nanostäbchen neue Erkenntnisse zur Morphogenese supramolekularer Aggregate.

List of Publications

- *Supramolecular Stereomutation in Kinetic and Thermodynamic Self-Assembly of Helical Merocyanine Dye Nanorods*

  Lohr, A.; Lysetska, M.; Würthner, F. *Angew. Chem., Int. Ed.* **2005**, *44*, 5071–5074.

- *Synthesis of Merocyanine Dye Nanorods: The Importance of Solvent, Kinetic and Thermodynamic Control, and Steric Effects on Self-Assembly (Feature Article)*

  Lohr, A.; Gress, T.; Deppisch, M.; Knoll, M.; Würthner, F. *Synthesis* **2007**, 3073–3082.

- *Circular Dichroism and Absorption Spectroscopy of Merocyanine Dimer Aggregates: Molecular Properties and Exciton Transfer Dynamics from Time-Dependent Quantum Calculations*

  Seibt, J.; Lohr, A.; Würthner, F.; Engel, V. *Phys. Chem. Chem. Phys.* **2007**, *9*, 6214–6218

- *Evolution of Homochiral Helical Dye Assemblies: Involvement of Autocatalysis in the "Majority-Rules" Effect*

  Lohr, A.; Würthner, F. *Angew. Chem., Int. Ed.* **2008**, *47*, 1232–1236.

- *Time-Dependent Amplification of Helical Bias in Self-Assembled Dye Nanorods by the Sergeants-and-Soldiers Principle*

  Lohr, A.; Würthner, F. *Chem. Commun.* **2008**, 2227–2229

- *Self-assembled π-stacks of functional dyes in solution: structural and thermodynamic aspects*

  Chen, Z.; Lohr, A.; Saha-Möller, C. R.; Würthner, F. *Chem. Soc. Rev.*, *accepted*.

- *Dipolar Aggregation of Bis(merocyanine) Dye Tweezers into Discrete Bimolecular π-Stacks*

  Lohr, A.; Grüne, M.; Würthner, F., *submitted*.

Poster Presentations

- Leopoldina Meeting, Dendrimers: Platforms for chemical functionality
  Heidelberg/D, March 18–19, 2005

  Lohr, A.; Lysetska, M.; Yao, S.; Würthner, F., *"Supramolecular Stereomutation in Kinetic and Thermodynamic Self-Assembly of Helical Merocyanine Dye Nanorods"*

- MC7, Materials for the 21th Century, Edinburgh/UK, July 5–8, 2005

  Lohr, A.; Lysetska, M.; Würthner, F., *"Supramolecular Stereomutation in Kinetic and Thermodynamic Self-Assembly of Helical Merocyanine Dye Nanorods"*

- The Seventh International Symposium on Functional π-Electron Systems (Fπ7)
  Osaka/JP, May 15–20, 2006

  Lohr, A.; Lysetska, M.; Würthner, F., "*Supramolecular Stereomutation and Amplification of Chirality in Self-Assembled Helical Merocyanine Dye Nanorods"*

- ORCHEM 2006, Bad Nauheim/D, September 7–9, 2006

  Lohr, A.; Lysetska, M.; Würthner, F., "*Supramolecular Stereomutation and Amplification of Chirality in Self-Assembled Helical Merocyanine Dye Nanorods"*

- 113th BASF International Summer Course, Ludwigshafen/D, July 23–August 3, 2007

  Lohr, A.; Lysetska, M.; Würthner, F., "*Supramolecular Stereomutation and Chiral Amplification in Self-Assembled Helical Merocyanine Dye Nanorods"*

- The 11th International Conference on Circular Dichroism, Groningen/NL, Sept 2–6, 2007

  Lohr, A.; Lysetska, M.; Würthner, F., "*Supramolecular Stereomutation and Chiral Amplification in Self-Assembled Helical Merocyanine Dye Nanorods"*

Danksagung

Herrn Prof. Dr. Frank Würthner danke ich für die interessante Themenstellung sowie für wertvolle Anregungen und Diskussionen. Darüber hinaus gebührt ihm ein großer Dank für die mir gewährte Freiheiten und das in mich gesetzte Vertrauen insbesondere beim Verfolgen eigener Ideen, sowie für seine uneingeschränkte Unterstützung.

Herrn Dr. Chantu Saha-Möller danke ich sehr herzlich für die exzellente Überarbeitung von Manuskripten, wertvollen Diskussionen und die gute Zusammenarbeit in allen Belangen des Publizierens.

Einen großen Dank möchte ich auch Frau Dr. Marina Knoll und Frau Dr. Shinobu Uemura aussprechen, welche mit der Durchführung von AFM- und STM-Messungen einen großen Beitrag zu dieser Arbeit leisteten.

Für die Aufnahme von Kernresonanz- bzw. Massenspektren möchte ich mich bei Herr Dr. Matthias Grüne und Frau Elfriede Ruckdeschel sowie bei Herr Dr. Michael Büchner und Herr Fritz Dadrich bedanken.

Herrn Stefan Geschwentner und Herrn Sascha Gruss danke ich für die Erstellung eines Computerprogramms für die Auswertung von Messdaten sowie für die Hilfestellung in mathematischen Belangen.

Herrn Prof. Dr. Volker Engel und Herrn Joachim Seibt danke ich für die gute Zusammenarbeit im Rahmen einer gemeinsamen Veröffentlichung.

Ein großer Dank gilt Herr Dr. Peter Osswald für unzählige wertvolle Diskussionen sowie zahlreiche Fahrgemeinschaften.

Für ihre Hilfsbereitschaft und Unterhaltung im Labor danke ich meinen Laborkollegen Herrn Joachim Bialas und Frau Manuela Deppisch.

Ein Dankeschön für die gute Zusammenarbeit und ihr Engagement gebührt weiterhin meinen Praktikanten Chris Hoggett, Ralf Schmidt, Felix Pasker und Mohan Wadekar, sowie meiner Auszubildenden Melanie Pavlov.

Herzlichen Dank an alle ehemaligen und aktuellen Mitarbeiter des AK Würthner für die gute Zusammenarbeit und das sehr gute und freundschaftliche Arbeitsklima.

Für all die schönen Abende und sonstige Freizeitunternehmungen möchte ich Conny, Felix P., Johann, Peter, Rainer, Ralf, Rüdiger und Marina, Stefanie, Suhrit und vor allem Valerie ein herzliches Dankeschön aussprechen.

Ein besonders großer Dank gebührt jedoch meiner Familie für Ihre immerwährend tolle Unterstützung.